Numerical study of the water experiment for XT-ADS windowless spallation target

A. Batta,[1] **A. Class,**[1] **K. Litfin,**[1] **M. Dierckx,**[2] **H. Jeanmart,**[3]
F. Roelofs,[4] **P. Schuurmans,**[2] **K. Van Tichelen**[2]
[1]FZK, Germany
[2]SCK•CEN, Belgium
[3]UCL, Mechanical Engineering Department, Belgium
[4]NRG, Netherlands

Abstract

Accelerator-driven systems require a coupling between a proton accelerator and a subcritical reactor core by means of a spallation target. Obviously there are only few options for the target design, e.g. a solid or a heavy liquid metal (HLM) target. For the case of a HLM target the proton beam can either hit the liquid metal directly (windowless or free-surface target) or it can pass through a solid window before it hits the liquid metal (window target). The windowless target resolves many of the material issues, since no solid structures are directly hit by the proton beam. Such a windowless target is currently developed in the Integrated Project EUROTRANS of the European Community. The windowless target is placed in the centre of the subcritical core and is subjected to a proton beam of maximum 3 mA and 600 MeV. In the target, HLM flows downwards through a feeder line surrounding the beam tube and forms a conical free surface which is subjected to the proton beam. The thermal-hydraulics of the target must ensure that the heat deposited into the HLM can be safely removed without jeopardising the vacuum of the proton beam line.

The design of the target is accompanied by numerical and experimental investigations which support the analysis of the target thermal-hydraulics. A water experiment built at UCL, Belgium is prepared for assisting the design of the XT-ADS spallation target as well as for validating the numerical methods that will be used in the analysis of the real HLM target. Volume of fluid methods in combination with cavitation models existing in Computational Fluid Dynamics codes like STAR-CD and CFX are used for the isothermal situation. In addition, the Euler-Euler method available in CFX is used. Based on preliminary numerical results as well as other experimental observations, design rules for the target are defined and applied. In this paper, the results of numerical simulations of the free-surface flow in different design versions of the target are shown. They have led to new design rules that ensure a stable free-surface configuration and an appropriate flow in the target feeder. It is also demonstrated that the design is insensitive to the flow rate within design limits and that the flow is insensitive to the pressure conditions far downstream the target. The resulting target design that will be experimentally tested is finally analysed.

Introduction

A windowless spallation target is currently being developed in the Integrated Project EUROpean Research Programme for the TRANSmutation of High Level Nuclear Waste in Accelerator-driven System (EUROTRANS). In this programme the first advanced design of an approximately 50 to 100 MWth eXperimental facility demonstrating the technical feasibility of Transmutation in an Accelerator-driven System (XT-ADS) is being developed [1]. The programme runs from 2005 to 2009. The target for XT-ADS is a heavy liquid metal (HLM). The proton beam hits the liquid metal directly through a free surface (windowless target), resolving many of the material issues encountered in the solid target. Figure 1(a) shows the design of the XT-ADS facility. The windowless target concept is schematically presented in Figure 1(b). The HLM flows downwards through an annular feeder line surrounding the beam tube and forms a conical free surface which is subjected to the proton beam. The thermal-hydraulics of the target must ensure that the heat deposited into the HLM can be safely removed. Thus, recirculation flow in the heat deposition region must be avoided. This requires geometrical optimisations of the target, where different target geometries are evaluated. Both numerical and experimental investigations assist the analysis of the target thermal-hydraulics. The numerical studies serve for testing and optimisation of the proposed target to be tested in the related experiment. Due to the complexity of measurements in HLM, a water experiment is performed firstly. The geometry for this experiment is representative for the final geometry but slightly adapted to the available experimental conditions and to simplify the manufacturing. The water experiment built at UCL, Belgium contributes to the design of the XT-ADS spallation target. It also provides data for the validation of the numerical methods that will be used in the analysis of the real HLM target. Figure 1(c) shows part of the target used in the first water experiments.

Figure 1: (a) XT-ADS design, (b) illustration of windowless target, (c) first design of XT-ADS target water experiment

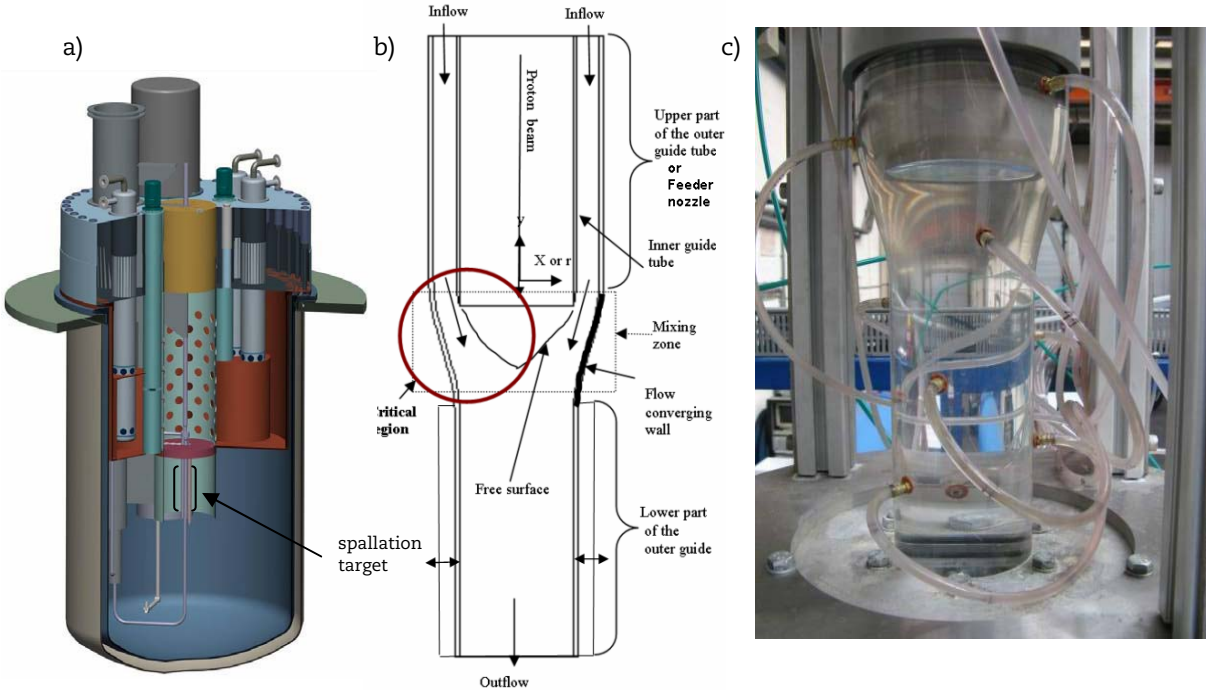

The water experiment studies the isothermal case. Numerical investigations using the fluid dynamics codes STAR-CD, STAR-CCM and CFX are performed to guide the design of the water experiment. The volume of fluid method (VOF) in combination with cavitation models existing in available codes CFX, Star-CD and STAR-CCM and the Euler-Euler method available in CFX code are used in the analysis. The Rayleigh cavitation model is applied in the used codes. The different design options for the feeder nozzle and geometrical parameters in the mixing zone are tested. Based on the extensive studies a final design for the water experiment is proposed.

Numerical investigation

Within this study the effect of different target geometrical parameters on the flow field are investigated. The focus is mainly on the minimisation of the recirculation zone and on the stability of the free surface. In order to minimise the circulation zone, application of a swirl or specific geometrical features of the target can be used. Accordingly, the effect of different swirl strengths and different target geometries are tested. Based on the results of earlier, it is more convenient to split the design of the target into two parts: the feeder and the target itself see Figure 1(b). Therefore, the study of the target is decoupled from the study of feeder. In most of the numerical studies reported here, the flow in the target is investigated assuming a suitable feeder outlet conditions at the target inlet. The design of the feeder can be achieved separately. After fixing the feeder and target design they are tested together. In the following sections the individual steps for the design of the target are shown. During the different design steps design rules are developed. These rules are applied in the latest design of the XT-ADS target for the water experiments.

Application of swirl

The application of a mild swirl in the windowless spallation target has been assessed in the water loop at the *Université catholique de Louvain* (UCL) in Belgium [2]. In this water experiments, the water circulates through a spallation target mock-up at a 1 to 1 scale. The loop is closed and the flow is driven by a centrifugal pump that can impose a flow rate from 0 to nearly 15 l/s. The swirl strength is varied by application of separately fabricated swirl devices, based on vertical twisted flow guides in the annular feeder of the target, with different angles of the flow guides. Three different swirl devices have been fabricated and evaluated. The angle of the swirl device is related to the resulting swirl strength, expressed in terms of the amplitude of the azimuthal component compared to the axial component of the flow velocity. The relationship between angle and swirl strength is given in Table 1.

Table 1: Equivalence between device angle and swirl strength

Device angle	3°	6°	9°
Swirl strength	5%	10.5%	15.6%

The experiments clearly showed that the guiding vanes direct the flow in order to create the required swirl. Unfortunately, the experiments also showed the occurrence of a vortex in the central downcomer. Such vortices were observed at swirl intensities of 10.5% and 15.6% and not at a swirl intensity of 5%. As these vortices are considered unacceptable from the point of view of surface stability, it is concluded that application of swirl strength of 10% or higher will lead to an unacceptable vortex in the central downcomer. Figure 2(a) shows flow visualisation at 10 l/s for a swirl intensity of 10.5% and Figure 2(b) shows the swirl device.

Figure 2: (a) Flow visualisation at 10 l/s for a swirl intensity of 10.5% [3], (b) swirl device, (c,d) instantaneous fluid patterns flow for 5% (c) and 10% (d) swirl intensity

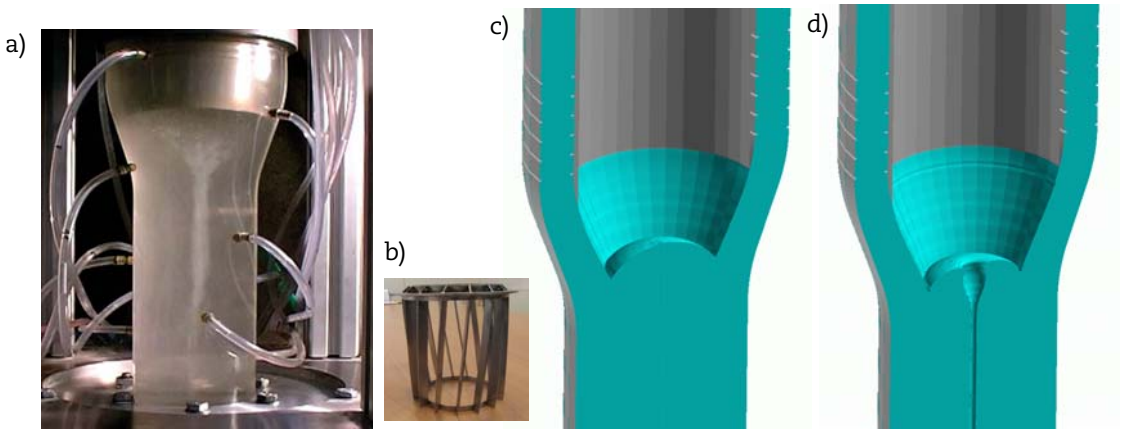

Previous to the experimental programme, numerical simulations were performed assessing the influence of various swirl strengths on the free surface behaviour. The computational model assumed axisymmetry, and contained about 10 000 computational volumes. Swirl intensities of 5%, 10% and 15% were assessed numerically. The numerical simulations focussed on the influence of application of a controlled swirl on the stability of the free surface. Figures 2(c) and 2(d) show the resulting flow fields for 5% and 10% swirl intensity. These results confirm the conclusion from the experimental programme that application of swirl strength of 10% or higher leads to an unacceptable vortex in the central downcomer. Furthermore, the numerical simulations show that application of a mild swirl of 5% has a small but stabilising effect on the LBE free surface. However, it should be noted that the addition of a mild swirl might hamper or even be in conflict with other design modifications, *e.g.* application of flow detachments and making optimal use of the available space for the feeder line. More details of this method can be found in [3].

Target geometrical design

Real-size water flow experiments performed at the *Université catholique de Louvain* (UCL) and LBE flow experiments that were done at the KALLA laboratory of the *Forschungszentrum Karlsruhe* (FZK) have shown that a more stable flow is achieved if some detachment of the HLM flow from the confining wall is allowed in the mixing region [4]. Accordingly, the geometry of the reference target investigated in the previous section is modified mainly in the converging zone right at the free surface level. The size of the recirculation zone has been predicted using CFD for different geometries, as shown in Figure 3(c). Compared to the reference design, wider guide tubes in the mixing zone and below are used as shown in Figures 3(a) and 3(b). The use of a wider guide tube will result in a detachment zone near the guide tube, *i.e.* the flow forms a free falling jet. Figure 3(c) compares the tested geometries. Flow rate 11.6 l/s was applied for Cases1-3 and 12.0 l/s for Case 4. Case 3 shows the smallest circulation zone and no cavitation at the converging wall. The geometry of this case is characterised by a small inclination angle. This result will be used in the next designs of the target, see [5] for more details.

Figure 3: Illustration of the proposed detachment zone and different contours of the outer walls of the mixing zone

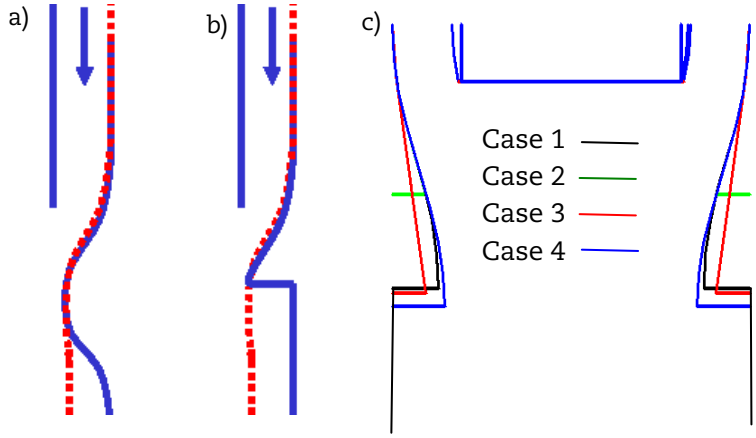

Feeder nozzle design

As starting point for the spallation target nozzle design, the design DG16.5 is taken [6]. This design is an evolution of older designs. The feeder line of DG16.5 nozzle is characterised by the presence of a so-called septum tube which vertically separates two inlet annuli. The septum wall increases the drag in the feeder line and in this way compensates for the hydrostatic pressure gain due to the acceleration of gravity. Indeed, the pressure should be at the local vapour pressure right at the free surface and higher above it. Without drag enhancement, the pressure would be too low in the feeder line, leading to flashing. This needs to be avoided since the resulting pressure fluctuations disturb the free surface.

Figure 4: VOF contours for the modified geometries of the studied cases of Figure 3, 1 denotes water and 0 denotes vapour

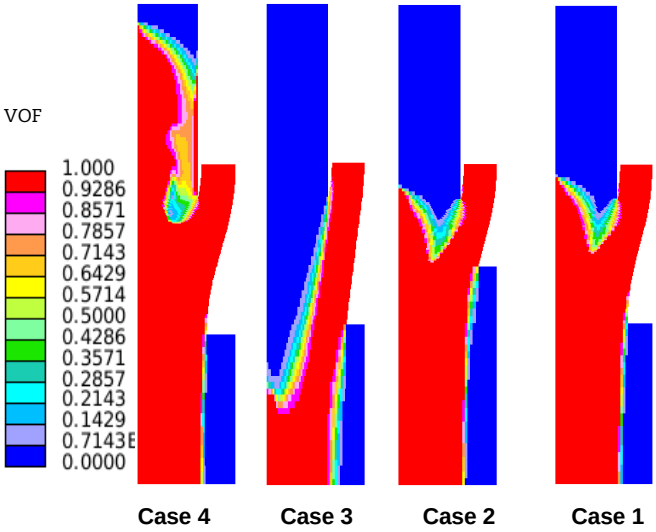

Furthermore, the inclination angle of the outer wall was minimised to 16.5° at that time in order to leave space for irradiation specimens in the region with the highest neutron fluxes. The hydraulic performance of this nozzle has been extensively studied in several experimental campaigns having water, mercury, and LBE as working fluids. On the other hand, these experiments have given input to simulation model developments (as in [7]). The experiments and the numerical simulations showed that a relatively stable recirculation zone could be achieved using this design. However, the septum wall would be difficult to fabricate and might not withstand erosion due to HLM. Other options are tested among them is the insertion of radial fins in the feeder tube which was extensively studied in [8]. Figure 5 shows the proposed fin design and associated computational domain. It shows also the pressure and vapour volume fraction contours obtained by including the feeder nozzle in the simulation.

Figure 5: Target geometry, computational domain, part of the mesh used in simulation, pressure and vapour volume fraction contours, 0 denotes water and 1 denotes vapour

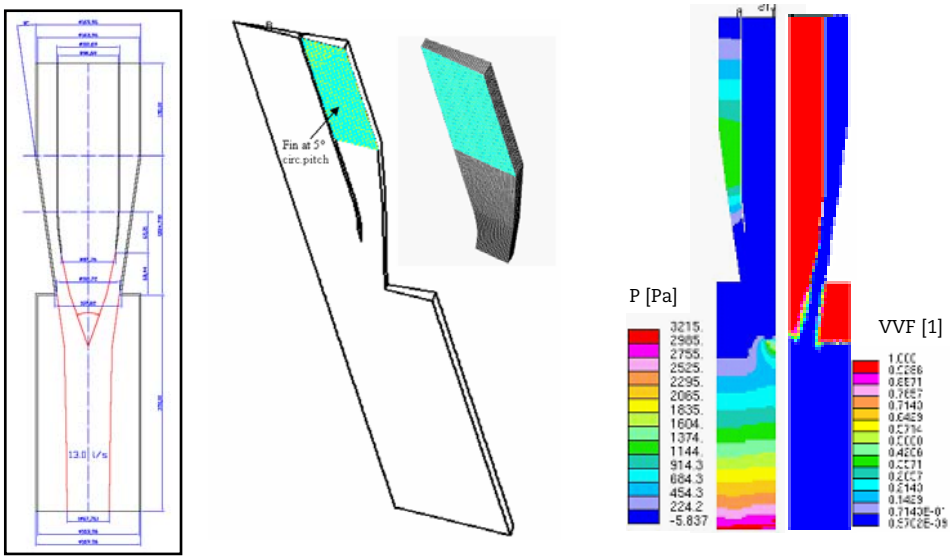

The results show that the required pressure drop in the feeder is achievable by using fins with a 5° pitch. Consequently no vapour is created in the feeder. It can be seen that a nearly linear pressure drop is obtained in the developing flow region.

A sensitivity study of the free surface of the target design given in Figure 5 with respect to inlet and outlet conditions is performed. Table 2 summarises the considered cases.

Table 2: Relative outlet static pressure and inlet velocities of the considered cases

Case number	Pressure Pa	Velocity m/s
i, reference case	3 000	1.0
ii	3 000	0.8
iii	2 000	1.0
iv	2 000	0.8

In [8] it has been proven that decoupling of the feeder from the rest of the target has negligible effect on the free surface compared to studies considering the feeder with the target for the numerical investigation. This is valid for cases where no cavitation exists in the feeder. Accordingly, the feeder will not be considered in the current sensitivity study.

Results have shown that all cases converge to steady state after a few seconds. A comprehensive illustration of the effect of the in- and outlet parameters on the free surface location and recirculation is given in Figure 6. Velocity vectors are coloured by the vapour volume fraction (blue is water and red denotes vapour). For better comparison of the studied cases a rectangle of identical size and position is shown on each result.

Figure 6: Velocity vectors for the cases of Table 2, coloured with vapour volume fraction scalar values, 1 denotes vapour and 0 denotes water

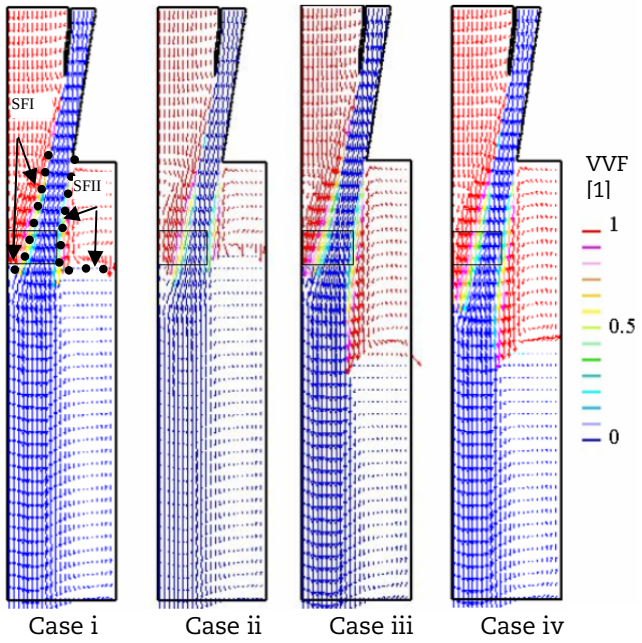

The comparison of Case ii to the reference Case i shows that reduction of inlet velocity results in an enlargement of the recirculation in the merging region and slightly raises the level of the free surface SFII. Comparing Cases i and iii indicates that lowering the outlet pressure lowers both free surfaces. Recirculation is almost eliminated for Case iii. Finally, comparing Cases iii and iv shows (similar as for Cases i and ii) that surface SFI is decreased in level while surface SFII is raised. For the lower outlet pressure this effect is more noticeable. Considering the criterion for operation stability where a stable free surface and a relatively small recirculation zone at the target centre are necessary to avoid high temperature in the recirculation zone, lower outlet pressures are preferred.

Proposed target for water experiment

The results presented above have been used for the latest design of the target nozzle of the XT-ADS target and the corresponding target for water experiment. The maximum allowable velocity in the nozzle of XT-ADS target is assumed to be about 2.5 m/s as corrosion is expected to play a major role during the lifetime of the nozzle. The radial fin option is used as a drag enhancer in the feeder. An analytical study investigated the effect of different fin lengths on the flow conditions at the nominal flow rate. Figure 7 illustrates the interaction between feeder pressure and fin geometry for the nominal flow in the water experiments, 10 l/s. The variation of some geometrical parameters and flow conditions has lead to the optimised design of the fins that should be used in the experiment. The previously defined design rules regarding the maximum allowable velocity, the necessity to have a detachment zone near the guide tube, minimising of the recirculation zone and avoiding cavitation in feeder nozzle are considered. The use of mild swirl is not considered as the proposed geometry is expected to result in a negligible recirculation. Figure 8 shows the target geometry and the computational domain used in the numerical investigation of the target where feeder and target are investigated together.

For the numerical study of this design the cavitation model in three different available codes in IKET at FZK are used. Figure 9 shows the water volume fraction results obtained from STAR-CD, STAR-CCM and CFX. The CFX results show more diffusion and a high recirculation zone, where STAR-CD results in relatively weak diffusion compared to the other codes. The proposed target geometry is currently constructed at UCL.

Conclusions

In this study different target designs for the water experiment are numerically tested. Based on numerical and experimental observations design rules are developed for the target:

- the maximum allowable velocity in feeder nozzle is 2.5 m/s;
- forced detachment by enlarging the guide tube is stabilising the free surface;
- suppression of cavitation in feeder nozzle is achieved by radial fins which induce the necessary pressure loss or drag;
- minimising of recirculation zone is achieved by a small injection angle at feeder nozzle outflow.

Finally, a target is designed for the XT-ADS water experiment which is expected to realise the necessary hydraulic conditions for stable target flow with a small recirculation near the free surface that can be avoided by the proton beam resulting in acceptable heat deposition loads at the surface.

Figure 7: Interaction between feeder pressure and fine geometry for nominal flow, 10 l/s

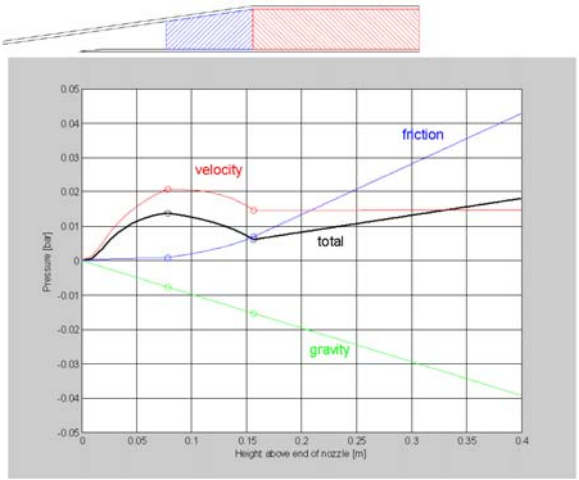

Figure 8: Target geometry and computational domain used in the analysis

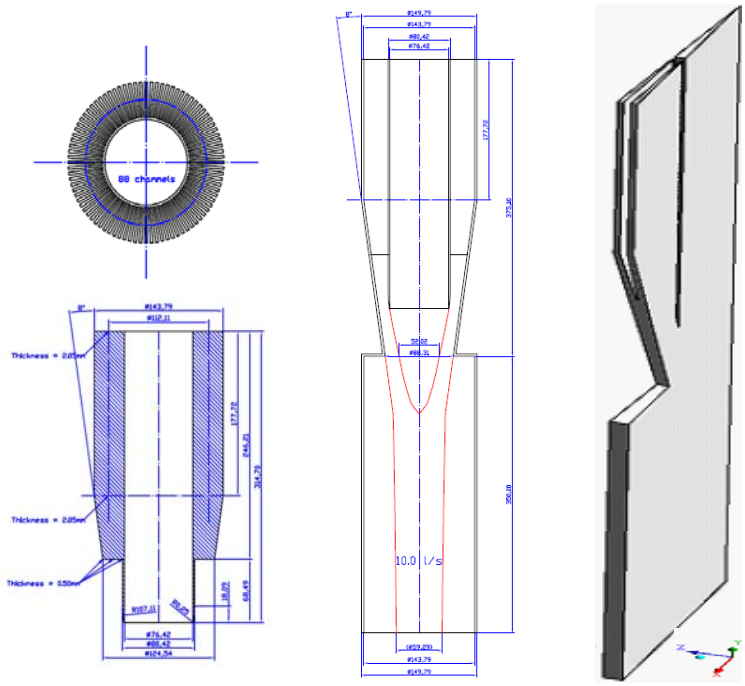

Figure 9: Water volume fraction results obtained from STAR-CD, STAR-CCM and CFX codes for nominal flow, 10 l/s, 0 denotes water and 1 denotes vapour

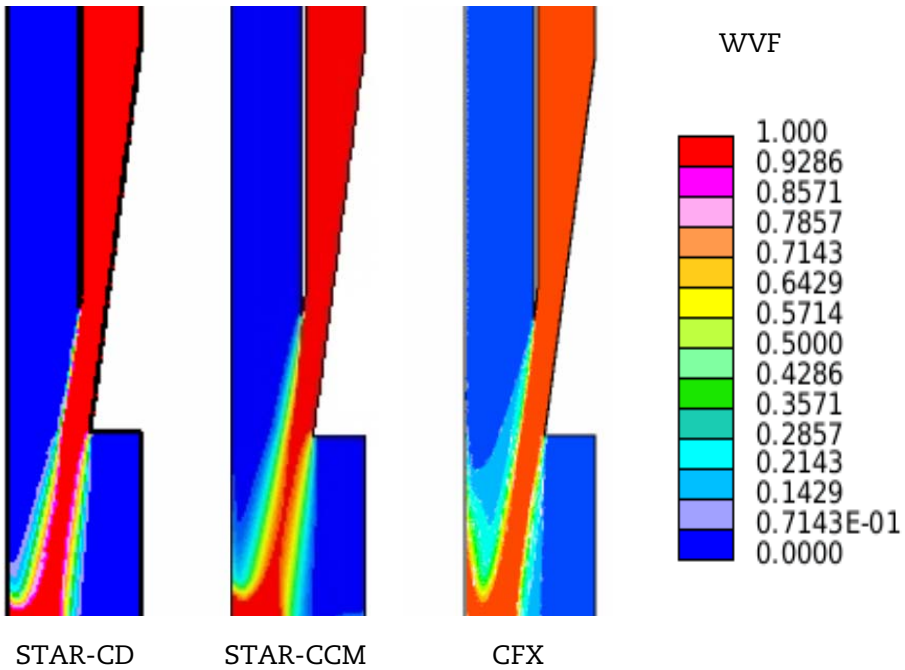

Acknowledgements

The work described in this paper was carried out in and supported by the FP6 EC Integrated Project EUROTRANS No. FI6W-CT-2004-516520.

References

[1] Annex I, EUROpean Research Programme for the TRANSmutation of High Level Nuclear Waste in an Accelerator Driven System, Project acronym: EUROTRANS, Contract no.: FI6W-CT-2004-516520, February (2005).

[2] Jeanmart, H., *et al*, *Investigation of the Impact of an Artificial Swirl on the Free Surface Stability of the Windowless Spallation Target in the XT-ADS*, EUROTRANS D4.12 (2008).

[3] Roelofs, F., *et al*., "Application of a Controlled Swirl in the XT-ADS Spallation Target", *Proc of ICAPP 2008*, Paper 8003, Anaheim, CA, USA (2008).

[4] Schuurmans, P., *et al*., "Design and Supporting R&D of the XT-ADS Spallation Target", *Ninth Information Exchange Meeting*, Nîmes, France, September (2006).

[5] Batta, A., Class, "A Numerical Investigations on Geometrical Designs of the Windowless XT ADS Spallation Target", *Proceedings of ICAPP*, Paper-Id 7479, Nice, France (2007).

[6] Tichelen, K. van, *et al*., "MYRRHA: Design of a Windowless Spallation Target for a Prototype Accelerator Driven System", *ICENES-2000*, Petten, Netherlands (2000).

[7] Roelofs, F., N.B. Siccama, S.M. Willemsen, "Development of an Euler-Euler Two-phase Model for Application in the Windowless XT-ADS Spallation Target Design", *Proceedings of ICAPP*, Paper 7092, Nice, France (2007).

[8] Batta, A., Class, "Free Surface Modeling and Simulation of the Water Experiment for the XT ADS Spallation Target", *Proceedings of ICAPP*, Paper-Id 8049, USA (2008).

Liquid-fuelled accelerator-driven transmutation system

Toshinobu Sasa, Kenji Nishihara, Takanori Sugawara, Hiroyuki Oigawa
Japan Atomic Energy Agency, Japan

Abstract

The management of radioactive waste is one of the important issues for sustainable nuclear energy production. To realise the nuclear fuel cycle based on MOX-fuelled LWR and FR, americium (Am) and curium (Cm) should be carefully treated because they may affect the soundness of nuclear fuels if they are commonly recovered and recycled with plutonium. On the other hand, disposition of Am and Cm will affect the design of the geological repository because of their long half-lives and radioactivity. A concept of accelerator-driven system using liquid molten-salt fuel is proposed for the effective transmutation of Am and Cm. In the concept, Am and Cm are separated from the spent fuel by the advanced aqueous reprocessing and converted to chloride molten salt fuel. With the adoption of such a liquid-type fuel, many defects on Am and Cm such as high radioactivity and heat release and chemical incompatibility can be overcome. The accelerator-driven system consists of a 10 MW-class cyclotron, tungsten disk spallation target and subcritical core. Molten salt fuel is reprocessed to separate fission products and adjusting the concentration of Am and Cm. Energy balance and subcriticality of the system is designed to recover overall electricity to drive system itself during the lifetime of the reactor. The concept of molten-salt-fuelled accelerator-driven system and dedicated fuel cycle will be introduced.

Introduction

Management of radioactive wastes from nuclear power plants is one of the important issues for sustainable nuclear power generation. To propose the way to reduce the environmental impact from disposal of high-level radioactive wastes and to improve the cost and space efficiency of geological disposal site, the long-term research and development programme for partitioning and transmutation (P&T) technology using accelerator-driven system [1] has been performed. In the concept of transmutation by a dedicated accelerator-driven system (ADS), minor actinides (neptunium, americium and curium) are separated by the four-group partitioning process and fabricated to the pellet nitride fuel. However, americium and curium and their daughter nuclides have some difficulties to handle these nuclides safely even in the P&T fuel cycle because of their high decay heat and radioactivity. These nuclides also give the chemical instability, namely the low vapour pressure of americium, which harms soundness of burn-up fuel pellet properties. In contrast, neptunium has similar chemical properties to uranium and plutonium and shows good compatibility not only in nitride fuel but also in oxide fuel. There are no significant difficulties to handle neptunium in a MOX fuel cycle.

To perform transmutation of minor actinides effectively, a fast fission reaction is desirable. However, because neutron capture reaction occurs simultaneously in a fast spectrum core, a large amount of minor actinides and high thermal output are required. Consequently, the currently proposed accelerator-driven transmutation systems must be connected to a high intensity proton linear accelerator.

Considering the above-mentioned characteristics of minor actinides and dedicated transmutation systems, we propose a liquid-fuelled ADS concept. There are two concepts for molten salt ADS, one reforms americium and curium into plutonium by neutron capture reaction and decay to reduce the burden in the fuel cycle. The other is dedicated system to burn minor actinides in a small closed fuel cycle. In this paper, outline of the both concepts of actinide reformer, neutronic performance including burn-up analysis and preliminary mass balance by introduction of the actinide reformer are described.

Outline of the system

Current LWR reprocessing process (PUREX process) aims at recovering uranium and plutonium from spent nuclear fuel. Through the process, americium and curium are easily separated from other actinides. However, to separate neptunium, whose chemical properties are close to plutonium, requires another recovering process within PUREX process. Because of the similarity of chemical and neutronic performance of neptunium and plutonium, it is not so difficult to treat them identically in the MOX fuel cycle and it is also effective for reduction of process, cost and secondary wastes.

The fuel cycle based on molten-salt-fuelled accelerator-driven system (ADS) concept is illustrated in Figure 1. When the ADS fuel cycle is adopted, neptunium in the spent fuel from power reactors is recovered and recycled with plutonium. Omission of neptunium separation process from current PUREX reprocessing process may give more cost effectiveness, safety and secondary waste reduction. From the reprocessing process, americium and curium are sent to the ADS cycle. At first, americium and curium are transformed to chloride molten-salt fuel. By using americium and curium as a molten salt fuel form, facilities such as fuel fabrication, storage, assembling/disassembling are not required. It is also needless to consider the engineering limitations of decay heat removal, linear power and chemical instability in solid fuel form. There also arise some demerits of liquid fuel: high radioactive nuclides spreads whole primary cooling circuit, risk of FP sedimentation formation and irradiation effect to chemical binding and so on. For these difficulties, system must be designed as simple as possible.

The chloride molten-salt may have limited compatibility with typical structural materials such as SUS316, SUS310S, Inconel 625 and Incoloy 825, fuel tank might be replaced at each burn-up cycle [2,3] to protect a fuel leakage accident by corrosion of structural materials.

For effective burning of molten-salt fuel by ADS, system composed of a 10 MW-class cyclotron, a tungsten spallation target and a molten-salt fuelled subcritical core. The engineering feasibility of the accelerator and the spallation target is in the range of the existing technology. In the viewpoint of neutronics, application of liquid fuel for subcritical system gives several advantages such as improved neutron economy, passive safety by fuel density effect, applicability of on-line adjustment of fuel composition. These neutronic characteristics are also useful to construct subcritical core. To compensate

Figure 1: Actinide reformer fuel cycle concept

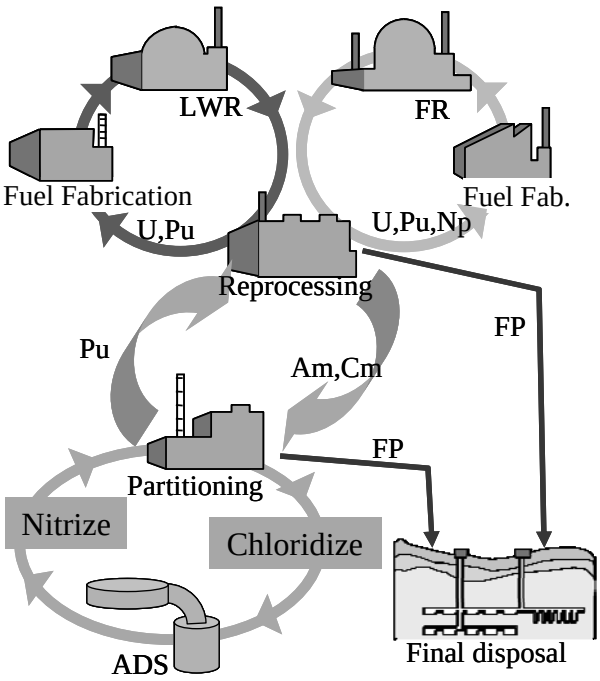

the demerit of liquid fuel, simple and small primary loop is considered. The power from fission reactions of actinides is recovered and used for electricity to operate its own accelerator. For reprocessing of spent molten-salt fuel, existing PUREX process and four group partitioning process, which is proved by laboratory scale, can be applied. By using four-group partitioning process together with PUREX process, spent fuel is roughly classified to minor actinides (mostly a remaining americium and curium), reformed plutonium and several fission product groups. The group containing MA is recycled in the actinide reformer cycle. In plutonium recovering case, recovered plutonium are returned to power reactor fuel cycle and used for power generation. Influences by inclusion of reformed plutonium into power reactor MOX fuel will be discussed at the following section.

Neutronic characteristics of system for plutonium recycling

Initial core configuration

To determine an optimum configuration of subcritical core dimensions and initial fuel composition, neutronic analysis of the subcritical core was performed. In the parametric survey to specify the core dimensions, the initial k-effective value is fixed around 0.98. It is also considered that the initial actinide inventory is set less than 2 tonnes to get high transmutation efficiency. Because of the rather high melting point of molten-salt, a spallation target is directly connected to the proton beam duct and is separated from a molten-salt fuel tank to reduce the coolant temperature of the spallation target in order to increase the structural strength of the beam window and apply water to coolant material. This spallation target configuration is useful to exchange the target without any fuel handling procedures. The radius of the spallation target is specified from a limitation of the proton beam current density, which is tentatively set to 20 $\mu A/cm^2$. Using these beam current density limitation and spallation target radius, maximum allowable proton beam power is set to 5 MW with proton energy of 800 MeV. Chloride molten-salt is loaded into the fuel region. The actinide-based molten salt [$(AmCm)Cl_3$] is mixed with 10% of lead-chloride [$PbCl_2$] to reduce the fission power density. Composition of actinides used in this calculation is 87.7% of Am and 12.3% of Cm, delivered from the standard PWR spent fuel. A stainless steel reflector is located around the fuel region to improve neutron economy and radiation shielding performance. The overall size of the subcritical core is about 120 cm diameter and 140 cm length. A two-dimensional cylindrical calculation model for the final core configuration is illustrated in Figure 2.

Figure 2: Neutronic analysis model

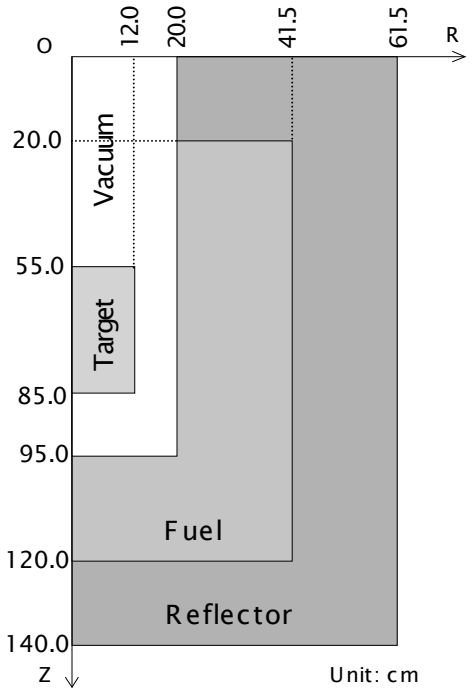

Table 1 summarises the analysis results obtained by using MCNPX-2.5 code [4] and JENDL-3.3 cross-section library [5]. An initial k-eff value of the subcritical core is determined around 0.98 with initial actinide inventory of 1 625 kg. Average power densities of the target region and the subcritical core region are 370 W/cm^3 and 380 W/cm^3, respectively. The power peaking factor, which usually gives rather higher value for subcritical system than for a critical reactor, has no limitation for liquid fuel. By the injection of rated proton beam power (800 MeV-5 MW), thermal output from subcritical core reaches around 170 MW. Figure 3 shows the average neutron energy spectrum in the subcritical core region. Because of the application of chloride molten-salt to the fuel, a hard neutron energy spectrum similar to that of fast reactor is obtained.

Table 1: Neutronic analysis results for initial core

Target radius/height [cm]	12.0/30.0
Target material/coolant	Tungsten/water
Fuel zone radius/height [cm]	41.5/100
Fuel density [g/cm^3]	5.70
Fuel fraction ($MACl_3$:$PbCl_2$)	90:10
Proton energy/power [MeV, MW]	800/5
Initial k-effective	0.9802
Thermal output [MW]	170
Av. power density (target) [W/cm^3]	368
Av. power density (core) [W/cm^3]	380
Initial MA loading [kg]	1 625

Burn-up analysis

Using the initial core configuration mentioned in the previous section, burn-up analysis was performed. To apply the simulation of on-line refuelling and fuel concentration adjustment for the burn-up calculation, ABC-SC code system (SLAROM-CITATION-ORIGEN) [6] and JENDL-3.3 based cross-section library were used. Decontamination factor (DF) of actinides (U, Np, Pu) and fission products (FP)

Figure 3: Average neutron energy spectrum

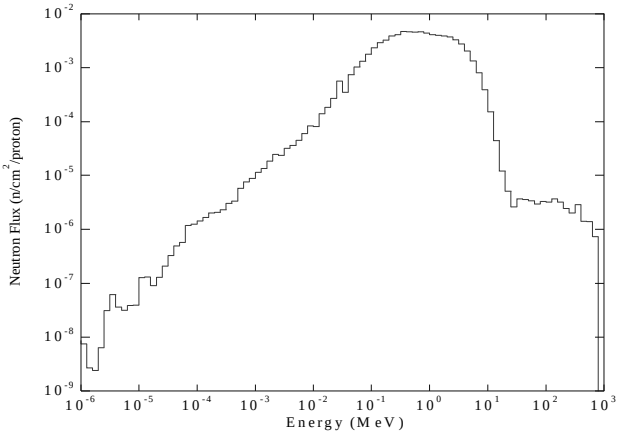

excluding rare earth elements were specified to 100 (99% recovery). DF for rare earth is assumed to be 2 (50% recovery). For this preliminary analysis, burn-up period is set to 300 EFPD (equivalent full power day) with 65 days cooling period.

Figure 4 summarises the removed nuclides amount for each burn-up cycle. From the contents of extracted nuclides, system reaches the equilibrium burn-up after the seventh cycle. By the definition of these analysis conditions, about 100 kg of americium and curium can be fed to one ADS annually at equilibrium cycle and then, 50.8 kg of FP and 42.3 kg of reformed actinides (plutonium and neptunium) are recovered simultaneously. To support the Rokkasho-scale reprocessing plant (430 kg of americium and curium are annually recovered), for example, five units of actinide reformers are required. Using five units of ADS, 500 kg of americium and curium can be loaded to ADS and then, about 212 kg of plutonium and neptunium are recovered and it can be recycled as a fuel for power generation.

Figure 4: Removed nuclides within each burn-up

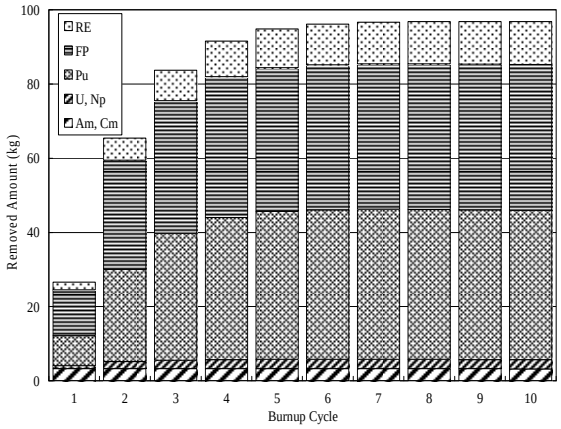

Influence by recycle of recovered plutonium

In the result of previous burn-up analysis, the isotope composition ratio of recovered plutonium is 57% of ^{238}Pu, 30% of ^{240}Pu and 13% of ^{242}Pu. In this section, engineering availability of recovered plutonium in power reactor fuel cycle is discussed.

Table 2 summarises the typical plutonium concentration of MOX fuels considered for both LWR and FR [7]. The table indicates that the FR-MOX with MA recycle case, which loads about 5% of MA in MOX fuel, gives higher concentrations of ^{238}Pu and ^{241}Am. In the cases of the molten salt ADS cycle, Am and Cm are sent to ADS and reformed to plutonium that is to be loaded into FR. Using the results

Table 2: Isotopic composition of plutonium in various reactor concepts

Nuclides (tonnes/year)	LWR-MOX fuel	FR-MOX fuel without MA recycle	FR-MOX fuel with MA recycle
Pu loading (incl. MA)	4.6%	19.7%	21.7%
^{238}Pu	0.19	0.24	0.70
^{239}Pu	3.85	26.07	26.40
^{240}Pu	1.12	12.50	13.21
^{241}Pu	1.15	1.19	1.21
^{242}Pu	0.66	1.23	1.65
^{241}Am	0.06	0.29	1.52
Others	0.0	0.0	1.08

of reformed plutonium amount, plutonium loading amount in LWR-MOX case are quite small. In the case of FR-MOX without MA recycle, it is also similar to LWR-MOX case. In contrast, FR-MOX with MA recycle case, which transmutes all MA in their fuel cycle and does not require the partitioning and transmutation concept, increasing ratio of ^{238}Pu and overall Pu gives much higher values than the other cases.

Figure 5 shows the comparison of fuel decay heat. Applying molten salt ADS for LWR and FR without MA recycle case, decay heat is not significantly increased. In contrast, FR-MOX with MA recycle case, MA is recycled together with plutonium in power reactor, shows large influences caused by ^{244}Cm. A similar characteristic arises for background neutron emission. In the viewpoint of power generation cost, it is desirable to handle more simple fuel like FR-MOX without MA recycle case. By applying molten salt ADS cycle, ^{244}Cm is confined in the ADS cycle and reformed plutonium gives rather small impact to the power reactor fuels.

Figure 5: Comparison of released decay heat

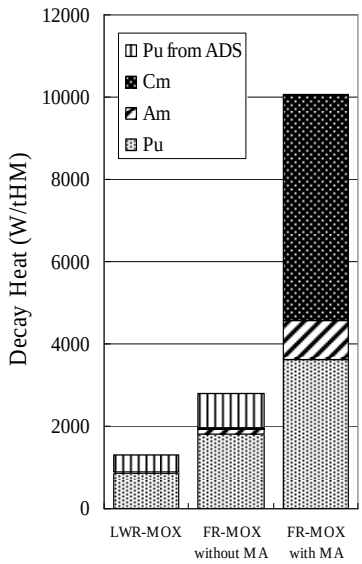

Neutronic characteristics for dedicated transmutation system

Initial core configuration

The first concept of liquid fuel ADS aims at reforming the harmful actinides, americium and curium to usable actinide, plutonium. However, there still exists rather small impact on commercial nuclear fuels and requires complicated process to separate plutonium from actinides in spent molten salt fuel.

If the molten salt ADS cycle is completely separated from power generation fuel cycle as double-strata fuel cycle, there is no significant impact to power generation cycle. In this chapter, dedicated molten salt fuel transmutation system focused on transmutation of americium and curium is considered.

Because the remaining actinides in spent molten-salt fuel can be commonly extracted in this case, the dry reprocessing method can be applicable for reprocessing of ADS fuel. The possibility of combination with dry-reprocessing will be discussed at the latter section.

One of the merits of the liquid fuel is flexible reactivity control through adjustment of the fuel concentration. This capability is more desirable especially for ADS which does not have reactivity control devices such as control rod. By adjusting subcritical level from time to time by on-line reprocessing, engineering requirement and construction cost of the accelerator can be reduced. In ordinary case of actinide burner, fissile material for fast system, plutonium, is produced at early burn-up cycles and at the equilibrium condition, k-eff values reaches higher value than that of early burn-up stages without any compensation. In the case of solid fuel, there are limited methods to control reactivity and then, in JAEA, plutonium is added into virgin fuel to compensate burn-up reactivity increase. For the effective transmutation of actinides, burn-up analysis with on-line reprocessing was applied.

Figure 6 shows the two-dimensional analysis model. The common specification of previously mentioned spallation target was applied. Burn-up analysis was performed with analysis conditions of 170 MW of rated power, 30 day period between batched on-line reprocessing. In the fuel reprocessing process, all fission products are separated and same amount of Am and Cm is added. At the reprocessing, two DF (20 as a realistic case and 10 000 for optimum case) were considered.

Figure 6: Two-dimensional analysis model

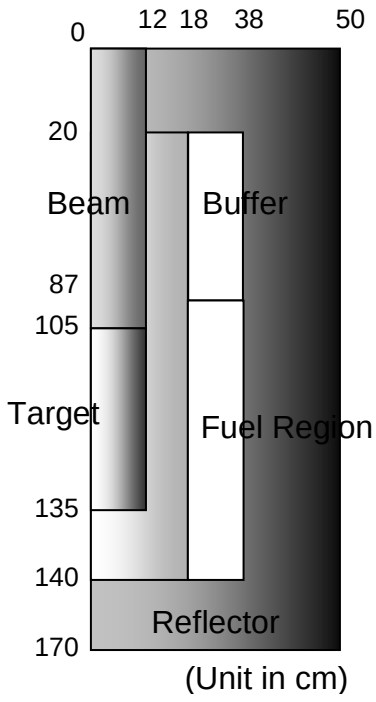

Figure 7 indicates a burn-up trend of k-eff with/without on-line reprocessing. The burn-up reactivity change gives drastically small values by adopting on-line reprocessing. The highest k-eff is tentatively set around 0.98 but it can be changed by trade off with actinide loading amount related to reprocessing capacity. In the case with on-line reprocessing, overall reactivity change during system lifetime is limited within the 1%Δk. The extra power for the accelerator for rated operation is only 30% and is corresponds to 1.5 MW of proton beam power. It is also seen that difference of DF does not give large differences to the system even the high DF case gives rather large value at BOC by the difference of remaining amount of FP in the fuel and rather small values of burn-up reactivity change.

Figure 7: Burn-up reactivity change

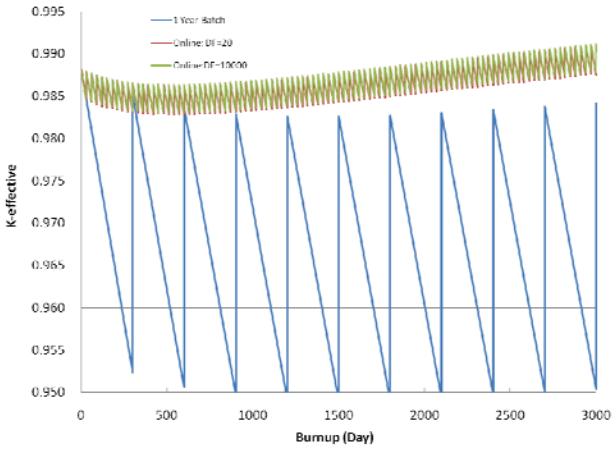

Reprocessing of molten salt

In this study, the system adopts the batch operation. From the neutronic analysis result, initial fuel loading is about 1 460 kg (1 300 kg of Am and 180 kg of Cm) in the core region. The burn-up fuel corresponds to one-year burn-up is 1 389 kg of actinides (Pu: 11 kg, Am: 1 181 kg, Cm: 197 kg and others) and 58 kg of FP. At the equilibrium cycle, about 670 kg of MA (405 kg of Am, 106 kg of Cm, and 147 kg of Pu) are stored in the core region annually. These actinides are transformed into 551 kg of MA (355 kg of Am, 107 kg of Cm, 81 kg of Pu, and others) and 56 kg of FP. To load about 430 kg of Am and Cm, eight units are required and about 13 tonnes of actinides, with consideration of the inventory in the piping and heat exchanger, must be reprocessed at the equilibrium cycle annually.

The design study for a dry reprocessing plant that can accept the high level waste from Rokkasho-scale reprocessing plant was performed at CRIEPI [8]. In the report, the plant was designed to accept about 25 mole of MA per batch, four batches per day, and 200 days operation per year. About 200 litres of chloride salt (LiCl-KCl) are used per batch. In such case, the annual amount of processed MA is about 5 tonnes and then, at least two processing lines are required for dedicated molten salt ADS plants. However, in this case, no processes are required for fuel disassembling, cutting, fabrication and re-assembling. Since MA is already chlorinated, the denitration and chlorination before the application of extraction processes can be also neglected. From the cost estimation of the plant, the cost of equipments decreases about 30% by eliminating these processes except for a Cd recovering process and MA re-chlorination process for recycling recovered actinides to molten-salt ADS.

Conclusion

To improve the safety, cost efficiency and waste reduction, two liquid-fuelled ADS concepts are proposed. The liquid-fuelled ADS aims at extracting americium and curium from current PUREX process based fuel cycle and reforms them into plutonium which has more chemical stability and safety in MOX fuel. The parameter of the components for liquid-fuelled ADS is set to the feasible values from the viewpoint of current engineering experiences. By adding these concepts to the current power generation cycle, fuels for power reactor can keep conventional fuel composition. It is useful to improve safety and cost efficiency of electric power generation.

From the preliminary analysis results, there is a possibility to make actinide reformer system by self-standing systems to reduce the environmental impacts by minor actinides. It is also found that dedicated actinide burner system reflecting liquid-fuelled ADS concepts also gives fairly good transmutation performance. Adoption of on-line reprocessing by batch manner, which requires not so high DF value, the reprocessing process line can be shared by the several numbers of modular-type molten-salt ADS. The construction cost of such on-line reprocessing process for highly radioactive nuclides will not so large compared with commercial reprocessing plant.

References

[1] Sasa, T., "Research Activities for Accelerator-driven Transmutation System at JAERI", *Progress in Nuclear Energy*, 47, pp. 314-326 (2005).

[2] Shiina, Y., Y. Kuriki, *Compatibility Tests Between Molten Salts and Metal Materials (I)*, JAERI-Tech 2002-065 (2002).

[3] Shiina, Y., Y. Kuriki, *Compatibility Tests Between Molten Salts and Metal Materials (II)*, JAERI-Tech 2003-070 (2003).

[4] McKinny, G.W., J.W. Durkee, J.S. Hendricks, M.R. James, D.B. Polowitz, L.S. Waters, F.X. Gallmeier, *MCNPX Overview*, LA-UR-06-206 (2006).

[5] Shibata, K., *Descriptive Data of JENDL-3.3*, JAERI-Data/Code 2002-026 (2003).

[6] Gunji, Y., T. Mukaiyama, H. Takano, T. Takizuka, *A Computer Code System for Actinide Transmutation Calculation in Fast Reactors – ABC-SC*, JAERI-M 92-032 (1992) [in Japanese].

[7] Nishihara, K., H. Oigawa, *Analysis on Introduction Scenario of Partitioning and Transmutation Cycle and its Benefit Based on Mass-balance Calculation of Actinides*, JAEA-Research 2006-081 (2006) [in Japanese].

[8] Kinoshita, K., M. Kurata, K. Uozumi, T. Inoue, "Estimation of Material Balance in Pyrometallurgical Partitioning Process for TRUs From HLLW", *Proc. 5th International Information Exchange Meeting on Actinide and Fission Product Partitioning and Transmutation* (1999).

Investigation of beam window structure for accelerator-driven system

Takanori Sugawara, Kazuhiko Suzuki, Kenji Nishihara,
Toshinobu Sasa, Yuji Kurata, Kenji Kikuchi, Hiroyuki Oigawa
Japan Atomic Energy Agency, Japan

Abstract

The investigations of the beam window – one of the most critical components for the accelerator-driven system (ADS) – were performed by Finite Element Analysis (FEA). Before applying the FEA, the simple assessment using a hemispherical model based on the "design by analysis" approach for nuclear power plant was carried out, and it was found that the buckling failure was the most severe failure mode for the beam window. Hence, the shape and the thickness of the beam window were optimised to prevent the buckling failure.

In the buckling analyses, the parametric survey for the thickness of the ellipse model was carried out by using the Finite Element Method (FEM) code (FINAS). The buckling analyses with initial imperfections were also performed to identify the level of the factor of safety (FS).

The results showed that a FS of 3 was conservative enough to ensure the integrity of the beam window. It was also shown that the ellipse shape concepts with the thickness of 2.0-2.4 mm at the top and the thickness of 2.0-4.0 mm at the transient part were acceptable under the current ADS design parameters. It was also confirmed that the structural robustness would be kept when the uniform change of the beam window thickness would occur due to the corrosion.

Introduction

To reduce the burden for the geological disposal of the high level waste (HLW), an accelerator-driven system (ADS) has been studied to transmute minor actinide (MA) included in the HLW. The ADS investigated in Japan Atomic Energy Agency (JAEA) is a lead-bismuth eutectic (LBE) cooled subcritical system [1]. A high intensity proton accelerator with 1.5 GeV beam energy and a subcritical core with 800 MW thermal power are designed to transmute 250 kg MA per year in the system. Figure 1 shows a conceptual diagram of the ADS.

Figure 1: Concept of LBE-cooled ADS

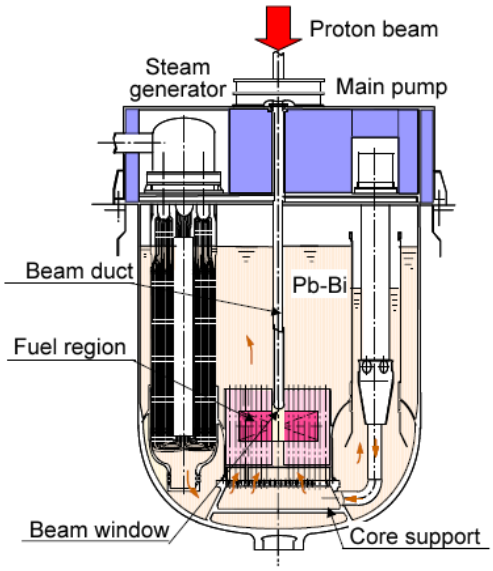

Since the ADS is a hybrid system of an accelerator and a nuclear reactor, there are many technical issues to be solved for the accelerator, the LBE as a coolant and a target and the subcritical core. Especially, the investigation of the beam window which is the boundary between the accelerator and the subcritical core is one of the most important issues in the ADS R&D. The beam window will be used in the following severe conditions: *i)* external pressure by LBE (accelerator side is vacuum); *ii)* heat generation by the proton beam; *iii)* creep deformation by high temperature; *iv)* corrosion by LBE; *v)* irradiation damage by neutrons and protons. Detail investigations for all of these conditions have not been carried out.

In this study, the investigations of the beam window to ensure the integrity in the unirradiated condition were performed by using Finite Element Analysis (FEA). In the previous study, the simple assessment using a hemi-spherical model based on the "design by analysis" approach for nuclear power plant was carried out [2]. From this assessment, it was found that the buckling failure was the most severe failure mode for the JAEA's beam window. Hence, the shape and the thickness of the beam window were optimised to prevent the buckling failure. Before this parametric survey, the buckling analyses with initial imperfections were performed to identify the level of the factor of safety (FS).

Calculation method

Calculation code and model

In this study, the FEA for the beam window was performed by the FINAS code [3] which is a finite element non-linear structural analysis system developed by JAEA and CTC corporation. Since this code was developed for structural analyses for a fast reactor mainly, it is able to treat not only general structural analyses but also effects for the creep or the irradiation by neutrons. Elastic-plastic large deformation buckling calculation without the effects of the creep and the irradiation was performed in this study.

The ellipse-shape model [4] shown in Figure 2 was employed as the reference model in the chapter of "Acceptable Factor of Safety for Beam Window". In the chapter of "Investigation for Feasible Beam Window Concept", a generalised model based on the reference model was treated for the parametric survey. For both investigations, Mod. 9Cr-1Mo steel was selected as the material.

Figure 2: Ellipse shape concept

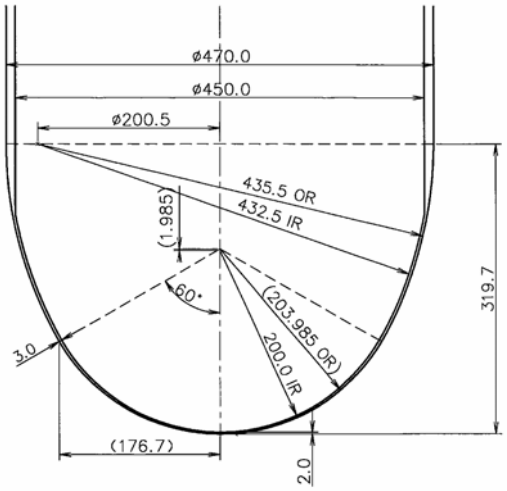

Temperature calculation

The buckling failure occurs by both the primary stress (ex. external pressure) and the secondary stress (ex. thermal stress). Detail temperature distributions were calculated and employed in the structure analyses since it was found that the main cause of the buckling failure was the thermal stress due to the proton beam in the previous studies [2,4].

The temperature distribution was calculated as a function for a thickness, a heat density and a coolant temperature. The temperature T_M at the thickness position t_M ($0 \le t_M \le t_0$, see Figure 3) was calculated by following equations:

$$T_0 = T_F(\theta) + Q_0(r) \cdot t_0 / \alpha$$

$$T_M = T_0 + Q_0(r) \cdot \left(\frac{t_0^2}{2} \right) \left\{ 1 - \left(\frac{t_M}{t_0} \right)^2 \right\} \Big/ \lambda$$

where T_0 is the temperature at an outer surface, $T_F(\theta)$ is the temperature of the coolant, t_0 is the thickness, $Q_0(r)$ is the heat density, α is the heat transfer coefficient between the coolant and the beam window (= 3.95 W/cm²/°C) and λ is the thermal conductivity for the beam window(= 0.27 W/cm/°C).

The heat transfer coefficient α was the average value calculated by the computational fluid dynamics (CFD) analysis, which was performed by STAR-CD [5] in Ref. [4]. The coolant temperature distribution $T_F(\theta)$ calculated by STAR-CD in Ref. [4] were also used in this survey. Although both the heat transfer coefficient and the coolant temperature distribution varied by changing the thickness and the shape of the beam window precisely, these values were treated as the constants in this study.

The heat density distribution Q0(r) was calculated by the cross-section data for heat generation [6]. The flux distribution above 20 MeV was calculated by PHITS code [7] which is a general-purpose particles and heavy ion transport Monte Carlo code, and the flux distribution below 20 MeV was calculated by TWODANT code [8] which is a deterministic neutron transport calculation code. Figure 4 shows the heat density distribution for the case of 1.5 GeV-20 mA proton beam. Temperature distributions calculated by this heat density distribution are presented in Figure 5. A large temperature difference between the inner and outer surface is observed at the top of the beam window.

Figure 3: Expression of variables for temperature calculation

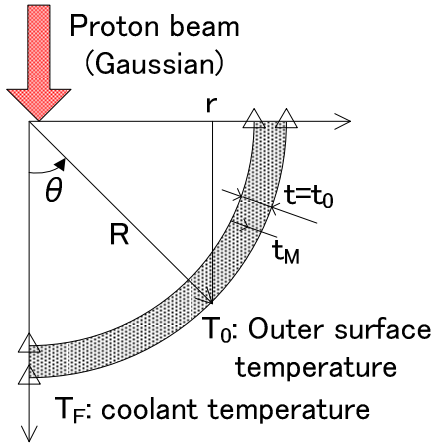

Figure 4: Heat density distribution

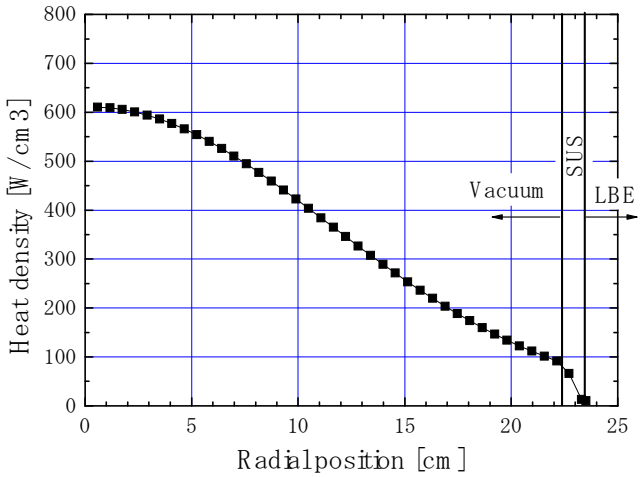

Figure 5: Temperature distribution

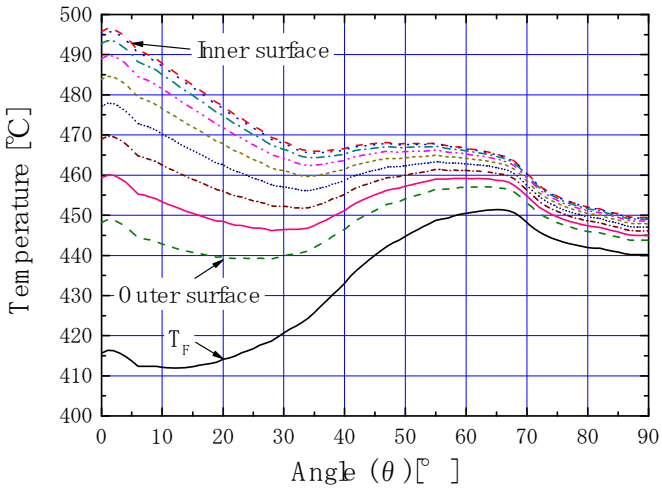

Acceptable factor of safety for beam window

For the level of the factor of safety (FS) for the beam window, it is required to set it with consideration for a synergistic effect between a heat strain by the proton beam and an initial imperfection. However, the previous investigation employed FS of 4 which is the value for the spherical shell [4] since there was no detailed knowledge for the synergistic effect.

ASME B&PV Code Section III Code Case N-284 (ASME N-284) [9] is known as the assessment procedure for the buckling with a reasonable FS which is based on the design by analysis. Calculations to get the knowledge for the synergistic effect and investigations based on ASME N-284 were performed to set an acceptable and reasonable FS for the beam window.

Calculation case

Buckling analyses with initial imperfections were carried out. The initial imperfections were set with consideration for fabrication, transportation, installation and ageing (Table 1 and Figure 6). The cases of (b) and (e) were based on the typical buckling modes shown in Figure 7. Imperfection amounts (Table 1) employed in these analyses were much larger than actual accuracies for the fabrication, the transportation, the installation and the aging because it was important to comprehend maximum effects to the buckling.

Table 1: Calculation cases for buckling analysis with initial imperfection

Case	Imperfection amount (δ) [mm]	Calculation model
(a) Imperfection for shape at the top	±2, ±5	2-dimensional
(b) Imperfection for shape at the top (the lowest order mode)	±1, 2	2-dimensional
(c) Imperfection for thickness at the top	±0.1, 0.2	2-dimensional
(d) Imperfection for circumferential direction of cylinder	5, 10	3-dimensional
(e) Imperfection for circumferential direction of cylinder with 10 waves	1, 2	3-dimensional

Figure 6: Calculation cases for buckling analysis with initial imperfection

For cases (d) and (e), views from the proton beam incident direction are presented

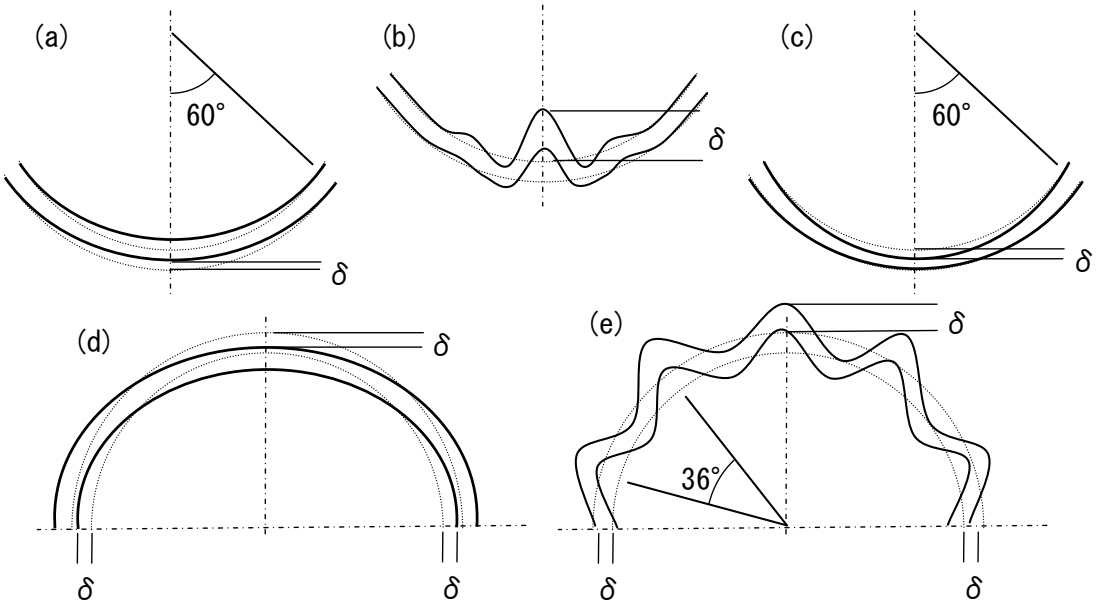

Imperfection for shape at the top

Figure 6(a) presents a concept with the imperfection for the shape at the top. It is supposed that this imperfection would occur at the time of the beam window transportation and installation. This calculation was performed with two-dimensional calculation model.

Imperfection for shape at the top (the lowest order mode)

A concept whose shape at the top is transformed to the buckling mode shown in Figure 7(a) is illustrated in Figure 6(b). It is supposed that this imperfection would not occur at the time of fabrication, the transportation and the installation, but would occur at the time the buckling failure happens. This calculation was also performed with two-dimensional calculation model.

Imperfection for thickness at the top

Figure 6(c) shows a concept with the imperfection for the thickness at the top. This imperfection would occur at the time of the fabrication and the aging due to the effect of the creep or the corrosion by LBE. Two-dimensional calculation model was also employed in this case.

Imperfection for circumferential direction of cylinder

A concept with the imperfection for circumferential direction of the cylinder is shown in Figure 6(d). It is also assumed that this imperfection would occur at the time of the transportation and the installation. This calculation was performed with three-dimensional calculation model since the two-dimensional calculation model was unable to treat this deformation.

Imperfection for circumferential direction of cylinder with 10 waves

Figure 6(e) illustrates a concept with the imperfection for circumferential direction of the cylinder with 10 waves. Although it is supposed that there is little possibility to occur this imperfection, this case is one of the typical buckling modes [Figure 7(b)]. Three-dimensional calculation model was also used for this case.

Figure 7: Typical buckling mode

(a) The lowest order mode

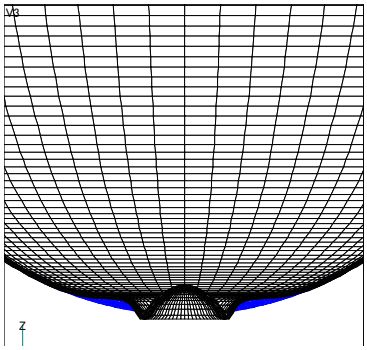

(b) For circumferential direction of cylinder with 10 waves

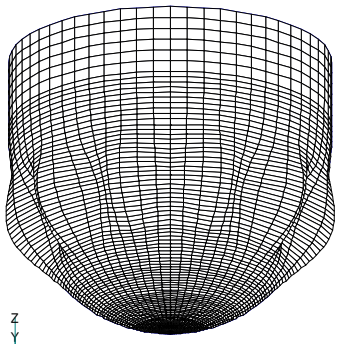

Calculation result for buckling analysis with initial imperfection

Calculation results for all cases are summarised in Table 2. In this table, “REF” means the calculation case without initial imperfection. Relative values of the buckling pressure against each REF case are also in this table. Because of the difference of the calculation model (2-D or 3-D), buckling pressures for REF between the 2-D model cases [(a), (b) and (c)] and the 3-D model cases [(d) and (e)] had slight differences about 2%.

Although initial imperfections which were much larger than actual accuracies were treated in these analyses, the maximum decrease of the buckling pressure was about 7% in the case (e). This result presents that the effect of the initial imperfection to the buckling pressure is very small for the beam window investigated in JAEA.

Discussion

The FS is generally defined as a ratio of the allowable stress to the design strength which is determined by a material property, a loading condition and so on. Though the value should be determined with consideration for various uncertainties such as an uncertainty of modeling or that of loading, it is determined based on empirical knowledge in many situations. In ASME N-284, FS of 2 is determined by performing analysis which is considering the uncertainty of the structure. Since the analyses with the initial imperfection discussed above corresponded to the analysis considering the uncertainty of the structure, the integrity of the beam window would be ensured if FS of 2 was ensured in the analyses.

Since the nominal external pressure for the beam window was 0.8 MPa, a design external pressure was set to 1.0 MPa which included a change of the external pressure or a measuring error. The FS is defined as (buckling pressure)/(design external pressure) in this case. From Table 2, it is found that the FS values for all cases are larger than 2 although the initial imperfections which were much larger than the actual accuracies were employed. So, the integrity of the beam window would be ensured with FS of 2 and with the actual accuracies for the fabrication, the transportation and the installation. For the FS value to use the assessment in this paper, however, more conservative value 3 was employed. This consideration includes differences between 2-D and 3-D calculation models (about 2%) or mesh structures (about 10% [2]).

Table 2: Calculation results for buckling analysis with initial imperfection

Case	Imperfection amount (δ) [mm]	Buckling pressure [MPa]	Relative value of buckling pressure (per each REF)	Buckling position
(a)	REF	3.85*1	1.00	Top part
	-2	3.70	0.96	Top part
	-5	3.70	0.96	Top part
	+2	3.87	1.01	Top part
	+5	4.16	1.08	Top part
(b)	REF	3.85*1	1.00	Top part
	-1	3.75	0.97	Top part
	-2	3.76	0.98	Top part
	+1	4.05	1.05	Top part
	+2	4.05	1.05	Top part
(c)	REF	3.85*1	1.00	Top part
	-0.1	3.80	0.99	Top part
	-0.2	3.76	0.98	Top part
	+0.1	3.80	0.99	Top part
	+0.2	3.84	1.00	Top part
(d)	REF	3.92*1	1.00	Top part
	5	3.77	0.96	Near top part
	10	3.68	0.94	Near top part
(e)	REF	3.92*1	1.00	Top part
	1	3.80	0.97	Transient part
	2	3.65	**0.93**	Transient part

*1: Because of the difference of the calculation model [(a), (b) and (c) are 2-D, (d) and (e) are 3-D].

Investigation for feasible beam window concept

Various factors such as the power of the proton beam or the depth position of the beam window relate to the buckling failure. The shape of the beam window is also one of the most important factors for the buckling failure and was focused in this study. The previous study has showed that simple hemispherical model is unable to be employed as the beam window for the JAEA's ADS because it has the possibility to cause the buckling failure [2], so the ellipse shape concept has been employed as the reference model. In this chapter, the parametric survey for the thickness of the beam window was carried out to create feasible beam window concepts to prevent the buckling failure.

Calculation condition

The generalised calculation model shown in Figure 8 was employed in the parametric survey. The generalised calculation model is an ellipse model which consists of a top part, a transient part and a cylinder part. Inner or outer surfaces of the top and transient parts are expressed as mathematical formulas and are connected at θ_f=60° smoothly. In this survey, t_1, t_2 and t_3 which were the thicknesses at the top, $\theta_f = 60°$, and a connection between the transient and cylinder parts were treated as parameters ($t_1 \le t_2 \le t_3$). The inner radius of the top part ($r_{1,i}$) and the radiuses for the cylinder part ($r_{3,I}$, $r_{3,o}$) were given the constant values (Figure 8).

Figure 8: Generalised calculation model

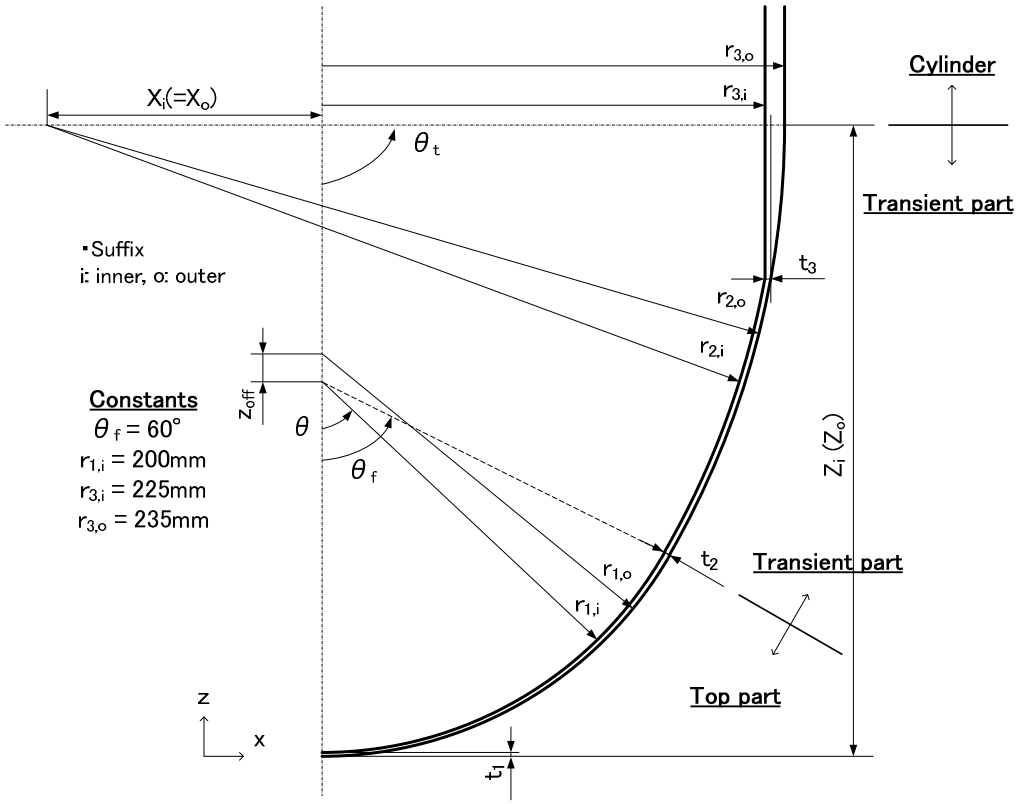

The parametric survey for $1.0 \le t_1 \le 3.0$ mm, $2.0 \le t_2 \le 5.0$ mm and $2.0 \le t_3 \le 5.0$ mm was performed with the condition $t_1 \le t_2 \le t_3$. In this survey, temperature distributions were calculated with consideration for the change of the thickness by the equations mentioned above.

Calculation result

Figure 9 presents results for the parametric survey. For the thickness t_3, two calculation cases were performed: t_1/t_2 = 2.0/3. and 2.0/2.0 mm. From Figure 9(a), it was observed that there were no changes for the buckling pressure by changing the thickness t_3. On the other hand, these results show that the change of the thickness t_2 has the possibility to change the buckling pressure.

It was also found that the buckling pressures for all cases were less than the previous result (3.85 MPa for 2-D model). This is because the fine mesh structure was employed in this survey to perform detailed investigation. The number of elements was 13 408 in this survey and that in the previous analysis was 664 (2-D model) for the reduction of the computational time. As mentioned above, the difference of the mesh structure causes the difference of the buckling pressure about 10%. In this survey, the difference of the buckling pressure against the previous result was about 9%.

Figure 9: Results of parametric survey

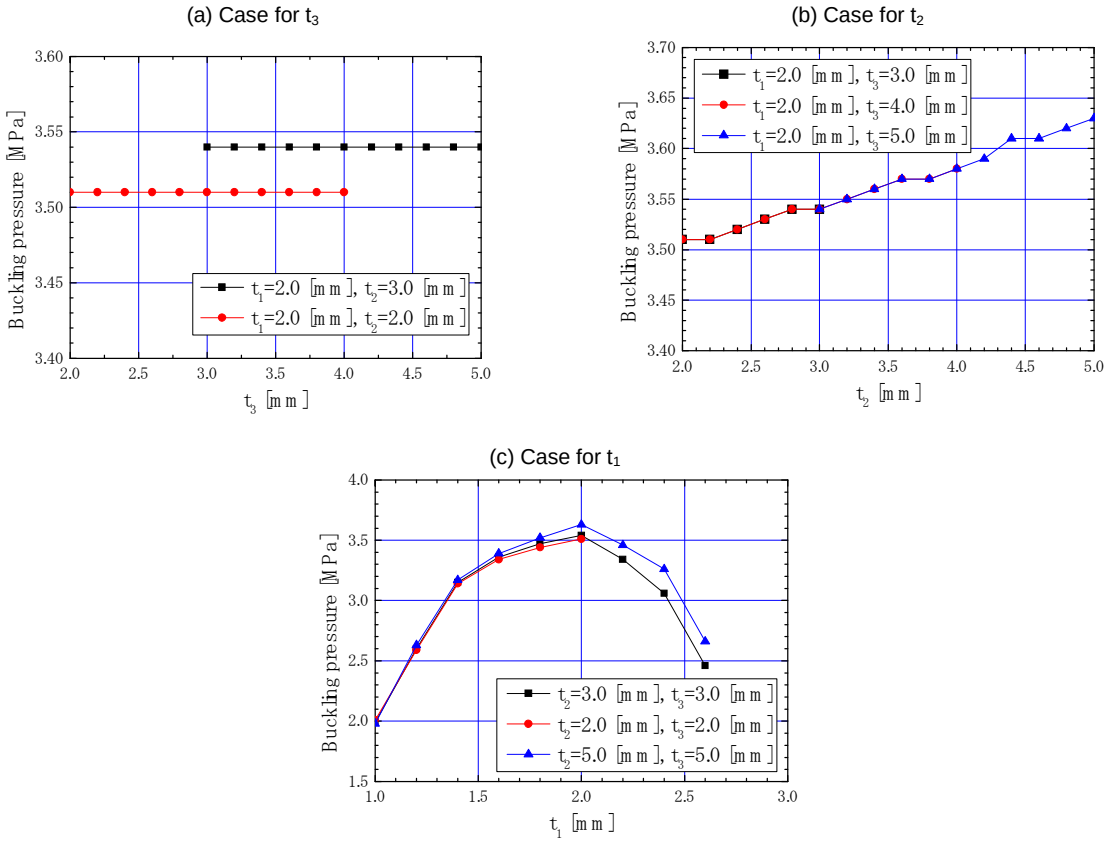

The results of the parametric survey for the thickness t_2 are illustrated in Figure 9(b). Three calculation cases, t_1/t_3 = 2.0/3.0, 2.0/4.0 and 2.0/5.0 mm were carried out. It was found that the buckling pressure was increased as the thickness t_2 was increased. The buckling pressure generally increases by the increase of the thickness, if the thermal stress does not increase widely. Since the heat density at the thickness t_2 was relatively low (about 200 W/cm³), it was supposed that the effect of the increase of the thermal stress was small in this case.

The results for the thickness t_1 are illustrated in Figure 9(c). Three calculation cases, t_2/t_3 = 3.0/3.0, 2.0/2.0 and 5.0/5.0 mm were performed. The results showed that the buckling pressure with t_1 = 2.0 mm was the largest in all cases. The decrease of the thickness from t_1 = 2.0 mm causes the decrease of the structural strength. Meanwhile, the increase of the thickness from t_1 = 2.0 mm causes the increase of the thermal stress and the buckling pressure decreases.

Discussion

Table 3 summarises the main results. Although the buckling pressure for the case $t_1/t_2/t_3$ = 2.0/5.0/5.0 was the largest in this survey, this case was not appropriate since the other parameters were also the largest and especially, the maximum strain was almost double against other cases.

From Figure 9(c) and Table 3, it was observed that the ellipse shape concepts with the thickness of 2.0-2.4 mm at the top (t_1) and the thickness of 2.0-4.0 mm at the transient part (t_2) were acceptable by the criteria FS of 3 and the design external pressure 1.0 MPa. Even though the concepts with the thickness of 1.4-1.8 mm at the top part satisfied the criteria in Figure 9(c), these were not conservative from the viewpoint of the corrosion by LBE and the creep deformation. Table 4 summaries the detail parameters for main concepts.

Table 3: Summary for parametric survey

Case[*1]	Max. temperature [°C]	Max. temperature difference [°C]	Max. stress [MPa] [*2]	Max. thermal stress [MPa] [*2]	Max. strain [mm/mm] [*3]	Buckling pressure [MPa]
2.0/2.0/2.0	496	47.6	107	98.9	5.14×10^{-4}	3.54
2.0/3.0/3.0	496	47.6	105	98.1	5.48×10^{-4}	3.54
2.0/4.0/4.0	503	55.4	103	104	6.48×10^{-4}	3.58
2.0/5.0/5.0	536	85.0	131	144	1.22×10^{-3}	3.63

*1: $t_1/t_2/t_3$ [mm].

*2: Von Mises stress.

*3: Total value for elastic strain, plastic strain and thermal strain.

Table 4: Summary for each model

Parameter[*1]	2.0/2.0/2.0[*2]	2.0/3.0/3.0[*2]	2.0/4.0/4.0[*2]	2.4/3.0/3.0[*2]
t_1	2.0	2.0	2.0	2.4
t_2	2.0	3.0	4.0	3.0
t_3	2.0	3.0	4.0	3.0
$r_{1,i}$	200.0	200.0	200.0	200.0
$r_{2,i}$	479.5	490.9	503.0	490.4
$r_{3,i}$	225.0	225.0	225.0	225.0
$r_{1,o}$	202.0	204.0	205.9	203.6
$r_{2,o}$	481.5	493.9	507.0	493.4
$r_{3,o}$	235.0	235.0	235.0	235.0
θ_f [degree]	60.0	60.0	60.0	60.0
X_i (= X_o)	-246.5	-258.9	-272.0	-258.4
Z_i	333.9	334.9	336.1	335.2
Z_o	333.9	335.0	336.2	335.2
z_{off}	0.000	1.985	3.941	1.195
Buckling pressure [MPa]	**3.51**	**3.54**	**3.58**	**3.06**

*1: Unit except θ_f and buckling pressure is [mm].

*2: $t_1/t_2/t_3$ [mm].

Corrosion tests for various steels were conducted in LBE [10] and results for Mod. 9Cr-1Mo steel were summarised in Table 5. The corrosion tests were performed for 3 000 h under the condition of high or low oxygen concentration and 450°C or 550°C. In Table 5, corrosion depths after 600 days ADS operation which were simply extrapolated by the corrosion test results were also presented. Based on these data, it was assumed that the maximum decrease of the thickness of the beam window would be about 0.24 mm in 550°C with the low oxygen concentration case. Even if the thickness of the beam window decreases uniformly from 2.0 mm to 1.76 mm by the corrosion, the results shown in Figure 9(c) indicates that the integrity of the beam window will be ensured. The concept with the thickness of 2.4 mm at the top will be a robust concept since its buckling pressure will increase by the decrease of the thickness due to the corrosion.

Table 5: Corrosion depth for Mod. 9Cr-1Mo in LBE [10]

Case	Oxygen concentration [wt.%]	Corrosion depth [μm/3 000 h]	Corrosion depth [mm/600 days]
450°C HO	3×10^{-4}	8.4	0.040
550°C HO	1×10^{-3}	14	0.067
450°C LO	5×10^{-8}	4.0	0.019
550°C LO	3×10^{-9}	50	0.240

HO – high oxygen concentration, LO – low oxygen concentration.

Conclusion

The investigations to create the feasible beam window concept were performed for the unirradiated condition. To identify the level of the factor of safety (FS) for the beam window, the buckling analyses with initial imperfections were carried out and discussed based on ASME N-284. From these analyses, it was found that FS of 3 was conservative enough to ensure the integrity of the beam window. Based on these analyses, the parametric survey for the thickness of the ellipse model was carried out and the estimation by FS of 3 was also performed. It was shown that the ellipse shape concepts with the thickness of 2.0-2.4 mm at the top and the thickness of 2.0-4.0 mm at the transient part were acceptable under the current ADS design parameters. It was also confirmed that the structural robustness would be kept when the uniform change of the beam window thickness would occur due to the corrosion.

Acknowledgements

The authors would like to express their great thanks to Drs. M. Arakawa, I. Saruyama and H. Ogawa of TEPCO SYSTEMS Corporation for the analysis and investigation of the factor of safety.

References

[1] Tsujimoto, K., *et al.*, "Neutronics Design for Lead-bismuth Cooled Accelerator-driven System for Transmutation of Minor Actinide", *J. Nucl. Sci. and Technol.*, 41 [1], 21-36 (2004).

[2] Sugawara, T., *et al.*, *Investigation of Beam Window Structure for Accelerator Driven System – Simplified Overall Integrity Assessment and Detailed Assessment on Buckling*, JAEA-Research 2008-026 (2008) [in Japanese].

[3] CRC Solutions Corp., Japan Atomic Energy Agency, *FINAS, Finite Element Nonlinear Structural Analysis System*, Commercial Code (2006) [in Japanese].

[4] Saito, S., K. Tsujimoto, K. Kikuchi, *et al.*, "Design Optimization of ADS Plant Proposed by JAERI", *Nuclear Instruments and Methods in Physics Research* A, 562, 646 (2006).

[5] Computational Dynamics Ltd., *STAR-CD*, CFD Commercial Code, London, England.

[6] Nishihara, K., K. Kikuchi, "Irradiation Damage to the Beam Window in the 800 MWth Accelerator-driven System", *J. Nucl. Material*, 377, 298-306 (2008).

[7] Iwase, H., K. Niita, T. Nakamura, "Development of General-purpose Particle and Heavy Ion Transport Monte Carlo Code", *J. Nucl. Sci. and Technol.*, 39, 11, 1142 (2002).

[8] Alcouffe, A.E., F.W. Brinkley, D.R. Marr, R.D. O'Dell, *User's Guide for TWODANT: A Code Package for Two-dimensional, Diffusion-accelerated, Neutral-particle, Transport*, LA-10049-M, Los Alamos National Laboratory (1990).

[9] ASME, *2004 ASME Boiler & Pressure Vessel Code Section III* (2004).

[10] Kurata, Y., M. Futakawa, S. Saito, "Corrosion Behavior of Steels in Liquid Lead-bismuth with Low Oxygen Concentrations", *Journal of Nuclear Materials*, 373, pp. 164-178 (2008).

Actinide burning performance of water-cooled thorium breeder

Naoyuki Takaki, Sidik Permana, Hiroshi Sekimoto*
Tokai University, *Tokyo Institute of Technology

Abstract

The core design condition and actinide burning performance of heavy water-cooled thorium breeder reactor has been studied. One thorium breeder reactor with 3 GWt rating that satisfies breeding capability and negative void reactivity coefficient could be feasible to consume minor actinides generated from two of the same class standard PWR. It can be concluded that an actinide-closed thorium breeder reactor based on conventional plant technology could be utilised as sustainable and symbiotic energy source with conventional LWR without actinide waste generation.

Introduction

The current LWR plant technology is in common use throughout the world and well-established technology by enormous operation experiences. This fact indicates that such water plant technology is reliable and acceptable for both public and utilities. Especially for utility company, transparent coolant is convenient for maintenance and there will be less need for thoroughly new education for operators in the introducing phase of breeder reactors, if it is possible to design a breeder by using water coolant.

The objective of this study is to find a design condition of water-cooled thorium breeder with actinides closed fuel cycle [1-3] which fulfils some characteristics required for future sustainable fission energy source such as: *i)* breeding capability; *ii)* negative void reactivity coefficient; *iii)* high burn-up; *iv)* simple homogeneous core design with large enough pin gap; *v)* small inventory of heavy metals and fissile material; *vi)* compact core size; *vii)* efficient actinide burning.

This paper especially focuses on the last provision "actinide burning". The core performances of heavy water-cooled thorium breeder reactors were evaluated for some MA loading cases in the make-up fuel in equilibrium state.

Calculations

An originally developed, very fast equilibrium burn-up calculation code (Equilibrium Cell Iterative Calculation System: ECICS) is used for various fuel cell designs and burn-up calculations. The MFR is varied from 0.3 to 1.5 by changing fuel pin configuration. The wide range of discharged fuel burn-up is examined by adjusting fuel discharge rate in the equilibrium fuel composition calculation. This equilibrium burn-up code employed 1 238 fission products and 129 heavy nuclides and is coupled with the PIJ cell calculation module of SRAC 2002 [4]. The JENDL3.2 nuclear data library is used [5].

Some basic core design parameters used in this analysis are summarised in Table 1. Based on the results of our previous study, a fixed fuel pin design is used and other important design parameters are treated as variables to find a feasible design condition of actinides closed thorium breeder.

Table 1: General design parameters

Thermal power output	[MWt]	3 000
Coolant		D_2O
Cladding material		Zircaloy-4
Fuel cycle option		All heavy metal closed
Make-up fuel		^{232}Th + MA from LWR spent fuel
MA content in make-up fuel	[%]	0-10
Fuel pellet diameter	[cm]	1.31
Fuel pin outer diameter	[cm]	1.45
Averaged pellet power density	[W/cc]	100-280 (140 for reference calc.)
Moderator to fuel ratio (MFR)	[–]	0.3-1.5 (1.0 for reference calc.)
Discharged burn-up	[GWd/t]	6-50 (36 for reference calc.)

The fuel cycle scheme considered in this study is illustrated in Figure 1. The make-up fuel to supplement heavy metals in the core is dominated by ^{232}Th and small portion of it is accounted by minor actinides that are generated in PWR with ^{235}U enrichment of 4.15% and discharged burn-up of 50 GWd/t. The contents of minor actinides in the make-up fuel vary from 0% to 10%.

Breeding capability

By increasing minor actinides contents in the make-up fuel, conversion ratio was slightly improved as shown in Figure 2. Some key design parameters as moderator to fuel ratio (MFR), power density in pellet and discharged burn-up are fixed on a set of preferable values in this calculation.

Figure 1: Fuel cycle of all actinide-closed thorium breeder

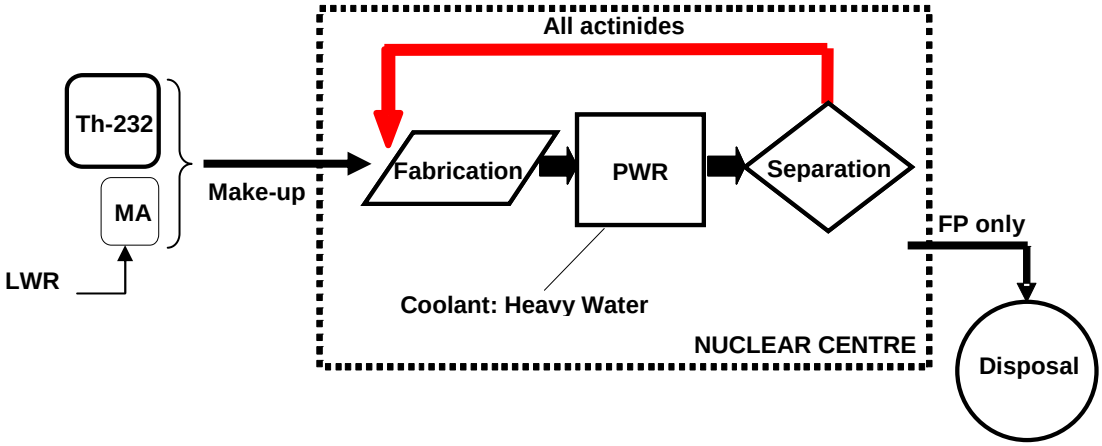

Figure 2: Conversion ratio and MA content in make-up fuel

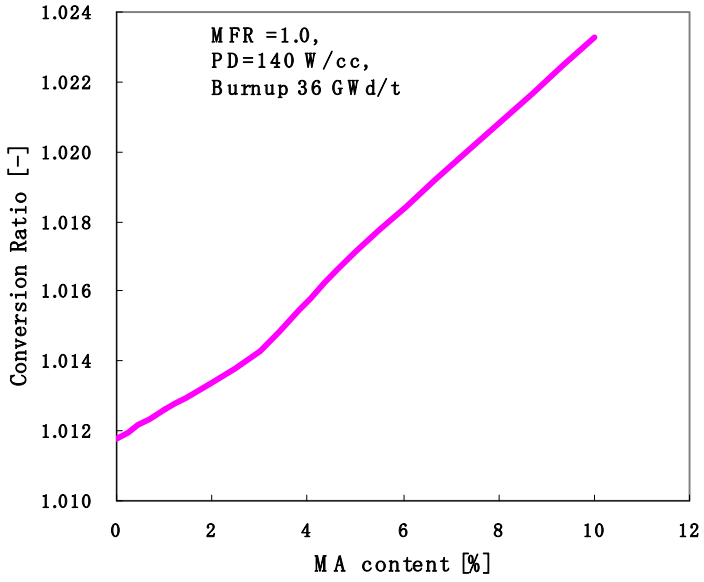

Neutron capture reactions by the loaded minor actinides that are mainly composed of even neutron nuclides contribute to generate fissile nuclides and consequently improve breeding performance. This trend can be seen for uranium cycle with minor actinides recycling.

Breeding capability can also be expressed as a function of discharged burn-up. The conversion ratio of a core that is designed as MFR = 1.0 and pellet power density of 140 W/cc with 5% minor actinides in make-up fuel is shown in Figure 3. To achieve higher burn-up, the cycle length must be extended and the criticality of core is worsened. As a result, conversion ratio decreased with increasing burn-up. The breeding capability of this core is lost for higher burn-up more than 45 GWd/t.

The moderator to fuel ratio (MFR) is a main design parameter to determine the neutronic performance of a core. Our past studies on water cooled thorium breeder reactor indicated that optimum MFR is around MFR = 1 to attain high breeding and burn-up performance simultaneously. Therefore limited MFR range is surveyed between 0.3 and 1.5 in the present study as shown in Figure 4. However lower MFR shows better conversion ratio, optimum MFR have to be chosen in a balance with safety parameters that will be discussed later.

Breeding capability monotonically decreases with increasing power density of fuel pellet. Figure 5 shows the fuel pellet power density must be less than around 200 W/cc to make the core breeder.

Figure 3: Conversion ratio and discharged burn-up

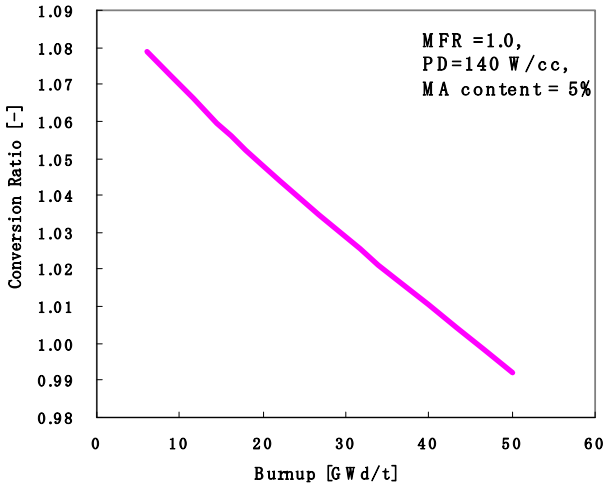

Figure 4: Conversion ratio and moderator to fuel ratio (MFR)

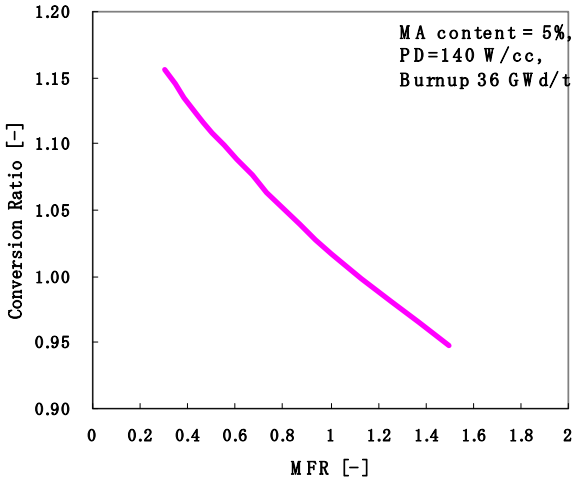

Figure 5: Conversion ratio and fuel pellet power density

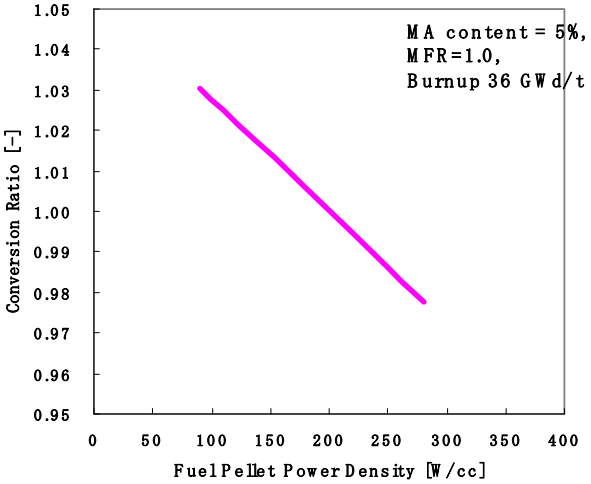

Void reactivity coefficient

Adding minor actinides into the make-up fuel of thorium reactor affects also on an important safety parameter, *i.e.* void reactivity coefficient. Figure 6 shows that void reactivity coefficients become less negative with increasing MA content. The authors calculated void reactivity coefficients for several voided fractions from 5 to 100% in order to find most conservative design condition, so several lines are illustrated in this figure. These values are for a core with MFR = 1.0 and pellet power density of 140 W/cc. Assuming 50% voided fraction for calculations, void reactivity coefficients are negative for all range of MA contents examined here.

Higher discharged burn-up also causes less negative void reactivity coefficients as can been seen in Figure 7 but the values are negative for all examined range of burn-up (<50 GWd/t) if assuming voided fraction of 50% or smaller.

Smaller MFR corresponds to harder neutron spectrum. Figure 8 indicates that void reactivity coefficients increase with reducing MFR, namely harder spectrum, for a core under design condition of burn-up of 36 GWd/t, pellet power density of 140 W/cc and 5% MA content. If the core is designed with MFR = 1, void reactivity coefficients calculated with 50% voided fraction can be kept in negative values.

The effect of pellet power density on void reactivity coefficients is shown in Figure 9. The design condition used in this evaluation is MFR=1.0, burn-up=36GWd/t and MA content=5%. Negative values of void reactivity coefficients can be achieved unless voided fraction exceeds 50%.

Figure 6: Void reactivity coefficient and MA content in make-up fuel

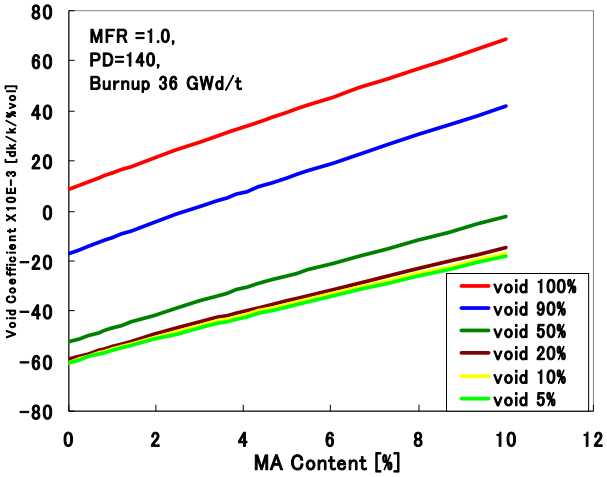

Figure 7: Void reactivity coefficient and discharged burn-up

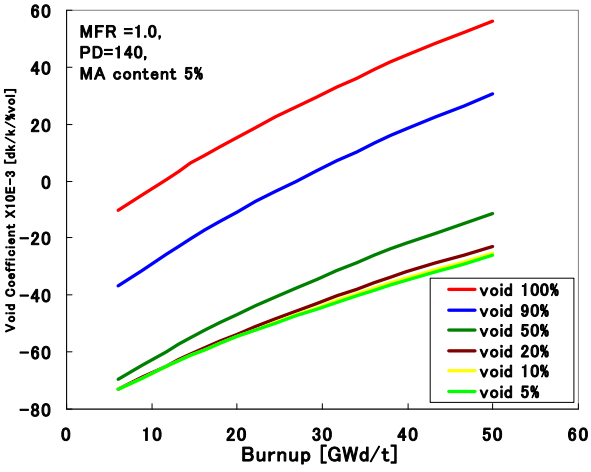

Figure 8: Void reactivity coefficient and moderator to fuel ratio (MFR)

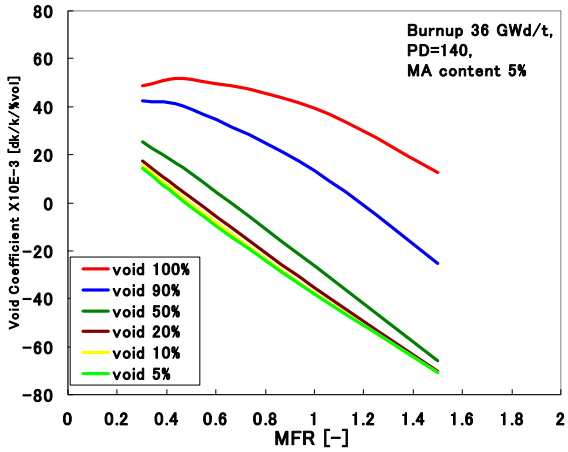

Figure 9: Void reactivity coefficient and fuel pellet power density

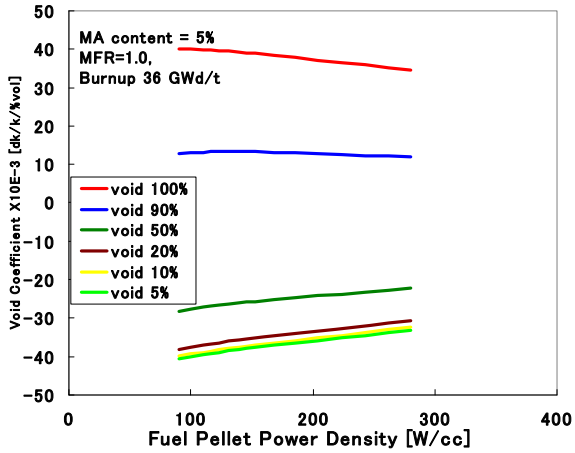

MA in the spent fuel

Minor actinides can be efficiently burnt by fission reactions in thorium-fuelled reactor compared to conventional uranium fuelled reactor because of far less precursors such as ^{238}U or plutonium that could produce new minor actinides. Figure 10 shows the spent fuel composition of the thorium reactor with additional minor actinides supply from standard PWR. The contents of minor actinides in the make-up fuel vary from 0% to 10%.

As for elements of Th, Pa and U, no remarkable difference in their compositions can be seen for each minor actinide contents. The concentrations of trans-uranium elements like Np, Pu, Am and Cm increase with increasing minor actinides content in the make-up fuel. However, the concentration increase for Np and Pu is less proportional with initial minor actinides content. Concerning higher TRU, concentrations for Am and Cm are more sensitive to the initial minor actinides content in the make-up fuel.

By loading 5% of minor actinides into make-up fuel, for instance, concentrations of Am and Cm are increased by more than one order of magnitude. Their concentration is still around one-hundredth of that of Th in the spent fuel. This means the thorium reactor works as a good minor actinide burner besides operating as a power reactor. In this actinides closed cycle, all actinides in the spent fuel are recovered and reloaded repeatedly into the reactor as fresh fuels and there is no generation of actinides waste except for their recovery loss in recycling process.

Figure 10: Spent fuel compositions as a function of MA content in make-up fuel

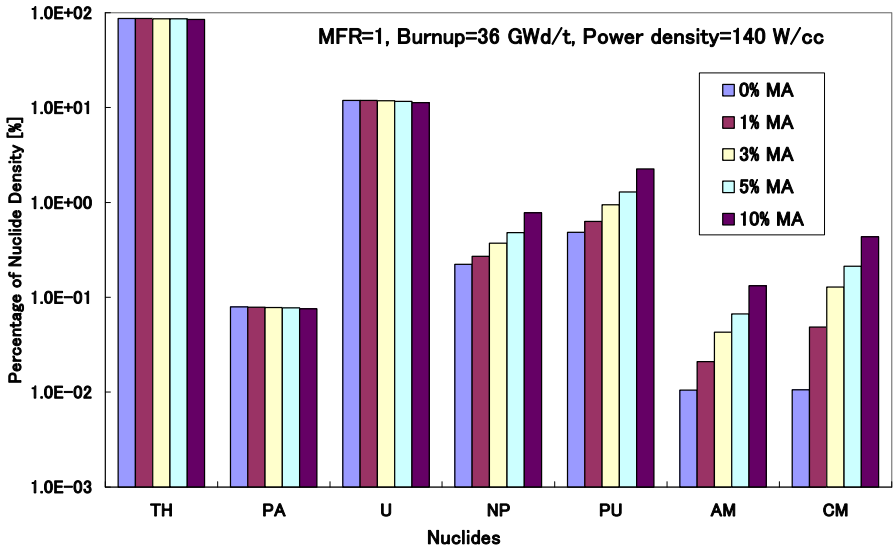

The ratio of residual minor actinides density in the spent fuel over initial minor actinides density in the make-up fuel is shown in Figure 11. This ratio implies how many minor actinides remains in the spent fuel after fuel discharge. Almost all of initially loaded ^{243}Am and ^{242}Cm are transmuted but more than 10% of ^{237}Np, ^{241}Am, ^{244}Cm remind in the discharged spent fuel. Especially ^{244}Cm is the most difficult isotope for thorough incineration even in thorium reactor but the concentration in the spent fuel is limited to around 0.8% in a case of initial minor actinides content of 5%.

Figure 11: Residual MA in spent fuel as a function of MA content in make-up fuel

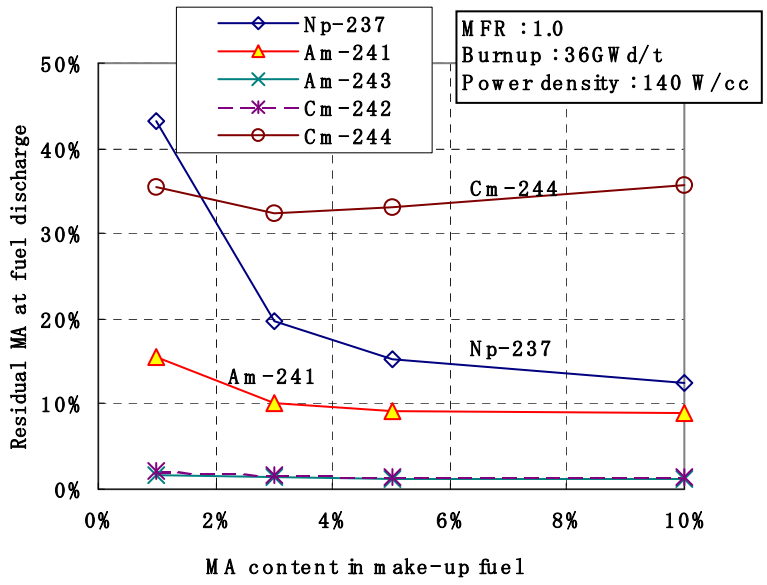

The loading rate of make-up fuel for this core is 1.14 tonnes/year and the loading rate of minor actinides in a case of 5% MA content is 57 kg/year. This value is almost double of minor actinides amount produced in a standard 3 GWt rating PWR. Consequently, is can be said that one thorium breeder reactor that satisfies breeding capability and burn-up of 36 GWd/t can consume minor actinides generated from two PWRs as illustrated in Figure 12.

Figure 12: An example of actinides-closed thorium breeder symbiotic system

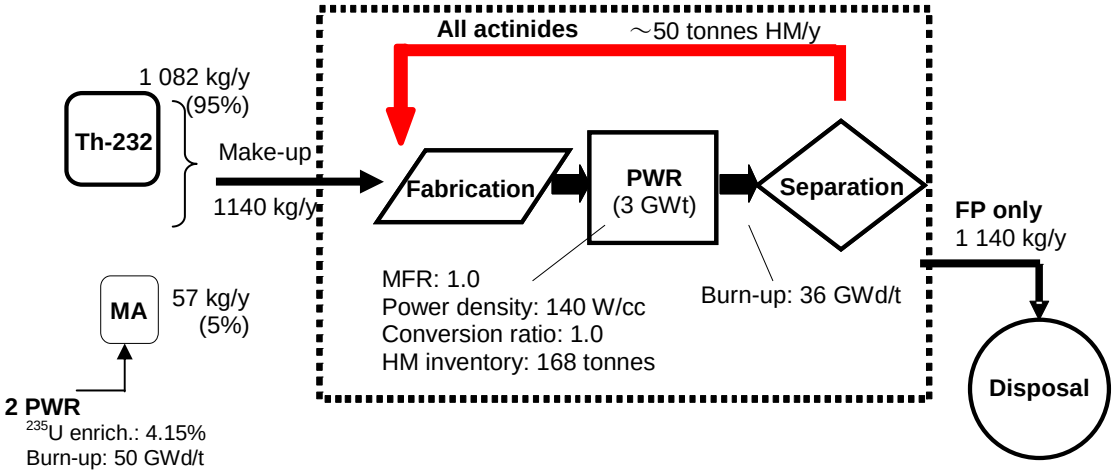

Conclusions

The core design condition and actinides burning performance of heavy water-cooled thorium breeder reactors have been studied for various and wide range of design parameters such as moderator to fuel volume ratio (MFR), discharged burn-up, minor actinides contents mixed in make-up fuel, etc.

Recycling all actinides in a closed thorium cycle makes the breeding and safety performances of the core worse but it could be possible to design thorium breeder reactor with negative void reactivity coefficient while consuming extra actinides produced in standard LWRs with uranium cycle. In case of 5% minor actinides content in make-up fuel, a 3 GWt rating thorium reactor that satisfies breeding capability more than 1.0 and burn-up of 36 GWd/t could be feasible to consume minor actinides generated from two of the same class standard PWR.

In conclusion, heavy water cooled, actinide-closed thorium breeder reactor based on conventional plant technology could be utilised as sustainable energy source and also as symbiotic system with conventional uranium fuelled LWR that generates no actinides as waste.

References

[1] Takaki, N., P. Sidik, H. Sekimoto, "Feasibility of Water Cooled Thorium Breeder Reactor Based on LWR Technology", *Proc. of GLOBAL 2007*, Boise, ID, USA (2007).

[2] Sidik, P., N. Takaki, H. Sekimoto, "Feasible Region of Design Parameters for Water Cooled Thorium Breeder Reactor", *J. Nucl. Sci. Technol.*, 44 [7], 946-957 (2007).

[3] Takaki, N., P. Sidik, H. Sekimoto, "Actinide Closed Water Cooled Thorium Breeder Reactor", *Proc. of Physor2008*, Interlaken, Switzerland (2008).

[4] Okumura, K., *et al.*, *SRAC95, General Purpose Neutronic Code System*, JAERI-Data/Code96-015, Japan Atomic Energy Research Institute (JAERI) (1996).

[5] Nakagawa, T., *et al.*, "Japanese Evaluated Nuclear Data Library Version 3 Revision-2: JENDL-3.2", *J. Nucl. Sci. Technol.*, 32, 1259 (1995).

Evaluation of the acceptable frequency of beam trips based on thermal responses of the ADS reactor system

Hayanori Takei, Kenji Nishihara, Kazufumi Tsujimoto, Hiroyuki Oigawa
Japan Atomic Energy Agency, Japan

Abstract

Frequent beam trips as experienced in existing high power proton accelerators may cause thermal fatigue problems in ADS components, which may lead to degradation of their structural integrity and reduction of their lifetime. On the other hand, the influence for the thermal shock damage on the ADS reactor system caused by beam trips has not been evaluated sufficiently. Conversely, it is not yet clear how many times of beam trips are acceptable for the ADS reactor system. Thermal transient analyses are underway to investigate the effects of beam trips on the reactor components, with objective to formulate ADS design considerations, and to determine the requirements of accelerator reliability. Preliminary analyses were made on thermal responses of four parts of the reactor structure, i.e. the beam window, the cladding tube, the inner barrel and the reactor vessel. As a result, the acceptable frequency of beam trips ranged from 43 to 2.5 $\times$104 times per year, depending on the beam trip duration.

Introduction

To realise effective transmutation of minor actinides (MA) by an accelerator-driven subcritical system (ADS), a high-power spallation target should be installed at the centre of the core. In the case of JAEA's reference ADS [1], proton beam power of ~30 MW is necessary to keep the thermal power at the subcritical core at 800 MW. Frequent beam trips, as experienced in existing high power proton accelerators, may cause thermal fatigue problems in ADS components which may lead to degradation of their structural integrity and reduction of their lifetime.

In general, beam trips are caused by two reasons: one is the failure of the accelerator components, and the other is the interruption by a Machine Protection System (MPS) to protect the accelerators against failures. For reference, the beam trip frequency caused by the "dead component" is assessed on the basis of techniques such as Failure Mode and Effect Analysis (FMEA) [2]. For these assessments, the reliability parameters of accelerator components, such as a failure rate, are usually used. However, the influence for the thermal shock damage on the ADS reactor system caused by beam trips has not been evaluated sufficiently. Conversely, it is not yet clear what times in the ADS reactor system are acceptable for the beam trips. The purpose of the present study is to evaluate of the acceptable frequency of beam trips from transient analyses of the ADS reactor system.

Conceptual design of ADS

General scheme

JAEA's reference design of ADS is a tank-type subcritical reactor, where lead-bismuth eutectic (LBE) is used as both the primary coolant and the spallation target, as shown in Figure 1. The subcritical core is composed of MA nitride fuel, with plutonium (Pu) added at the initial loading of the first cycle to reduce the bum-up swing reactivity. The proton accelerator for the ADS must have high power intensity, more than 20 MW, with good economic efficiency and reliability. To realise such an accelerator, energy efficiency must be enhanced to assure the self-sustainability for electricity of the whole system. Taking account of these requirements, the superconducting linac (SC-linac) is regarded as the most promising choice. Considering the production efficiency of the spallation neutrons in LBE, the accelerated energy of the SC-linac was set at 1.5 GeV. This value will be optimised in the future taking into account the trade-off between the cost of the accelerator for higher energy and the engineering difficulty associated with higher current. In order to keep the thermal power at 800 MW, the beam current was adjusted from 8 to 18 mA (*i.e.* 12 to 27 MW) depending on the effective multiplication factor (k_{eff}). Taking into account these requirements, the maximum beam current of the SC-linac was set at 20 mA.

Figure 1: Concept of 800 MWth, LBE-cooled, tank-type ADS

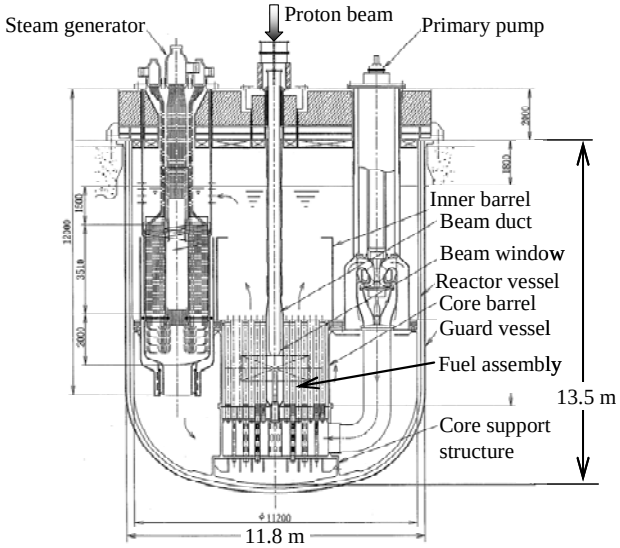

Basic parameters of the SC-linac, such as the number of cryomodules, the output power of the klystron and the total length of the SC-linac, were optimised for accelerated energies from 100 MeV to 1.5 GeV [3]. The SC-linac consists of a series of 89 cryomodules, which were designed for a 972 MHz RF wave. One klystron was provided for each cryomodule giving a total of 89 klystrons. These klystrons were classified into three categories, according to rated output power: 197, 425 and 750 kW. The total length of the SC-linac was estimated as 472 m, using the effective length of equipment, such as the quadrupole magnet and the cryomodule, for the SC-linac of the J-PARC project as reference.

Cooling system

The ADS plant was assumed to have a primary LBE cooling system and a water/steam system for power conversion through a saturated steam cycle. As shown in Figure 1, all other components of the primary system, including four steam generators, two primary pumps and auxiliary heat exchangers, are accommodated within the reactor vessel. The heat generated in the target and the subcritical core is removed by forced convection of the primary LBE, and transferred through the steam generators to water/steam for power conversion.

Figure 2 is a simplified flow diagram of the ADS. Primary LBE coolant flows upward through the subcritical core and exits into an upper plenum. Then, the coolant flow divides equally among four steam generators. The flow passes through heat transfer sections in the steam generators and enters a lower plenum. The LBE coolant is then returned back into the subcritical core by primary pumps. The water/steam system has four steam drums, four re-circulation water pumps, a turbine generator unit, and a feed-water pump. Steam generated in the steam generators is directed to the steam drums. The steam from all four steam drums is combined and drives the turbine generator unit. The steam is cooled down into water in a condenser at the turbine exit, and the feed-water pump returns the water back to the steam drums through a feed-water heater that is not shown in the figure. The re-circulation water pump delivers the water from the steam drum to the steam generator.

Figure 2: Simplified flow diagram of ADS plant

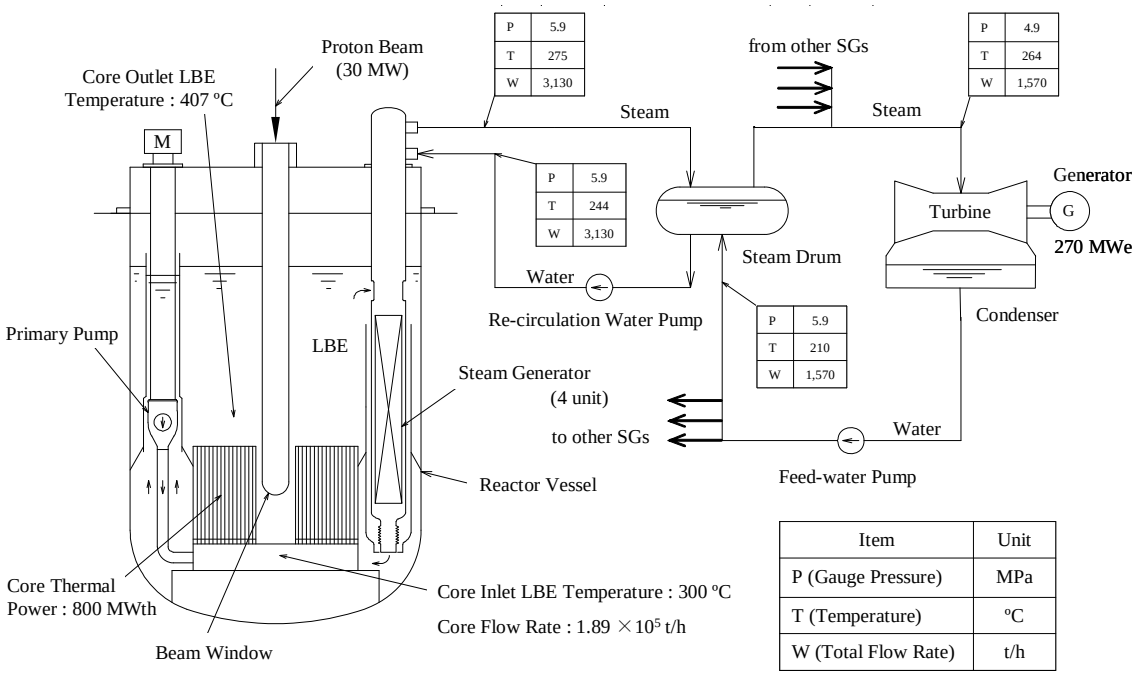

Item	Unit
P (Gauge Pressure)	MPa
T (Temperature)	ºC
W (Total Flow Rate)	t/h

Preliminary analysis was performed for transients in the ADS plant caused by the beam trip [4]. The primary LBE cooling system and the water/steam power conversion system were modelled with a simple one-dimensional flow network. As a result, about 400 seconds of turbine operation may be possible without the beam. When the duration of the beam trip exceeds this limit, the pressure of the steam drum and the LBE temperature become too low to prevent its freezing.

Estimation of acceptable beam trip frequency

Restriction from the subcritical reactor

As shown in Figure 3, four parts of the reactor component, *i.e.* the beam window, the cladding tube, the inner barrel and the reactor vessel, were picked as representatives to discuss the influence of thermal shock. In the following discussion, the expected life time of the subcritical reactor is defined as 40 years and no replacement of the inner barrel and the reactor vessel is assumed during this period. On the other hand, the replacement of the beam window and the cladding tube is assumed once every two years. And the harshest conditions for the thermal load were applied.

Figure 3: Influence of beam trip transient on reactor structure

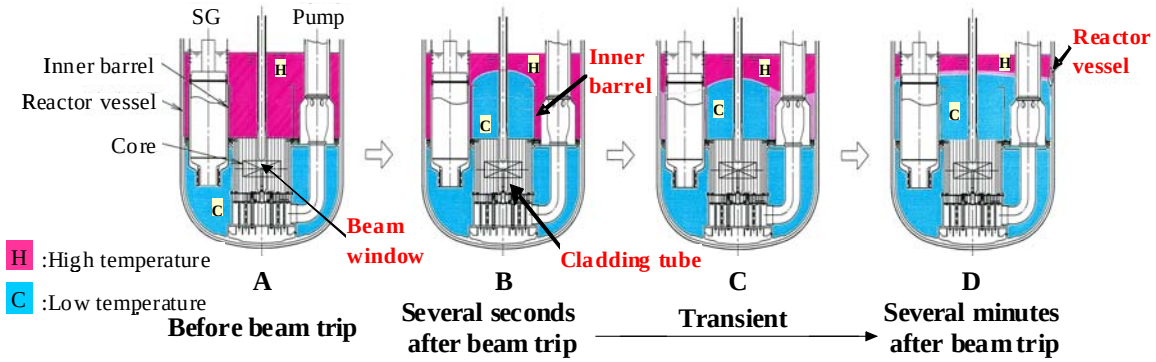

As for the beam window, a beam trip causes a rapid temperature drop, which in turn causes thermal stress because of the temperature difference between the inner and the outer surfaces of the beam window. The temperature response of the beam window (inner diameter: 450 mm, thickness: 2 mm, material: 9Cr-1Mo steel, beam power: 30 MW) was evaluated using the finite element method FINAS code [5]. In the evaluation, the beam is assumed to be restarted five seconds after the beam trip. Figure 4(a) shows the temperature change for the apical region of the beam window. On the beam trip at $t = 0$, the surface temperature starts to drop rapidly and asymptotically approaches the coolant temperature within about three seconds. The maximum thermal stress of 179 MPa is expected at a time 0.5 seconds after the beam trip. This thermal stress is much lower than what would cause buckling failure. The acceptable number of these thermal shocks is estimated to exceed 10^5, which means that several beam trips per one hour may be acceptable for two years of the expected lifetime of the beam window (about 15 000 hours). It should be noted that this estimate is based on the material data without radiation damage, and therefore experimental verification for the effect of the proton and neutron irradiation is indispensable.

As for the cladding tube, a beam trip causes a rapid temperature drop similar to that for the beam window. The temperature response of the cladding tube was evaluated using the finite element method ABAQUS code [6]. Design parameters used for the evaluation are listed in Table 1. The distance from the centre of the active core to the cladding tube was 27.9 cm. In the evaluation, the beam is assumed to be restarted 10 seconds after the beam trip. And the corrosion depth of the outer surface is estimated as 125 μm. Figure 4(b) shows the change of the surface temperature in such a position that the strain range caused by the beam trip and restart becomes the maximum of 6.2×10^{-4}. This position is located on the outer surface at 50.4 cm below from the top of the active core. After the beam trip, the temperature difference between the inner and outer surface starts to drop rapidly and asymptotically approaches zero within about five seconds. Considering the magnitude of the strain range, the acceptable number of beam trips for the cladding tube is estimated to exceed 10^6 times.

The inner barrel is a cylindrical structure, as shown in Figure 1, made of 3 cm thick 9Cr-1Mo steel and installed to straighten the LBE flow above the subcritical core. During normal operation, it is kept at the average outlet temperature 407°C. In the case of the beam trip, the inner surface of the cylinder is immediately cooled by the cold LBE (about 300°C), causing a temperature difference between the inner and outer surfaces. The temperature for 120 seconds after the beam trip was calculated by means of the ABAQUS code. In the calculation, the temperature for the outer surface is taken to be the

Figure 4: Change of the surface temperature after the beam trip for (a) the beam window and (b) the cladding tube

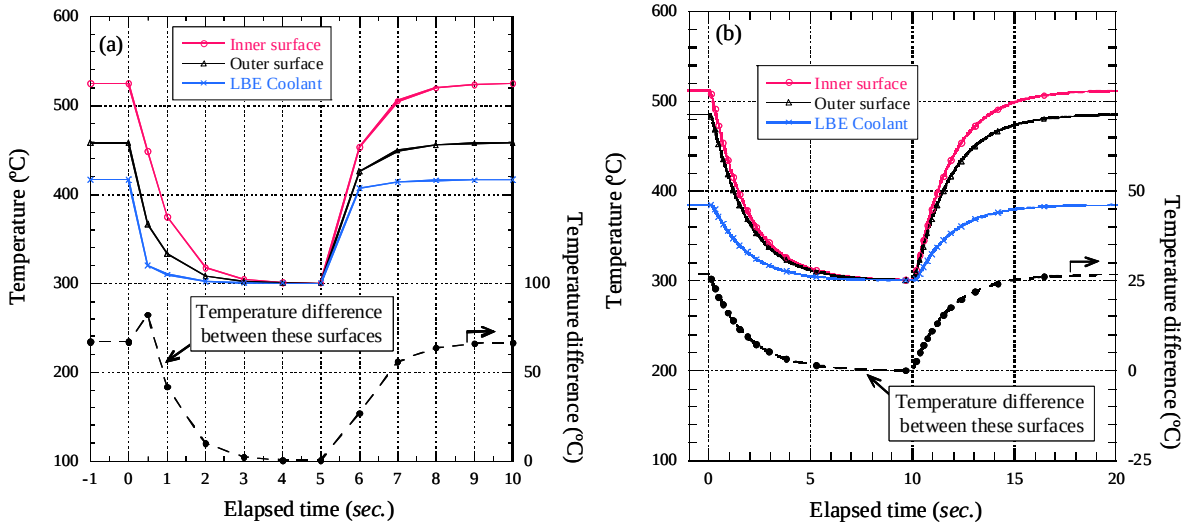

Table 1: Parameters used for the evaluation of the cladding tube

Fuel composition	(Pu+MA)N+ZrN *
Bond	He
Cladding	9Cr-1Mo steel
Pin outer diameter	7.65 mm
Thickness of cladding tube	0.5 mm
Pellet smear density	95%
Pin pitch	11.48 mm
Pin length	3 050 mm
Active height	1 000 mm
Gas plenum height	1 050 mm
Production rate of fission product (FP) gas	27%
Release rate of FP gas	100%
Linear power rating	343 W/m (average)
Coolant velocity	2.0 m/s
Inlet temperature	300°C

* Fuel is composed of 50.3% (MA+Pu)N, which is a mixture of MA nitride (MAN) and Pu nitride (PuN), and 49.7% zirconium nitride (ZrN) in weight basis.

steady value, 407°C, because it is difficult for the cold LBE to reach the outer surface in a short period of time. And the beam is assumed to be restarted 30 seconds after the beam trip. According to the results, shown in Figure 5(a), the temperature difference of 54°C will be observed at 24 seconds after the beam trip, which will cause maximum stress of 144 MPa. At the re-start of the beam, the stress in the inverse direction will be added to the inner barrel. The stress range for fatigue evaluation, therefore, is 159 MPa. Considering this magnitude of stress, the acceptable number of beam trips for the inner barrel is estimated at about 10^5 times. If the duration of the beam trip is less than 24 seconds, the stress to the inner surface becomes smaller than the maximum. In this example, the stress at the inner surface at five and ten seconds after the beam trip is 74 and 121 MPa, which is roughly equivalent to exceed 10^6 and 10^6 beam trips, respectively. Therefore, the influence of the thermal shock to the inner barrel could be reduced, provided that the beam was reinjected into the subcritical core within about ten seconds after the beam trip.

As for the reactor vessel, the beam trip causes a temperature change between the inner and outer surfaces similar to that for the inner barrel, and the formation of temperature stratification and the lowering the LBE level because of thermal shrinkage both cause thermal stress. The stress range for the fatigue evaluation was estimated for the reactor vessel made of 5 cm thick 9Cr-1Mo steel under

the assumption that the beam is restarted 400 seconds after the end of the beam trip. The result is shown in Figure 5(b). We observed that the peak value of the temperature difference between the surfaces occurred just before the beam restart. The maximum stress range calculated from the axial and circumferential stress was about 270 MPa. Considering this magnitude of the stress, the acceptable number of beam trips for the reactor vessel is estimated at about 10^4 times.

Figure 5: Change of the surface temperature after the beam trip for (a) the inner barrel, and (b) the reactor vessel

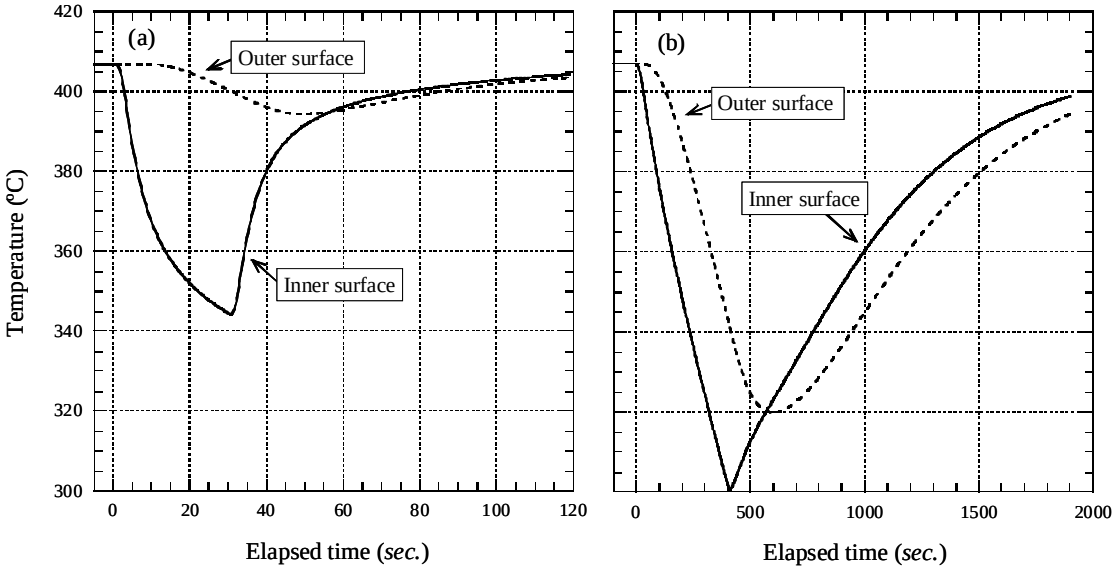

Acceptable number of beam trips per year

Taking account of the above discussions, the acceptable number of the beam trips for each component is summarised in Table 2. In this table, the elapsed time after the beam trip when the stress range or the strain range is maximised and the expected life time for each component are also listed. The acceptable frequency of beam trips, obtained by dividing the acceptable number of beam trips by the expected life time for each component, ranges from 250 to 5×10^5 times per year. For the beam trip duration over 400 seconds, it was assumed that the acceptable frequency of beam trips was restricted by the availability of the system because the restart procedure of the system usually takes a long period of time, typically several hours, once the power generation turbine stops.

Table 2: Acceptable number of the beam trip for each component

Component	Expected lifetime (year)	Beam trip duration* (sec.)		Acceptable number (times)	Acceptable frequency (times/year)
Beam window	2	$0 \le T \le 5$	(0.5)	$> 10^5$	$> 5 \times 10^4$
Cladding tube	2	$0 \le T \le 10$	(0)	$> 10^6$	$> 5 \times 10^5$
Inner barrel	40	$0 \le T \le 5$	(5)	$> 10^6$	$> 2.5 \times 10^4$
		$5 < T \le 10$	(10)	10^6	2.5×10^4
		$10 < T \le 120$	(24)	10^5	2.5×10^3
Reactor vessel	40	$0 \le T \le 400$	(293)	10^4	250

* The value in parentheses represents the elapsed time after the beam trip when the stress range or the strain range is maximised.

Therefore, the acceptable frequency of beam trips was classified by three criteria, according to the beam trip duration, as shown in Table 3. The acceptable frequency of beam trips for the inner barrel was adopted for the criteria for a beam trip of 10 seconds or less, because the acceptable frequency of

Table 3: Distribution of the beam trip duration

Criteria	Acceptable value (times/year)
0 *sec.* ≤ *T* ≤ 10 *sec.*	25 000
10 *sec.* < *T* ≤ 5 *min.*	2 500
T > 5 *min.*	43

beam trips for the inner barrel was lower than that for the beam window and the cladding tube. For the medium beam trip duration (10 sec. < *T* ≤ 5 min.), the acceptable frequency of beam trips for the inner barrel was adopted. For the beam trip duration over five minutes, the acceptable frequency of beam trips was assumed to be once a week so that the system availability was 70% or more. In this estimation, the effective full power days was assumed to be 300 for one year, that is, 43 weeks per year.

Conclusion

Frequent beam trips as experienced in existing high power proton accelerators may cause thermal fatigue problems in ADS components which may lead to degradation of their structural integrity and reduction of their lifetime. Thermal transient analyses were performed to investigate the effects of beam trips on the reactor components. These analyses were made on the thermal responses of four parts of the reactor components; the beam window, the cladding tube, the inner barrel and the reactor vessel. Our results indicate that the acceptable frequency of beam trips ranges from 43 to 2.5×10^4 times per year, depending on the beam trip duration.

As the acceptable frequency of beam trips is different for each ADS reactor system design, this solution for the beam trip problem is not valid for all ADS accelerators. However, we believe that this evaluation technique of the beam trip is of potential utility in ADS system planning. In the future, it will be necessary to include the following items in the study of beam trip problems.

References

[1] Tsujimoto, K., *et al.*, "Research and Development Program on Accelerator Driven Subcritical System in JAEA", *Journal of Nuclear Science and Technology*, 44, 483 (2007).

[2] Burgazzi, L., P. Pierini, "Reliability Studies of a High-power Proton Accelerator for Accelerator-driven System Applications for Nuclear Waste Transmutation", *Reliability Engineering and System Safety*, 92, 449 (2007).

[3] Ouchi, N., *et al.*, "Development of a Superconducting Proton Linac for ADS", *Proc. of 4th Workshop on Utilisation and Reliability of High Power Proton Accelerators*, 175 (2004).

[4] Takizuka, T., *et al.*, "Responses of ADS Plant to Accelerator Beam Transients", *Proc. of 2nd Workshop on Utilisation and Reliability of High Power Proton Accelerators*, 321 (1999).

[5] *Finite Element Nonlinear Structural Analysis System (FINAS)*, ITOCHU Techno-Solutions Co., 2-5, Kasumigaseki 3-chome, Chiyoda-ku, Tokyo 100-6080, Japan.

[6] *Unified Finite Element Analysis ABAQUS*, Dassault Systemes Simulia Corp., Rising Sun Mills, 166, Valley Street, Providence, RI 02909-2499, USA.

Monte Carlo simulation of thermally-induced reactivity variations in the GUINEVERE facility

Pedro Teles,[1] **Antonio Lafuente,**[2] **Baudouin Arien,**[3] **Peter Baeten,**[3]
José Maria Martinez-Val,[2] **Yuriy Romanets,**[1] **Pedro Vaz**[1]
[1]Instituto Tecnológico e Nuclear, Portugal
[2]Escuela Técnica Superior de Ingenieros Industriales, Universidad Politécnica de Madrid, Spain
[3]SCK•CEN, Belgium

Abstract

The Generator of Uninterrupted Intense NEutrons at the lead VEnus REactor (GUINEVERE) consists in a set of experiments conducted by a European consortium, sponsored by the European Union in the framework of the FP6 IP-EUROTRANS project. It will involve the coupling of a modified (to work in subcritical mode) version of the VENUS reactor core with a modified GENEPI deuteron accelerator (used for the past MUSE experiments). The behaviour of this coupled system will be studied in order to obtain an accurate methodology for the reactivity monitoring of ADS and to assess its operating characteristics.

In a first period, the reactor will be working in a critical mode, and several safety restrictions must apply. The maximum reactivity that can be inserted in the GUINEVERE reactor without causing any damage to the core assemblies must be investigated. For such purpose, a 2-D thermal-hydraulic model coupled to a point-kinetics model has been developed, which take into account the particular specifications of the GUINEVERE reactor.

In the framework of this point-kinetics model, the feedback reactivity of the system responding to thermal variations must be quantified. To do so, the reactivity must be re-calculated taking into account the feedback effects produced by Doppler broadening of the capture resonances and the expansion of the fuel. In order to do so we have thoroughly analysed these two effects: i) thermal expansion effect; ii) Doppler effect.

We have implemented a generic calculation of this in a systematic way, using the state-of-the-art NJOY and MCNPX code systems.

Introduction

Safety benchmarks

Safety benchmarks for GUINEVERE require the precise knowledge of this system's feedback effects arising from reactivity variations. In fact, licensing procedures require systematic cross-checking of results [1,2].

For the GUINEVERE system, a straightforward approach based on the point-kinetics model has been envisaged [1].

Some of the point kinetic parameters have been determined by several institutions, and in Table 1 we show the comparison between our estimation of k_{eff} and β_{eff} and that of the UPM and the SCK for the steady-state configuration:

Table 1: Kinetic parameters k_{eff} and β_{eff} for the steady-state configuration of GUINEVERE

	UPM results	SCK•CEN results	ITN results
K_{eff}	1.01698 ± 0.0002	1.01403 ± 0.00008	1.01375 ± 0.0002
β_{eff} (pcm)	700.11 ± 28	743 ± 11	685 ± 27

Most of the simplifications to the initial steady state system have been shown to be conservative [1-3], and it has been demonstrated [1] that it would suffice to undertake a precise analysis of the 2-D thermal effects to understand the behaviour of this system, in case of accidental reactivity insertion. These simplifications include the assumption that the temperature is uniform in the fuel rods, that it increases most rapidly in them before being evacuated and that there is no heat flux between each fuel cell, amongst others. Vertical heat conduction is also neglected [3]. We can thus determine reactivity feedbacks in the GUINEVERE system, by only taking into account what happens in the fuel cells when reactivity excursions occur.

These studies are needed to assess the appropriate procedures that must be undertaken in case of any type of accidental reactivity insertion in the system. So, the present document gives a deeper insight into some important results considered in "Reactivity accidents in the GUIENEVERE facility" [3]. This report contains the rationale and the guidelines to address, by means of the code MCNPX, some of the reactivity feedback effects to be considered in core safety analysis.

Reactivity excursions will induce thermal-mechanical variations in the fuel cells. Thermal variations usually imply both changes in the density of the fuel, and in the neutron capture cross-sections; both effects must be considered when studying these effects.

In the present paper, we aim at clarifying the role of the density variations in the fuel cells, as well as the effect of Doppler broadening in the overall reactivity feedback of the system, considering them both as separate and/or coupled effects, using the Monte Carlo radiation transport code MCNPX.

Finally, for the sake of clarity, we will refer to the multiplication constant k_{eff} in this study, but we know that the reactivity is related to k_{eff} by the following expression:

$$\frac{1-k_{eff}}{k_{eff}} \tag{1}$$

Thermal expansion

The density dependence of the macroscopic cross-sections of neutron reactions can be written as:

$$\sum_{ix} f_i \rho \sigma_x \tag{2}$$

σ_x being a type of microscopic cross-section (fission, capture, scattering) and i the isotope. f_i is the isotope abundance in the fuel, and ρ is the density. By differentiating this equation we obtain the approximate equation (assuming 2nd order terms to be negligible, as well as no variation of f):

$$\Delta\left(\sum_{ix} f_i \rho \sigma_x\right) \approx \sum_{ix} f_i \cdot \Delta\rho \cdot \sigma_x + \sum_{ix} f_i \cdot \rho \cdot \Delta\sigma_x + ... \tag{3}$$

One of the main objectives of this paper is to consider these two effects separately:

$$\sum_{ix} f_i \cdot \rho \cdot \Delta\sigma_x \text{ and } \sum_{ix} f_i \cdot \Delta\rho \cdot \sigma_x \tag{4}$$

And then consider them in the more general coupled form $\Delta(\sum_{ix} f_i \cdot \rho \cdot \sigma_x)$, in order to see the main contributions of each term.

Thermal expansion will modify the original geometry, and lead to a decrease in the density of the material constituting the fuel. The term for the variation of density of the fuel with temperature (*T*) can be written as:

$$\rho(T) = \rho_0(1 + \beta\Delta T)^{-3} \tag{5}$$

where ρ_0 and T_0 are the initial density and temperatures respectively, β is the thermal expansion factor and $\Delta T = T - T_0$ is the variation of temperature in the fuel. This, in general, embodies a decrease in reactivity and a small increase in neutron leakage [5]. We shall see that this dependence with temperature can be further adapted to the problem at hand.

Doppler broadening

Another very important feedback effect in the kinetic evolution is the Doppler broadening of the cross-section resonances, which corresponds to an increase in the neutron captures in the fuel as temperature increases [5].

This effect has to be calculated for each specific fuel, and counters the power trip (to some extent) because it represents a negative feedback effect. For this effect to be relevant, the contents of fertile nuclei (such as ^{238}U, ^{240}Pu) in the fuel must be very high [3], and the neutron spectrum must be soft enough for many neutrons to be slowed-down until the energy range (from 1 eV up to 1 keV) where most capture resonances lie. The effect decreases as fuel temperature increases. It can be approximately expressed as [2,3]:

$$\frac{\partial}{\partial T} k_{eff}(T) = -\frac{C_D}{T^{3/2}} \tag{6}$$

where C_D is the value that we intend to calculate.

Calculations

Our calculations were performed using the MILIPEIA cluster (LDA, Coimbra, Portugal), which consists of 2 and 130 management and computational nodes respectively, with a maximum of 4 processors per node, each processor running at 2.2 GHz.

We have performed our calculation using the MCNPX code, version 2.5.0. Finally, we have used two different libraries for the nuclear data of Uranium, one was compiled by us from the ENDF/B-VII.0 library [6], using NJOY 99.259 [7] for different temperatures (referred to as .71c). The other one is the JEFF-3.1 library [8], already compiled, at room temperature (300 K), referred to as .03c.

Results and discussion

Introduction

It is quite straightforward to conceive that a sudden temperature increase of the fuel rods will induce a decrease of their density, as thermal expansion occurs [Eq. (5)]. In our case, a simplification can be made to this equation by considering that variations will occur mostly radially (due to the radial symmetry of the problem). We will thus have, for the radial expansion, as a function of the temperature (*T*):

$$r(T) = r_0(1 + \alpha\Delta T) \Rightarrow \rho(T) = \rho_0 \frac{r_0^2}{r^2(T)} \tag{7}$$

Values for the linear expansion coefficient (α) as well as the initial radius of the fuel rod (r_0) are known from [2]. From this expression, we can determine the expected variation in density and radius with temperature, as summarised in Table 2.

Table 2: Values of β, α, r and ρ for several temperatures using Eqs. (2-7)

T (K)	T (°C)	β (°C^{-1})	α (°C^{-1})	R (cm)	ρ (g/cm^3)	ρ (atoms/cm^3)
290	17	4.19297E-05	1.39766E-05	0.628174	18.481	0.04716246454
320	47	4.24636E-05	1.41545E-05	0.628441	18.465	0.04712243631
350	77	4.30988E-05	1.43663E-05	0.628715	18.449	0.04708126371
400	127	4.44523E-05	1.48174E-05	0.629198	18.421	0.04700909770
450	177	4.61137E-05	1.53712E-05	0.629719	18.390	0.04693133525
500	227	4.7913E-05	1.5971E-05	0.630281	18.358	0.04684769155
550	277	4.96743E-05	1.65581E-05	0.630878	18.323	0.04675899322
600	327	5.12916E-05	1.70972E-05	0.631503	18.287	0.04666647617
650	377	5.27662E-05	1.75887E-05	0.632152	18.249	0.04657082949
700	427	5.42025E-05	1.80675E-05	0.632827	18.210	0.04647142347
750	477	5.57654E-05	1.85885E-05	0.633545	18.169	0.04636614873
800	527	5.75964E-05	1.91988E-05	0.634325	18.124	0.04625228207

In terms of MCNPX calculation procedures, there are several means of modelling the variation of density and radius. For this, we shall perform several adaptations to the initial input file (corresponding to the steady state system).

However, several problems arise. Should we change the input file to reflect both the variation of the radius and of density, or just the former or the latter? And how do we take into consideration the Doppler effect, as temperature is increased in the same way? To solve this problem we have decided to start our estimations by considering these effects separately, and then coupled. So, in this work, we will start by determining the variations of $k_{eff,}$ due to thermal expansion, first by considering density variations only, and then by considering density variations accompanied with increases in the radius of the fuel rods. After quantifying these changes, we will determine the effect of the Doppler broadening, first considering it separately, and then coupled to the thermal expansion effects. Proceeding in this way will permit us to determine how each of these contributions is important in the overall variation of the reactivity.

Another small problem arises with the geometric definition of the core. In fact the fuel rods are surrounded by a thin layer of nickel, and in the MCNPX input file, this layer is in direct contact with the outer stainless steel (SS) cladding of the assemblies. In fact, in reality, the fuel rods are surrounded by air and there is no such contact. However, in MCNPX, a direct increase of the radii of the fuel rods is therefore not possible in such a configuration, as it would lead to a juxtaposition of the layer and the cladding. In order to perform the calculations, and to avoid significant alterations in the initial configuration, we have thus removed the thin layer of Ni which permitted us to expand the radius of the fuel rods up to 0.635 cm, which is the length of the stainless steel casements in which the fuel rods are placed. It should be emphasised that we are talking about very slight variations.

Thermal expansion

The three different approaches to the calculations of k_{eff} vs. *T* due to thermal expansion are as follows: *i*) the PERT card; *ii*) direct changes in the input file, varying only density; *iii*) direct changes to the input file, varying both the density and the radius, accounting for the real thermal expansion.

The PERT card

The MCNPX code, in reactivity calculations, allows by means of using the control card PERT [10], to calculate the reactivity variations resulting from the variation of density, as a second order perturbation. This computation is performed without significantly changing the calculation time. Therefore, we have used the PERT card as a first step to determine the variations of k_{eff} with density.

The results are summarised in Figure 2 which show a linear descent of the reactivity as the fuel density diminishes (with the increase in temperature). This is a first approximation to the problem.

Figure 1: Fuel assembly

Fuel rod in dark green, nickel coating in light red, SS cladding in blue and lead in light green

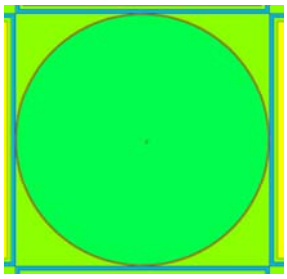

Figure 2: Comparison between the PERT card results and the results obtained varying just the density. Equations are linear fits to the results.

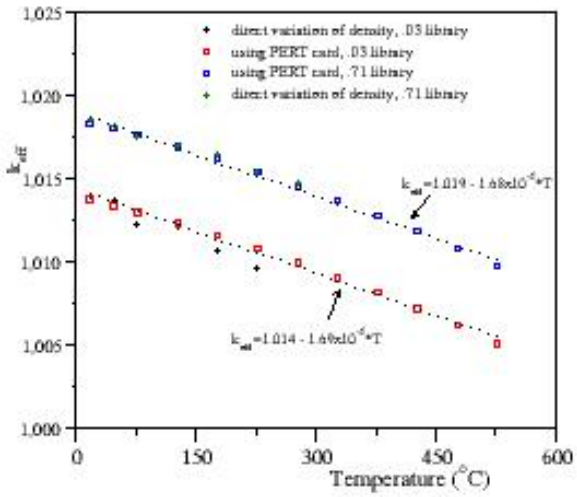

Direct changes to the input code

We can also introduce the values of density and radii estimated in Table 2 directly in the MCNPX input file. It takes a lot more computational time to obtain the desired results in this procedure, as we have to run the codes for each pair of values of density and radius.

As discussed previously, we have tried this in two different ways: one in which both the radius of the fuel rods and the density of the material are varied, and another one in which only the density is varied. As we have seen before, due to limitations related to how the input file is built, varying the radius of the fuel rods is impossible without removing the Ni coating involving these rods. This does not produce any significant changes in the final reactivity of the system (some 30 pcm), at 300 K. The obtained results have been summarised in Figures 2 (varying just the density) and 3 (both the density and radius of the fuel rods were changed).

We can see that the variation in k_{eff} with temperature, when only density is varied, is exactly the same as the one obtained when using the PERT card (see Figure 2). This demonstrates to some extent what this card is calculating, as well as puts in perspective that geometric expansion is not considered when this card is used. When both the radius and the fuel density are varied, the decrease in k_{eff} is far less pronounced (Figure 3). However, this is a more realistic approach as it is what is precisely expected in reality.

To note that, for the sake of completeness, we have performed these calculations using both atoms/cm^3 and g/cm^3 as units for the values of density, which seems to affect the obtained results in absolute terms, but not in the variations. From Figure 3, changes are not extremely pronounced for our calculations and correspond to just a few pcm and a very slow descent in reactivity as temperature rises.

Figure 3: Comparison between several calculations where density and radius of the fuel rods were changed to reflect temperature increase

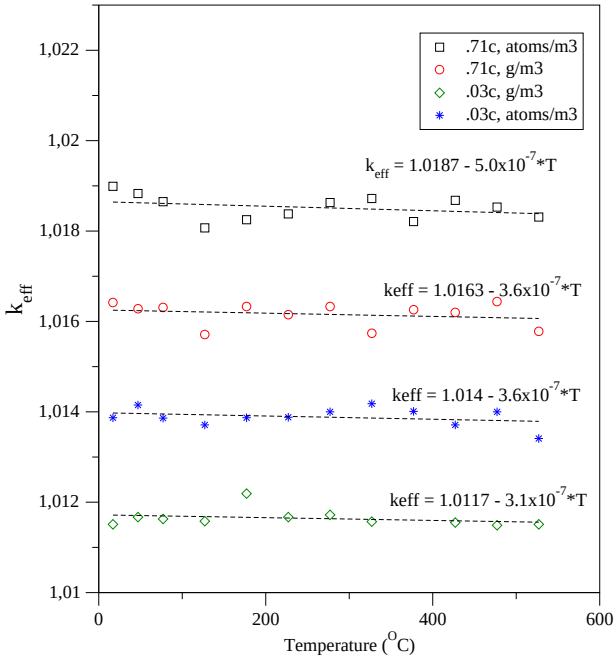

Doppler effect

As temperature increases, the cross-sections of the nuclei of both ^{235}U and ^{238}U present in the fuel will change due to Doppler broadening. We have used the NJOY 2.59 code to determine the cross-sections at different temperatures from the ENDF/B-VIII Library(.71c). These cross-sections were then used on the MCNPX code to calculate the variations in reactivity with temperature due to this effect. Results are displayed in Figure 4.

Figure 4: k_{eff} versus temperature, illustrating how Doppler broadening reduces the reactivity

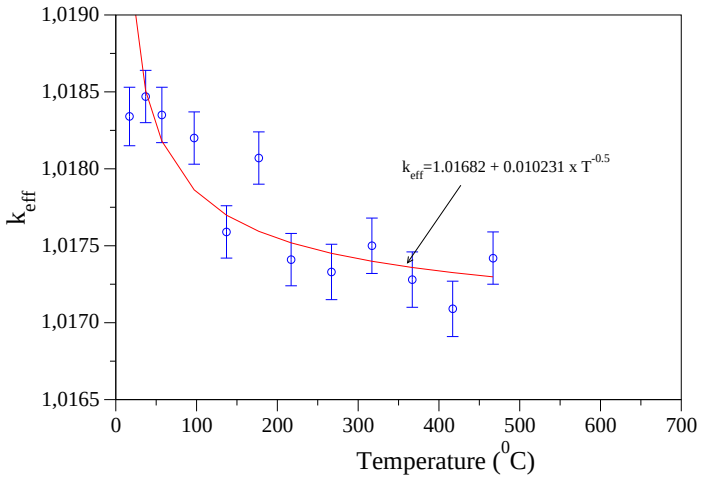

The fit of the data points using the parameterisation of Eq. (6) gives satisfactory results ($\chi^2 = 1.22 \times 10^{-6}$ and $R^2 = 0.80$). The parameterisation of k_{eff} variation with temperature as indicated in Figure 4.

Coupling both effects

Finally, we have also proceeded to the determination of the changes in reactivity when coupling both the density variation and the Doppler effect with temperature. This is shown in Figure 5. By comparing Figures 5 and 6, we can see how the variation of k_{eff} is not so different from the one obtained when taking only the Doppler broadening into account. However there is a change in the values of the fitting equation, which will be used to determine thermal-mechanical safety restrictions, and this variation is important.

Figure 5. Results obtained when the Doppler broadening effect is coupled to the variations in density and radius

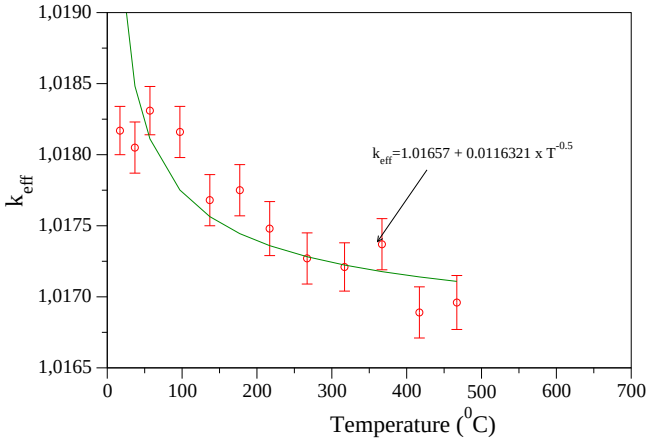

Finally, we can also compare the results when applying the direct methodology, where we modify density, volume and cross-sections with temperatures at the same time (Figure 5), with the decoupled method, where we study both effects separately and add the contributions in the end (see Figure 6, summation of results). In Figure 6, we summarise our results, where we show a comparison between the different results obtained using the different methodologies.

Figure 6: Comparison between methodologies

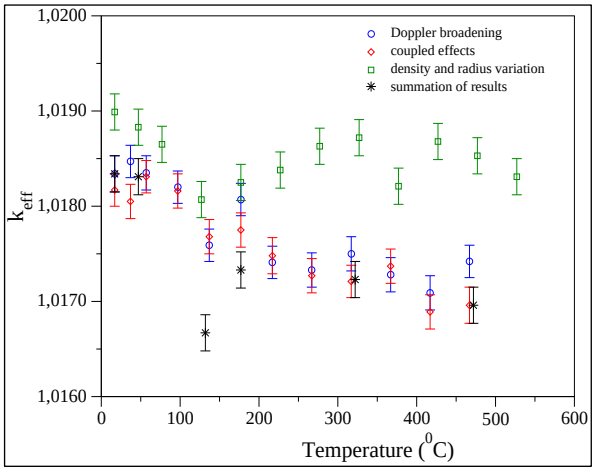

Conclusions

The feedback reactivity variations estimated here are needed to quantify which initial conditions should be used to avoid inducing massive damage to the core and its constituents, due to thermal-mechanic effects in the case of an accident. When estimating the different safety parameters [3], the variation of k_{eff} with temperature, as given in Eq. (6), will influence the maximum reactivity insertion that can be reached for different initial powers, without inducing prompt-criticality in the system. Thus, the calculations of the systems' reactivity feedbacks presented here is of extreme importance to this type of safety studies.

For the thermal expansion, one must consider not only the density variation but also the volume changes. The thermal expansion feedbacks are far less pronounced than the Doppler ones, but, nevertheless, should be introduced in the calculation to relax the constraints of the problem.

We have been able to develop a realistic methodology – which we present here. This methodology permitted us to estimate the variation of the reactivity with temperature using the MCNPX and NJOY codes in a systematic and efficient way.

Acknowledgements

The authors appreciate the efforts of all the scientists and institutions involved in EUROTRANS, as well as the financial support of the European Commission FP6 IP-EUROTRANS/ECATS project. Pedro Teles would like to thank his FCT post-doctoral grant. Finally, the authors would like to thank the computer resources, technical expertise and assistance provided by the Laboratory for Advanced Computing at the University of Coimbra, Portugal.

References

[1] Arien, B., P. Baeten, *Envelope Determination for Core Certificate Procedure: Analysis of Linear Reactivity Insertion Excursion in the GUINEVERE Experiment*, internal report.

[2] Aoust, Th., *GUINEVERE: études de sûreté, modélisation neutronique*, internal report, SCK•CEN-ThA/tha-3910.B045003 – 516/07-19, 6 December 2007.

[3] Lafuente, A., *et al.*, *A New Proposal for the Envelope Determination Within the Core Certificate Procedure: Analysis of Linear Reactivity Insertion Excursion in the GUINEVERE Experiment for Core Configuration Number One*, ITN-UPM report (2008); A. Lafuente, *et al.*, "Reactivity Accident in the GUINEVERE Facility", these proceedings.

[4] Lafuente, A. *et al.*, "Dynamic Response of an Accelerator Driven System to Accelerator Beam Interruptions for Criticality Monitoring", *Nuclear Inst. and Methods in Physics Research A*, forthcoming.

[5] Martinez-Val, J.M., *et al.*, "An Analysis of the Physical Causes of the Chernobyl Accident", *Nuclear Technology*, 90, 371 (1990).

[6] Chadwick, M.B., *et al.* "ENDF/B-VII.0: Next Generation Evaluated Nuclear Data Library for Nuclear Science and Technology", *Nuclear Data Sheets*, 107, 12 (2006).

[7] MacFarlane, R.E., D.W. Muir, *The NJOY Nuclear Data Processing System Version 91*, LA-12740-M, Los Alamos National Laboratory (1994).

[8] Koning, A.J., *et al.*, "The JEFF Evaluated Data Project", *Proceedings of the International Conference on Nuclear Data for Science and Technology*, Nice (2007).

[9] Koning, A.J., O. Bersillon, R.A. Forrest, R. Jacqmin, M.A. Kellett, A. Nouri, P. Rullhusen, "Status of the JEFF Nuclear Data Library", *Proceedings of the International Conference on Nuclear Data for Science and Technology*, Santa Fe, p. 177 (2004).

[10] Pelowitz, D.B. (Ed.), *MCNPX Users Manual(2.5.0)*, Los Alamos National Laboratory, April (2005).

Neutron flux characteristics of the YALINA-Booster core based on experiments in comparison with MCNP calculations

Milan Tesinsky,[1] **Carl Berglöf,**[1] **Andrei Fokau,**[1] **Boris Martsynkevich,**[2]
Ivan Serafimovich,[2] **Victor Bournos,**[2] **Anatoly Khilmanovich,**[2] **Yurii Fokov,**[2]
Sergey Korneev,[2] **Christina Routkovskaia,**[2] **Hanna Kiyavitskaya,**[2] **Waclaw Gudowski**[1]
[1]Royal Institute of Technology (KTH), Stockholm, Sweden
[2]Joint Institute of Power and Nuclear Research, Sosny, Belarus

Abstract

The foil activation technique was used to describe the fast neutron spectrum at two distinguished positions and to characterise the radial distribution of thermal and epithermal neutrons of the YALINA-Booster facility. Monte Carlo calculations done by MCNP are directly compared with experimentally measured neutron characteristics including neutron flux and spectrum. The comparison of experimental and simulated data resulted in good agreement.

Introduction

The possibility to transmute nuclear waste in dedicated, accelerator-driven systems (ADS) was extensively studied since the 1990s [1,2]. The main advantage of ADS compared to critical reactors is the possibility to reduce safety problems related to presence of high concentrations of minor actinides (*e.g.* Am and Cm) in the core. During the last decade an extensive experimental programme called "Multiplication with an External Source" (MUSE) helped to understand the physics of ADS [3,4]. An experimental programme on ADS called YALINA has been ongoing also at the Joint Institute of Power and Nuclear Research in Sosny, outside Minsk, Belarus [5,6]. With an outlook to further development of the knowledge, a new project GUINEVERE devoted to studies of ADS-related neutron physics is about to start [7,8].

The main objective of this work is to study neutron characteristics of the YALINA-Booster core and compare experimental results with calculations obtained from MCNP. Only a direct comparison of different physical quantities between experiments and calculations done by MCNP can justify a future usage of MCNP and the selected model to predict other quantities, such as k_{eff}. In this respect, the following two experiments were performed in February 2006 at YALINA-Booster using the foil activation technique: threshold activation of different foils inside the core and characterisation of radial distribution of the neutron flux.

YALINA-Booster

The YALINA-Booster facility is a neutron source coupled to a two-zone subcritical core. The inner fast zone is closely packed to the neutron source while the thermal zone surrounds the fast zone. Consequently, the facility is well suited for studies of neutron physics for ADS.

The neutron source takes advantage of the fusion reaction between two deuterons (D) or a deuteron and a triton (T). It consists of two parts: accelerator and target. The accelerator can operate in pulse or continuous mode. (For this experiment, the continuous mode was used). Accelerated deuterons enter the core and hit a Ti-D or Ti-T target in the centre of the core. One of the following reactions occurs:

$$D + D \rightarrow {}^{3}He + n$$

$$D + T \rightarrow {}^{4}He + n$$

In case of the (D,T)-reaction the neutron yield is $4.4 \cdot 10^{10}$ ns^{-1} and the Q-value of this reaction is 17.6 MeV (values from February 2006). Thus the neutrons have an energy around 14 MeV. The maximal yield of the (D,D) reaction is significantly lower.

The neutron source is located inside the booster zone, surrounded by the thermal zone and a reflector. A vertical cross-section of the core is given in Figure 1 (February 2006 core configuration; names of the experimental channels as in June 2008). Both the thermal zone and the booster zone contain axial experimental channels. There are four experimental channels in the booster zone, three channels in the thermal zone and three channels in the reflector (two axial and one radial).

The standard full-sized booster zone (as in February 2006) is composed of a lead lattice and consis of two parts with two different enrichments of fuel pins. The inner part closest to the target contains 132 fuel pins made of metallic uranium with 90% enrichment. The outer part contains 563 fuel pins made of 36% enriched UO_2. The two outermost layers of fuel rods form a thermal neutron filter. The filter is transparent to fast neutrons passing through, but it stops thermal neutrons coming into the booster zone from the thermal zone. The filter consists of one layer of fuel rods made of natural uranium (0.7% enrichment) and one layer of rods made of borated polyethylene B_4C, as denoted in Figure 1. The natural uranium absorbs neutrons and transforms some of them into fast neutrons by fission while the boron serves as an absorber.

The thermal zone has a polyethylene lattice and there are up to 1180 fuel pins EK-10 with uranium dioxide enriched to 10% in cylindrical geometry. There is also a possibility to insert three B_4C control rods in the thermal zone (withdrawn during the measurements).

Figure 1: Vertical cross-section of the YALINA-Booster core (configuration with 1 180 EK-10 fuel pins)

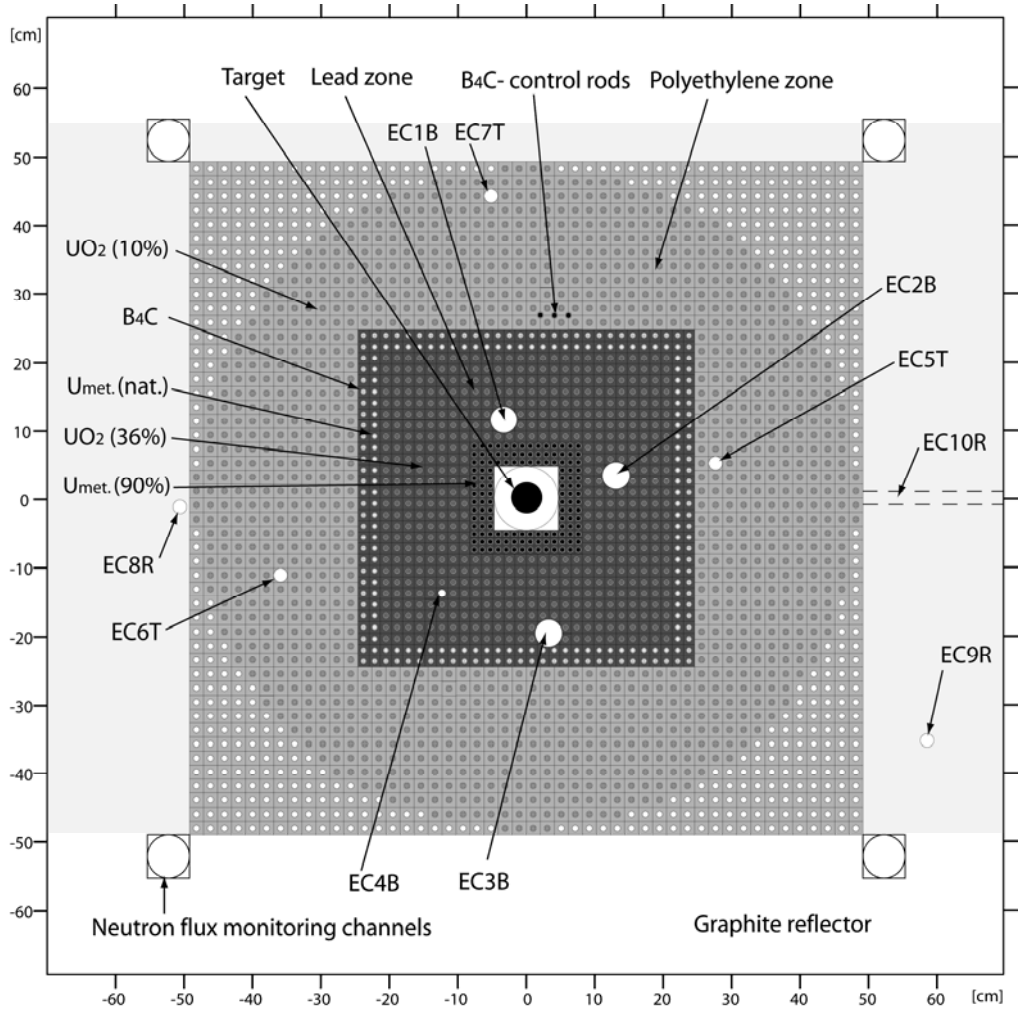

Methodology

The following two experiments are elaborated below: threshold activation of different foils inside the core and characterisation of radial distribution of the neutron flux. Each of the experiments was performed under specific conditions.

Neutron spectrum characteristics

For this experiment the (D,T) reaction was utilised and there were 1 180 EK-10 pins in the thermal zone. Two identical sets of activation foils were placed at two distinguished positions – one in the fast zone and one in the thermal zone. Each set of the foils was coated in a cadmium container, so that reactions induced by thermal neutrons are eliminated. The cadmium containers with the foils inside were inserted in the middle of the EC2B and EC6T experimental channels (Figure 1). The choice of the experimental channels is guided by the need to measure the neutron flux in the middle of the zones, away from their radial boundaries. Both sets were activated during the same run, which lasted for 100 minutes.

Materials for measurements using activation foils were chosen according to the need to cover energy interval of fast neutrons by as broad range of threshold reactions as possible. The list of foil materials is given in Table 1 and the list of employed reactions in Table 2.

The shape of the foils was cylindrical, excluding the golden foil, which had a square cross-section. Most of the cylindrical foils had a diameter, D, of 12 mm and height, L, of approximately 2 mm. There were two exceptions, titanium and indium, which had different dimensions. Although the samples were called foils, they had a rather cylindrical shape with a relatively high thickness. For this reason, a correction for gamma self-shielding during the measurements was introduced. Neutron self-shielding during the activation process was negligible.

Table 1: List of the foil materials D - diameter, m – mass, L – height

Sample	D [mm]	Set #1, EC2B		Set #2, EC6T	
		m [g]	L [mm]	m [g]	L [mm]
Cd	12.0	1.933	1.98	2.080	2.13
Co	12.0	2.043	2.03	2.057	1.34
Ti	12.0	2.419	4.71	2.404	4.68
Fe	12.0	1.873	2.11	1.789	2.11
Cu	12.0	1.747	1.72	1.948	1.92
CF_2	12.0	0.437	1.76	0.500	2.01
Ni	12.0	2.151	0.21	2.164	0.22
Pb	12.0	2.566	2.00	2.755	2.15
Mg	12.0	0.339	1.72	0.394	2.00
Al	12.0	0.552	1.81	0.490	1.61
Zn	12.0	1.576	1.96	1.534	1.90
Au	8.0 x 8.0	0.133	0.12	0.143	0.12
In	10.0	0.404	0.70	0.404	0.70

Table 2: List of activation reactions employed for neutron activation measurements with the corresponding thresholds and γ-energies of the activation products

Reaction	Threshold [MeV]	Eγ [keV]
$^{27}Al(n,p)^{27}Mg$	3	844
$^{27}Al(n,\alpha)^{24}Na$	7	1 369
$^{59}Co(n,p)^{59}Fe$	5	1 099
$^{59}Co(n,\alpha)^{56}Mn$	8	847
$^{65}Cu(n,p)^{65}Ni$	4	1 480
$^{19}F(n,2n)^{18}F$	12.8	511
$^{56}Fe(n,p)^{56}Mn$	5	847
$^{54}Fe(n,p)^{54}Mn$	1.5	835
$^{24}Mg(n,p)^{24}Na$	6	1 369
$^{46}Ti(n,p)^{46}Sc$	2.5	1 121
$^{47}Ti(n,p)^{47}Sc$	12	159
$^{48}Ti(n,p)^{48}Sc$	8	1 311
$^{64}Zn(n,p)^{64}Cu$	1	1 347

Radial distribution of thermal and epithermal neutrons

During this experiment the (D,T) reaction was used and the number of the EK-10 pins was 1180. A set of indium foils was irradiated at different positions inside YALINA-Booster. Namely, there were two foils in the fast zone (experimental channels EC1B and EC3B), three foils in the thermal zone (experimental channels EC5T, EC6T and EC7T) and nine foils in the reflector (EC10R). The foils were irradiated for 10 min. All the foils were placed in the middle of the experimental channels. The mass of the activation samples was 0.202 g each.

Results and discussion

Neutron spectrum characteristics

To be able to compare experimental values and MCNP calculations, reaction rates are utilised. In this context the reaction rate is defined as the number of activation reactions that occur during the irradiation inside a foil within one second normalised by the number of atoms in the activation foil. Values calculated by MCNP (C) are divided by experimental values (E) and normalised to the average C/E value. In this way, the number of source neutrons is not needed.

The comparison is depicted in Figure 3 and Figure 4. The error bars cover errors of the experimental as well as the calculated values. The depicted error of the experimental values comes mainly from the peak-fitting procedure during analysis of the activated foils, while the displayed error of the calculated values arises mainly from the statistical error of the Monte Carlo calculation.

Using the same nuclear data library (ENDF/B-VI.8) and the same model, the neutron spectrum was calculated at the positions of the foils using MCNP. This spectrum is depicted for both locations in Figure 2. Based on good agreement of the measured and calculated reaction rates (see Figures 3 and 4) it is possible to conclude that MCNP can reliably reproduce neutron spectrum at these positions using the selected model and data library.

Radial distribution of thermal and epithermal neutrons

The isotope ^{115}In is activated mainly by thermal and epithermal neutrons to ^{116m}In. As in the case of the threshold reactions in the previous chapter, it is the reaction rate that is compared between measured and calculated values. In this case, however, the same reaction is used, while the location of the foils is changing.

Figure 5 illustrates changes of the reaction rates over the distance from the centre of the core as measured and calculated by MCNP using the ENDF/B-VI.8 library. As expected, there are virtually no thermal or epithermal neutrons in the fast zone which corresponds to the first two data points. On the other hand, the number of thermal and epithermal neutrons is the highest in the thermal zone and decreases gradually in the reflector. Correctness of the calculation is confirmed by comparison with measured data as depicted in Figure 6.

Figure 2: Neutron spectrum at the locations of the foil activation calculated by MCNP

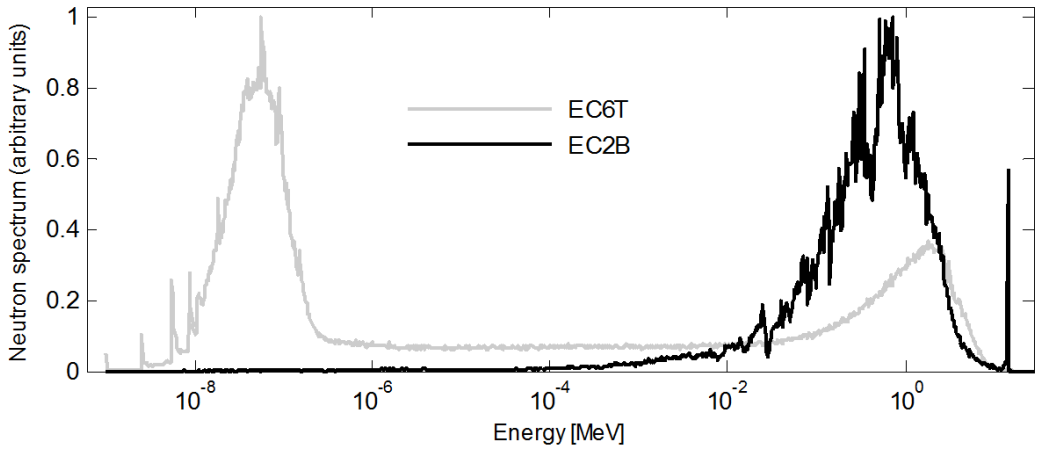

Figure 3: C/E values of the reaction rates in the fast zone (EC2B) normalised to the average value

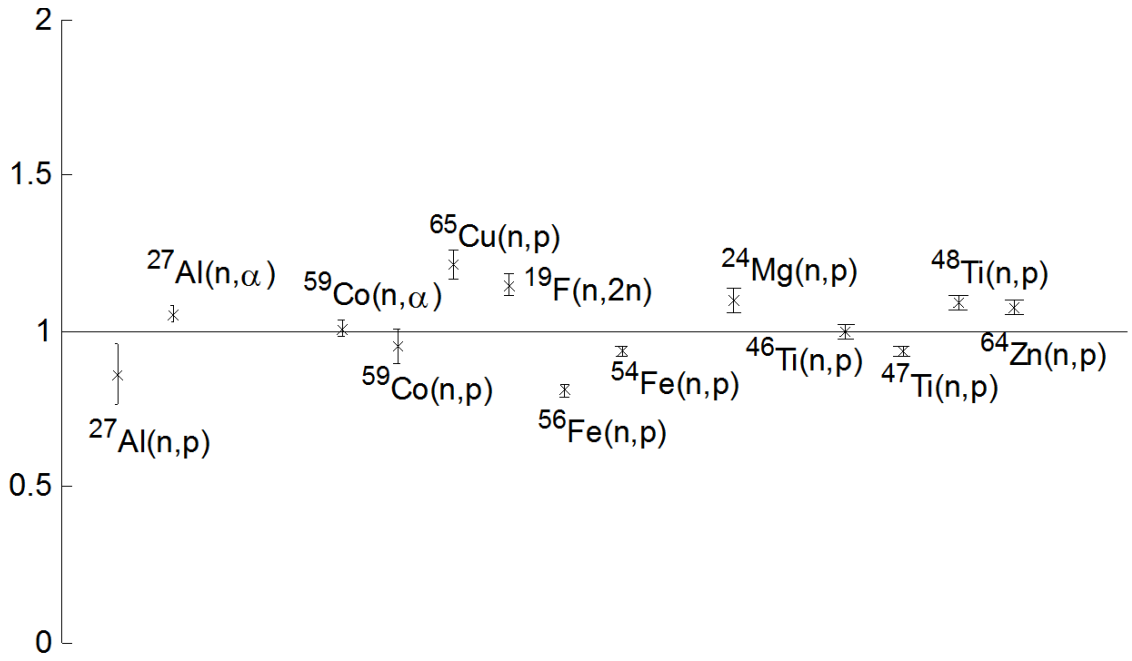

Figure 4: C/E values of the reaction rates in the thermal zone (EC6T) normalised to the average value

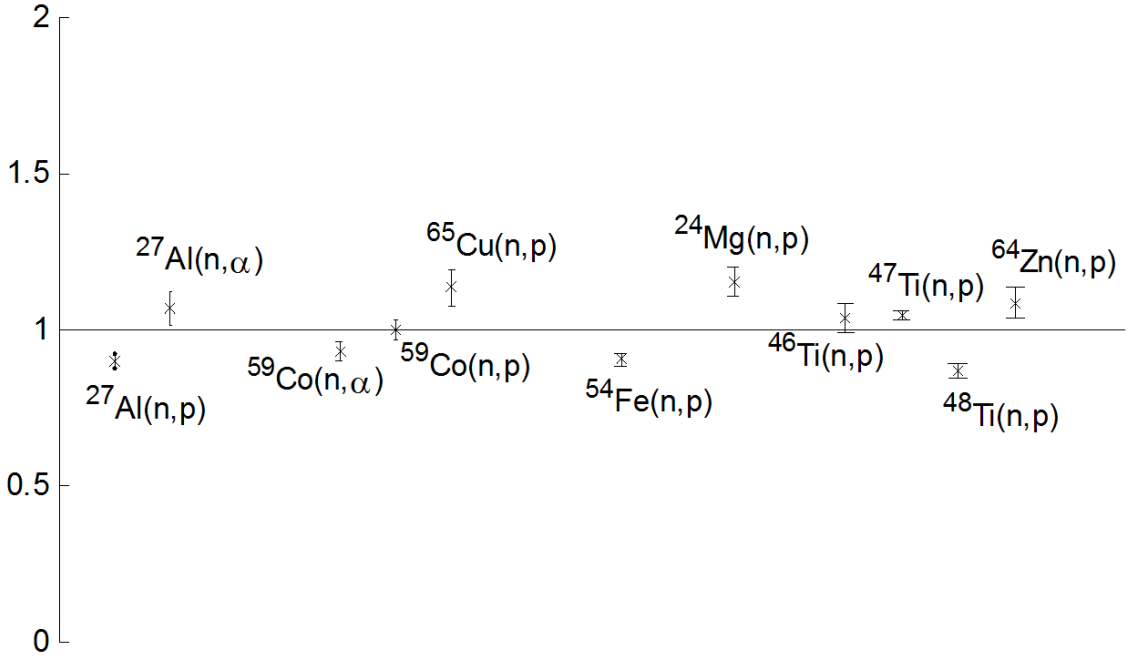

Figure 5: Reaction rate of the ^{115}In to ^{116m}In reaction as a function of distance from the centre of the core (experimental values together with MCNP calculation)

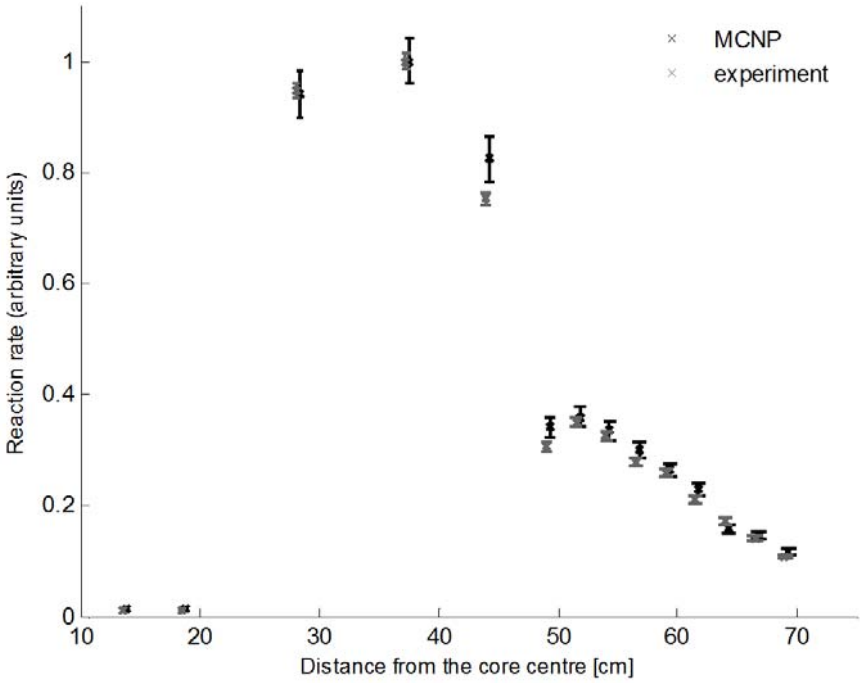

Figure 6: C/E values of the reaction rates depicted in Figure 5 (normalised to the average value)

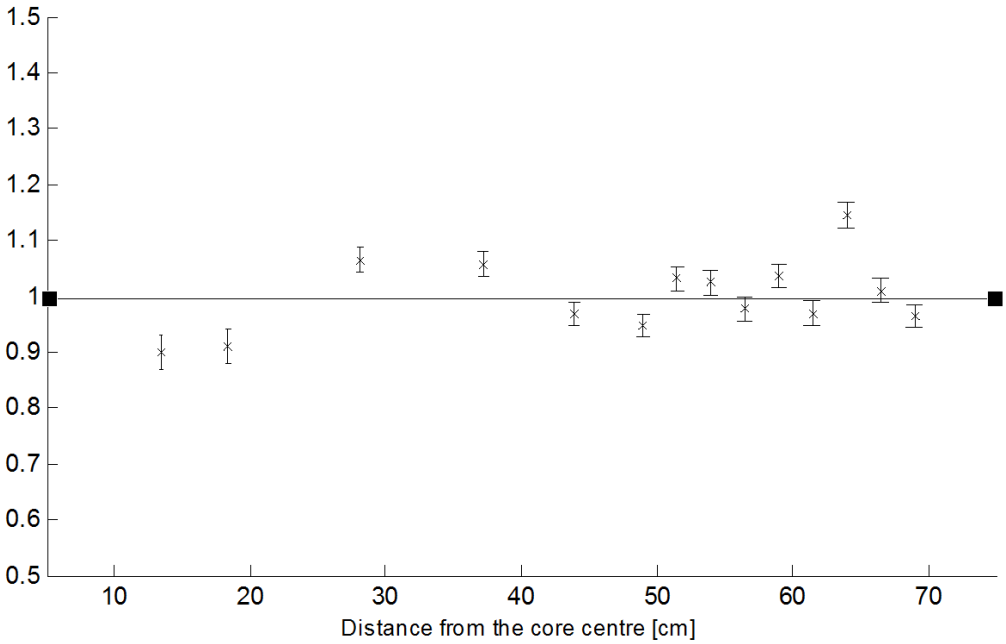

Conclusions

Different neutron characteristics connected to neutron flux and neutron spectrum were studied experimentally as well as through simulations by Monte Carlo calculations. Direct comparison of calculated and experimental values was performed resulting in good agreement.

The foil activation technique was used to experimentally describe fast neutron spectrum at two distinguished positions inside YALINA-Booster and to describe radial changes in the thermal and epithermal flux. In both cases, the observed effects were reproduced by MCNP calculations with good precision.

Acknowledgements

The authors would like to express their gratitude to the YALINA-Booster staff (S. Mazanik, A. Adamovich and A. Nesterovich) whose experience and hospitality is greatly appreciated. The YALINA-Booster facility was built as a part of the Belarus State Scientific Programme "Instruments for Scientific Research". This work was financially supported by the Swedish Institute through the Visby Programme.

References

[1] Salvatores, M., *et al.*, "Physics Characteristics of Nuclear Power Systems with Reduced Long-term Radioactivity", *Nuclear Science and Engineering*, Vol. 120 (1995).

[2] Salvatores, M., *et al.*, "The Transmutation of Long-lived Fission Products by Neutron Irradiation", *Nuclear Science and Engineering*, Vol. 130, pp. 309-319 (1998).

[3] Soule, R., *et al.*, "Neutronic Studies in Support of Accelerator-driven Systems: The MUSE Experiments in the MASURCA Facility", *Nuclear Science and Engineering*, Vol. 148, pp. 124-152 (2004).

[4] Lebrat, J-F., *et al.*, "Global Results from Deterministic and Stochastic Analysis of the MUSE-4 Experiments on the Neutronics of Accelerator-driven Systems", *Nuclear Science and Engineering*, Vol. 158, pp. 49-67 (2008).

[5] Persson, C-M., *et al.*, "Pulsed Neutron Source Measurements in the Subcritical ADS Experiment YALINA-Booster", *Annals of Nuclear Energy* (2008), doi:10.1016/j.anucene.2008.07.011.

[6] Fernandez-Ordonez, M., *et al.*, "Reactivity Monitoring of the YALINA Subcritical Assembly Using Beam Trips and Current-to-flux Experiments", these proceedings.

[7] Billebaud, A., *et al.*, "Prompt Multiplication Factor Measurements in Subcritical Systems: From MUSE Experiment to a Demonstration ADS", *Progress in Nuclear Energy*, Vol. 49, pp. 142-160 (2007).

[8] Granget, G., *et al.*, "GUINEVERE Program for the reactivity Monitoring of an ADS System Using the GENEPI-C Accelerator", *AccApp'07*, Pocatello, Idaho (2007).

A source efficient ADS for minor actinide burning*

S. Ishida, A. Fokau, Y. Zhang, J. Wallenius
Reactor Physics, KTH
Stockholm Sweden

Abstract

Taking advantage of the good neutron economy of nitride fuel, a compact ADS for burning of minor actinide fuels has been designed, based on the fuel assembly geometry developed for the European Facility for Industrial Transmutation (EFIT) within EUROTRANS. The small core size permits to reduce the size of the spallation target region, which enhances the source efficiency by about 40%, compared to the reference oxide version of EFIT. In this contribution we present values for proton and neutron source efficiencies, beam power amplification, burn-up swing, safety coefficients and transient behaviour of this nitride-fuelled ADS, calculated with MCB and SAS4A.

* The full paper being unavailable at the time of preparation of this CD-ROM, only the abstract is included.

Efficiency estimation criteria of the different ADS burners

A. Gulevich,[1] **A. Degtyarev,**[2] **A. Kalugin,**[2] **O. Kolyaskin,**[2]
V. Konev,[3] **L. Ponomarev,**[2] **V. Seliverstov,**[3] **E. Zemskov**[1]
[1]Institute of Physics and Power Engineering, Russia
[2]Russian Research Centre "Kurchatov Institute", Russia
[3]Institute of Theoretical and Experimental Physics, Russia

Abstract

The problem of minor actinides (MA) in the closed nuclear fuel cycle (NFC) is a one of the most important for future nuclear energetic. There are several approaches for MA transmutation but there are no of common criteria for the comparison of their efficiency. In paper [1] we turned out the attention to the importance of taking into account the duration of the closed NFC in addition to a usual criterion of the neutron economy. In accordance with these criteria the different ADS-burners are considered: LBE-cooled reactor (fast neutron spectrum), molten-salt reactor (intermedium spectrum) and heavy water reactor (thermal spectrum).

Introduction

We define MA as a mixture of isotopes Np, Am and Cm and the process of MA transmutation as the direct and indirect fission of MA in the closed fuel cycle. The direct MA fission is the fission of the loaded MA, and the indirect one is the fission of transuranium (TRU) isotopes originated by the loaded MA in its transformation chains, as well as TRU produced by the other fissile elements (*e.g.* Pu). Therefore the mass of the non-transmuted TRU in NFC is equal to the mass of all TRU originated by MA and Pu loading in reactor.

Plutonium is necessary for the ADS subcriticality level maintaining. The inclusion of TRU produced by Pu in the total balance of TRU certainly worsens the overall MA transmutation efficiency but it makes all consideration more realistic.

Time of transmutation

The transmutation of any TRU is a stochastic process which can be characterised by the probability density function $\omega(t)$. In the closed fuel cycle (without taking into account the small reprocessing fuel losses) the function $\omega(t)$ is normalised by the condition:

$$\int_0^\infty \omega(t)dt = 1 \tag{1}$$

and the mean time τ_{in} of the TRU transmutation in reactor is:

$$\tau_{in} = \int_0^\infty t \cdot \omega(t)dt \tag{2}$$

As an example the functions $\omega_{MA}(t)$ and $\omega_{Pu}(t)$ for Pu and MA (including Np) for thermal reactor with molten salt fuel cooled by heavy water (its main parameters are given in Table 1) are presented in Figure 1.

Figure 1: The transmutation probability density functions for ADS with thermal spectrum

In this case τ_{MA} = 67 years; τ_{Pu} = 46 years

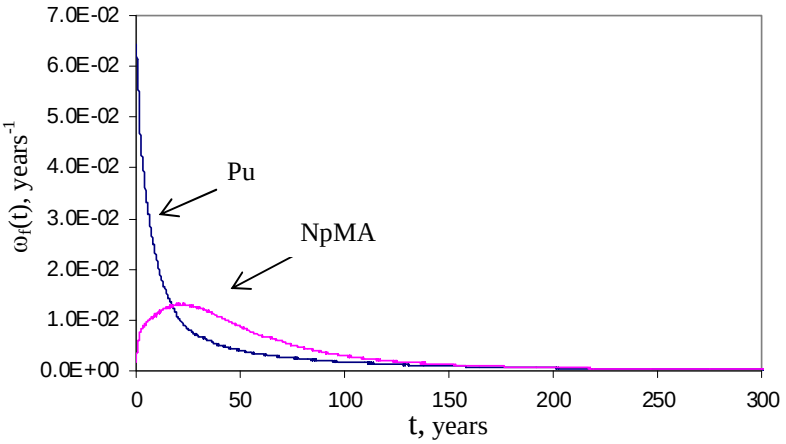

There are two approaches to MA transmutation: the first one considers ^{239}Pu as the radioactive waste which should be burned together with all MA; in the second approach ^{239}Pu is the valuable nuclear fuel which must be eliminated from the burning TRU balance. This difference should be taken into account at the calculation of function $\omega(t)$. In what follows we calculate function $\omega(t)$ for the set of TRU originated in reactor by MA and Pu loading, *i.e.* for all isotopes of Am and Cm, ^{237}Np and all isotopes of Pu. We choose the initial MA composition which corresponds to those in the PWR spent fuel.

Table 1: Characteristics of ADS burners chosen for the comparative study

Reactor characteristics	Neutron spectrum		
	Fast	Intermediate	Thermal
Subcriticality, Δk	0.05	0.05	0.03
ADS power, *MW*	330	800	500
Neutron flux, *n/cm²·s*	$1.5 \cdot 10^{15}$	$3 \cdot 10^{14}$	$5 \cdot 10^{13}$
Equilibrium Pu/MA loading, *tonnes*	0.9/2.3*	4.7/1.6	2.7/1.4
Pu/MA feeding content, ε	0.4	2.9	3.0
Ttransmutation MA rate, q_{MA}, *kg/year*	–	70	40
Transmutation time τ_{in}, *years*	–	~75	~50

* Initial loading.

The transmutation time τ_{in} can also be determined via the equilibrium mass G_{TRU}^{equ} of TRU in reactor and the rate of MA feeding q_{MA} [kg/year]. The probability $\xi(t)$ that TRU generated by MA and Pu loaded at the time moment $t = 0$ will be transmuted (*i.e.* fissioned directly or indirectly) at the time moment t is equal:

$$\xi(t) = \int_0^t \omega(t)dt \tag{3}$$

The non-transmuted TRU mass $G_{TRU}(t)$ accumulated to time moment t due to MA loading with the rate q_{MA} is equal to:

$$G_{TRU}(t) = q_{MA} \cdot \int_0^t \eta(t)dt, \quad \eta(t) = 1 - \xi(t) \tag{4}$$

After integral transformation, taking into account Eqs. (1-4):

$$\int_0^t \eta(t)dt = t \cdot \eta(t)\Big|_0^t + \int_0^t t \cdot \omega(t)dt \underset{t\to\infty}{=} \tau_{in} \tag{5}$$

The total equilibrium mass of TRU $G_{TRU}^{in} = G_{TRU}(\infty)$ is equal to:

$$G_{TRU}^{in} = q_{MA} \cdot \tau_{in} \tag{6}$$

The equilibrium TRU mass G_{TRU}^{equ} originated by both MA and Pu loading in the closed NFC is equal to:

$$G_{TRU}^{equ} = q_{MA} \cdot \tau \tag{7}$$

where $\tau = \tau_{in} + \tau_{out}$ and τ_{out} is the duration of outer NFC, *i.e.*:

$$\tau_{in} = \frac{G_{TRU}^{in}}{q_{MA}}, \qquad \tau = \frac{G_{TRU}^{equ}}{q_{MA}} = \frac{G_{TRU}^{in}}{q_{MA}}\left(1 + \frac{\tau_{out}}{\tau_{in}}\right) \tag{8}$$

where G_{TRU}^{out} is the amount of TRU in the outer NFC:

$$G_{TRU}^{equ} = G_{TRU}^{in} + G_{TRU}^{out}, \qquad \frac{G_{TRU}^{in}}{\tau_{in}} = \frac{G_{TRU}^{out}}{\tau_{out}} \tag{9}$$

In the equilibrium closed NFC the MA feeding rate q_{MA} is equal to the MA transmutation rate considered usually as a main parameter in the all previous estimations of the reactor-burner efficiency. But in the closed NFC one more parameter G_{TRU}^{equ} is essential, which can be represented by the transmutation time τ. The third parameter $\varepsilon = q_{Pu}/q_{MA}$ is the ratio of MA and Pu feeding. In our opinion it is more informative as the number of neutrons, necessary for one MA nucleus transmutation, which is usually discussed.

Number of the fuel reprocessing cycles

As a rule the duration τ_{cycle} of a single fuel cycle, which consists of the time of fuel irradiation in reactor and prefabrication in the outer NFC is much less than MA transmutation time τ. This means that TRU initiated by MA loading in reactor have to be reprocessed many times. The number of the single reprocessing cycles is equal to ratio:

$$n_{rep} = \frac{\tau}{\tau_{cycle}} \tag{10}$$

The total fraction Q_{loss} of MA losses due to the fuel reprocessing is:

$$Q_{loss} = n_{rep} \cdot \chi_{cycle} \tag{11}$$

where χ_{cycle} is the relative MA losses per one reprocessing cycle.

At τ_{cycle} ~5-10 years the number of reprocessing is n_{rep} ~10 in all the cases and this fact leads to sharp restrictions for the MA losses Q_{loss} in closed NFC. Particularly the value $Q_{loss} \leq 10^{-3}$ can be achieved at $\chi_{cycle} < 10^{-4}$ only. Such a level of the spent fuel purification is discussed now in the molten salt technology only.

Results

For illustration of the presented approach we have chosen three types of ADS burners:

- heavy water ADS (thermal neutron spectrum) [2];
- molten salt ADS (intermedium spectrum) with cascade schema of neutron flux multiplication [3];
- lead-bismuth ADS (fast neutron spectrum) [4] based on Russian submarine reactor as prototype [5].

The main characteristics of these reactors are presented in Table 1. In all the cases there are fixed the accelerator power (W_a = 10 MW, I_a = 1 mA, E_a = 1 GeV) and initial fuel composition (spent VVER-1000 fuel, 30 MW·years burning after 30 years storage, enriched with ^{239}Pu to the level necessary for keeping the fixed subcriticality Δk).

It is clear from Table 1 that the transmutation time τ_{in} is comparable with the lifetime of the reactor and this fact should be taken into account at all the discussions on closed NFC. It is clear also that minimal amount of TRU in closed NFC cannot be less than G_{TRU}^{equ} which essentially exceeds q_{MA} during the all period of the MA burner functioning. In this sense reactor-burner can be considered also as a storage of the concentrated TRU and its elimination is the special problem of the back end of nuclear power.

The contribution of fissile nuclides ε can be reduced essentially at the neutron flux high enough (see Figure 2). For the essential reduction of G_{TRU}^{equ} it is necessary to reduce τ and ε. The molten salt reactors has a definite advantage because in this case τ_{out} = 0 and the nuclear fuel reprocessing is essentially simplified.

Conclusion

The transition to the closed NFC requires the modification of the general approach to the efficiency estimations of the different reactor-burners and their NFC. Particularly in this case it is essential to turn attention not only on the MA transmutation rate q_{MA} but also on the equilibrium mass G_{TRU}^{equ} in total NFC which can be represented via transmutation time τ.

Figure 2: Dependence ε on the neutron flux Φ for different value k_∞ of molten salt reactor

At k_∞ = 1.12 (Δk = 0.05), $\Phi = 3 \cdot 10^{14}$ cm^{-2}·s^{-1} and ε = 2.9

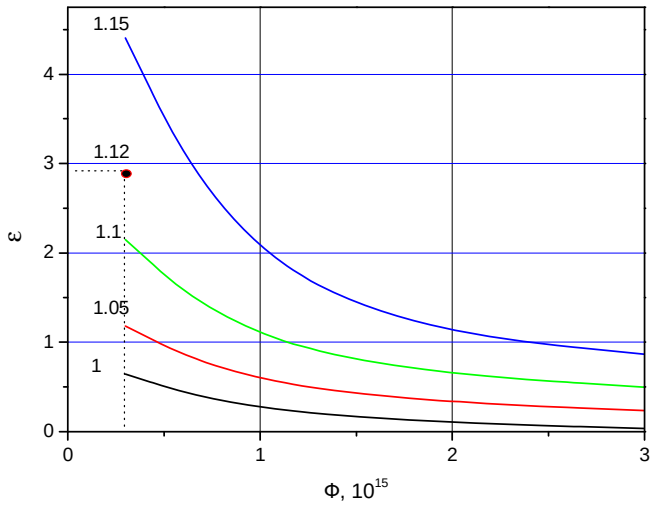

For comparison of the MA transmutation efficiency of ADS burners in the closed NFC we suggest to use three basic parameters:

- rate of MA transmutation, q [kg/year];
- transmutation time, τ [year];
- fraction of fissile nuclides (*e.g.* Pu), $\varepsilon = q_{Pu}/q_{MA}$.

Now we cannot make the final conclusion concerning the transmutation efficiency of the considered ADS burners because calculations are not yet completed. We will do this in the nearest future and compare the results with the efficiency of the critical reactor-burners using the same set of the comparison parameters.

Acknowledgements

This work was supported by grants of FAAE RF. We thank for E. Chekunov, O. Feinberg, O. Komlev, A. Myasnikov,K. Melnikov and M. Seregin for help and discussions.

References

[1] Gulevich, A., A. Kalugin, L. Ponomarev, V. Seliverstov, M. Seregin, "Comparative Study of ADS for Minor Actinides Transmutation", *Progress in Nuclear Energy*, 50, March-August, p. 358 (2008).

[2] Konev, V., V. Seliverstov, "Concept and Main Physics Characteristics of the Heavy Water Moderated Blanket with LEU fuel. Report on the Meeting on Use of LEU in ADS Assemblies", IAEA, Vienna, 10-12 October. In proceedings, IAEA-NEFW-651-T1-TM, 28939, p. 79 (2005). ISTC Project #17 (1996).

[3] Degtyarev, A.M., A.K. Kalugin, L.I. Ponomarev, "Cascade Subcritical Molten Salt Reactor (CSMSR): Main Features and Restrictions", *Progress in Nuclear Energy*, 47, 1-4, p. 99 (2005). See also A.M. Degtyarev, A.K. Kalugin, O.E. Kolyaskin, *et al.*, "Cascade Subcritical Molten-salt Reactor for Burning of the Transplutonium Elements", *Atomnaya Energiya*, 101, 2, p. 116 (2006).

[4] Pavlopoulos, P., C. Rubbia, A. Zrodnikov, *Nuclear Waste Burner (NWB) – an ADS Industrial Prototype for Minor Actinides Elimination*, IPPE, Obninsk (2003).

[5] Dragunov, Yu.G., N.M. Klimov, O.G. Komlev, *et al.*, "Nuclear Power Development in Market Conditions with Use of Multi-purpose Modular Fast Reactor SVBR-75/100", *Nuclear Engineering and Design*, 236, p. 1490 (2006).

Micro-hetero nuclear fuel related developments for near-perfect burning*

L. Popa-Simil
LAVM LLC
Los Alamos, NM, USA

Abstract

The actual nuclear reactors are using less than 30% of the present ^{235}U at a single pass through, that makes the total uranium resources usage to be about 0.2%, driving towards fuel cost increase and most probably to "uranium peak". The usage of low enriched largely mixed fuel pellets drives towards a high isotopic complexity nuclear waste, with a plurality of issues.

There is no doubt that the fission products are dangerous but the actual philosophy of sequestration on spot of the fission products, applied in the actual solid fuels making the nuclear reactor design similar to a high security prison, with more than seven layers of confinement applied successively to fission products turns to be counterproductive making any small enhancement very expensive. The new concept does not set free the fission product but offers them the chance to be removed from the nuclear reactor hot area, preventing neutron driven transmutation and the possibility of being separated and chemically stabilised leaving the reactor with less accumulated radioactivity.

The new fuel concept represents an extension of the 1 950th dispersion theory that gave birth to cermet materials, replacing the metal matrix with a neutron compliant liquid washing the fuel made like a beaded mesh soaked in the drain liquid. The main feature of the fuel is that it is made by several microns small fissile bead supported on a metal wire or fibre. The range of the fission products is bigger than the fuel bead diameter being at the base of the drastic nuclear fuel damage reduction.

Fission occurs inside the bead, giving birth to two fission products sharing about 170 MeV and flying apart and leaving the bead and stopping in the surrounding drain liquid insensitive to nuclear recoil damage. After stopping in the drain liquid the fission products are transported outside the high neutron flux zone, preventing further neutron-induced transmutations. Running under this mechanism the mass of the fuel bead is decreasing driving down the criticality. To compensate for this reactivity decrease there is possible to use the fuel's mesh elastic property and to compress the used fuel in order to compensate for the criticality loss by varying the drain liquid to fuel ratio. This feature generates new reactor designs that allow high fuel compression rate driving to ultra high burn-up at the limits of the micro-fuel safety limits. Burn-up factors higher than 90% are expected, driving to near perfect burning in OTTO cycle. The new "cerliq" fuel has the thermal conductivity increased by several times, allowing higher operating temperatures with higher conversion efficiency.

The fission products extraction capability with potential progressive separation is driving to new fuel waste management procedure, transforming the waste fuel into a very special ore for the technologies of the future. Though the work is still in progress, some preliminary results are presented.

* The full paper being unavailable at the time of preparation of this CD-ROM, only the abstract is included.

Nanograin-based fuel for ^{232}Th, and DU transmutation*

L. Popa-Simil
LAVM LLC
Los Alamos, NM, USA

Abstract

The actual nuclear fuel usage is of about 0.2%, driving towards fuel cost increase and most probably to "uranium peak", in the absence of significant improvements. The transmutation of ^{232}Thorium opens the way to resources over 1.5 10^9 kg of fuel, while the transmutation of ^{238}Uranium is making accessible for burning the entire amount of 35 10^9 kg, representing unrestricted energy for all the planetary needs, and space for several thousands of years if smartly used complementarily with renewable energies.

The usage of nanograin based nuclear fuel washed in a drainage liquid makes the fissile material extraction by using the recoil separation effect of the nuclear reaction, doubled by the exceptional properties of self repairing and enhanced defects rejection present in nanograins. The reaction is based on neutron absorption in nuclear reactor structures that drives to a transmuted isotope recoiled out of the lattice, directly by the nuclear recoil or rejected by the chemical incompatibility with the lattice and cluster enhanced defect rejection rate.

The nanograins are immersed in a drain liquid that collects the transmuted isotope and by gentle flow carries it outside the neutron flux zone, into a direct separation device. This procedure makes that the application of Urex or Purex processes to be significantly reduced, while the cost of newly produced fuel is decreasing, toward the cost of DU or thoria ore.

The design of such transmutation fuel has to consider all the parameters for the fuel used in the specific location of the nuclear reactor. The nanograin recoil separation is easily applicable for other material those radioactive isotopes are of medical or industrial importance, while for the transmutation of the nuclear fuel waste it presents separation and fabrication issues.

Though the work is still in progress, some preliminary results are presented.

* The full paper being unavailable at the time of preparation of this CD-ROM, only the abstract is included.

Parametric studies of an EFIT core with CERMET fuel

Xue-Nong Chen,[1] **Werner Maschek,**[1] **Ping Liu,**[1] **Andrei Rineiski,**[1] **Shisheng Wang,**[1]
Claudia Matzerath Boccaccini,[1] **Vitaly Sobolev,**[2] **Youpeng Zhang**[3]
[1]Forschungszentrum Karlsruhe, IKET, Karlsruhe, Germany
[2]SCK•CEN, Belgian Nuclear Research Centre, Mol, Belgium
[3]Reactor Physics Department, Kungliga Tekniska Högskolan (KTH), Stockholm, Sweden

Abstract

Within the framework of the EUROTRANS programme a European Facility for Industrial Transmutation (EFIT) is under development. This paper deals with the design and safety analyses of an EFIT core with Mo-matrix based CERMET fuel. A three-zone core design was developed, which satisfies the EFIT general and specific requirements. The fuel/matrix ratio in each zone is determined for a suitable subcritical level at a k_{eff} of about 0.97 and a total power peaking factor around 1.5.

The Pu/MA ratio determines the transmutation rate and the burn-up characteristics. The initial reference value is taken as Pu/MA = 46/54 at.%. Then it is reduced down to 35/65 at.% for optimising the reactivity swing and the MA transmutation efficiency. The effect of reduced Pu/MA ratio on the reactivity needs to be compensated by increasing the fuel volume fraction, which can be realised by reducing the pin number per SA and increasing the pin diameter. It is shown that the original coolant/clad thermal hydraulic conditions can be preserved, as the pin number is reduced and the fuel volume is increased. A good transmutation efficiency and an almost zero reactivity swing have been achieved by a 61-pin arrangement with Pu/MA = 35/65 at.%.

Based on the preliminary core design, the following parametric safety studies are performed: i) impact of subcriticality on the power shape and the clad temperature in the ULOF case; ii) impact of pressure drop on ULOF. It is shown that there is an optimal point at k_{eff} = 0.98, where the power peaking factor and the clad temperature under the ULOF condition are minimal. The pressure drop variation shows that the core is able to survive the ULOF under quite high pressure drop conditions.

Introduction

The European Facility for Industrial Transmutation (EFIT) is a conceptual design of an accelerator-driven transmuter (ADT) in an industrial scale. A key issue of the R&D work is the choice of an adequate fuel to be used in such an ADT. Within the EUROTRANS programme, especially in the AFTRA domain, various fuel forms have been assessed and CERCER and CERMET fuels, specifically the Mo and MgO matrices, have finally been selected and are now under closer investigation. The final recommendation on fuels by AFTRA gave a ranking of these fuels based on a number of criteria. The composite CERMET fuel $(Pu_{0.5},Am_{0.5})O_{2-x}$–Mo (with the isotope ^{92}Mo comprising 93% of the molybdenum) has been recommended as the primary candidate for the EFIT. This CERMET fuel fulfils adopted criteria for fabrication and reprocessing, and provides excellent safety margins. Disadvantages include the cost for enrichment of ^{92}Mo and a lower specific transmutation rate of minor actinides. The composite CERCER fuel $(Pu,MA)O_{2-x}$–MgO has therefore been recommended as a back-up solution as it may offer a higher consumption rate of minor actinides for a same Pu/MA ratio, and can be manufactured for a lower unit cost.

In the current investigation we concentrate on an EFIT with CERMET fuel. A three-zone core design was carried out, which satisfies the EFIT general and specific requirements and especially fits into the overall ANSALDO plant design for the EFIT [1]. According to the optimisation of the minor actinides (MA) transmutation, a so-called "0-42 approach" can be achieved by optimising the Pu/MA ratio, where Pu and MA are burned at rates of ~0 and ~42 kg/TWhth, respectively [2]. Therefore the Pu/MA ratio was initially fixed at 46/54 at.% for the current CERMET reference core design and the transient analyses, which is close to the optimised value 45.7/54.3 for the CERCER core [2]. The fuel/matrix volume ratios are used for flattening the radial power profile with an upper limit of the fuel content of 50 vol.%. The numbers of subassemblies (SA) and the associated fuel/matrix ratios in three zones are determined by the plant design, for a targeted subcritical level at k_{eff} about 0.97 and a required total peaking factor around 1.5.

A parametric study of the transmutation efficiency is made by changing the Pu/MA ratio. Generally reducing Pu/MA ratio is favourable to the MA transmutation efficiency. But this leads to a lower subcriticality k_{eff}. To compensate this effect, more fuel is needed in the core, where the Pu content has to be rather constant in order to keep k_{eff}, to be at a certain level. On the other side the good thermal conductivity of the CERMET fuel makes the fuel temperature not be a constraint and therefore allows thicker pins in the design. However, just simply to increase pin diameter will deteriorate the thermal hydraulic performance. An optimal solution is to reduce the pin number per SA and to enlarge the pin diameter in order to obtain more fuel and an equivalent thermal-hydraulic performance. Burn-up calculations are performed by an FZK code TRAIN [3] for Pu/MA = 46/54, 40/60 and 35/65. Promising results are obtained.

The preliminary core design has been analysed with SIMMER parametrically for variation of subcriticality under the operating condition and unprotected loss of flow (ULOF) conditions and for variation of pressure drop in the ULOF case. Because of the high fuel thermal conductivity, the fuel temperature is not a concern in all of cases investigated, but the clad temperature is generally the constraint in the core design. The variation of subcriticality shows that there is an optimal point at $k_{eff} = 0.98$ in this three-zone arrangement, where the power peaking factor and the clad temperature under the ULOF condition are minimal. The variation of the pressure drop shows that the core can survive a ULOF in a quite high pressure drop condition. It is concluded that the core has been designed, examined and optimised by possible parameter variations from the viewpoints of safety and transmutation.

Design of EFIT CERMET core

The ADT has a subcritical core. Protons from an accelerator hit a central lead target. As the result of a spallation process, neutrons will be supplied to the core. The heat removal in the pool design is established via forced convection flow through eight steam generators. In the past, various preliminary core design proposals were investigated in the AFTRA domain. The results have been reported in [4,5]. The current CERMET three-zone core design is adapted to the most recent EFIT overall plant design by [1,2]. The CERMET fuel has a high thermal conductivity and the restriction on the power density and the fuel temperature as for CERCER fuel can be relaxed. This means a larger pin

diameter can be chosen. To flatten the radial power profiles the "variable matrix technique" is applied. The cross plane of the current three-zone core and the SA/pin design are schematically depicted in Figure 1. Geometric SA/pin data are given in Table 1.

Figure 1: Cross plane of current AFTRA three-zone core and its SA and CERMET fuel pin arrangement

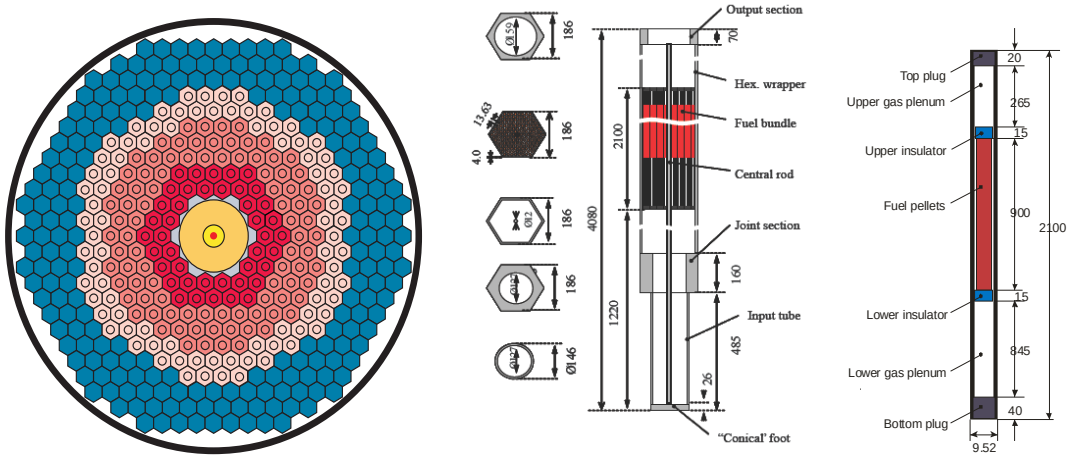

Table 1: SA and pin geometrical data

Parameter	CERCER-EFIT Inner/middle zone	CERMET-EFIT
Fuel SA pitch	191 mm	191 mm
Wrapper inner width	178 mm	178 mm
Wrapper thickness	4.0 mm	4.0 mm
Active core height	900 mm	900 mm
Fuel SA number	182	216

Parameter	CERCER-EFIT Inner/middle zone	CERMET-EFIT
Fuel pins per SA	168	168
Fuel pin pitch	13.63 mm	13.54 mm
Fuel pin diameter	8.62 mm	9.52 mm
Cladding thickness	0.6 mm	0.6 mm
Fuel pellet diameter	7.10 mm	8.00 mm

The main core and safety parameters are given in Table 2. The minor actinide vector of the fuel is typical for MOX fuel reprocessed 30 years after irradiation [6]. Because of the MA load, the safety parameters deteriorate: small beta-eff, no Doppler effect and a significant coolant void worth (about +7 300 pcm). A whole core voiding has a very low probability. However a partly core voiding and reactivity addition could be triggered, *e.g.* by a pin failure with helium fission gas release. The calculated void worth distribution is shown in Figure 2.

CERMET fuel pellet fabrication and its thermal property measurements have been carried out in AFTRA [7]. The calibrated thermal conductivities for this three zone design are presented in Figure 3. A T91-cladding creep test was recently carried out by CIEMAT experiments [8]. From these data one can extrapolate in a first guess the creep temperature limits for various fission gas pressures by the so-called Larson-Miller parameter, which is shown in Table 3. Recent results [9] suggest more pessimistic data and lower limits, but have not been taken into account in the current study.

Table 2: Thermal-hydraulic and neutronic parameters

Parameter	Value
Nominal thermal power	400 MW
Average linear power	122 W/cm
Av. fuel volumetric power	244 W/cm^3
k_{eff}	0.97336
Void worth	7 335 pcm
Inlet coolant temperature	673 K
Average coolant velocity	0.885 m/s
Axial peaking factor	1.174
Peak pin factor	1.075

Parameter	Value
Zone and total fuel assemblies	42 + 98 + 84 = 216
Fuel/matrix ratio in three zones	35:65, 43:57, 50:50
Pu/MA ratio	46/54 at.%
Effective beta	168.6 pcm
Doppler constant	68 pcm
Outlet coolant temperature	753 K
Overall pressure drop	1.1 bar (ref. value)
Radial peaking factor	1.230
Total peaking factor	1.552

Figure 2: Void worth distribution

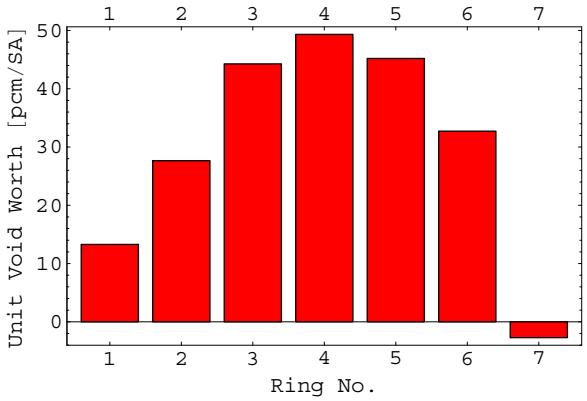

Table 3: Creep failure temperature limits in K for CERMET T91 steel pin

Gas pressure \ Failure time	0.1 s	1 s	10 s	2 min	30 min	10 h
1 MPa	1 342.58	1 279.97	1 222.94	1 166.83	1 111.27	1 055.66
5 MPa	1 315.21	1 253.87	1 198.00	1 143.04	1 088.61	1 034.14
10 MPa	1 281.77	1 222.00	1 167.55	1 113.99	1 060.94	1 007.85

Parametric studies

Burn-up calculations

It was shown and discussed in the past that MgO matrix (CERCER) fuel is slightly better than the Mo matrix (CERMET) fuel in the aspect of transmutation in the case of the same pin/SA geometry and same Pu/MA ratio. However, the much higher thermal conductivity of CERMET fuel makes a core design with thicker pins so suitable that the transmutation efficiency is improved.

A simple increase of the pin size without changing the pin number can reduce the Pu/MA ratio and can consequently improve the transmutation efficiency only to a certain extent, because the thermal-hydraulic performance becomes worse in this case, *e.g.* the clad temperature is significantly increased, especially in the ULOF case. Therefore this is not an optimal solution. But if we reduce the pin number per SA, we can obtain more fuel without deteriorating the thermal hydraulic/elastic performance.

Two variations of pin number are considered:

- *Variation 1*: To keep the coolant area, the clad thickness and the pin gap unchanged.
- *Variation 2*: To keep the coolant flow rate and the pressure drop unchanged and the clad thickness and the pin gap are increased proportionally to the pin diameter.

Variation 1 is straightforward. The pin diameter and the fuel volume fraction are given in Table 4. As the pin number is reduced, the pressure drop coefficient becomes smaller and therefore the thermal-hydraulic performance becomes better. But the clad/fuel thermal elastic performance becomes obviously worse. Variation 2 is not as explicit as Variation 1, but it provides really equivalent thermal-hydraulic/elastic conditions. The constant pressure drop and flow rate conditions provide a relationship between the coolant area and the hydraulic diameter, from which the pin diameter is determined. The results are shown in Table 5. Fortunately, for a certain pin number, both variations yield almost same fuel volume fraction. Therefore the neutronic burn-up calculations can be just performed for one variation and its results are approximately valid for the other as well.

Table 4: Pin number Variation 1: the coolant area, the clad thickness and the pin gap are unchanged

Pin number per SA	Pin diameter	Hydr. diameter	Clad thickness	Gap	Fuel diameter	Fuel vol. frac.
168+1 (12 mm)	9.52 mm	10.82 mm	0.6 mm	0.16 mm	8.00 mm	26.73%
127	11.00 mm	12.28 mm	0.6 mm	0.16 mm	9.48 mm	28.38%
91	13.00 mm	14.19 mm	0.6 mm	0.16 mm	11.48 mm	29.79%
61	15.87 mm	16.80 mm	0.6 mm	0.16 mm	14.35 mm	31.24%
61* out zone	16.87	15.97 mm	0.6 mm	0.16 mm	15.35 mm	35.74%

Table 5: Pin number Variation 2: the coolant flow rate and the pressure drop are unchanged, the clad thickness and the pin gap are proportional to the pin diameter

Pin number per SA	Pin diameter	Eff. hydr. diameter	Clad thickness	Gap	Fuel diameter	Fuel vol. frac.
169	9.520 mm	10.87 mm	0.6 mm	0.16 mm	8.00 mm	26.88%
127	11.274 mm	11.54 mm	0.71056 mm	0.18948 mm	9.47 mm	28.34%
91	13.695 mm	12.39 mm	0.86312 mm	0.23016 mm	11.51 mm	29.96%
61	17.233 mm	13.48 mm	1.08613 mm	0.28964 mm	14.48 mm	31.80%

Burn-up calculations are performed by applying the TRAIN code [3] with nuclear data JEFF-3.1 for Variation 1. The results are shown in Table 6. Thus the reactivity swing and the transmutation efficiency can be improved by reducing the Pu/MA ratio. For keeping the same k_{eff}, almost the same Pu mass is needed. This cannot be fully realised in the case of 61-pin. Therefore we have to use even thicker pins in the outer zone to compensate for the fuel shortage.

Table 6: Burn-up calculation results of pin number Variation 1

Pin number per SA	168+1	91	61	61 + thicker pins in outer zone
Pu/MA atom ratio over all	**46/54**	**40/60**	**35/65**	**35/65**
Power	**400 MW**	**400 MW**	**400 MW**	**400 MW**
Fuel vol. fraction in the core/the outer zone	26.73%	29.79%	31.24%	31.24%/35.75%
k_{eff} initial	0.9820	0.9724	0.9428	0.9667
k_{eff} after three years	0.9593	0.9625	0.9455	0.9660
Pu initial mass	3 055 kg	2 966 kg	2 726 kg	2 899 kg
MA initial mass	3 610 kg	4 479 kg	5 056 kg	5 377 kg
Pu consumption [kg/TWhth]	5.71	-1.06	-7.95	-7.22
U consumption [kg/TWhth]	-0.48	-0.49	-0.50	-0.51
Am consumption [kg/TWhth]	46.80	54.72	63.40	62.40
Cm consumption [kg/TWhth]	-9.70	-10.70	-12.27	-11.76
Np consumption [kg/TWhth]	0.86	0.96	0.60	0.44
MA consumption [kg/TWhth]	37.96	44.98	51.73	51.08

For the original Pu/MA = 46/54 the 400 MW core has a quite large reactivity loss of 2 324 pcm after a three-year operation. Its Pu and MA consumption rates are 5.71 and 37.96 kg/TWhth, respectively. For the optimised Pu/MA = 35/65 the reactivity loss is almost zero and the Pu and MA consumption rates are -7.22 and 51.08 kg/TWhth, respectively. This means that the CERMET fuel disadvantage of low transmutation efficiency can be completely overcome by using thicker pins and lower Pu/MA ratio.

Effect of subcritical level on the radial peaking factor

The steady-state equilibrium can be calculated by the SIMMER code, see [10]. The current three-zone arrangement with the suitable fuel/matrix ratios makes the radial temperature profiles quite flat and the total peaking factor less than 1.6.

The peaking factors, especially the radial peaking factor, are strongly dependent on the subcritical level, *i.e.* k_{eff}. In order to investigate its influence, we fix the zone arrangement and the fuel/matrix ratios, but change artificially the macroscopic neutron generation cross-section to get the desired

parametric k_{eff}. The results are presented with the radial power profiles at the core mid-plane in the left plot of Figure 5 and the total peaking factors in the right plot of Figure 5. It is well known that the peaking factor decreases as k_{eff} increases to approach one. But it is less well known that if k_{eff} is sufficiently close to one, *i.e.* larger than 0.98 in this case, the peaking factor stays almost constant and the peak fuel temperatures radially move from the inner zone to the middle zone. The k_{eff} is fixed for the design because of operational and safety reasons, but the results have some impact on the core behaviour under transient or accidental conditions, in case of a reactivity insertion. The main motivation of the study was to assess the pin failure propagation potential in the core regions with the high void worth under accidental reactivity increase conditions.

Figure 5: The radial power profiles at the core mid-plane (left) and the total peaking factors vs. k_{eff} (right)

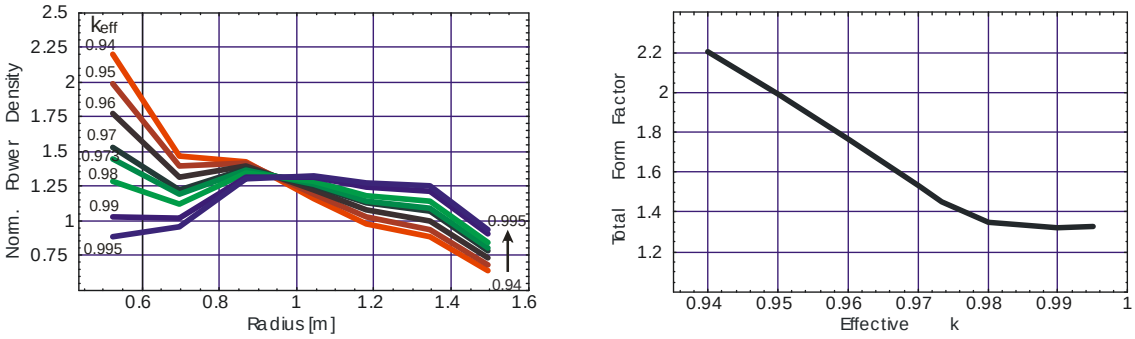

ULOF calculations

The unprotected loss of flow (ULOF) is taken as a typical accident for assessing the core safety behaviour. Favourably the core should survive this transient. As the liquid lead has good natural convection properties, after the primary coolant pump coasts down, the natural convection takes over the cooling function at a certain reduced mass flow rate. The remaining mass flow rate depends mainly on the pressure drop in the primary loop, the coolant temperature difference between the core outlet and inlet and the height of the steam generating units (SGU). The last two have been already fixed in the EFIT design, *e.g.* the SGU height (from core mid-plane to SGU mid-plane) is 3.7 m and the nominal temperature rise through the core is 80 K. The total pressure drop given in the ANSALDO design [1] was under discussion for a long time and therefore own parametric studies have been performed to optimise the pressure drop via design of the primary pump, the steam generating units, the subassembly in-and outlets and the grid spacers in the core. To study the pressure drop influence a range of parametric values has been investigated for the total pressure drop (from 0.64 bar to 1.6 bar under operational conditions). Due to the positive coolant feedback, the power increases about 1.6-2.6% during the ULOF transient for pressure drops varying from 0.64 to 1.6 bar.

In the ULOF case, the power increase is small and the fuel temperature is not a problem. Therefore only the maximal clad temperature and the maximal coolant velocity for various pressure drops are shown in Figure 6. We see that the maximal clad temperature will stabilise, after the pump coast down, at 960 K in the case of 0.64 bar pressure drop and at 1 050 K in the case of 1.6 bar. The former temperature value is well below the clad safety margin and the latter value means that the pin may withstand more than half an hour without clad creep failure under a high pin gas pressure of 5 MPa, assumed as pressure limit in the plenum (see Table 3).

Another issue here is to investigate the influence of subcritical level on ULOF. In Figure 7 the maximal clad temperature vs. k_{eff} curves are shown for the ULOF at the condition of 0.64 bar pressure drop. The maximal clad temperature has a minimum at about k_{eff} = 0.98. Due to the increasing peaking factor the clad temperature increases as k_{eff} decreases. Since the positive coolant feedback has an increasing effect on power as k_{eff} approaches unity, the clad temperature will also increase, as k_{eff} is close to one under the ULOF condition.

Figure 6: The maximal clad temperature and coolant velocity transients for difference drops for a slow pump stop process

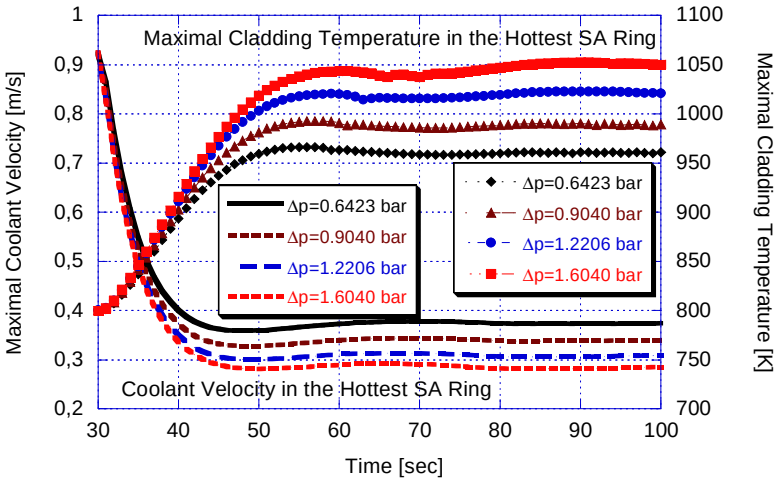

Figure 7: Maximal clad temperatures at steady state (lower) and in the ULOF case (upper) at the 0.64 bar pressure drop condition

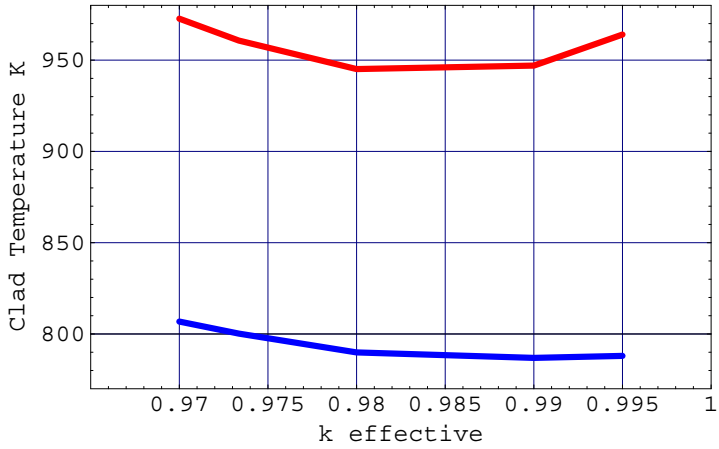

Conclusions

The conclusions of the present study are summarised as follows:

- An EFIT core with Mo-matrix based CERMET fuel has been developed fulfilling the required operational and safety criteria.
- The Pu/MA ratio has been optimised for better transmutation efficiency and an almost zero reactivity swing in a three-year operation. Because the fuel temperature is not a constraint for the current design due to the high thermal conductivity of CERMET fuel, the pin number reduction together with the increase of pin diameter provides an equivalent thermal-hydraulic condition, where more fuel in the core, consequently a lower Pu/MA ratio, can be realised. A CERMET core can be designed with a similarly good transmutation efficiency and limited reactivity swing as a CERCER core. As the fuel safety margins for CERMET are very high, one could also increase the power density of the core under the condition that the clad safety limits are not violated under transient conditions.

- Parametric safety studies show there is an optimal point for this core design at k_{eff} = 0.98, where the radial peaking factor in the operation condition and the clad temperature in the ULOF case are minimal.
- The CERMET EFIT core can survive a ULOF transient, even under high pressure drop conditions, *i.e.* without short time pin creep failures.

Acknowledgement

The authors appreciate the effort and support of all the scientists and institutions involved in IP EUROTRANS, as well as the financial support of the European Commission through the contract FI6W-CT-2004-516520.

References

[1] Mansani, L., *et al.*, *Main Components Functional Sizing of EFIT*, Deliverable D1.24, 6th Framework Programme EUROTRANS, DM1 DESIGN (2007).

[2] Sarotto, M., C. Artioli, V. Peluso, *Preliminary Neutronic Analysis of the Three Zones EFIT-MgO/Pb Core*, EUROTRANS-DM1-WP.1.2-Task 1.2.4, FPN-P9EH-002 (2007).

[3] Rineiski, A., "Decay Heat Production in a TRU Burner", *Progress in Nuclear Energy*, 50, 377-381 (2008).

[4] Maschek, W., X-N. Chen, C. Matzerath Boccaccini, A. Rineiski, J. Wallenius, V. Sobolev, P. Smith, R. Thetford, J-P. Ottaviani, S. Pillon, D. Haas, "First Results of Safety Analyses for ADTs with CERCER and CERMET Fuels Within the EUROTRANS-AFTRA Programme", *Actinide and Fission Product Partitioning & Transmutation, 9th Information Exchange Meeting*, Nimes, France, OECD/NEA, Paris (2006).

[5] Maschek, W., X-N. Chen, F. Delage, A. Fernandez-Carretero, D. Haas, C. Matzerath Boccaccini, A. Rineiski, P. Smith, V. Sobolev, R. Thetford, J. Wallenius, "Accelerator-driven Systems for Transmutation: Fuel Development, Design and Safety", *Progress in Nuclear Energy*, 50, 333-340 (2008).

[6] Sobolev, V., *et al.*, *Neutronic Performances of EFIT-400 (AFTRA) Reference Cores at the Beginning of Operation*, Deliverable D3.2, 6th Framework Programme EUROTRANS, DM3 AFTRA (2007).

[7] Staicu, D., *et al.*, *Measurement of Thermophysical Properties of the Inert Matrix Fuels (Zr,Pu,Am)O_2 + Mo, (Pu,Am)O_2 + Mo, ($Pu_{0.2}$,$Am_{0.8}$)O_2 + MgO and ($Pu_{0.5}$,$Am_{0.5}$)O_2 + MgO*, Deliverable D3.40b, 6th Framework Programme EUROTRANS, DM3 AFTRA (2006).

[8] Schikorr, M., D. Struwe, "Temperature Limits for XT-ADS Clad Material T91", *EUROTRANS: DM1 WP1.5 Safety Meeting*, Lyon, 10-11 October (2006).

[9] Fazio, C., "Progress in Structural Materials for Transmutation Devices", *EURATOM PARTRA Cluster Meeting*, FZK, Karlsruhe, Germany, 25-26 February (2008).

[10] Maschek, W., *et al.*, "SIMMER-III and SIMMER-IV Safety Code Development for Reactors with Transmutation Capability", *M&C 2005*, Avignon, France (2005).

New developments in actinide burning with symbiotic LWR-HTR-GCFR fuel cycles: Perspectives and challenges

E. Bomboni,[1] **N. Cerullo,**[1,2] **G. Lomonaco**[1]
[1]DIMNP – University of Pisa – CIRTEN – Pisa, Italy
[2]DIPTEM – University of Genova – Genova, Italy

Abstract

The long-term radiotoxicity of the final waste is currently one of the main drawbacks of nuclear power. Indeed, isotopes of neptunium and plutonium along with some long-lived fission products are dangerous for more than 100 000 years. Actually, 96% of the spent light water reactor (LWR) fuel consists of actinides, hence it is able to produce a lot of energy by fission if recycled. The effective exploitation of uranium resources is intrinsically connected with an effective actinides burning. At the moment, it is clear that these goals can be achieved only by combining different concepts of nuclear cores in a "symbiotic" way, as suggested in the frame of the Generation IV Initiative.

Light Water Reactor – (Very) High Temperature Reactor [(V)HTR] – Gas-cooled Fast Reactor (GCFR) symbiotic cycles have good capabilities as far as the integral actinide exploitation is concerned. Particularly, HTR fuelled by plutonium oxide is able to reach an ultra-high burn-up and to burn neptunium and plutonium effectively. In contrast, not negligible amounts of americium and curium build up in this core, although the total mass of heavy metals (HM) is strongly reduced. Americium and curium are characterised by a high radiological hazard as well. Nevertheless, at least plutonium from HTR (which is rich in non-fissile nuclides), neptunium and, if appropriate, americium can be used as a "driver" fuel for the GCFR along with large amounts of depleted uranium (DU): that is feasible with this kind of core thanks to its very good neutron economy.

This paper focuses on the potentialities of the LWR-HTR-GCFR fuel cycle, highlighting also the challenges (both from the technological and neutronic points of view) to face with while realising such a cycle. On the basis of the main technological constraints three possible (original) LWR-HTR-GCFR are proposed and their capabilities in actinides burning are assessed as well. Finally, some hints about designing an Am-Cm dedicated assembly are supplied.

1 Introduction

The main drawback of LWR technology is the limited exploitation of uranium resources coupled with the high-level long-term radiotoxicity of the final waste [it takes more than 100 000 years to balance the level of mine (LOM)]. Indeed, 96% of the LWR spent nuclear fuel (SNF) is composed of uranium, plutonium (see Table 1) and minor actinides (MA, *i.e.* neptunium, americium and curium, see Table 2).

Table 1: Spent LWR Pu composition (burn-up 33 GWd/tHM; initial enrichment 3.2% ^{235}U; 5 years cooling) [1]

	Isotope	Quantity [g/t HM]	Mass fraction [%]
Pu	^{238}Pu	140	1.5
	^{239}Pu	5 470	59.0
	^{240}Pu	2 230	24.0
	^{241}Pu	956	10.3
	^{242}Pu	486	5.2

Table 2: Spent LWR MA composition (burn-up 33 GWd/tHM; initial enrichment 3.2% ^{235}U; 5 years cooling) [1]

	Isotope	Quantity [g/t HM]	Mass fraction [%]
MA	^{237}Np	437	51.6
	^{241}Am	296	35.0
	^{243}Am	83.8	9.9
	^{242}Cm	6.2	0.7
	^{244}Cm	24	2.8

The long-term radiotoxicity of the nuclear waste is essentially due to transuranic (TRU) elements, and they can produce energy by fission directly or by means of transmutation into fissile nuclides. Consequently it is very promising to burn all HM as a fuel for nuclear reactors. For some extent this idea follows the older ones of (U,Pu) or (U,Th) cycles, observing that MA can be fertile or fissile as well. The choice of using innovative gas-cooled reactors (both HTR and GCFR) allows obtaining very high discharge burn-ups (typical of the fuel adopted for these reactors). Of course, burning all HM is not straightforward due to a lot of technological and neutronic open issues. Some of them are related to the very strong gamma and neutronic emissions of many MA nuclides as well as to the different dynamic behaviour of cores with a non-negligible MA inventory. Nevertheless, some reactor concepts seem to be particularly suitable for burning Pu and, for some extent, MA, such as helium-cooled thermal and fast reactors. This paper represents a first approach of design a kind of symbiotic LWR-HTR-GCFR fuel cycle, aiming at burning the nuclear waste producing meanwhile energy, and taking into account the current technological constraints to face with. Some approximations have had to be applied at this stage of development. Indeed the considered HTR pebble-bed core has been simulated by an infinite lattice of pebbles. In addition, neither a temperature profile nor a fuel equilibrium composition has been taken into account for GCFR.

In this connection, it is interesting to underline that the problem is a very complex one, and, at the moment, there are no codes that are able to fully simulate such a fuel cycle. Nevertheless these preliminary results can be considered a useful starting point in order to find out one among the possible ways to pursue in order to close the nuclear fuel cycle.

2 The potentialities of He-cooled reactors in plutonium and minor actinide burning

Some previous works have shown the very good capability of HTR cores in Pu and Np burning [2-4]. With its proven characteristics of "intrinsic" safety, HTR is one of the most promising core concepts in the frame of Generation IV Initiative [5]. Particularly, HTR can be loaded with a lot of different fuel compositions (also fertile-free fuels) without deterioration of their safety parameters, and they are able to reach ultra high burn-up (up to 750 GWd/tHM when fuelled with Pu oxide) thanks to their

peculiar fuel element, *i.e.* coated particles embedded, with low packing factors, in a graphite matrix. The flexibility in the fuel choice as well as the capability to reach high burn-up rates are important advantages in the frame of waste burning, although relatively large amounts of Am and Cm build up because of the high fluency reached by Pu-based fuel at end of cycle (EOC). In order to complete Pu[1] burning and to reduce Am and Cm amounts, a fast spectrum is probably a good choice, with some moderated regions if necessary. If compared with other fast reactor (FR) concepts, GCFR [2,6] is particularly flexible from the fuel choice point of view, essentially thanks to its very good neutron economy and the inert gaseous coolant. Indeed, the GCFR core is constituted of carbides (or nitrides) of HM, SiC as fuel matrix and structural material and He as coolant. Carbides and nitrides are characterised by a higher mass density of HM per unit volume than oxides, while using He as coolant and SiC as structural material makes lower the probability of parasitic capture. Additionally, the gaseous coolant reduces the positive void coefficient (typical of FR) strongly. These are the key features of the GCFR core, which is able to reach criticality with small fractions of "bad" quality Pu in large amounts of DU, as we are going to show in Section 4. That is of particular importance as far as the intrinsic safety of the core is concerned: indeed, large fractions of DU assure a quite large delayed neutrons fraction as well as a more negative fuel temperature coefficient.

3 Technological challenges in plutonium and minor actinide burning

As partially anticipated in previous paragraphs, closing the nuclear fuel cycle[2] would permit the possibility to close all the open issues regarding nuclear power, while assuring the energy supply world wide for the future centuries. Of course, there are some challenging aspects at the moment as far as partitioning and transmutation (P&T) are concerned. Probably, the best way to close the nuclear fuel cycle would be an integral fuel cycle (as proposed for GCFR reactors [5]). In such an approach, the reprocessed spent fuel from LWR is part of the feed for FR. Then, the spent fuel of FR is reprocessed *in situ*, and all HM are recovered together (*i.e.* without chemical separation of the different elements) and reused to produce new fuel for the same FR fleet (multiple *homogeneous* recycle), while FP constitutes the final waste. Such a strategy is at the moment quite challenging [7], because an economically feasible process is needed, allowing the possibility to treat highly radioactive materials and to extract HM with a very high efficiency (more than 99%). What's more, treating non-negligible quantities of MA (particularly Cm, due to its strong γ and neutron emissions) seems to be quite difficult due to radioprotection problems, particularly in large facilities and along with large amounts of all the other HM [7]. Additionally, all the processes involved should be very effective as far as the separation of HM from FP and the recoverability of reactants are concerned. Hence, at the moment it seems to be more feasible recycling U, Pu and Np and, if appropriate, Am. Indeed, Np can be partitioned during the PUREX process, although this procedure has not yet been developed on the industrial scale [7]. Regarding Cm, it seems to be advisable to store it temporarily, while waiting for its decay into Pu (the half-life of ^{244}Cm is around 18 years). Meanwhile, it is also challenging to separate it from Am due to their similar chemical behaviour [7]. Then, storing Cm substantially entails to store Am together as well, at least at the moment. On the other hand, Am and Cm could be recovered in some smaller dedicated facilities [7] and reused in dedicated assemblies (heterogeneous recycle) for critical reactors or for accelerator-driven systems (ADS). In this connection it is important to take into account that [8]:

- Recycling Cm produces non-negligible quantities of ^{252}Cf, which is a very strong neutrons emitter (much stronger than Cm itself) and, consequently, it is very difficult to be managed.
- The opportunity of recycling Am without Cm has to be deeply assessed: indeed, it does not reduce the long-term radiotoxicity very much (not more than a factor 10 or less, due to the production of Cm by neutron capture). That means, a challenging procedure of partitioning could eventually not be very effective from the long-term radiotoxicity reduction point of view.
- In principle, building dedicated facilities for Am and Cm recycling could not be economical.

1. After irradiation in a HTR, Pu isotopic vector is very "degraded", *i.e.* rich in ^{240}Pu and ^{242}Pu. Though such an isotopic composition is unsuitable for any thermal reactor, it can successfully be used as driver fuel in fast ones.
2. For example, all HM from mine is exploited to produce energy by fission, directly or indirectly by transmutation, it is then reprocessed and recycled; the final nuclear waste consists of only FP.

Of course, it is important to remember that there is still a lack of knowledge of MA-based advanced fuels (like carbides and nitrides), and new fabrication techniques have to be developed (*e.g.* to face with Am carbide and nitride volatility) [7].

As far as transmutation is concerned, a single reactor concept is probably not enough to burn HM effectively, but this purpose can be reached by chains of different reactors, each doing what the others are not able to do. LWR can be considered the starting point of all the possible chains, due to their current large diffusion world wide, their proven technology and reliability as well as, last but not least, the large amounts of LWR SNF world wide. Additionally, as shown above, LWR SNF is rich in fissionable elements. Nevertheless, it is not possible to burn HM completely in LWR because of neutronic reasons. Instead, FR can exploit Pu by breeding ^{238}U [2], thus increasing largely the availability of nuclear fuel, and their good neutron enables us to transmute even Pu isotopes and MA as well. Of course, thorough analyses are requested in order to use these new fuels, particularly concerning the dynamic behaviour of the core. Indeed, the introduction of relatively large fractions of Pu and MA tends to make worse the safety parameters like the fuel temperature coefficient (FTC) and the effective delayed neutrons fraction (β_{eff}). In this connection it is clear that cores with a high neutron economy are advisable, since they are able to reach and to maintain the criticality with small fractions of Pu.

On the basis of the considerations outlined until now, a fuel cycle scheme is proposed in the following paragraphs that involves current LWR, (V)HTR and GCFR in a "symbiotic" way in order to exploit nuclear waste (adding Pu, Np and depleted uranium from reprocessing plants if necessary) as fresh fuel, reducing strongly its initial quantity.

4 A general assessment of a LWR-HTR-GCFR fuel cycle

On the basis of what is explained in Section 3 and in [4], a LWR-HTR-GCFR cycle has been simulated using Monteburns© [9-11] and JEFF-3.1 libraries [12]. This cycle is aiming at producing energy by means of materials considered waste in a once-through cycle: Pu, MA and DU. In this way, a strong reduction of the total amount of waste (*i.e.* fission products, Am and Cm) per unit energy produced is envisaged. Indeed, GCFR is able to reuse its U, Pu and Np. Then, Pu and Np from GCFR do not have to be seen as waste but as fresh fuel for multiple recycles.

The main approximations introduced in our calculations are the following:

- HTR pebble-bed reactor modelled as a single pebble with white reflection as boundary condition [3].
- GCFR (2 400 MW_{th}, core "E" [6]) modelled explicitly but with axially and radially constant temperatures and fuel compositions. Each material (fuel, structural, coolant) is at a temperature that is different from the temperature of the other materials.
- The initial core of GCFR has been considered instead of the equilibrium core.

Three initial fuel compositions have been used for HTR, as explained in Figure 1.

Each composition is burnt in HTR, then it is reprocessed. Pu and Np are recovered and used as driver fuel of the GCFR core, while Am and Cm along with FP go to the repository. Figure 1 shows that Am and Cm could be recovered in a dedicated facility and loaded in some dedicated assemblies to burn in a GCFR. Of course, composition II (*i.e.* Pu+Am+Np *tout venant* from LWR, see Figure 1) might not be feasible, nevertheless it has been considered on the basis of [13]. Additionally, it could be useful in order to evaluate the impact of Am in the fuel. It is interesting to observe that HTR is able to reach very high burn-ups with all the proposed compositions (*i.e.* more than 500 GWd/tHM) and that GCFR is able to work with only 18% of Pu+Np. Considering the low quality of Pu coming from HTR, the very good neutron economy of the GCFR is highlighted. Fuel compositions at end of cycle (EOC) are shown in Figures 2 and 3.

Figure 1: Sketch of the proposed cycle

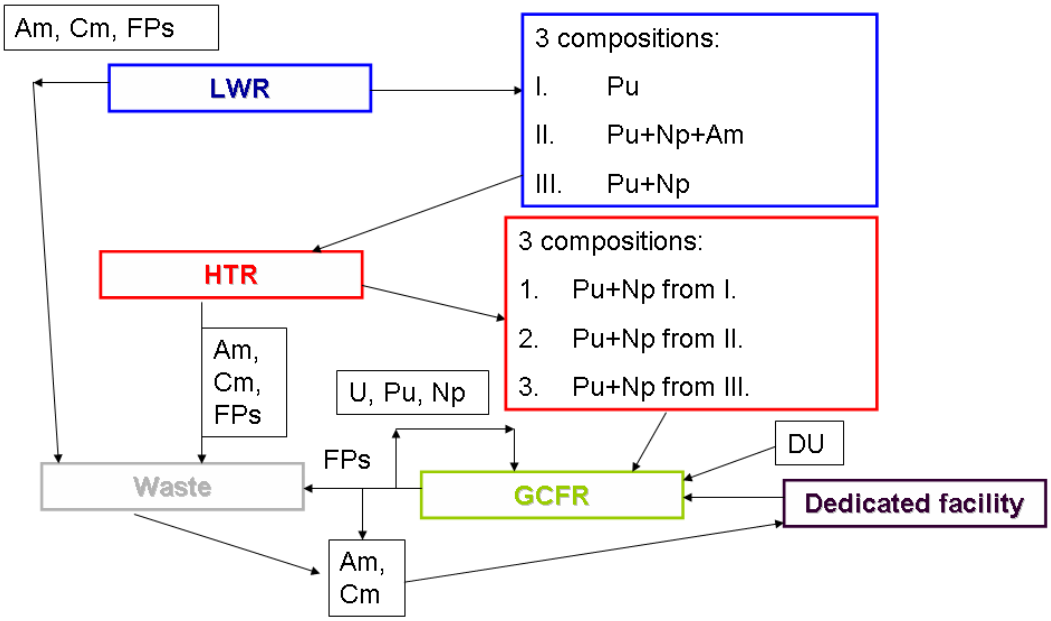

Figure 2: Masses of TRU nuclides at EOC for the three initial compositions in HTR

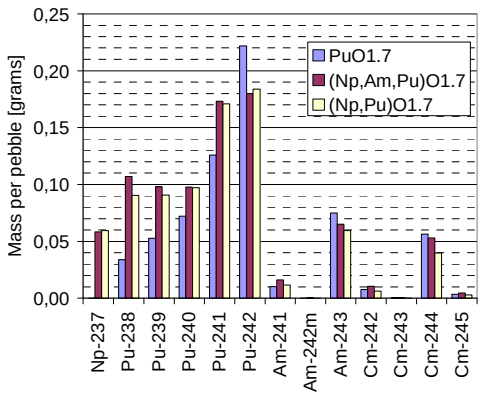

Figure 3: Masses of TRU nuclides at EOC for the three initial compositions in GCFR

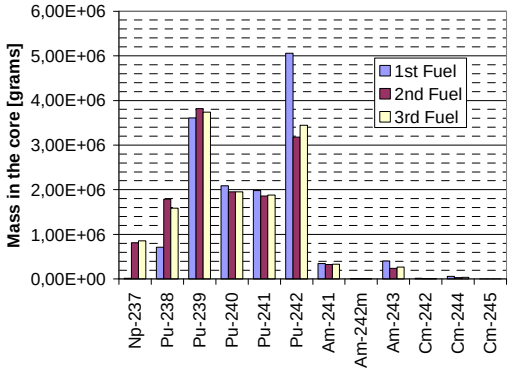

Tables 3 and 4 show fuel temperature coefficient (FTC) of HTR and FTC, void coefficient (VC) and effective delayed neutron fraction (β_{eff}) of GCFR at beginning of cycle (BOC) respectively, as a function of the fuel compositions. The other results are summarised in Tables 5 and 6. Negative values in Table 5 mean burning of the considered element. Values in the last three rows in Table 6 have been calculated taking into account the mass balance on the whole cycle. In this connection, it is to remember that each reactor of the considered chain is completely different from the others in kind, size, fuel inventory. Consequently, to assess the performances of the whole cycles, it has been assumed that all the useful material from a reactor (*i.e.* Pu, or Pu+Am+Np, or Pu+Np from LWR, and Pu+Np from HTR) is integrally recycled by a proper number of reactors staying in the following ring of the chain. Additionally, the residence times of the fuel in the different cores have taken into account as well.

Table 3: Fuel temperature coefficient (FTC) of HTR at BOC

Fuels	Pu	Pu+Am+Np	Pu+Np
FTC [pcm/K]	-2.16	-2.11	-1.16

Table 4: FTC, VC and β_{eff} of GCFR at BOC

	FTC [pcm/K]	VC [pcm/%void]	β_{eff} [pcm]
1st fuel	-1.56	1.81	443
2nd fuel	-0.69	1.61	434
3rd fuel	-1.87	1.57	537

Table 5: Mass produced per unit energy for the different kind of core and fuel compositions

	Np [g/GWh$_e$]	Pu [g/GWh$_e$]	Am \ [g/GWh$_e$]	Cm [g/GWh$_e$]
LWR – 33 GWd/tHM (initial enrichment: 3.2% ^{235}U) [1]	0.42	9.51	0.36	0.028
HTR I (Pu oxide) - ~650 GWd/tHM	4.54E-03	**-97.65**	5.83	4.19
HTR II (Pu+Am+Np oxide) – ~600 GWd/tHM	**-5.90**	**-85.91**	7.57E-03	5.03
HTR III (Pu+Np oxide) – ~550 GWd/tHM	**-6.05**	**-90.76**	5.29	3.72
GCFR (Pu+Np from spent HTR-I) – ~100 GWd/tHM	0.69	**-11.78**	23.17	2.35
GCFR (Pu+Np from spent HTR-II) – ~100 GWd/tHM	**-8.94**	**-1.81**	7.29	1.42
GCFR (Pu+Np from spent HTR-III) – ~100 GWd/tHM	**-9.56**	2.96E-03	18.30	1.56

Table 6: Mass of waste per unit energy for the different kind of core and for the proposed symbiotic cycles

	$\left[\frac{g_{Am+Cm}}{GWh_e}\right]$	$\left[\frac{g_{waste}}{GWh_e}\right]$
LWR – 33 GWd/tHM	0.39	951.29
HTR I (Pu oxide) - ~650 GWd/tHM	10.02	97.56
HTR II (Pu+Am+Np oxide) - ~600 GWd/tHM	5.03	92.60
HTR III (Pu+Np oxide) - ~550 GWd/tHM	9.02	97.33
GCFR (Pu+Np from spent HTR-I) – ~100 GWd/tHM	25.52	112.93
GCFR (Pu+Np from spent HTR-II) – ~100 GWd/tHM	8.72	96.12
GCFR (Pu+Np from spent HTR-III) – ~100 GWd/tHM	19.87	107.27
Cycle I	1.16	6.50
Cycle II	0.67	5.65
Cycle III	1.12	6.10

In agreement with previous works [2,3], HTR results a very good Pu and Np burner, while GCFR burns Np and keeps substantially constant the amount of Pu by breeding ^{238}U. Indeed, a close to zero breeding gain (BG) is envisaged for this core [6].

From the analysis of the results obtained, it is possible to deduce that:

- The smallest amount of Am+Cm per unit energy can be obtained separating as less as possible.
- Meanwhile, a higher average mass number produces larger quantities of Cm per unit energy.
- Recycling the most of HM together reduces the achievable burn-up and makes worse some safety parameters (*e.g.* reactivity coefficients).
- Both HTR and GCFR seem to be strongly proliferation resistant because of the composition of Pu coming from them, regardless of their initial fuel composition.
- The LWR-HTR-GCFR cycle is able to produce a lot of energy reducing strongly the mass of waste per unit energy and exploiting what is considered "waste" in the current once-through cycle.
- A symbiotic cycle, in which each sort of reactor uses the spent fuel of the previous one as fresh fuel, is more efficient than a cycle involving only one kind of reactor as far as the total amount of waste per unit energy is concerned.

Even though the performances of the LWR-HTR-GCFR cycle appear good, the final waste still contains a non-negligible quantity of Am and Cm. Then, the long-term radiotoxicity of the final waste is still an open issue.

5 The open issue of americium and curium burning

As explained in Section 3, homogeneous recycling is a very challenging strategy because of the strong γ and neutron emissions of Cm nuclides, as well as the problematic and not always well-known behaviours of Am- and Cm-based fuels. On the other hand, the results shown above as well as some previous works [2] have proven that Am and, above all, Cm amounts tend to increase when they are irradiated along with U and Pu.

Consequently, treating Am and Cm in some dedicated facilities and inserting these elements in dedicated assemblies is not only advantageous from the technological point of view, but also as far as their net reduction is concerned.

The design of such an assembly is a very complex work, because what follows has to be taken into account contemporarily:

- The assembly have to be compatible with materials, temperatures and irradiations conditions of the core in which it has to be inserted.
- Its composition has to be chosen in order to obtain a reasonable burning rate of Am and particularly of Cm: indeed, Cm is characterised by a quite small absorption cross-section, except for a narrow range between 100 eV and 500 eV [14]. The smaller the cross-section, the larger the fluency needed to transmute the considered nuclide.
- In order to obtain an effective transmutation rate, slightly moderated assemblies have to be used for Am and Cm burning in fast reactors, so that the high fluency that is a FR feature, can be coupled with larger cross-sections.
- If Am could be separated from Cm quite easily, it would be a good choice to design a dedicated assembly for Cm alone, as shown in [2].

Then, some preliminary analyses suggested us to design a dedicated assembly for GCFR, inserting carbides of Am and Cm in a SiC matrix [15]. Moreover, an opportune cooling time has also to be assessed for the decay of Cm in Pu. However, at this stage of development, the destruction rates obtained are not enough and a deep work of design and optimisation has still to be performed.

6 Conclusions

The flexibility both of HTR and GCFR cores allows us to design a fuel cycle boosted by the waste of the current once-through cycle (*i.e.* LWR Pu and Np). In that case, as a main consequence, the ratio between waste unloaded and energy produced falls down, passing from 950 grams of waste per GWh_e to less than 10 grams per GWh_e. Since Cm is difficult to be treated and to be separated from Am, we supposed that they are stored with FP, and, if necessary, they are recovered in some dedicated assemblies for GCFR. As a rule of thumb, homogeneous recycling tends to decrease the mass of waste per unit energy, but it increases the Cm inventory and it makes worse the safety parameters of the cores involved. Additionally, the higher the average mass number of the fuel, the higher the final amount of Cm at EOC. The isotopic composition of spent Pu from HTR and from GCFR makes it useless for proliferation purposes. Finally, designing a dedicated assembly to burn Am and, above all, Cm (along with the optimisation of cooling times) is probably the most promising way to close the LWR-HTR-GCFR cycle as well.

Acknowledgements

The work presented in this paper was partly funded by the European Union 6th Framework Programme, under contracts GCFR, PuMA and RAPHAEL. First of all we would like to thank Dr. Somers of ITU, Dr. Mitchell of AMEC-NNC, Dr. Kuijper and Dr. van Heek both of NRG, Prof. Kloosterman of TUD, Dr. von Lensa of FZJ for the collaboration. Finally we want to thank Prof. Forasassi of DIMNP for his strong support and Dr. Bufalino of SORIT for his precious suggestions and help.

References

[1] *Nuclear Fuel Cycle Simulation System (VISTA)*, IAEA-TECDOC-1535, IAEA, Vienna, February (2007).

[2] Bomboni, E., N. Cerullo, G. Lomonaco, V. Romanello, "A Critical Review of the Recent Improvements in Minimizing Nuclear Waste by Innovative Gas Cooled Reactors", *Science and Technology of Nuclear Installations*, Volume 2008, Article ID 265430, 18 pages, Hindawi Publishing Corporation, doi:10.1155/2008/265430.

[3] Bende, E.E., *Plutonium Burning in a Pebble-bed Type High Temperature Nuclear Reactor*, Ph.D. Thesis, NRG Petten (2000).

[4] *www.puma-project.eu*.

[5] US DOE Nuclear Energy Research Advisory Committee and the Generation IV International Forum.

[6] *www.gcfr.org*.

[7] Somers, J., Private communication, Karlsruhe, May 2008.

[8] Salvatores, M., C. Chabert. I. Slessarev, G. Youinou, "Intercomparison of Systems for TRU Recycling at Equilibrium", *Proceedings of GLOBAL 2005*, Tsukuba, Japan, 9-13 October 2005.

[9] Poston, D.L., H.R. Trellue, *User's Manual Version 2.0 for Monteburns 1.0*, LA-UR-99-4999, September (1999).

[10] Briefmeister, J.F., *MCNP™ – A General Monte Carlo n-Particle Transport Code*, Los Alamos National Laboratory, Version 5, LA-CP-03-0245.

[11] Croff, G., *A User's Manual for the ORIGEN2 Computer Code*, ORNL/TM-7175, July (1980).

[12] Haeck, W., B. Verboomen, *A Validated MCNP(X) Cross Section Library based on JEFF3.1*, Open Report, SCK•CEN-BLG-1034 Rev0, October (2006).

[13] Haas, J.B.M. de, J.C. Kuijper, *A Simplified Pebble Bed HTGR Design*, Under contract of the EU FP6 Project PUMA – Contribution to Deliverable D121, NRG, Petten, The Netherlands, 04 June (2008).

[14] *www.atom.kaeri.kr.re*.

[15] Verrall, R.A., M.D. Vlajic, V.D. Krstic, "Silicon Carbide as an Inert Matrix for a Thermal Reactor Fuel", *Journal of Nuclear Materials*, 274, 54÷60 (1999).

Development of PASCAR (proliferation-resistant, accident-tolerant, self-sustainable, capsular, assured reactor) design and safety analysis*

I-S. Hwang, M-H. Kim, H-G. Joo, B. Yoo, M-H. Kim, S-R. Oh, K-W. Yi, J-Y. Lim, D-Y. Han, J. Lim, H-O. Nam, J-H. Cho, K-Y. Lee, M-H. Bae, S-Y. Choi, C-H. Kim, S-H. Kim
Nuclear Transmutation Energy Research Centre of Korea (NUTRECK)
Seoul National University
Seoul, Republic of Korea

Abstract

Liquid lead-bismuth eutectic has outstanding property as a fast reactors coolant: natural circulation ability, shielding capability of chemically stable and fair neutron spectrum for transmutation. Based on these qualities, a lead-bismuth coolant fast reactor, PASCAR (Proliferation-resistant, Accident-tolerant, Self-sustainable, Capsular, Assured Reactor) was designed by NUTRECK (Nuclear Transmutation Energy Reach Centre of Korea). The class of design employs a pool-type integral reactor capsule including a core of metallic fuel rods in open-square lattice and coolers in the outer downcomer. It can deliver thermal power of up to 100 MW by LBE natural circulation between the core near its bottom and coolers near the top. The natural circulation capability leads to uncompromised accident-tolerance and the corrosion-resistance of materials ensures up to 60 years of capsule life are being demonstrated with the help of HELIOS experiments and MARS® computer simulation code. The elimination of the rotating machineries from the primary system and the utilisation of the advanced structural materials as well as the reduction of hot-leg temperature enable maintenance-free continual operations such a long time. To tolerate severe seismic loadings, the entire capsule is to be placed on a monolithic underground foundation through overhung supports with three-dimensional seismic isolations. The modularised core and steam generators can be replaced with new ones if necessary and the spent fuel module is sent to a pyroprocess plant at the end of life. This paper attempts to describe the design of PASCAR and assess the safety of the reactor.

* The full paper being unavailable at the time of preparation of this CD-ROM, only the abstract is included.

Main results of IAEA CRP "Studies of Advanced Options for Effective Incineration of Radioactive Waste": Case for molten salt transmuter

V. Ignatiev,[1] **D. Da Cruz,**[2] **S. Dulla,**[3] **O. Feynberg,**[1] **M. Kormilitsin,**[4]
E. Malambu,[5] **W. Maschek,**[6] **P. Ravetto,**[3] **A. Rineiski,**[6] **M. Schikorr,**[6]
A. Stanculescu,[7] **V. Subbotin,**[8] **M. Szieberth,**[9] **J. Uhlir,**[10] **R. Zakirov**[8]
[1]RRC-KI, Russia; [2]NRG, Netherlands; [3]Politecnico di Torino, Italy; [4]RIIAR, Russia; [5]SCK•CEN, Belgium; [6]FZK, Germany; [7]IAEA, Austria; [8]VNIITF, Russia; [9]BUTE, Hungary; [10]NRI, Czech Republic

Abstract

The main goal of the IAEA Co-ordinated Research Project (CRP) on "Studies of Advanced Reactor Technology Options for Effective Incineration of Radioactive Waste" was to deepen the understanding of the dynamics of transmutation systems, to qualify the available methods, specify their range of validity, and formulate requirements for future theoretical developments. Twenty institutions from 15 member states and three international organisations have actively participated in this CRP. The comparative investigations cover burner reactors and transmuters both containing fertile and fertile-free fuels. The systems are designed either as neutronically critical or subcritical (hybrid) driven by an external neutron source. The neutron spectra of the reactors extend from low thermal to fusion neutron energy levels. Further, both systems with solid fuels and molten salt fuels are compared. The solid fuel systems investigated cover also the impact of various coolants from sodium to heavy liquid metals and gas.

Within this CRP critical fertile and fertile-free fuel concepts of the thermal molten salt reactor (MSR) were investigated in their transmutation capabilities, their safety related parameters (reactivity coefficients, effective delayed neutron fraction, etc.) and transient analyses for simulating relevant hypothetical accidents as well as fuel cycle reprocessing implications. In this paper the main focus is placed on transient analyses of single stream Li, Na,Be/F Molten Salt Actinide Recycler and Transmuter (MOSART) system fuelled with compositions of plutonium plus minor actinide trifluorides (AnF_3) from UOX LWR spent fuel without U-Th support.

Introduction

Recent years have demonstrated a growing interest in the nuclear energy systems employing the technology of molten salt fluorides. Among the systems selected in GIF Generation IV, molten salt reactors (MSR) present a promising flexible option in response to the goals and criteria assigned to future nuclear systems: fuel cycle sustainability, safety, environmental impact, proliferation resistance, diversity of applications and economics [1].

Molten salt reactor (MSR) systems have been under development since 1947 and extensive experience with fluoride-based salts has been accumulated [2,3]. Various compositions of UF_4 and ThF_4 dissolved in ^7LiF-BeF_2 system have been considered for fuel salt. The most likely choice for reference Molten Salt Breeder Reactor (MSBR) designs was dealt with 72LiF-16BeF_2-12ThF_4 (mole %) mixture. TRU burning was not the original development goal for the MSBR concept. The main questions arising from TRU fuelling include: evaluation of alternative fuel salt composition, adequate constituent solubilities, new redox buffer for systems without uranium, analytical chemistry instrumentation, corrosion and container chemistry, suitable fuel processing, waste form development and safety aspects.

Several design options of the thermal molten salt reactor concept were investigated within the CRP framework in their transmutation capabilities, their safety characteristics, and fuel cycle reprocessing implications. As reference design was selected the MSBR as designed by ORNL during the early 1970s. From this, two AMSTER concepts, as proposed and designed by EdF, are investigated in more detail. One AMSTER concept (AMSTER-Incinerator) focuses on the transmutation of actinides, the other concept (AMSTER-Breeder) focuses on optimising the fissile fuel sustainability as well as incineration [4].

Graphite thermalised incinerator concepts offer the advantages of both a small fissile inventory, concept and inherent safety features. But they absolutely require using a Th support in case of multiple recycle of minor actinides. Whatever graphite moderated MSR incinerator is considered, the amount of minor actinides, and especially ^{244}Cm and ^{252}Cf, is very large (several hundred of kg of ^{244}Cm at equilibrium per 1 Gwe), and would rise very serious safety, criticality and maintenance problems, and surely an awkward complication of the fuel salt reprocessing. The total temperature coefficient for MSBR, has values close to zero, if erbium is not added to the graphite matrix. Moreover, both fuel and graphite coefficients display non-negligible variations with temperature, leading to quite complex and unpredictable long term transient behaviour (if the operator does not intervene, of course) [1].

Another system studied within the CRP framework is Molten Salt Actinide Recycler and Transmuter (MOSART) concept with fertile-free fuel [5,6]. This non-moderated MSR is efficient for actinide burning because fast spectrum is favourable for TRU burning. This is due to the probability of fission per neutron absorbed which is much higher in fast spectrum than in thermal spectrum, and especially for isotopes non fissionable by thermal neutrons (^{244}Cm, ^{242}Pu, ^{240}Pu, ^{241}Am…). Optimal MSR burner has no fertile elements (Th or ^{238}U). Constraint with that type of reactor is to stay below the $TRUF_3$ solubility limit. Non-moderated MSR burners allow fuel without fertile isotope (with a very bad Doppler effect) thanks to the highly negative salt dilatation coefficient. In-core fluid fuel expansion due to a rise in temperature in the reactor core reduces not only fluid density, but also the amount of fissile material in the core thus reducing reactivity. The system without moderator offered the prospect therefore have being self-regulating and the reactor experiments that were operated showed that the classical control rod absorber system was not necessary. Non-moderated MSR breeders are the only breeder with a negative coolant dilatation (or void) effect (unlike solid fuel FBR) [1].

The CRP study on MSR consisted of two main parts: *i*) neutronics analyses benchmarks on computing safety parameters (reactivity coefficients, effective delayed neutron fraction, etc.); *ii*) transient analyses, which are supported by neutronics studies, for simulating relevant hypothetical accidents. Results of Part 1 studies were described in detail earlier [3]. This paper is focused on transient analyses of MOSART concept, which are supported by neutronics studies, for simulating relevant hypothetical accidents.

General description of MOSART concept

MOSART is a single-stream fast-spectrum MSR fuelled with different compositions of plutonium and minor actinides from LWR SNF without the use of uranium or thorium. The start-up and feed material

scenarios include plutonium and minor actinides from PWR enriched uranium (Scenario 1) or mixed-oxide SNF (Scenario 2). The fuel-salt mixture is 15LiF-58NaF-27BeF_2 (mole %) with a melting point of 479°C. Depending upon the feed material, the salt at equilibrium contains 1.05 to 1.3 mole % of actinide trifluorides. Transient to equilibrium in the 2 400-MW(t) MOSART core requires about 10 years. Masses of plutonium and minor actinides in the primary circuit at equilibrium for Scenario 1 and Scenario 2 are respectively 7 320 kg and 9 346 kg. The specific salt was chosen, in part, because of its high solubility (> 2 mole % at 600°C) for actinide and lanthanide trifluorides – a requirement for TRU burning. The salt is sparged for removal of tritium, xenon, and krypton. The salt processing system removes the soluble fission products (rare-earth trifluorides) with an average residence time in the reactor of 300 effective full-power days. More rapid processing would reduce parasitic neutron losses but it would also increase the losses of actinides to the waste stream. The lithium is enriched to 99.99% ^{7}Li. There is, of course, not one possible arrangement of MOSART unit. Figure 1 show the preliminary design configuration that is used here to evaluate its neutronics and thermal-hydraulics feasibility. Design parameters of MOSART fuel circuit are summarised in Table 1.

The 2400-MW(t) MOSART system has a homogeneous core with intermediate-to-fast neutron spectrum. The core diameter is 3.4 m with a core height of 3.6 m. The core has 0.2-meter radial and axial graphite reflectors. The specific power is 43 W/cm^3, with an effective neutron flux of about 1 x 10^{15} n cm^{-2} s^{-1}. The salt inlet temperature is 600° with an average outlet temperature of 715°C. The core inlet structure is designed to assure (1) the maximum temperature of the solid reflectors is controlled to assure reasonable lifetimes and (2) no reverse or stagnate flow. The mechanical design of the balance of the nuclear system includes four pumps operating in parallel with an out-of-core circulation time of ~4 s. Pumps circulate salt through heat exchangers and return it to a common plenum at the bottom of the reactor vessel. Heat is transferred from the primary salt to the power conversion system using a secondary NaF-$NaBF_4$ salt with a composition of 8–92 mole%. Provisions are made for maintaining fission products at low required level by continuous fuel salt processing.

Table 1: Design parameters of MOSART fuel circuit

Thermal capacity, MWt	2 400
Reactor vessel ID, m	6.77
Vessel wall thickness, cm	5.5
Vessel design pressure, N/m^2	$5.2 \cdot 10^5$
Core height, m	3.6
Radial thickness of reflector, cm	20
Volume fraction of salt in core	1
Average core power density, MW/m^3	75.0
Peak core power density, MW/m^3	163
Average neutron flux, n·cm^{-2}·s^{-1}	10^{15}
Max graphite damage flux, n·cm^{-2}·s^{-1}	$1.45 \cdot 10^{14}$(>180 keV)
Graphite temperature at max graphite damage, K	1 084
Estimated useful life of graphite, yrs	3-4
Total weight of graphite in the reactor, t	20
Average flow velocity of salt in core, m/s	0.5
Total fuel salt in reactor vessel, m^3	40.4
Outer diameter of one heat exchanger, D_2, m	1.05
Total number of tubes in four heat exchangers, N	18 591
Length of one heat exchanger, l, m	6.6
Total volume of fuel salt in heat exchangers tubes, V, m^3	6.2
Heat transfer coefficient, α_1, W/m^2	17 100
Heat transfer coefficient, α_2, W/m^2	17 656
Overall heat transfer coefficient, K_Σ, W/m^2	5 700
Pressure drop in heat exchangers, ΔP_h, kPa	660
Pressure drop in core, kPa	3.7
Pressure drop in main circulation pipes, kPa	180
Total pressure drop in the fuel circuit, kPa	840

Figure 1: MOSART core

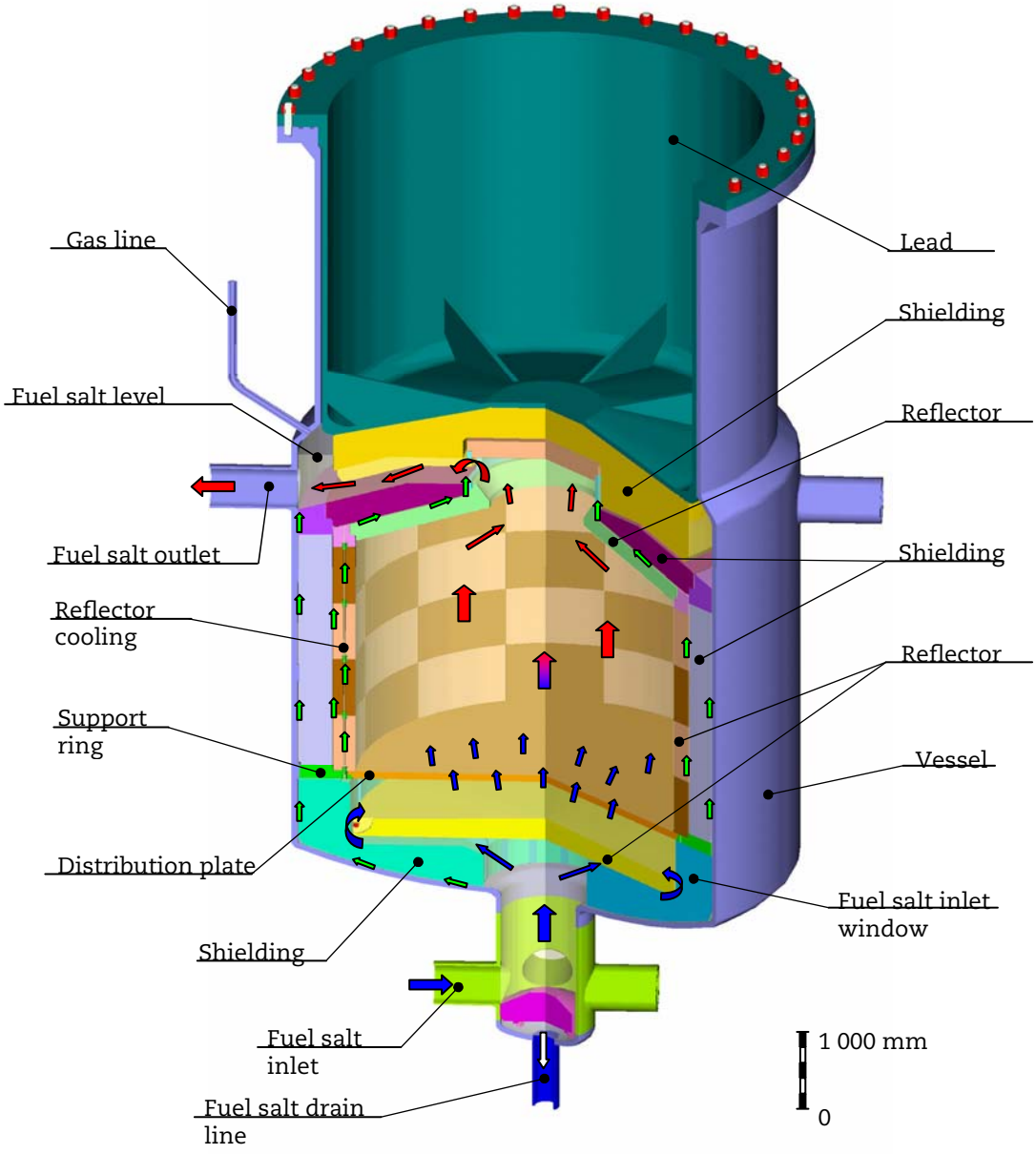

Safety-related issues and possible transient initiators for detailed analysis

MSR can be operated with acceptable effect on the environment and safety of the public provided that the radioactive liquids and gases that circulate throughout much of the plant are managed carefully. Because the MSR processing plant is attached directly to the reactor, there is no need for shipment of short-cooled fuel. Fission products extracted from the fuel salt are stored as solids or concentrated noble gases for shipment after long decay.

With regard to safety from severe accidents, the use of fluid fuel places some special requirements on the design and operation of an MSR. At the same time, it eases or eliminates some requirements that are important in solid fuel reactors (*e.g.* mitigation of severe accidents with core meltdown). Although it is clear *a priori* that different measures must be taken to ensure safety, whether these measures are more or less complex and expensive in an MSR than in other reactor systems can be determined only by a comprehensive analysis that begins with the most basic considerations.

The general principles of nuclear safety in MSR are the same as for all reactors. Small fluctuations in reactivity should produce only highly dumped power oscillations. Large, rapid increases in reactivity should be difficult to produce and be easily controlled before the resulting power excursions produce damaging temperature or pressure excursions. The continuous removal of fission products and the adjustment of fissile inventory in the fuel salt during operation of the MSR minimise amount of excess reactivity that must be compensated by control rods and hence limit the potential for rapid increases in reactivity associated with this excess.

Special initiating events, which could lead to the reactivity changes in MSR are summarised below [2]:

- change of the effective delayed neutron fraction due to the stopping and starting fuel circulation;
- increase of the fissile materials concentration in the fuel;
- changes in the fuel composition and density (voiding of fuel channels, changes in the gas fraction in the fuel and a primary circuit overcooling).

In all of these transients, we can assume that the xenon continuous extraction from the salt was ~100% efficient, so that no significant amount of xenon remains inside the fuel salt.

A unique consideration in fluid-fuel reactors is the possibility of inhomogeneity of the fissile material in the circulating fuel. Specifically of concern is gradual segregation of fissile material outside the core, followed by rapid introduction with the incoming stream. The MSR fuel salt is quite stable over a range of conditions much wider than the anticipated deviations. In Th-U MSR segregation of uranium could conceivably be produced by introduction of reducing agents or oxygen into the salt, but adequate protection against this should be provided in the MSR (*e.g.* gettering action of the ZrF_4 for H_2O major impurity). The principle components of MOSART fuel mixture do not form intermediate compounds with PuF_3. It is anticipated therefore that in concentrations at which PuF_3 would be used, it would not be deposited preferentially from the bulk salt during the inadvertent freezing, nor at locations such as in freeze valves.

MOSART operation would require routine additions of fresh fissile fuel in the amount of about 20 kg per week. Also, the fissile material in the processing systems amounts to about 1% of the reactor inventory. If these materials could be added to the reactor, the excess reactivity would be increased up to 500 pcm or even less. Furthermore, conceivable rates of introduction are quite inconsequential, and any unwanted reactivity increase from these sources can easily be stopped.

The response of the nuclear power to reactivity increases is governed by the temperature coefficients of reactivity and the action of the control rods and safety rods. Because the delayed neutron fraction will be unusually small in case of U-Th system and TRU incinerator, the MSR power responds rapidly to reactivity increases.

MOSART safety assessments show that the parameters are favourable for reactor safety, primarily because of the large negative density and fuel Doppler effects. The temperature reactivity coefficients vary from -4.125 (Scenario 1) to -6.625 pcm/°C (Scenario 2), depending upon the feed [6]. This is for a pure actinide burner with no uranium or thorium. The option exists to add a thorium-containing salt blanket to produce fissile material.

Transients analysed for MOSART

Four basic transients have been analysed with the SIM-ADS code in the MOSART concept [7]:

- An unprotected loss of flow (ULOF), assuming loss of forced circulation in the primary system due to pump failure. The core inlet temperature is assumed to remain constant. The mass flow rate of the fuel salt is assumed to stabilise after 7 seconds at about 4% of its nominal value (natural convection).
- An unprotected loss of heat sink (ULOH) in which the heat sink is assumed to totally fail.
- An unprotected primary circuit overcooling transient, with the inlet temperature reduced by 100°C in 60 sec.

- Several unprotected transients over power (UTOP) due to a +200 pcm and a +500 pcm reactivity insertion. This transient is assumed initiated by a particle becoming dislodged from the walls of the loop (fissile fuel agglomeration due to precipitation); two different cases will be investigated. In one case, the particle is assumed to become lodged inside the core region (this case is somewhat hypothetical in the MOSART design since no surface areas inside the core region are foreseen aside of possible flow diverters and the reflector surfaces); the second case assumes that the particle transits repeatedly the core region; the core inlet temperature is assumed to remain constant during all UTOP transients.

The transient initiators selected for detailed analyses are listed in Table 2. Also listed in the table are the underlying assumptions under which the specific transients were analysed. The results of the unprotected loss of flow (ULOF), unprotected loss of heat sink (ULOH), overcooling transient of the core, and the unprotected transient overpower transient (UTOP) are displayed in Figures 2 to 6. For each transient two figures are provided. In the first figure, the dynamic response of the normalised thermal reactor power, neutron flux and mass flow rate are displayed. In the second figure, the dynamic response of the molten salt core outlet-, average core-, core inlet-, and average bulk graphite temperatures are shown.

Table 2: List of transients analysed

Number	Transient	Description
MOSART		
U-1	ULOF	Loss of forced circulations in primary and secondary system, core inlet temperature is assumed to remain constant
U-2	ULOH	Loss of heat sinks (HX failure)
U-3	Over-cooling of primary side	Core inlet temperature drops by 100°C in 60 sec
U-4a	UTOP	200 pcm jump in reactivity at HFP due to agglomerated fissile particle that is assumed to remain lodged inside the core region, coolant inlet temperature will remain constant
U-4b	UTOP	200 pcm jump in reactivity at HFP due to agglomerated fissile particle that is assumed to repeatedly transit the core region, coolant inlet temperature will remain constant
U-5a	UTOP	500 pcm jump in reactivity at HFP due to agglomerated fissile particle that is assumed to remain lodged inside the core region, coolant inlet temperature will remain constant
U-5b	UTOP	500 pcm jump in reactivity at HFP due to agglomerated fissile particle that is assumed to repeatedly transit the core region, coolant inlet temperature will remain constant

ULOF transient

For the ULOF transient, Figure 2, the mass flow rate drops to the natural convection flow rate (about 4% of nominal flow is assumed) shortly after pump failure. Control rods are postulated not to insert into the core. The loss of flow rate in circulating fuel reactors implies an insertion of positive reactivity. In the case of MSBR, with β_{eff} *static* = 340 pcm, this reactivity insertion due to the loss of fuel circulation is +82.9 pcm (β_{loss} = -82.9 pcm), or +24.4%.

Both fuel average and fuel outlet temperatures are observed to rise rapidly to ~740°C and ~880°C respectively at about 50 sec into the transient as a result of the fast decreasing mass flow rate. Since the temperature coefficient of the fuel is strongly negative, namely ~-4.125 pcm/°C, sufficient negative reactivity is being inserted into the reactor to counterbalance the positive reactivity increase associated with the loss of fuel circulation. The net effect is a fast decrease in the power level to below 10% after 50 s into the transient.

Concurrent with the initial fast rise in the fuel temperatures is the relatively slow rise in the reflector graphite temperature. Due to the negative graphite reactivity coefficient of ~-0.04 pcm/°C, another negative reactivity is now slowly inserted into the core. After 240 sec into the transient, both outlet fuel temperature and bulk graphite temperature assume about the same value, namely 770°C. The net reactivity, *i.e.* the sum of the fuel and the graphite coefficient remains negative, namely

~-4.165 pcm/°C. This assures a continued decrease in reactor power with a concurrent decrease of both fuel average and outlet temperatures after the peak temperatures 50 sec into the transient have been reached.

Temperature exposure of the vessel and the outlet loop exceeding 850°C is observed to be limited in time to ~130 sec. The system is expected not be seriously challenged by this transient since all temperatures will be below nominal temperatures after ~350 sec after initiation of this transient.

Figure 2: Unprotected loss of flow (ULOF)

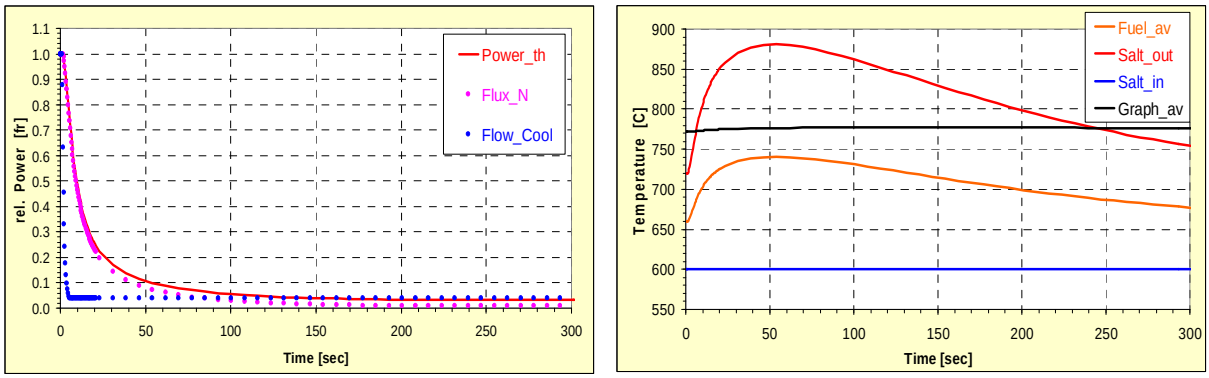

ULOH transient

For the ULOH transient, Figure 3, the heat transfer into the secondary system is assumed to fail at t = 0. Control rods are postulated not to insert into the core. The loss of heat sink implies the core inlet temperature will increase on account of lack of cooling via the heat exchangers. The only heat sink remaining will be radiation via the vessel surface to the reactor containment atmosphere. As can be observed in Figure 3, the core inlet temperature will increase from 600°C to about 740°C within 300 sec after transient initiation. As a result, the core average and outlet fuel temperatures will be at ~740°C within 150 sec into the transient causing negative reactivity to be inserted into the core on account of the strongly negative fuel reactivity coefficient, namely ~-4.125 pcm/°C. The net effect is a fast decrease in the power level to below 10% after 60 sec into the transient. Since the power level continues to decrease, the core fuel temperatures do not rise above 750°C. As can be observing in Figure 3, all fuel temperatures reach an asymptotic level of about 740°C about 300 sec into the transient. The graphite temperature gradually also decreases from 770°C to 740°C.

Figure 3: Unprotected loss of heat sink (ULOH)

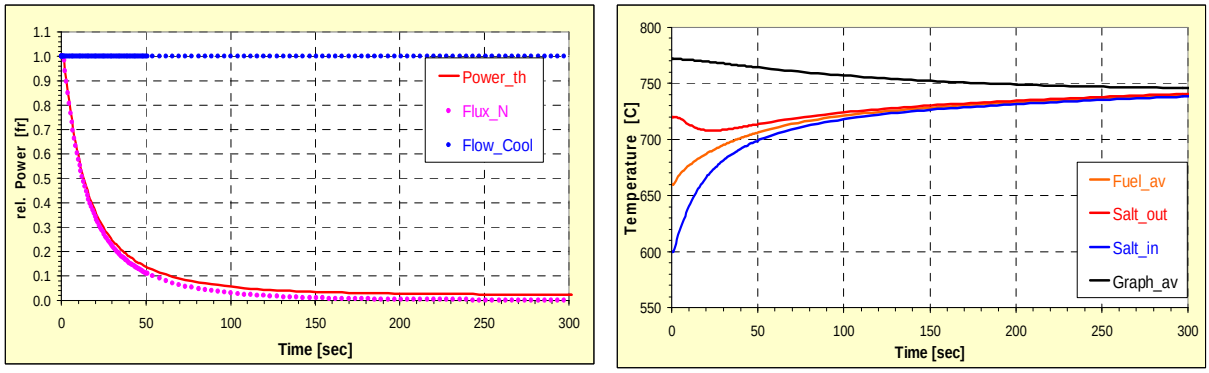

Overcooling transient

In the case of the overcooling transient, Figure 4, the decreasing core inlet temperature leads to a decrease in the average fuel temperature whereas the fuel outlet temperature increases from 720°C to ~830°C. Since the reactivity coefficient of the fuel is negative, a positive reactivity is inserted into the reactor leading to a power rise of a factor 2.7 about 60 sec into the transient. Due to the gradual increase in the temperature of the bulk graphite, additional negative reactivity is inserted into the core leading to a levelling off of the power level at a factor of 2.7. Correspondingly, the core outlet temperature remains constant at ~820°C. The mechanical integrity of the hot loop must now be carefully monitored on account of potential long-term exposure of vessel and loop components exceeding temperatures of 800°C unless rectifying countermeasures are activated at some reasonable time into this transient. The reactor design is however inherently stable under this transient condition.

Figure 4: Unprotected overcooling transient

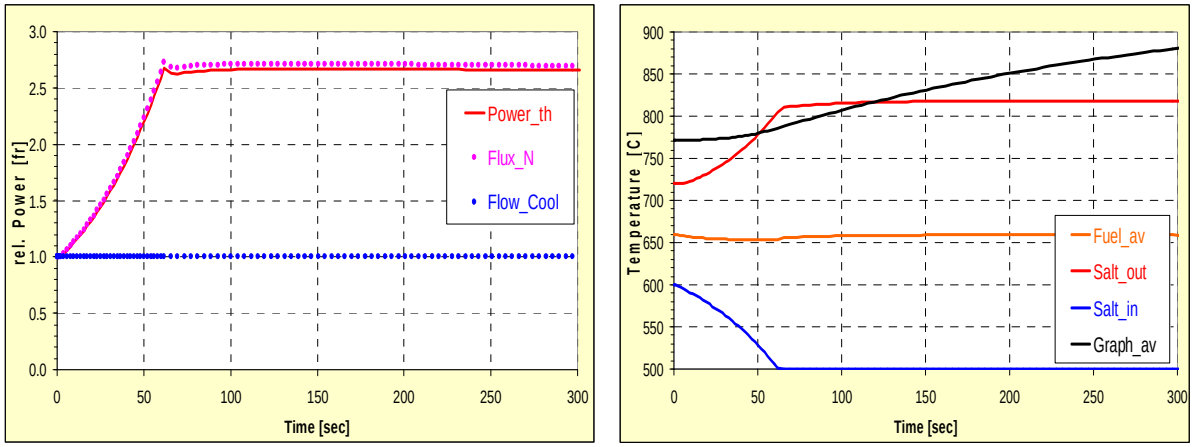

UTOP transients

In the case of the unprotected overpower transient caused by an assumed agglomerated fissile fuel particle to become lodged inside the core region, Figure 5(a), the insertion of +200 pcm reactivity, or ~60 cents, leads to an initial power spike of factor 4.5. The correspondingly fast rise in average and outlet fuel temperatures add quickly negative reactivity into the core, reducing the power to a factor 1.8 at about 6 s into the transient. The slowly increasing graphite temperature inserts additional negative reactivity which will cause the power level to become stabilised. The core outlet temperature reaches about 820°C and stabilises at ~81°C. These temperatures are only ~100°C above nominal conditions and no serious challenge to the mechanical integrity of the system is expected under these transient conditions assuming rectifying countermeasures are activated at some reasonable time into this transient (several minutes).

Unless power is reduced (by control rod shutdown or reduction of the fuel inlet temperature) some reasonable time after transient initiation (*i.e.* several minutes) in order to reduce fuel outlet temperatures, piping or vessel failure at the core outlet must be anticipated at some point into this transient.

In the case of the overpower transient caused by a fuel particle (+200 pcm) sweeping through the core region in ~7 sec to return in another ~4 sec (loop time) a cyclic power spiking will be observed [see Figure 5(b)]. The power spikes subsequent to the first power cycle (power factor ~4.5) are dampened (power factor ~2.4) because of the lower power level (below nominal) from which these power spikes are initiated (the drop in power below nominal after particle transit is due to elevated average fuel temperatures). Fuel outlet temperatures quickly rise to ~820°C within 1 sec after the initiation of the transient, and decrease to ~760°C after the particle has left the core region. The fuel outlet temperature cycles between these limits during subsequent particle transits through the core region. These temperatures are only ~100°C above nominal conditions and no serious challenge to the integrity of the system is expected under these transient conditions.

Figure 5: Unprotected overpower transient (UTOP + 200 pcm)

(a) Agglomerated fuel particle lodged inside core

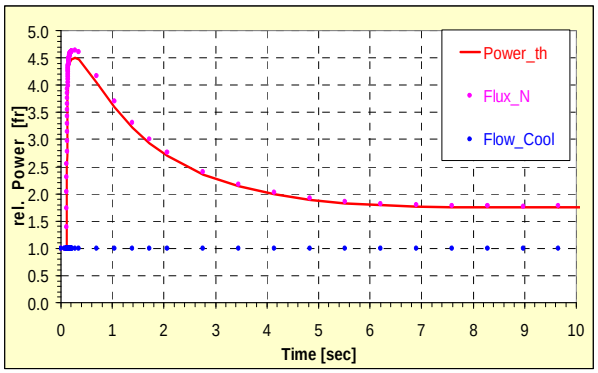

(b) Agglomerated fuel particle swept through core

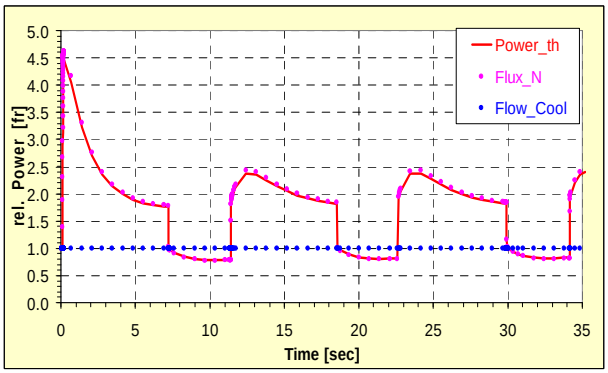

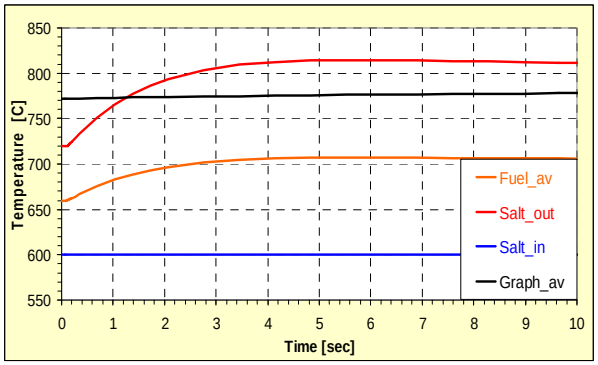

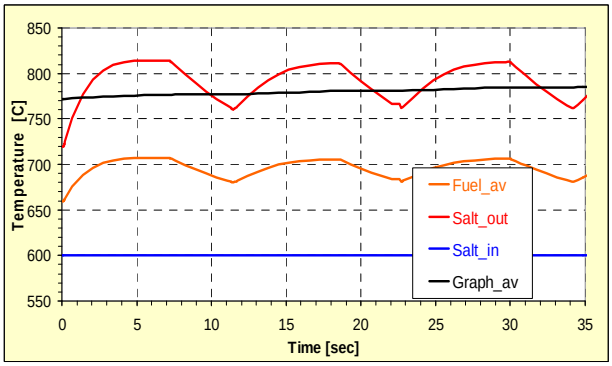

In the case of the unprotected overpower transient caused by an assumed agglomerated fuel particle to become lodged inside the core region, Figure 6(a), the insertion of +500 pcm reactivity, or ~+1.5$, leads to an sharp power spike of factor ~1 000. The correspondingly fast rise in average and outlet fuel temperatures add quickly negative reactivity into the core, reducing the power to a factor ~3 at about 3 s into the transient. The slowly increasing graphite temperature inserts additional negative reactivity which will cause the power level to become stabilised. The core outlet temperature reaches a maximum of ~1 010°C to decrease thereafter. These temperatures are ~300°C above nominal conditions presenting a possible challenge to the mechanical and structural integrity of the upper vessel and loop components. Since the time duration of these excessive temperatures is relatively short (several seconds) the system is not expected to fail catastrophically as rectifying countermeasures are assumed to be activated at some reasonable time into this transient (several tens of seconds).

In the case of the unprotected overpower transient caused by a +500 pcm fuel particle repeatedly sweeping through the core region in ~7 sec to return in another ~4 sec (loop time), a cyclic power spiking (power factor ~1 000) will be observed [see Figure 6(b)]. Again, the power spikes subsequent to the first power spike are dampened (power factor ~30) because of the lower power level (below nominal) from which these power spikes are initiated (the drop in power below nominal after particle transit is due to elevated average fuel temperatures). Maximum fuel outlet temperatures quickly rise to ~1 010°C within 1 sec after the initiation of the transient, and decrease to ~840°C after the particle has left the core region. In subsequent power cycles, the temperatures range from 960°C to 840°C. These temperatures are ~300°C above nominal conditions presenting a possible challenge to the mechanical and structural integrity of the upper vessel and loop components. Rectifying countermeasures should be activated soon after initiation of this transient (several minutes) in order to assure long-term structural integrity of the hotter parts of the systems. Short-term catastrophic system failure is however not expected in this transient.

Figure 6: Unprotected overpower transient (UTOP + 500 pcm)

(a) Agglomerated fuel particle lodged inside core

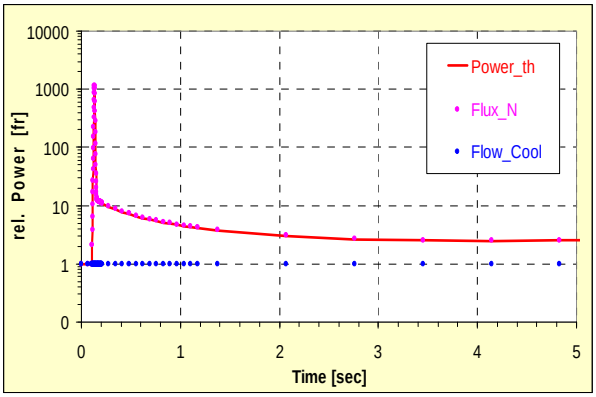

(b) Agglomerated fuel particle swept through core

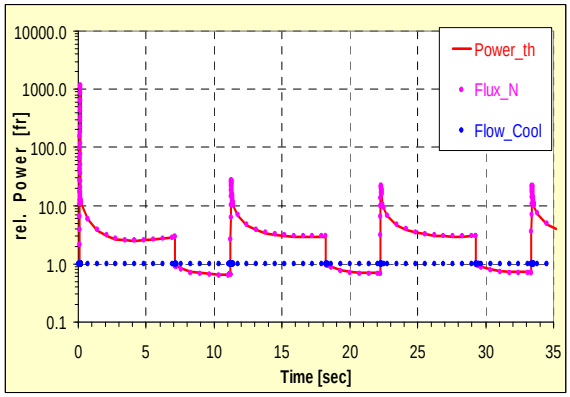

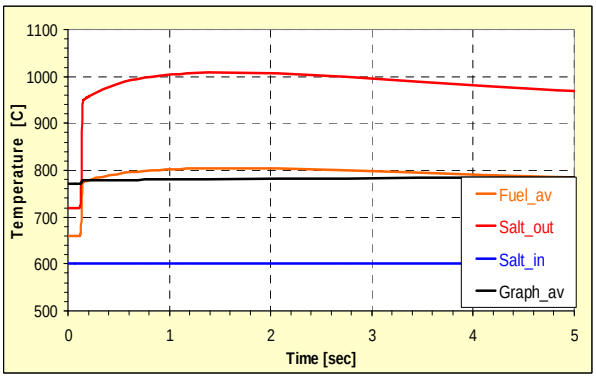

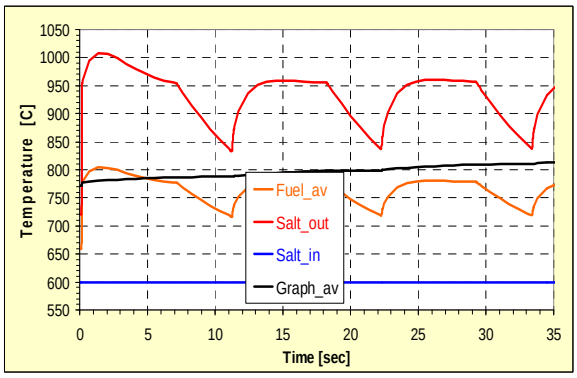

Conclusions

Most important neutronic and thermal–hydraulic considerations can be satisfied by the 2 400 MWt MOSART core of homogeneous configuration: *i*) the AnF_3+LnF_3 concentration in fuel salt is truly within the solubility limit for molten 58NaF-15LiF-27BeF_2 (mole %) at minimum fuel salt temperature in primary circuit of 600°C for fuel cycle scenario under consideration; *ii*) core with 0.2 m graphite reflector in the temperature range 600-1 200°C has strong negative temperature reactivity coefficients; *iii*) regions of reverse, stagnant or laminar flow are avoided; *iv*) the maximum temperature of solid reflectors is low enough to allow it use for suitable time.

Several nuclear data libraries, codes, and computation models were employed to compute safety-related neutronics parameters for the 2 400 MWt MOSART system. The results show that the parameters are favourable for reactor safety, mainly due to the strong density and fuel Doppler effect. The results are in principal agreement with respect to the major reactivity effects.

Preliminary calculations of kinetic and dynamic characteristics of the MOSART system indicate that it would exhibit high levels of controllability and safety. The system would also posses inherent dynamic stability and would require only modest amounts of reactivity control capability.

The transient study has demonstrated that the MOSART design is an inherently stable reactor design on account of its large, negative fuel temperature coefficient (-4.125 pcm/°C) in combination with its negative graphite reflector reactivity coefficient (-0.04 pcm/°C). The MOSART reactor is expected not to be seriously challenged by the major, unprotected transients such as ULOF, ULOH, overcooling or even UTOP. The system was shown to buffer reactivity insertion of up to +1.5$. System temperatures are expected to rise only ~300°C above nominal under these severe transient conditions.

The mechanical and structural integrity of the system is not expected to be impaired assuming countermeasures are facilitated within a reasonable time period after initiation of the 1.5$ UTOP transient (several minutes).

A full safety analysis of MOSART has not been performed because it would require a much more comprehensive design than is currently available.

While a substantial R&D effort would be required to commercialise MOSART, there are no killing unresolved issues in the needed technology. The major technical uncertainties in the conceptual design are in the area of tritium confinement, fuel salt processing and behaviour of some fission products.

References

[1] Forsberg, W., V. Ignatiev, C. Lebrun, E. Merlet-Lucotte, C. Renault, "Liquid Salt Applications and Molten Salt Reactors", *Revue Generale Nucleaire,* 4, Jullet-Aout, 63 (2007).

[2] Weinberg, A., *et al.*, "Collection of Papers on the Molten Salt Reactor Experiment", *Nuclear Application and Technology,* 8 (1970).

[3] Robertson, R., *Conceptual Design Study of a Single Fluid Molten Salt Breeder Reactor*, *ORNL-4541*, USA, June (1971).

[4] Maschek, W., A. Stanculescu, V. Ignatiev, *et al.*, "Report on Intermediate Results of the IAEA CRP on Studies of Advanced Reactor Technology Options for Effective Incineration of Radioactive Waste", *Proc. of CENES 2007*, Istanbul, Turkey, June (2007).

[5] Ignatiev, V., *et al.*, *Experimental Study of Molten Salt Technology for Safe, Low-waste and Proliferation Resistant Treatment of Radioactive Waste and Plutonium in Accelerator Driven and Critical Systems*, ISTC-1606 Project Final Report, International Scientific Technical Centre, Moscow (2008).

[6] Ignatiev, V., *et al.*, "Progress in Integrated Study of Molten Salt Actinide Recycler and Transmuter System", *Actinide and Fission Product Partitioning and Transmutation, 9th Information Exchange Meeting*, Nîmes, France, September, OECD/NEA, Paris (2006).

[7] Schikorr, M., "Assessment of the Kinetic and Dynamic Transient Behaviour of Sub-critical Systems (ADS) in Comparison to Critical Reactor Systems", *Nuclear Engineering and Design*, 210, 95 (2001).

Accelerator-driven systems and fast reactors cooled by lead-208: A possibility for reducing initial fuel load and increasing the transmutation rate

G.L. Khorasanov, V.V. Korobeynikov, A.P. Ivanov, A.I. Blokhin
Institute for Physics and Power Engineering named after A.I. Leypunsky
Obninsk, Russian Federation

Abstract

Long-term scenarios of nuclear energy evolution over the world scale predict deployment of FR from 2020-2030 and achievement near 2050 the world installed nuclear power equal to 1 500 GW_e with essential increasing the FR number. For several countries which policies are based on a sharp increase of nuclear production, at the stage near 2030-2040 when Pu from PWR spent nuclear fuel is consumed, the Pu lack will stimulate minimising its loading in FR. The period of Pu deficiency will be prolonged until the years when breeding gain equal to 0.2-0.3 in FBR is obtained.

In the present paper one potential opportunity of reduction the initial quantity of uranium-plutonium nitride fuel in FR is considered: it is related to using a low neutron capturing ^{208}Pb as a coolant.

As is known, lead natural, ^{nat}Pb, contains ~52% of the stable isotope ^{208}Pb characterised by a small cross-section of radiation neutron capture: it is shown in the paper that its mean values averaged upon a neutron spectrum of the ADS subcritical core are by 3.7-4.5 times less than these for the natural mix of lead isotopes ^{nat}Pb. This circumstance allows minimising fuel load of the FR and ADS core for achievement its criticality or small subcriticality, accordingly. It is shown that replacement of the ADS core coolant from ^{208}Pb to ^{nat}Pb results in reduction the neutron fluxes by 1.5 times and decreasing the effective multiplication factor of neutrons from the initial value K_{eff} = 0.970 down to the value equal to K_{eff} = 0.953. In these conditions, thermal power of the core, at preservation the proton beam power, is below nominal by 1.5 times. In this case, to achieve the rated core power, N = 80 MW it is required to increase Pu enrichment by 1.5 times, or, at preservation Pu loading, to increase by 1.5 times the current and power of the proton beam in the target.

Due to the ^{208}Pb low neutron absorbing ability, neutron fluxes in the ADS and FR peripheral zones are higher than those for the installations cooled by ^{nat}Pb that allows increasing transmutation rate of MA and LLFP being inserted into these zones.

As is known, for the small-sized FR, SVBR-100 type, correctly designed from the coolant minimisation point of view, a specific need for the lead coolant weight related to FR thermal power makes about 0.65 tonne/$MW_{thermal}$. Then, the minimum quantity of the coolant from ^{208}Pb for the ADS blanket of thermal power equal to 80 MW will make ~60 tonnes, and the quantity of the ^{208}Pb coolant for the critical LFR with thermal power of close to 280 MW makes about 180 tonnes.

The limiting factor of usage highly enriched ^{208}Pb as the coolant is its high price in the world market. In the ISTC #2573 project, executed in the RF, the opportunity of creation of the plant for separation of lead isotopes using selective photoreactions was considered. The complex of calculations and theoretical works was carried out, the outline sketch of the separation installation was developed, and economic and technical estimations of industrial production of highly enriched ^{208}Pb were made. Developers of the ISTC #2573 project expect that at the scale of manufacture equal to 150-300 kg of ^{208}Pb per year its price will be of $200/kg.

Introduction

Long-term scenarios of nuclear energy evolution over the world scale predict deployment of fast reactors (FR) from 2020-2030 and achievement on 2050 the world installed nuclear power equal to 1 500 GWe with essential increasing the FR number. For several countries (*i.e.* Russia, Japan) which policy is based on a sharp increase of nuclear production, at the stage near 2030-2040 when Pu from the PWR spent nuclear fuel is consumed, the Pu lack will stimulate minimising its loading in FR. The period of Pu deficiency will be prolonged until the years when breeding gain (BG) equal to 0.2-0.3 in FBR is obtained which corresponds to Pu inventory doubling time of 44-24 years.

Ways of minimisation of initial loading of fuel in BR are well-known – they have been partially described in Ref. [1]. In the specified paper it is offered to use high density uranium-plutonium (^{238}U+Pu)^{15}N nitride fuel, wrapperless fuel assemblies, low neutron absorbing nitrogen isotope ^{15}N in nitride fuel contents, structural materials with low cross–section of neutron capture, etc.

In this paper one more potential opportunity of reduction the initial quantity loaded in the FR uranium-plutonium fuel is considered: it is it is related to using a low neutron capturing ^{208}Pb as a FR coolant. As is known, lead natural contains the stable isotope ^{208}Pb (~52% in the mix of lead isotopes) characterised by a small cross-section of radiation capture of neutrons.

The possibility of using stable lead isotopes – low activation ^{206}Pb and low neutron absorbing ^{208}Pb – in emerging nuclear systems has been earlier pointed by authors in Refs. [2-6].

An ADS subcritical core with a coolant from ^{nat}Pb and ^{208}Pb. Mean cross-sections $<\sigma_{n,\gamma}>$, averaged upon the ADS core neutron spectra, for ^{nat}Pb and ^{208}Pb

In this paper advantages of using ^{208}Pb instead of ^{nat}Pb as a FR coolant are demonstrated on the model of the ADS core offered for transmutation minor actinides (MA) in a number of nowadays developed scenarios of destruction nuclear plant waste.

Calculations of neutron and physical characteristics of the subcritical ADS core have been performed by means Monte Carlo technique with the MCNP/4A code [7-9] and NJOY program specially developed with the help of the library of cross-sections on the basis of ENDF/B-VI evaluated nuclear data files.

As initial data the following ones were taken:

- annular subcritical core with an external source of neutrons – a proton beam target on its axis;
- calculated spectrum of spallation neutrons in the target consisted of the modified lead-bismuth eutectic – ^{208}Pb(80%)-Bi(20%) [2];
- proton beam energy – E_p = 600 MeV;
- the effective multiplication factor of the subcritical core cooled by ^{208}Pb – K_{eff} = 0.970;
- thermal power delivered in the subcritical core in the rated regime – N = 80 MW;
- core coolant – ^{208}Pb (100%).

For reduction the core dimensions and minimisation the quantity of the coolant, the mix of mononitrides of the depleted uranium, Pu and MA from the PWR spent nuclear fuel as the ADS core fuel was considered. Pu and MA content in uranium-plutonium mix was accepted equal to 15%.

The calculated basic technical parameters of the 80 $MW_{thermal}$ ADS core cooled by ^{208}Pb and satisfied the initial data are resulted in Table 1.

Calculations have shown that, in such a core, at use ^{208}Pb as the coolant, delivering the nominal thermal power N = 80 MW will need a proton beam current I_p = 2.8 mA and proton beam capacity N_p = 1.68 MW to which corresponds an intensity of spallation neutrons from the modified Pb-Bi target equal to $S = 2.3 \cdot 10^{17}$ neutron/s.

Table 1: Main parameters of the 80 $MW_{thermal}$, ADS core cooled by ^{208}Pb

Parameters	Values
Subcritical core thermal power	80 MW
Annular core outer diameter	123.7 cm
Annular core inner diameter	56.0 cm
Annular core height	110.0 cm
Core fuel	$(U+Pu+MA)^{15}N$
Total fuel inventory	5 410 kg
Total heavy metal inventory	5 090 kg
Total Pu and minor actinide inventory	765 kg
Mean pin linear power	188 W/cm
Mean volume power density	118 W/cm^3
Effective multiplication factor for the core cooled by ^{208}Pb	K_{eff} = 0.970

At use ^{nat}Pb as the coolant the effective multiplication factor of neutrons in the working regime falls from the initial value K_{eff} = 0.970 down to the value equal to K_{eff} = 0.953. Replacement of the coolant from ^{208}Pb to ^{nat}Pb also results in reduction the neutron fluxes in the core. In Figure 1 the neutron fluxes in the core centre near its inner diameter are shown. It is visible that the fluxes in the core cooled by ^{nat}Pb are lower by 1.5 times as compared with the fluxes in the core cooled by ^{208}Pb.

Figure 1: Neutron fluxes in the core per one neutron from the target

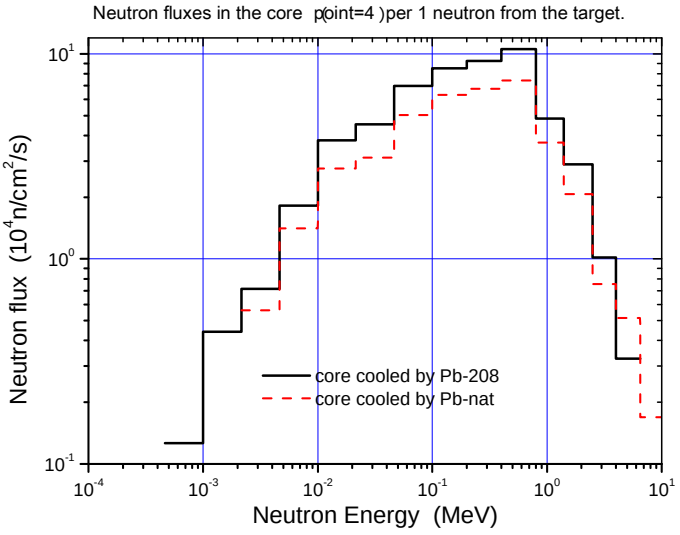

On replacement the coolant the thermal power of the core, at preservation the proton beam power, is below nominal by 1.5 times. For achievement the rated core power N = 80 MW, at preservation the proton beam power, it is required to increase the fissile material – Pu enrichment from the initial 15% up to the 22.5% or, at preservation fuel loading, to increase by 1.5 times the current and power of the proton beam: I_p = 4.3 mA, N_p = 2.58 MW. Accordingly, the intensity of spallation neutrons will increase up to $S = 3.55 \cdot 10^{17}$ neutron/s.

These advantages of the usage ^{208}Pb as the ADS core coolant are caused by its small neutron absorbing ability. In Figure 2 microscopic cross-sections of radiation neutron capture by the lead isotopes and by the natural mix of lead isotopes in the ABBN-93 system [8] of 28 neutron energy groups are resulted. Cross-sections are received on the basis of files of the evaluated nuclear data ENDF/B-VI. It is visible, that, practically, for all the 28 neutron energy groups of the ABBN-93 system, the values of radiation neutron capture by the lead isotope ^{208}Pb considerably concede to the values of radiation neutron capture by the mix of lead isotopes ^{nat}Pb, and this distinction is especially strong, in orders of magnitudes, for low and intermediate energies of neutrons, E_n < 50 keV.

Figure 2: Cross-sections of radiation neutron capture $\sigma_{n,\gamma}$ by stable lead isotopes and the natural mix of lead isotopes in the ENDF/B-VI version and for 28 neutron energy groups of the ABBN-93 system [8]

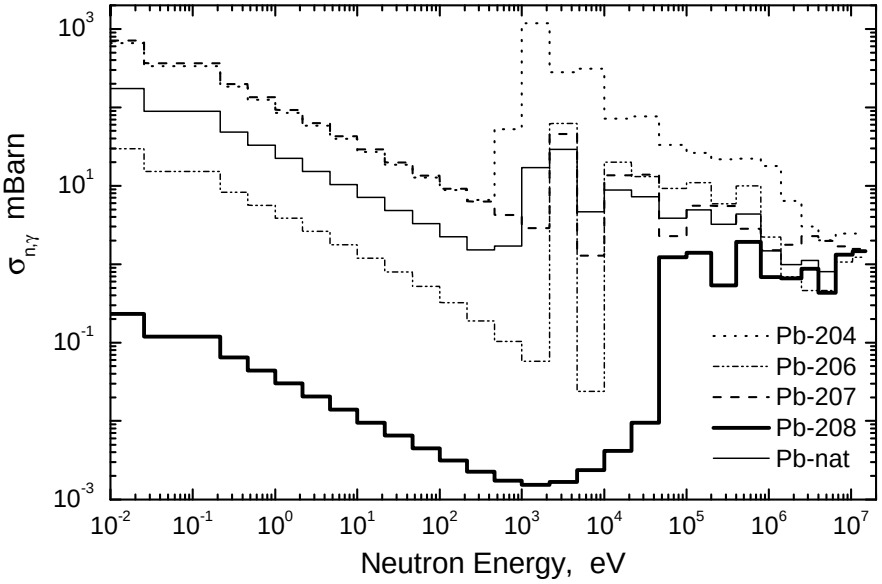

On the basis of the resulted cross-sections $\sigma_{n,\gamma}$ in the 28 group approximation and neutron spectra calculated by means the MCNP/4A code for subcritical core cooled with ^{208}Pb or ^{nat}Pb the mean values of cross-sections $<\sigma_{n,\gamma}>$ of radiation neutron capture by the isotope ^{208}Pb and by the mix of isotopes ^{nat}Pb averaged on corresponding neutron spectra of zones #4, 5, 6 and 9 of the ADS subcritical core have been calculated. The arrangement of zones in the ADS annular subcritical core is shown in Table 2.

Table 2: Scheme of zone positions in the annular subcritical core

Target zone	Zone 1	Zone 2	Zone 3	ΔH_3 = 36.7 cm
	Zone 4	Zone 5	Zone 6	ΔH_2 = 36.7 cm
	Zone 7	Zone 8	Zone 9	ΔH_1 = 36.7 cm
R = 28 cm	ΔR_1 = 11.2 cm	ΔR_2 = 11.2 cm	ΔR_3 = 11.2 cm	

For the zone # 4 of the ADS core cooled by ^{208}Pb and ^{nat}Pb the calculated spectra of neutrons are resulted in Figure 1. Neutron fluxes Φ_n related to one external neutron, mean neutron energies $<E_n>$ and mean cross-sections $<\sigma_{n,\gamma}>$of radiation neutron capture by ^{208}Pb and ^{nat}Pb averaged upon neutron spectra for four zones, #4-6 and #9, of the ADS core are given in Table 3.

Table 3: Total neutron flux per 1 external neutron, Φ_n, mean neutron energy, $<E_n>$, and mean radiation neutron capture cross-section, $<\sigma_{n,\gamma}>$, for the isotope ^{208}Pb/ natural mix of isotopes ^{nat}Pb. $<E_n>$ and $<\sigma_{n,\gamma}>$ are averaged upon the neutron spectra of the ADS core zones.

Parameters	^{208}Pb used as a core coolant				^{nat}Pb used as a core coolant			
	Zone 4	Zone 5	Zone 6	Zone 9	Zone 4	Zone 5	Zone 6	Zone 9
Φ_n (n/cm^2/1n)	$5.67\cdot10^{-3}$	$4.57\cdot10^{-3}$	$2.45\cdot10^{-3}$	$1.01\cdot10^{-3}$	$4.08\cdot10^{-3}$	$2.99\cdot10^{-3}$	$1.58\cdot10^{-3}$	$6.67\cdot10^{-4}$
$<E_n>$(keV)	482±24	538±27	370±18	315±16	558±28	467±23	375±19	329±16
$<\sigma_{n,\gamma}>$ (mbarn)	0.97±0.05	0.95±0.05	0.88±0.04	0.78±0.04	3.62±0.18	3.70±0.19	3.63±0.18	3.52±0.18

From the resulted data follows that the mean values of the cross-section $<\sigma_{n,\gamma}>$ for the mix of lead isotopes ^{nat}Pb are by ~3.7-4.5 times greater than the mean values of the same cross-sections for the lead isotope ^{208}Pb.

In peripheral zones of the core this relation achieves its greatest value, ~4.5, that allows increasing transmutation rate of MA and LLFP being inserted into these zones.

A critical LFR core with a coolant from ^{nat}Pb. Mean cross-sections $<\sigma_{n,\nu}>$ averaged upon the LFR core neutron spectra for ^{nat}Pb

Calculations of neutron and physical characteristics of the critical LFR core have been performed by means of the Monte Carlo technique with the MCNP/4A code and NJOY program specially developed with the help of the library of cross-sections on the basis of ENDF/B-VI files.

As initial data these ones from the paper [1] were taken:

- thermal capacity of the core – N = 700 MW;
- core fuel – $(U+Pu+MA)^{15}N$;
- Pu and MA contents in fuel – 13.5%;
- core coolant – natural lead, ^{nat}Pb (100%).

In Figure 3 neutron spectra in the zones #4, 5 and 12 of the 700 $MW_{thermal}$ FR core with the coolant from ^{nat}Pb is presented. Calculations of the critical LFR core for a case of its cooling by ^{208}Pb were not carried out.

Figure 3: Neutron spectra in the zones # 4, 5 and 12 of the 700 $MW_{thermal}$ LFR core

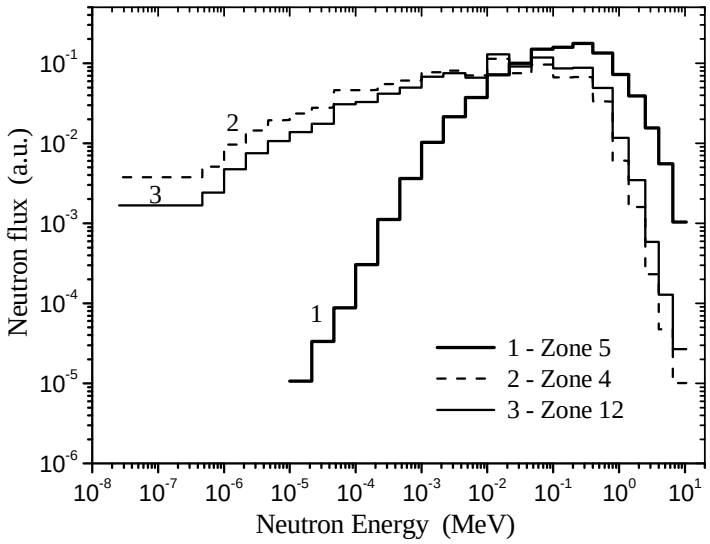

On the basis of the microscopic cross-sections, $\sigma_{n,\gamma}$, taken in the ABBN-93 group approximation and calculated neutron spectra for several zones of the LFR core, the mean values of $<\sigma_{n,\gamma}>$ for ^{nat}Pb averaged upon corresponding neutron spectra of the zones have been received. They are given in Table 4. Total neutron fluxes and mean energies of neutrons averaged upon corresponding neutron spectra of the core zones are also resulted in Table 4.

From the data it follows that values $<E_n>$ and $<\sigma_{n,\gamma}>$ for the critical LFR with uranium-plutonium nitride fuel and the coolant from natural lead insignificantly differ from the same values calculated for the ADS subcritical core.

Table 4: Total neutron flux, Φ_n, mean neutron energy, $<E_n>$, and mean radiation neutron capture cross-section, $<\sigma_{n,\nu}>$, by the natural mix of isotopes ^{nat}Pb. $<E_n>$ and $<\sigma_{n,\gamma}>$ are averaged upon the neutron spectra of the 700 $MW_{thermal}$ critical LFR core zones.

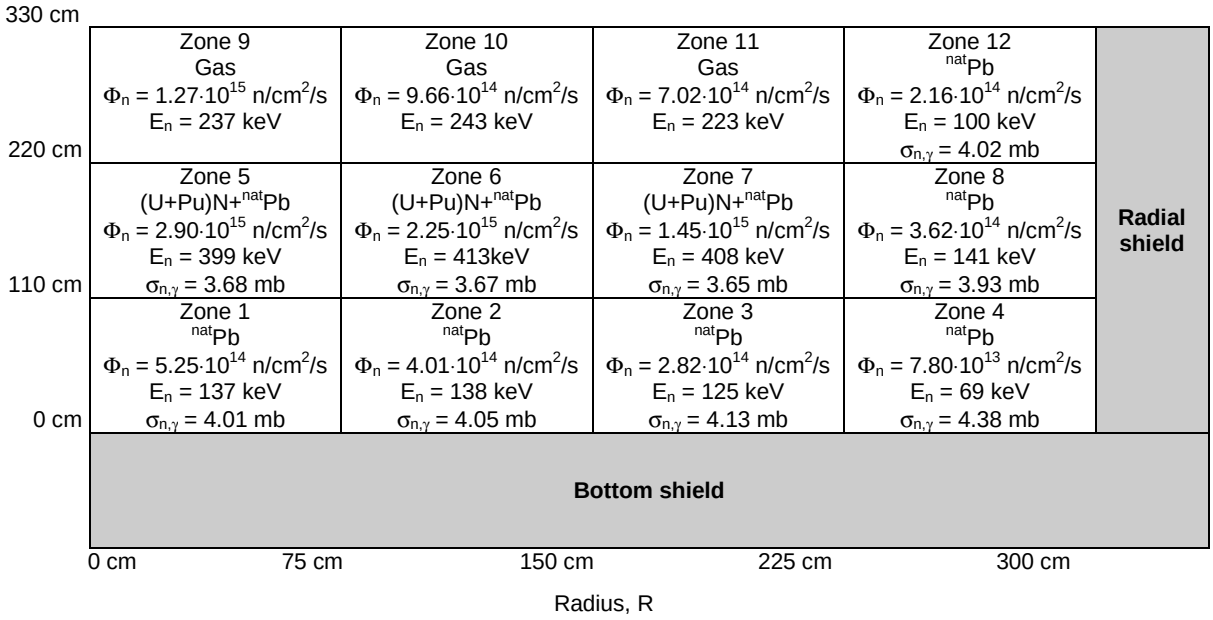

In this case, it is possible to expect, that the relations of values of mean cross-section $<\sigma_{n,\gamma}>$ for natural mix of lead isotopes ^{nat}Pb and lead isotope ^{208}Pb, will be kept approximately at the same level, as for the ADS core, *i.e.* about ~3.7-4.5, that will cause a smaller fuel load of the LFR in using the coolant from ^{208}Pb.

An estimation of a minimum quantity and economically acceptable cost of the ^{208}Pb used as the LFR coolant

In Ref. [10] it is shown that in the correctly designed LFR, from the point of view of coolant minimisation, a specific need for the lead coolant weight related to the LFR thermal power, makes about 0.65 tonne/$MW_{thermal}$. Then, the minimum quantity of the coolant on the basis of highly enriched ^{208}Pb for the ADS with thermal power equal to 80 MW will make ~60 tonnes.

In transition to the coolant from ^{nat}Pb and preservation other parameters of the ADS core, the enrichment of Pu fuel must be increased up to the value of 22.5% of heavy metal masses to deliver the nominal power. In this example it is demonstrated that at delivering about 80 MW thermal power an economy of 370 kg of Pu can be reached, only due to using the coolant from ^{208}Pb instead of the coolant from ^{nat}Pb.

In several projects published last time the plutonium enrichment in the uranium-plutonium fuel is equal to from 13.5 up to 27% of heavy metal masses in the core. The minimum plutonium enrichment, 13.5%, is given in the paper [1]. In using the coolant from ^{208}Pb the Pu enrichment value might be additionally decreased that will preserve the valuable fissile material for initial loading the next FR fleet.

The minimum quantity of the coolant from ^{208}Pb for the LFR with thermal power less than 300 MW makes several tens or hundreds of tonnes. For example, in Ref. [11] it is pointed that small-sized FR named as SVBR-100 (280 MW thermal) needs about 180 tonnes (~18 m^3) of Pb-Bi coolant. To avoid severe unprotected accidents in small-sized LFR, less than 300 $MW_{thermal}$, an additional passive cooling system by means the heat transfer through the core vessel is possible, as was shown in the SVBR-100 project.

The limiting factor of usage highly enriched ^{208}Pb as a coolant is its high price in the world market. In the ISTC #2573 project [12], executed in the Russian Federation in 2004-2005 with the authors' participation, the opportunity of creation of the plant for separation of lead isotopes using selective photoreactions was considered. In the Efremov Institute (St. Petersburg) and the Institute for Semiconductor Physics RAS (Novosibirsk) the complex of calculations and theoretical works was carried out, the outline sketch of the separation installation was developed, and economic and technical estimations of industrial production of highly enriched ^{208}Pb were made.

Advantages of a photochemical method of lead isotope separation consist in one-photon excitation of atoms, an opportunity of using commercially accessible highly effective semiconductor lasers and high efficiency of lead isotope separation in the reactionary chamber. The technique of selective photoreactions operates with such working substance as lead vapour and does not require conversion of lead into a volatile substance and its return transformation into a desired product as it takes place in the technique of gas separation centrifuges.

All this allows hoping for reception of large quantities (tens or hundreds of tonnes) of the lead isotope ^{208}Pb with 95-99% enrichment under the price acceptable to nuclear engineering.

Developers of the ISTC #2573 project expect that at large scale manufacture (for example, more than 150-300 kg of ^{208}Pb per year), in using the photochemical technique the product ^{208}Pb can be produced for a price of close to $200/kg [13].

Conclusions

- Molten lead isotope ^{208}Pb as a low neutron absorbing material is the ideal coolant for the subcritical or critical core of reactors on fast neutrons. In the paper it is shown that for the accelerator-driven system subcritical core with thermal power of 80 MW, the mean cross-sections of radiation capture of neutrons by the lead isotope ^{208}Pb, $<\sigma_{n,\gamma}>$, averaged upon ADS core neutron spectra are by ~3.7-4.5 times less than the same cross-sections for a natural mix of lead isotopes ^{nat}Pb. This circumstance allows minimising the fuel load of the FR and ADS core for achievement its criticality or small subcriticality, accordingly.
- For pick-up the 80 MW ADS core heat by means the ^{208}Pb coolant about 60 tonnes (~6 m^3) of this lead isotope are required. Expenses for obtaining this quantity of expensive ^{208}Pb can be compensated due to reduction the power of a high energy proton beam which cost is also great enough.
- For a safe LFR with thermal power of close to 300 MW about 180 tonnes (~18 m^3) of lead will be enough, as it is shown in the SVBR-100 project. Expenses for reception this quantity of ^{208}Pb can be compensated due to the economy of a uranium-plutonium fuel and relatively fast breeding of plutonium in LFR with a high breeding gain, BG = 0.1-0.2.
- The considered benefits of using the stable lead isotope ^{208}Pb in the next generation ADS and LFR are the background for the R&D and industrial deployment of new laser photochemical technique for lead isotope separation and obtaining large quantities of ^{208}Pb.

Acknowledgements

The study is performed under the financial support of the State Corporation for atomic energy "Rosatom".

References

[1] Orlov, V.V., A.I. Filin, V.S. Tsikunov, *et al.*, "Tasks and Requirements for BREST-OD-300 Pilot and Demonstration Reactor Design", *Proc. of the Conf. on Heavy Liquid Metal Coolants in Nuclear Technology*, Obninsk, SSC RF IPPE, Vol. 2, pp. 411-418 (1999).

[2] Khorasanov, G.L., A.P. Ivanov, A.I. Blokhin, "Reduction of the Induced Radioactivity in an ADS Target by Changing the Target Material Isotope Composition", *Nuclear Engineering and Design*, Vol. 236, Nos. 14-16, pp. 1606-1611 (2006).

[3] Khorasanov, Georgy L., Anatoly P. Ivanov, Anatoly I. Blokhin, Leonid Yu. Sosnin, Anatoly N. Cheltsov, "Isotopic Tailored Materials for Nuclear Engineering", *Proceedings of the 9th International Workshop on Separation Phenomena in Liquids and Gases (SPLG 2006)*, 18-21 September 2006, Beijing, China, Tsinghua University Press, Beijing, pp. 82-87 (2007).

[4] Khorasanov, Georgy L., Anatoly P. Ivanov, Anatoly I. Blokhin, "Neutronic and Physical Characteristics of the ADS Target and Subcritical Core with a Lead-208 Coolant", *Proc. of the 14th Int. Conf. on Nuclear Engineering (ICONE 14), 17-20* July 2006, Miami, Florida, USA, Paper # ICONE 14-89153 (2006).

[5] Khorasanov, G.L., A.P. Ivanov, A.I. Blokhin, "Neutronic and Physical Characteristics of an Accelerator-driven System with a Coolant from the Lead Isotope ^{208}Pb", *Actinide and Fission Product Partitioning and Transmutation, 9th Information Exchange Meeting, Nîmes, France, 25-29 September 2006*, OECD/NEA, Paris, No. 6282, pp. 499-507 (2007).

[6] Khorasanov, G.L., A.P. Ivanov, A.I. Blokhin, "Neutronic Parameters of the ADS Installation with Lead-208 Isotope as a Coolant Material", *Issues of Atomic Science and Technology, Series: Nuclear Constants,* Issue 1-2, pp. 94-100 (2005) (in Russian).

[7] Briesmeister, J.F., *MCNP-4 General Monte Carlo Code for Neutron and Photon Transport*. LA-7396-M-Rev. 2 (1987).

[8] Manturov, G.N., M.N. Nikolaev, A.M. Tsiboulia, "Group Constant System ABBN-93. Part 1: Nuclear Constants for Calculation of Neutron and Photon Emission Fields", *Issues of Atomic Science and Technology, Series: Nuclear Constants,* Issue 1, p. 59 (1996) (in Russian).

[9] Orsi, R., M. Pescarini, A.I. Blokhin, *ENDF/B-VI Multi-Temperature Neutron Library for MCNP*, ENEA KT-SCG-2 (1998).

[10] Grigoriev, O.G., G.I. Toshinsky, S.K. Leguenko, "Demands for Commercial Usage of SVBR-75 Reactor Installation for Solving Different Tasks", *Proc. of the Conf. Heavy Liquid Metal Coolants in Nuclear Technology*, Obninsk, SSC RF IPPE, Vol. 2, pp. 514-520 (1999).

[11] Zrodnikov, A.V., G.I. Toshinsky, O.G. Komlev, *et al.*, "Nuclear Power Development in Market Conditions with Use of Multi-purpose Modular Fast Reactor SVBR-75/100", *Nuclear Engineering and Design*, Vol. 236, Nos. 14-16, pp. 1490-1502 (2006).

[12] ISTC Project # 2573: "Investigation of Processes of High-Performance Laser Separation of Lead Isotopes by Selective Photoreactions for Development of Environmentally Clean Perspective Power Reactor Facilities", Project Manager: A.M. Yudin (RF, St-Petersburg, Efremov Institute, NIIEFA), Project Submanagers: G.L. Khorasanov (RF, Obninsk, Leypunsky Institute, IPPE) and P.A. Bokhan (RF, Novosibirsk, ISP) (2005).

[13] Bortnyansky, A.L., V.L. Demidov, S.A. Motovilov, F.P. Podtikan, Yu.I. Savchenko, V.A. Usanov, A.M. Yudin, B.P. Yatsenko, "Experimental Laser Complex for Lead Isotope Separation by Means of Selective Photochemical Reactions", *Proc. of the Int. Conf. Physical and Chemical Phenomena in Selection of Atoms and Molecules,* 3-7 October 2005, Moscow, TSNIIATOMINFORM, pp. 76-82 (2005).

Experimental investigation of subchannel flow distribution in a hexagonal rod bundle experiment

K. Litfin, A.G. Class, M. Daubner, S. Gnieser, R. Stieglitz
Forschungszentrum Karlsruhe GmbH
Institute for Nuclear and Energy Technologies
Karlsruhe, Germany

Abstract

In the framework of accelerator-driven subcritical reactor systems (ADS), heavy liquid metals (HLM) like lead or lead-bismuth eutectic (LBE) are considered as coolant for the reactor core and the spallation target due to their efficient heat removal properties and high production rate of neutrons.

The excellent heat conductivity of LBE-flows expressed by a low molecular Prandtl number of the order of 10^{-2} leads to modelling problems of the turbulent heat transfer. Although various models for thermal-hydraulics of LBE flows are existing, validated heat transfer correlations for ADS-relevant conditions are still missing. In order to validate the used subchannel codes and computational fluid dynamics (CFD) codes used to design fuel assemblies the comparison with experimental data is inevitable.

Therefore, a series of experiments has been initiated at the KArlsruhe Liquid metal LAboratory (KALLA) of the Forschungszentrum Karlsruhe. In order to quantify and separate the individual phenomena occurring in the momentum and the energy transfer domain of a fuel assembly the experimental programme is composed of three major experiments.

In a first step, a single electrically heated rod is placed in a hydraulically developed turbulent LBE pipe flow in the regime of forced, mixed and buoyant convection, where radial and axial temperature fields and pressure are measured. The second experiment is a 19-pin hexagonal rod bundle that is tested in a turbulent water flow. In the third experiment the same rod bundle design is placed in a hydraulically developed turbulent LBE flow.

Because of the opaqueness of the liquid metal flow the rod bundle water experiment is necessary to gain information about the flow distribution and the pressure drop in the subchannels by means of Laser Doppler Anemometry (LDA). Furthermore, measurements by Ultrasonic Doppler Velocimetry (UDV) technique and a movable pitot tube is used to characterise the subchannel flow distribution. The experimentally gained data of the water experiment serves as a numerical benchmark of subchannel analysis codes and commercial CFD software packages and is discussed in this paper.

Introduction

Liquid metals are often considered as coolant for an efficient heat removal of thermally high loaded surfaces. Due to their high thermal conductivity heavy liquid metals allow rather simple geometries of the heat transfer unit employed. However, the high conductivity leads to a violation of the analogy of turbulent heat and momentum transfer. The spatial extension of viscous and thermal boundary layer is different and the concept of a constant turbulent Prandtl number does not apply. While for momentum transport the turbulent contribution is dominant, the molecular contribution is of equal or even stronger importance for heat transfer. The common turbulence models in commercially available code packages (like k-ε model, Reynolds stress model, k-ω model) lead to considerable errors compared to the experimentally obtained temperatures.

Only the detailed knowledge of the convective-diffusive heat transport phenomena in laminar and turbulent liquid metal flows enables an adequate design of heat transfer units near highly heat loaded surfaces such as fuel bundles. This problem is particularly prominent in the weakly turbulent Reynolds number regime, where buoyancy plays a non-negligible role. Moreover, in most technical applications the flows are thermally developing so that the heat exchange trough the boundary layer plays a significant role. Only the detailed knowledge of the momentum and energy transfer in the thermal boundary region allows the understanding of the discrepancies between computational results and the experimental observation. Therefore, a series of experiments has been initiated at the KArlsruhe Liquid metal LAboratory (KALLA) of the Forschungszentrum Karlsruhe. In order to quantify and separate the individual phenomena occurring in the momentum and the energy transfer domain of a fuel assembly the experimental programme is composed of three major experiments.

In the LBE single rod experiment a single electrically heated rod is placed in a hydraulically developed turbulent LBE pipe flow in the regime of forced, mixed and buoyant convection. Radial and axial temperature fields are measured with a thermocouple rake and a movable thermal probe that also contains a pitot tube for pressure measurements. The experimental data are compared to numerical simulations simultaneously conducted by various groups in the context of the EUROTRANS programme. Furthermore, this experiment allows testing the heater performance and the validation and qualification of the used measurement techniques. In the second experiment an isothermal hexagonal rod bundle is placed in a turbulent water flow where the flow distribution and the pressure drop in the subchannels is measured by Laser Doppler Anemometry (LDA), Ultrasonic Doppler Velocimetry (UDV) and a movable pitot tube. This experiment also serves as a test for flow-induced vibrations of the set-up because the same experimental geometry is used for the LBE set-up. The third experiment is an electrically heated hexagonal rod bundle that will be tested in a hydraulically developed turbulent LBE flow in regime of forced, mixed and buoyant convection. Measurements of temperature distribution and velocity fields are planned by means of UDV sensors and movable thermocouple rakes inside the rod bundle. The experimentally gained data of all three experiments serves as a numerical benchmark of subchannel analysis codes and commercial CFD software packages. The set-up of both water- and LBE-cooled rod bundle experiment and first experimental data on the water rod bundle measurement is described below.

Rod bundle design

The set-up of the test rod bundle is of hexagonal shape and contains 19 electrically heated fuel pin simulators. It represents part of the fuel assembly proposed for the PDS-XADS (Preliminary Design Studies of an eXperimental Accelerator-Driven System) that contains 91 pins. The active heated length is 870 mm, the power distribution is constant over the active length. The design parameters of two proposed PDS-XADS geometries together with the experimental set-up are listed in Table 1. The design of the rod bundle in Figure 1.

The entire fuel bundle simulator is composed of four modules flanged to each other and is fabricated from stainless steel. For the LDA measurements in the water experiment some parts of the test section are replaced by windows made of polymethylmethacrylate (PMMA). The first part is the foot where at low velocity the incoming fluid is guided into a vertical tube through six vertical slits of 80 mm height and 6.5 mm width at fuel bundle conditions. The second part is the flow conditioning a venturi nozzle generating a hydraulically fully developed flow. The third part is the test section containing the 19 fuel pin simulators in a hexagonal arrangement. The transverse position of the pins

is fixed by three vertically equal positioned spacers and an entrance guide. The spacer design is identical to that proposed for the XADS. The fourth part at the top is a head which is flanged to the test section and guides the fluid sideways to the outlet. This is necessary in order to mount the simulators to the electric power supply.

Figure 1: Picture of spacer and disassembled test section area (left), drawing of rod bundle experimental set-up with marked pressure positions P1 to P6 (right)

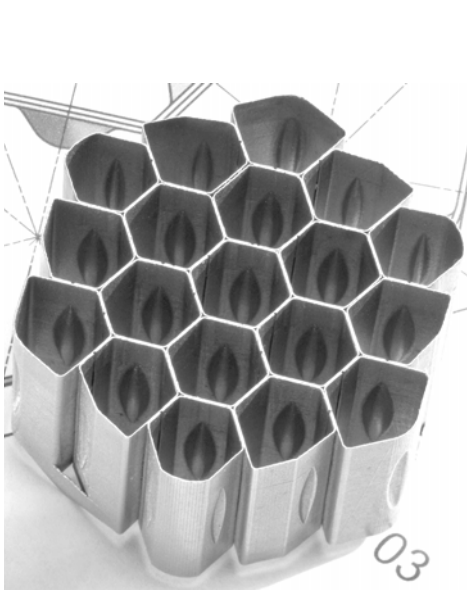

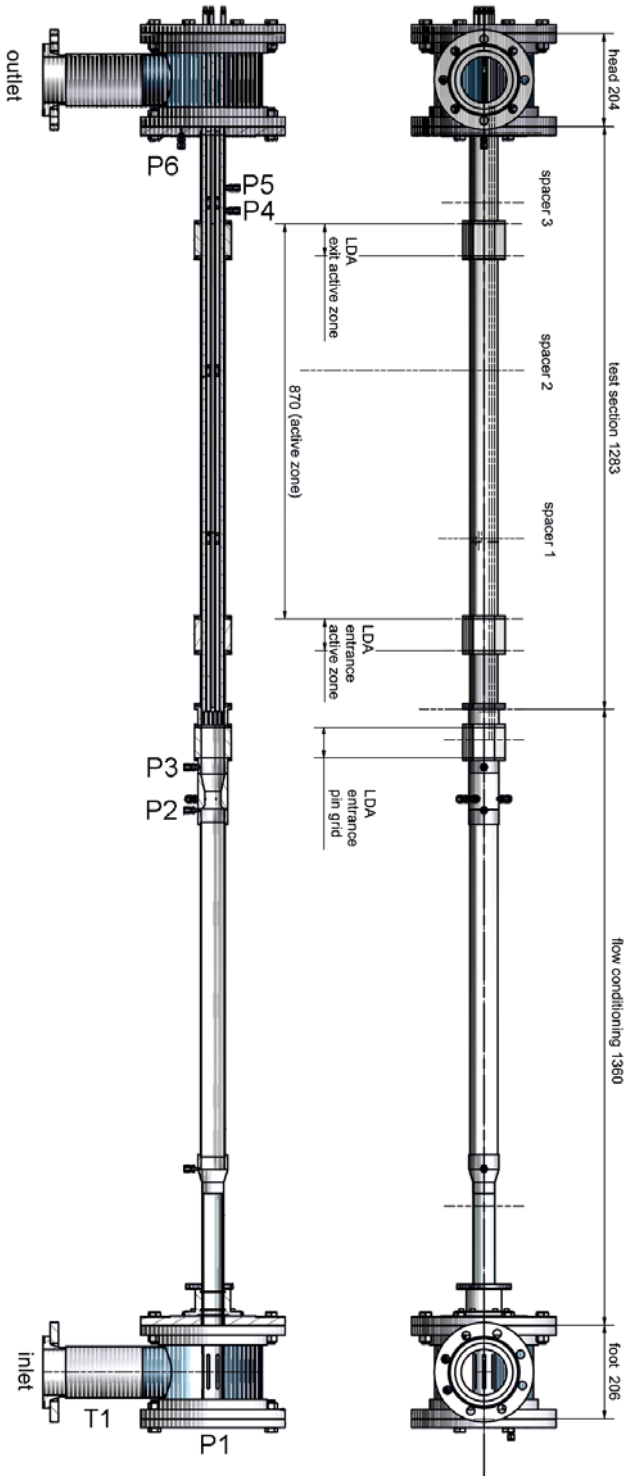

Table 1: Design parameters for the PDS-XADS fuel assemblies as well as the water and the electrically heated rod bundle experiment

	PDS-XADS	MYRRAH	Exp. H_2O	Exp. LBE
Geometry	Hexagonal	Hexagonal	Hexagonal	Hexagonal
Total power	0.775 MW	1.466 MW	–	0.43 MW
Fuel pins	90	91	19	19
Pin diameter	8.5 mm	6.55 mm	8.2 mm	8.2 mm
Pitch	13.41 mm	8.55 mm	11.48 mm	11.48 mm
Pin length	1 272 mm	1 200 mm	1 272 mm	1 272 mm
Active height	870 mm	600 mm	870 mm	870 mm
Grid spacer	3	3	3	3
Mean velocity	0.42 m/s	2.5 m/s	10 m/s	2 m/s
Mass flow	~41 kg/s	~71 kg/s	~13 kg/s	~26 kg/s
Subchannel area	9 330 mm²	2 760 mm²	1 260 mm²	1 260 mm²
Max. heat flux	150 W/cm²	131 W/cm²	-	100 W/cm²
Inlet temperature	~300°C	~200°C	~25°C	~300°C
Outlet temperature	~400°C	~337°C	~25°C	~415°C

Numerical calculations

Subchannel analysis

By means of subchannel analysis of the test section the expected pressure losses are calculated and the wall distance is optimised to provide a homogenous temperature distribution for all subchannels in the rod bundle. For this purpose, the thermal-hydraulic analysis code MATRA (Multi-channel Analyser for steady states and Transients in Rod Arrays) based on the subchannel analysis tool COBRA-IV-I, was used. It was initially developed at the Korean Atomic Energy Research Institute (KAERI) to provide an improved structure, additional functions and models, a convenient user environment and increased numerical accuracy.

For the analysis of heavy liquid metal cooled fuel assemblies several modifications to the MATRA code were necessary as the original code does not include the thermo physical properties of liquid metals. Therefore, the thermophysical properties of the used heavy liquid metal LBE was implemented into the MATRA code [1].

The single phase turbulent friction factor is obtained using the Rehme correlation for triangular rod arrays [2]. Detailed knowledge about turbulent mixing in-between adjacent subchannels in LBE flows is still missing. A CFD-based systematic study of the turbulent mixing in heavy liquid metal cooled rod bundles conducted by Cheng [3] showed that the turbulent mixing, *i.e.* the velocity fluctuation across the gap, is proportional to the mean axial flow velocity with a factor of 0.02.

The rod bundle layout is shown in Figure 2. Subchannel calculations are performed for different wall distances w in the range between 5.1 mm and 8.1 mm. Constant mean LBE flow velocity of 2.0 m/s and a channel inlet temperature of 300°C is assumed. The channel exit temperatures of all channels for three different values of w are also shown in Figure 2.

Due to the constant mean flow velocity the average temperature decreases with increasing wall distance w. Obviously the outer channels 25 to 42 are highly affected while the temperature for the inner channels 1 to 24 remains nearly constant. Simulation for a wall distance of 5.1 mm (squares) shows an about 20 K higher channel exit temperature for the outer channels, while for a wall distance of 6.1 mm (triangles) the temperature is about 10 K lower.

The optimised wall distance of 5.7 mm leads to a minimal temperature difference between all channels. This reduces thermal stresses and minimises differential elongation. An average pressure loss of 0.20 MPa and an average channel exit temperature of 413°C is computed. The maximum temperature variation among all rods over the test section is as low as 4.9 K, while the variation of the subchannel temperature shows a much higher value of 9.2 K. This is due to the high temperature in the corner channels with the smallest channel area. The maximum temperature difference between the rods and its corresponding subchannel at a given height does not exceed a value of 33 K.

Figure 2: Rod bundle layout with modelling parameter wall distance w (left) and channel exit temperatures of the subchannels for three different wall distances w (right)

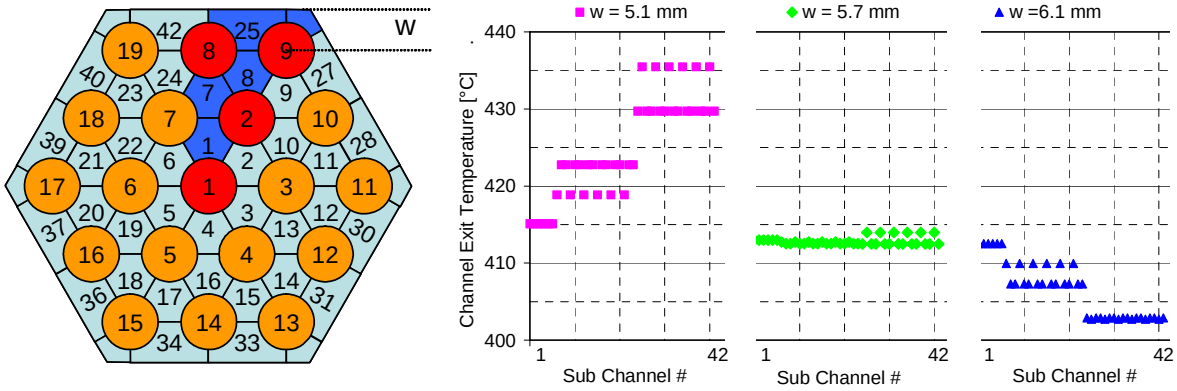

Spacer

A crucial element of a rod bundle is the spacer which ensures at all operational conditions a constant P/D ratio and thus guarantees a defined neutronic and thermal-hydraulic performance of the reactor system. The spacer design is kept as close as possible to the original developed in the context of the PDS-XADS and is shown in Figure 1. It is composed of a honeycomb structure requiring four different subchannel types to fit into the hexagonal shape of the rod bundle cross-section. The rods are focused by point contacts embossed in the honeycombs to compensate lateral and axial expansion of the rods. Moreover, the point contact reduces the extent of the hot spot. Optimisations regarding enhanced flow conditioning have not been evaluated as these are not regarded to be necessary for liquid metal flows. In contrast to the original design which suggests bending and welding of steel plates, the spacers fabrication employs by selective laser melting. An additional surface treatment reduces surface roughness from 30 µm to 15 µm after polishing. This is of the same order as the laminar viscous sublayer thickness in the liquid metal subchannel flow.

The material thickness is 0.5 mm in the inner structure and 0.25 mm at the outer subchannels respectively. This leads to an average blockage ratio for the honeycomb structure without embossed point contacts of 0.15. It increases to 0.30 if the whole cross-section of the spacer including point contact structures is taken into account. The resulting loss coefficient calculates with the Rehme correlation [4]:

$$C_D = 7 \cdot \left(\frac{A_S}{A} \right)^2$$

to C_D = 0.16 without point contacts and to C_D = 0.65 with point contacts respectively. One should expect that pressure loss measurements are close to the higher C_D value as the influence of the point contacts is supposed to have a significant effect onto the rod bundle flow. For the isothermal water rod bundle experiments the same input values have been used on the optimised geometry. The resulting estimated pressure loss for the spacer and the test section are listed in Table 2 together with the results for the LBE rod bundle flow with inlet temperatures of 200°C and 300°C.

Table 2: Results of pressure loss calculations with MATRA on the optimised rod bundle geometry for low and high spacer influence at nominal operating conditions

	H_2O exp.	LBE exp 200°C	LBE Exp 300°C
Spacer pressure loss low C_D	0.14 bar	0.10 bar	0.10 bar
Spacer pressure loss high C_D	0.38 bar	0.20 bar	0.20 bar
Test section pressure loss low C_D	1.84 bar	1.96 bar	1.91 bar
Test section pressure loss high C_D	2.58 bar	2.26 bar	2.21 bar

CFD

CFD calculations with the commercial software package STAR-CD 3.26 have been carried out for the foot section, the flow conditioning and the head section. The geometry of these parts has been optimised with respect to a minimal pressure loss while requiring a homogeneity of the flow of 98%.

For the lower vessel part of the foot several designs were discussed to homogenise the flow in the upstream tube. In the original PDS-XADS design this vertical tube ends directly in the lower part of the reactor vessel where the fluid is almost stagnant. By means of a deflector plate low uniform fluid velocities and uniform pressure conditions as shown in Figure 3 could be obtained. The resulting pressure loss shown in Table 3 is quite high so that the shape and length of the entrance slits was maximised in the actual fabrication process of the foot vessel. A picture of the manufactured rising tube is shown on the right side in Figure 3. The resulting pressure loss of that second design is now reduced by approximately 25%. A summary of the optimised geometric dimensions and pressure losses at nominal operating conditions for both designs are given in Table 3.

Figure 3: Results of a CFD aided optimised foot module geometry showing pressure loss (left) and velocity distribution (middle). Picture of manufactured riser tube (right).

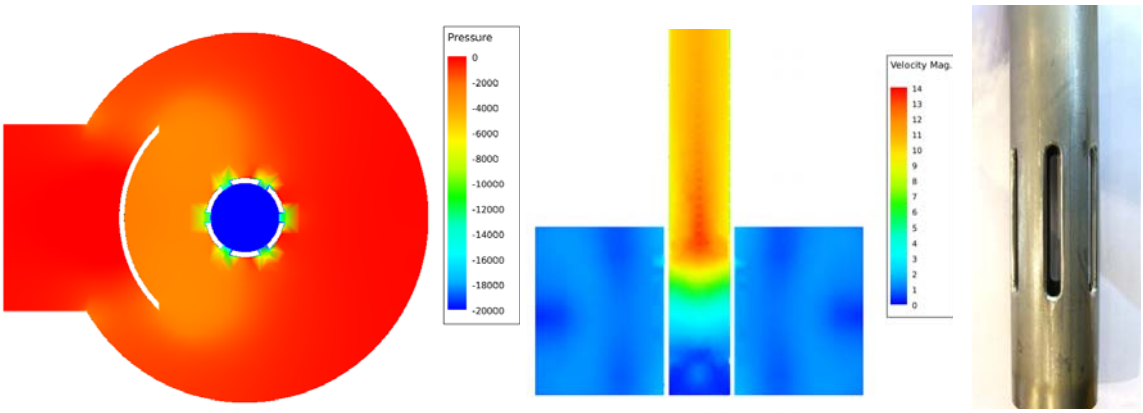

Table 3: CFD Results of optimisation of foot geometry at nominal operating conditions

	First foot design	Second foot design
Length of foot vessel	110 mm	110 mm
Diameter of foot vessel	213 mm	213 mm
Diameter of riser tube	40 mm	41.1 mm
Number of entrance slits	6	6
Height of entrance slits	70 mm	80 mm
Width of entrance slits	6.5 mm	6.5 mm chamfered
Pressure loss H_20 at 25°C	1.15 bar	0.89 bar
Pressure loss LBE 200°C	0.86 bar	0.75 bar
Pressure loss LBE 300°C	0.85 bar	0.74 bar

Sensor instrumentation

The intended sensor instrumentation for pressure and fluid velocity measurements of the water rod bundle experiment is shown in Figure 1. To ensure the comparability of both water and LBE rod bundle measurements, the geometrical design and material used are identical except for the windows made of polymethylmetacrylate (PMMA) that are required in the water experiment for the Laser Doppler Anemometry (LDA) measurements determining the velocity distribution. For the isothermal water experiment subchannels temperature measurements are not necessary. In case of the LBE experiment LDA measurements are not possible due to the opaqueness of the fluid.

Pressure and temperature measurements are foreseen at positions T1, P1 and P6 to characterise the overall inlet and outlet conditions. Additionally pressure sensors are installed to measure the pressure loss of the foot and flow conditioning (P2-P1), overall test section loss (P6-P3) and the spacer induced pressure loss (P5-P4). To characterise the pressure distribution in each individual subchannel, it is planned to integrate a movable pitot tube into the collector head. Due to the small distance of the rods a maximum diameter of 1.7 mm is allowed to reach the inner subchannels. This domain is not accessible with a Prandtl tube that would allow for more precise measurements. In the water experiment, fluid velocities can be easily and accurately measured by LDA. Therefore, optical access is foreseen by PMMA windows as marked in Figure 1. The velocity distribution is measured in the rod bundle downstream the venturi tube to characterise the inlet conditions, upstream the first spacer to characterise the lateral flow distribution due to the bundle and upstream the last spacer to characterise the spacer induced pressure loss and lateral flow redistribution. Due to the rod bundle geometry only for the outer subchannels the full area is optically accessible as shown in the left drawing of Figure 4 together with the UDV sensor instrumentation and the position of the thermocouple rakes.

Figure 4: Rod bundle test section with LDA measurement capabilities (left), positions for UDV sensor instrumentation (middle) and thermocouple rake (right). Size of the thermocouple rake is exaggerated in this view and will be much smaller in reality.

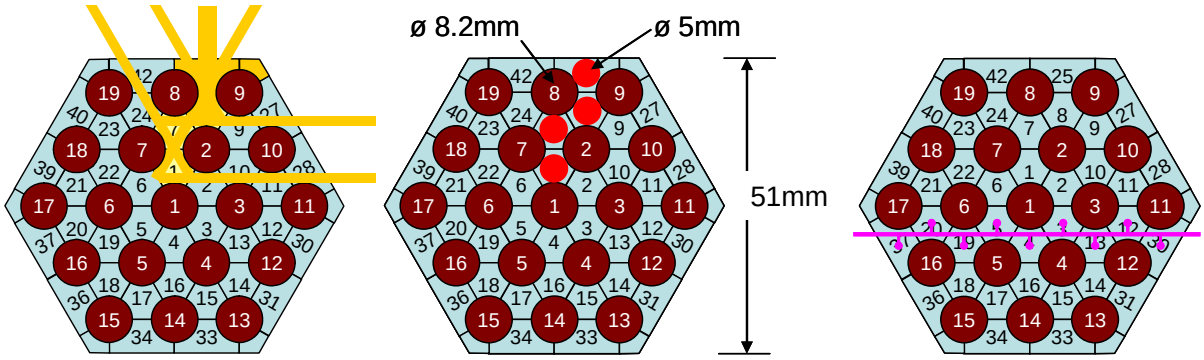

In the LBE experiment subchannel temperature measurements over the whole heated test section are necessary to gather information regarding the thermal-hydraulic behaviour of the flow. For this purpose, three traversable thermocouple rakes are installed in the test section. They are movable along the assembly between the spacer positions.

Ultrasonic Doppler Velocimeter (UDV) measurements are carried out for both water and LBE experimental set-up. For this purpose small UDV-transducers of 3 mm diameter will be positioned between the rods at the head exit position. However, capturing of the flow rate is limited because of the beam divergence of the ultrasonic measurement signal. In this set-up the maximum depth is 100 mm from the top so that it will be possible to determine the flow rate at the test section exit.

Measurements

Water rod bundle pressure measurements

Pressure loss measurements on the water rod bundle experiment were carried out at temperatures of 25°C and fluid flow rates from 0 m³/h up to 45 m³/h resulting in fluid velocities up to 5 m/s in the flow conditioning section and velocities up to 10 m/s in the rod bundle test section area. Differential pressure sensors have been used at positions P1 to P6 as described above. The results are shown in Figure 5.

The measured pressure loss in the foot design turns out to be in the range of what was expected from the CFD calculations for the second foot design. For the pressure loss of the test section and the spacer the calculated values for the high blockage ratio of the spacer match the experiments well. The calculations for the low blockage ratio are far too low compared to the measurements.

Figure 5: Measured pressure loss along the foot, the rod bundle test section and the last downstream located spacer as a function of flow rate

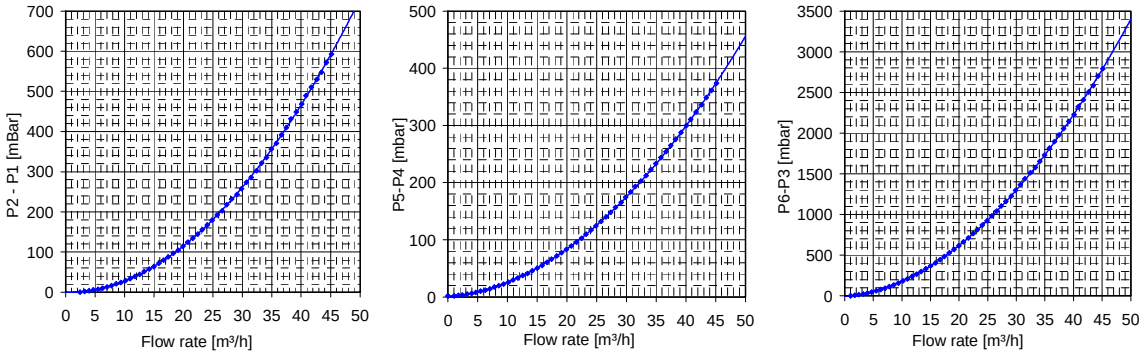

Loss coefficient was calculated for the rod bundle test section and the uppermost spacer using the formula:

$$C_D = \frac{\Delta p}{0.5 \cdot \rho \cdot u^2}$$

with the pressure loss Δp, fluid density ρ and fluid velocity u. The hydraulic diameter for the rod bundle test section can be calculated to d_h = 7.58 mm and was also used for the spacer region. This leads to Reynolds numbers up to 10^5 in the measured area. The results of the measured loss coefficients are shown together with the MATRA pre-calculations for the low and high spacer influence in Figure 6.

Figure 6: Comparison of numerically predicted and measured loss coefficient for one spacer (left) and for the test section area (right) together with calculated values as a function of Re

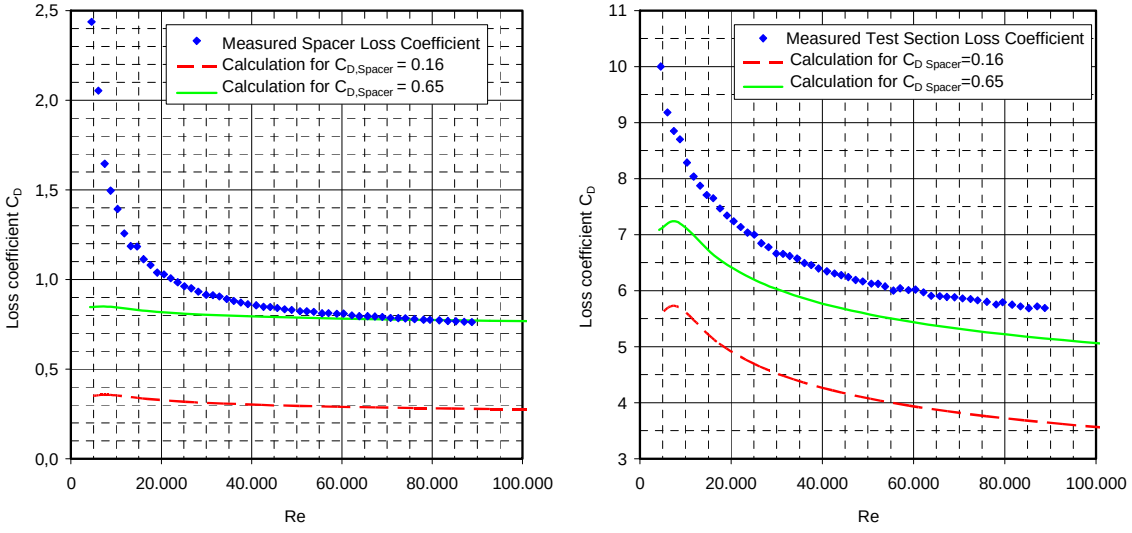

It can be seen that the estimated pressure loss of the spacer for the calculated high blockage ratio agrees almost perfectly with the measurements in the high flux region for Reynolds numbers higher than 40 000 where the flow is fully turbulent. In the transitional flow regime with Reynolds numbers between 5 000 and 35 000 the influence of the secondary flow is relatively high and leads to a rising loss coefficient.

For the complete rod bundle test section the numerical predicted pressure loss underestimates the measurements by approximately 10% leading to a slightly lower loss coefficient. In contrast to the spacer pre-calculations the variation stays constant also in the transitional flow regime for lower

Reynolds numbers giving reasonable agreements down to Re = 10 000. One possible reason for the difference between and measurement and calculations is the entrance guide at the beginning of the test section that has to be taken into account as an additional blockage for the subchannel analysis. Another reason can be found in the flow separation at the upper vessel leading to additional momentum losses.

Conclusions

In this paper a scaled liquid metal cooled fuel rod bundle simulation experiment performed within the IP-EUROTRANS project is presented. Its modular design admits measurements in water and liquid metal flows with minimised modifications of the experimental set-up. CFD and subchannel analysis aided geometry optimisation leads to an optimal set-up with minimised pressure losses.

First pressure loss experiments at selected positions in the water rod bundle experiment show an excellent agreement with pre-calculations made by subchannel analysis code MATRA in the fully turbulent flow regime. For smaller Reynolds numbers the influence of secondary flow has to be taken into account. The comparison between CFD and experiment with a 45% overestimated pressure loss at nominal working conditions show a quite reasonable agreement.

Acknowledgements

The work is supported in the framework of the IP-EUROTRANS project; contract number FI6W-CT-2004-516520.

References

[1] Litfin, K., R. Stieglitz, "Sub-channel Analysis of Heavy Liquid Metal Cooled Fuel Assemblies", *Proc. Jahrestagung Kerntechnik 2006*, INFORUM Verlag, Berlin, 674 (2006).

[2] Rehme, K., "Pressure Drop Performance of Rod Bundles in Hexagonal Arrangements", *Int. J. Heat Mass Transfer*, 15, 2499 (1972).

[3] Cheng, X., N. Tak, "CFD Analysis of Thermal-hydraulic Behavior of Heavy Liquid Metals in Sub-channels", *Nuclear Engineering and Design*, 236, 18, 1874 (2006).

[4] Rehme, K., "Pressure Drop Correlations for Fuel Element Spacers", *Nuclear Technology*, Vol. 17, pp. 15-23 (1973).

Feasibility of FBR core concept with two different TRU composition regions

Shuhei Maruyama
Japan Atomic Energy Agency, Japan

Abstract

A new FBR core concept which has two different TRU-composition regions is proposed in this paper. A conventional sodium-cooled MOX fuel core consists of two different Pu-enrichment fuels in the radial direction to flatten the radial power distribution. As the fuels burn, power contribution of outer core is getting smaller while inner core getting larger, which results from the difference of the content of fissile materials between two kinds of fuel, as long as the both fuels have the same TRU composition. The new core concept is devised to suppress the difference of burn-up characteristics between inner and outer cores by utilising feature of nuclides. As a result of survey calculations for various combinations of TRU composition, an adjustment of MA content in inner and outer core fuels is found to be most effective and practically feasible. By increasing the MA content of outer core fuels while decreasing that of inner core fuels, it is possible to reduce power distribution change along with burn-up, which leads to the reduction of required coolant flow rate. Moreover, this concept improves the safety parameters such as sodium-void reactivity and Doppler coefficient. Assuming an advanced aqueous reprocessing process with Am-Cm extraction, we have prepared inner and outer core fuels in which Am-Cm is concentrated on the latter ones, namely, U-Np-Pu for inner core fuels, U-Np-Pu-Am-Cm for outer core fuels. But the outer core fuels have difficulties in fuel design, for instance, the large Am-Cm content conduces to a large amount of helium production. These difficulties are relieved by implementing two TRU composition regions also in the axial direction. It is found that not only avoiding the fuel design difficulties, the two TRU composition regions both in radial and axial directions can enhance the above-mentioned merits in core characteristics effectively.

Introduction

Recently, conceptual studies of sodium-cooled fast breeder reactor (FBR) core in Japan have taken much interest in the transition stage from light water reactors (LWR) to FBR [1]. In this stage, we need to suppose to use the fuels which are recovered from LWR spent fuel (SF). Various transuranic (TRU) compositions for these SF result from discharge burn-up, cooling time, and initial fuel composition. For example, as cooling time increases, SF accumulates minor actinide (MA) which is mainly ^{241}Am due to beta-decay of ^{241}Pu. Differences in LWR SF compositions influence FBR core characteristics because of variety in cross-section and decay constant for these nuclides. Especially, MA has significant influence on core and fuel design. This paper contrives a new FBR core concept that has the potential acceptability of high-MA-content TRU from LWR SF. The author pursued possibility of improvement of core characteristics by using nuclide characteristics for different fuel compositions, and then proposed the core concept that has two different TRU-composition regions.

Assumptions and conditions for this study

The reference core

For a reference core in this study, the author employed the "high-internal-conversion (HIC) type" sodium-cooled MOX fuel core that is the principal core concept obtained in the Feasibility Study on Commercialised Fast Reactor Cycle System (FS) Phase-II in Japan [2]. Since this study mainly concerned the LWR-FBR transition stage, the "breeding core" that has radial blanket was selected. Major core and fuel specifications are listed in Table 1. Core configuration and fuel assembly are illustrated in Figure 1. The HIC type core was designed to achieve a high internal conversion ratio by adopting fuel pins of large diameter. This feature reduces the amount of blanket, which results in an economical advantage due to reducing the fuel fabrication cost. To flatten radial power distribution, the reference core uses two kinds of Pu-enrichment fuel assembly (inner core and outer core assembly) in radial direction, which is the same as conventional FBR cores.

Fuel composition

As a typical FBR core fuel composition in the reactor transition stage, a TRU composition recovered from LWR SF was employed in this study. In FS Phase-II, several typical TRU compositions from LWR SF had been evaluated, and they were based on a scenario of FBR deployment. The TRU composition selected is one of those compositions. When recovering TRU from SF, an advanced aqueous reprocess with Am-Cm extraction was assumed in this work. Usually, Am and Cm are accompanied by a certain amount of rare earth nuclides in an Am-Cm extraction process. For the uranium isotopic composition in core and blanket fuels, the depleted uranium composition was used. These nuclides compositions are as follows:

TRU composition [wt.%]
^{238}Pu/^{239}Pu/^{240}Pu/^{241}Pu/^{242}Pu/^{237}Np/^{241}Am/^{243}Am/^{244}Cm = 1.9/47.2/24.0/2.4/7.0/6.4/9.4/1.5/0.2
Residual FP fraction [wt.%]
Residual FP / (Am+Cm) = 10.0
Uranium composition [wt.%]
^{235}U/^{238}U = 0.3/99.7

In this paper, reference core with inner and outer core fuels which have TRU composition presented above is called "reference case".

Calculation method

The core characteristics were calculated using the neutron diffusion theory code for two-dimensional R-Z geometry. The cross-sections considered the self-shielding effect were prepared for a homogeneous cell representation by using the adjusted cross-section library ADJ2000R [3,4]. The corrections for neutron transport effect, spatial mesh effect, and cell-heterogeneity effect were taken into account to calculation values.

Table 1: Core and fuel specifications of the reference core

Items	Value
Reactor power (thermal/electric) [MW]	3 570/1 500
Coolant temperature (outlet/inlet) [°C]	550/395
Operation cycle length [month]	26.3
Refuelling batch (core / radial blanket) [-]	4/4
Core height [cm]	100
Axial blanket thickness (upper/lower) [cm]	20/20
Envelope diameter of radial shielding [m]	6.77
Fuel pin diameter (core/radial blanket) [mm]	10.4/11.7
Fuel pin cladding thickness (core/radial blanket) [mm]	0.71/0.42
Number of fuel pin per assembly (core/radial blanket) [-]	255/217

Figure 1: Core configuration and fuel assembly of the reference core

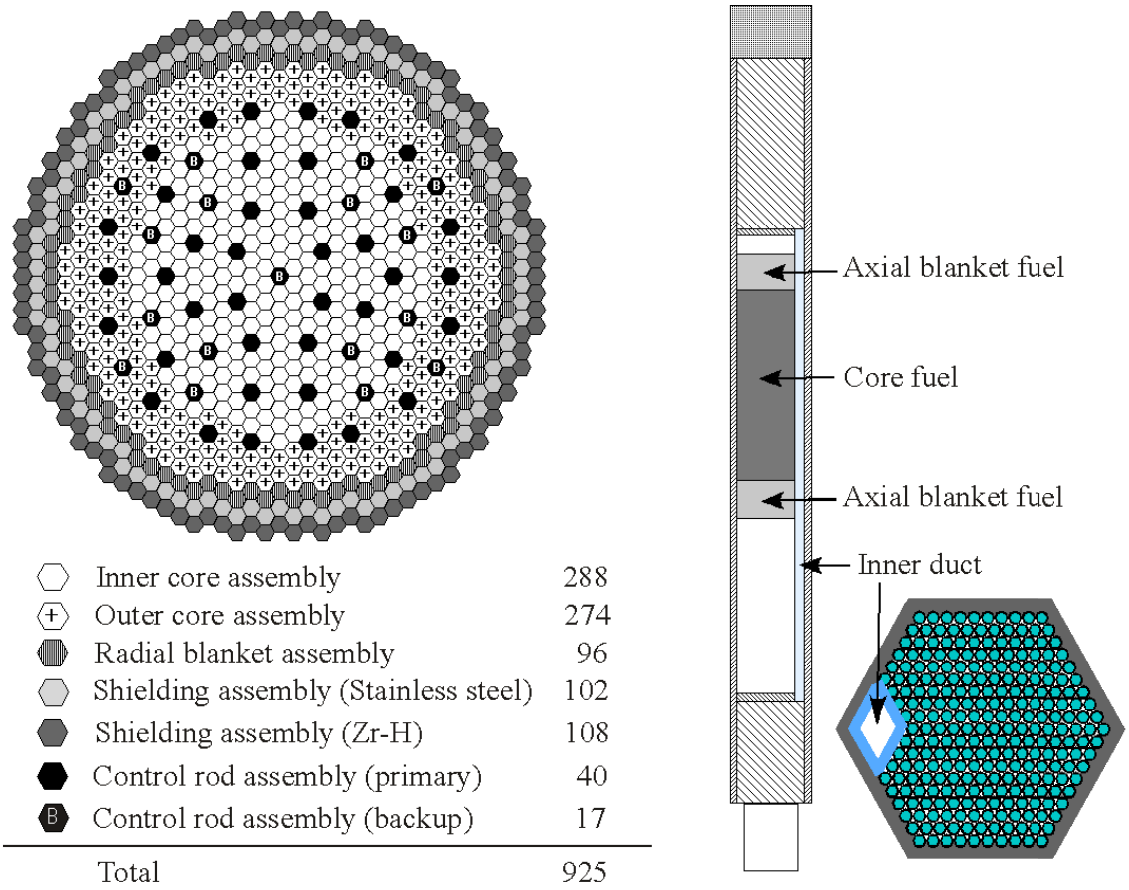

Core concept with two different TRU-composition regions

This section describes a core concept with two different TRU-composition regions. The concept is introduced to improve safety parameters (*i.e.* sodium void reactivity and Doppler coefficient) and power distribution change by controlling the MA content of inner core and outer core fuel. At first, the reference core configuration is employed for this study. Then, the configuration is improved, because this concept may bring some difficulties in fuel design. Finally, attractive core concepts with two different TRU-composition regions core are selected as representative cases, and their core characteristics are compared to the reference case.

Control of Am and Cm fraction in inner and outer core fuels

As described in Introduction, we need to suppose to use the high-MA-content fuels recovered from LWR SF in the reactor transition stage. MA fed into FBR core fuel consists mainly of fertile. Compared to typical fertile ^{238}U, the MA has the following characteristics. In fast neutron energy region, fission cross-section has threshold and as neutron energy increases, neutron production is getting higher. In intermediate neutron energy region (middle energy range between fast neutron and thermal neutron), capture cross-section is higher. Therefore, in the case of using MA as core fuel, neutron importance at fast energy region becomes higher, while it becomes lower at intermediate energy region. This energy distribution of neutron importance causes increment of sodium void reactivity and decrement of Doppler coefficient in absolute value. MA also shows the ability of high conversion from fertile to fissile.

As a way of suppressing the influence on safety parameters and utilising the ability of high conversion, the author proposes the core concept with two different TRU-composition regions, in which MA content of inner core fuel is lowered, while outer core fuel is heightened. A conventional sodium-cooled MOX fuel core consists of two different Pu-enrichment fuels in the radial direction to flatten the radial power distribution. As the fuels burn, power contribution of outer core is getting smaller while inner core getting larger due to the difference of fissile materials content in two different Pu-enrichment fuels, as long as the both fuels have the same TRU composition. This power distribution change can be suppressed by using higher MA content fuel for outer core. The safety parameters are also getting better than the reference case, because of setting MA at outer core where the neutron flux and importance are lower.

On those assumptions, the survey calculations for safety parameters and enveloped reactor power* were performed by parametrically changing the Am-Cm content of inner and outer core fuels. Owing to the Am-Cm extraction process, Am-Cm content in fuel can be adjusted. If Am-Cm is concentrated in outer core fuel, then Am-Cm content of inner core fuel becomes lower. That means TRU composition is kept constant in entire core fuel whenever the Am-Cm contents of inner and outer cores are changed. The results of this calculation are shown in Figure 2. The leftmost mark in the graphs means all Am-Cm are added in inner core fuels, and then the outer core fuel becomes U-Pu-Np fuel. The rightmost mark means *vice versa*. Shaded marks mean inner and outer core fuels have the same TRU composition, which corresponds to the reference case.

Figure 2: Safety parameters and enveloped reactor power

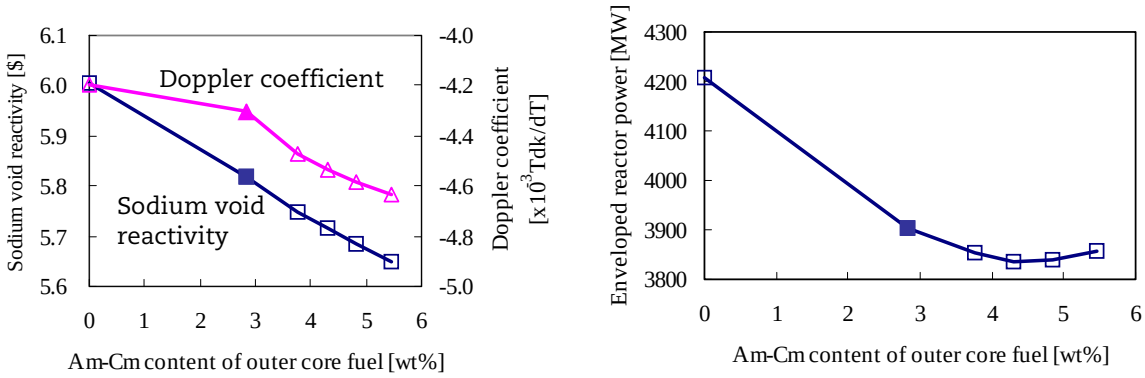

The results show that the enveloped reactor power tends to be lower when Am-Cm content of outer core fuel is higher than the reference case because of suppressing the mismatch of power distribution. And also, the less MA content of inner core fuel leads to the better safety parameters. Therefore, as the fuels of two different TRU-composition regions, U-Pu-Np fuel is employed as inner

* A parameter related to the required coolant flow. The coolant flow region i was set tentatively for each assembly layer in the two dimension core modelling. The enveloped reactor power P_E was estimated as follows:

$$P_E = \sum_i p_i n_i$$

where p_i is the maximum assembly power of the i-th coolant flow region during the life, and n_i is the number of assembly in the i-th coolant flow region.

core fuel and U-Pu-Np-Am-Cm fuel is employed as outer core fuel (the rightmost mark in Figure 2). This core may become an effective loading concept in terms of safety parameters when TRU with high MA content is fed from LWR SF.

Employment of axial outer core region

The concept described above is good for safety parameters and required coolant flow. However, the increment of Am-Cm content in outer core fuel causes lowering of allowable linear heat rate because of lowering of fuel melting point and thermal conductivity. Moreover, it increases the helium production in outer core fuel pin mainly by the (n,γ) reaction of ^{241}Am as described in Figure 3. Although it was possible to change fuel specifications such as fuel pin diameter, gas plenum length, and cladding thickness, this study pursued a way to decrease MA content and/or to suppress the maximum linear heat rate and the neutron fluence (related to rare gases production included helium gas production) of outer core fuel pin by modifying the core configurations.

Figure 3: Helium gas production process

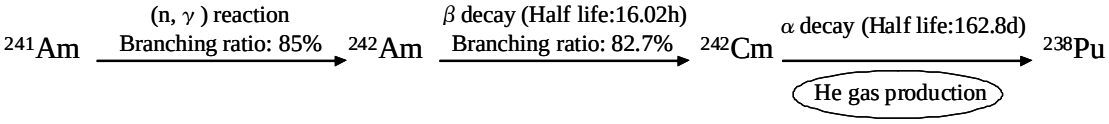

To prevent Am-Cm concentration, outer core fuel region (high MA content fuel region) should be taken more widely. But, if outer core region is extended toward inner core region, safety parameters would be getting worse. So, we focused on the upper and lower part of inner core assembly. Safety parameters are insusceptible to MA here, because neutron flux and importance at the upper and lower part of core are lower than the central part. Moreover, by setting two different Pu-enrichment fuel regions in axial direction as well as in radial direction, we can expect the suppression of the maximum linear heat rate and the neutron fluence of outer core fuel pin due to flatten neutron flux and power distributions. Thus, the core concept with two different TRU-composition regions is adopted in axial direction as well as in radial direction. The outer core fuel (high TRU content U-Pu-Np-Am-Cm fuel) encloses the inner core fuel (low TRU content U-Pu-Np fuel) as illustrated in Figure 4.

Figure 4: Core with two TRU composition regions in radial and axial directions

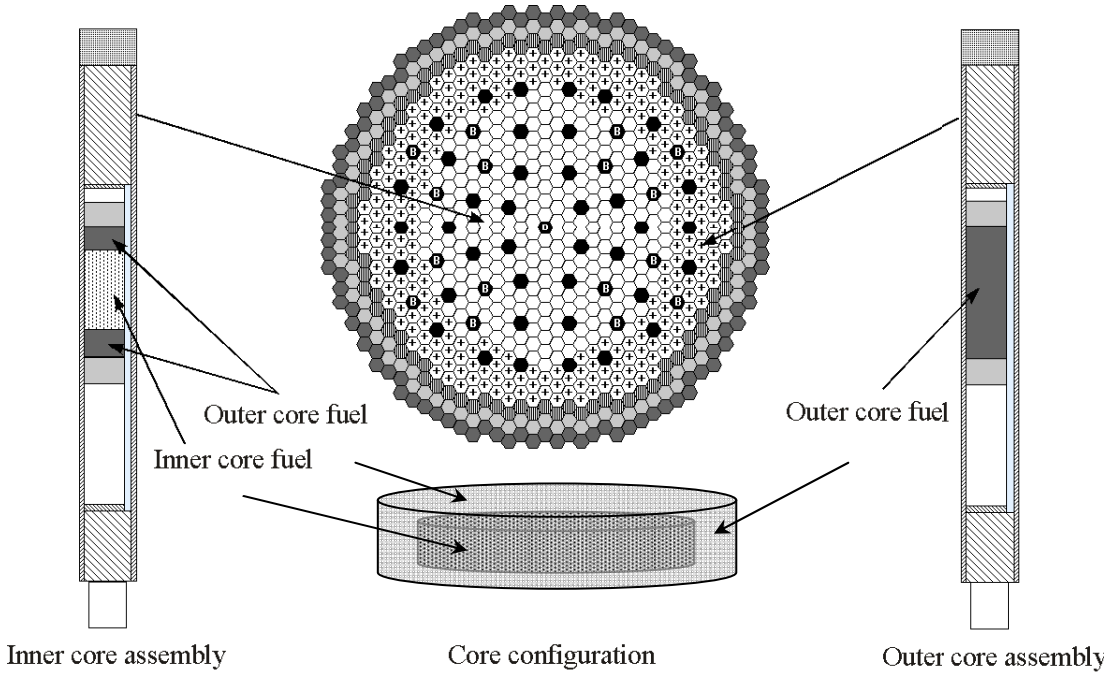

In order to investigate the effect on core characteristics when outer core fuel was employed to the upper and lower part of inner core assembly, outer core fuel region in inner core assembly was increased step by step and core characteristics were evaluated. The results were shown in Figure 5. Am-Cm content of outer core fuel decreases when outer core region is extended. By increasing the outer core region, the maximum linear heat rate and the neutron fluence of outer core assembly are also getting lower. Safety parameters show gradual increments, but Doppler coefficient is somewhat less sensitive than sodium void reactivity due to compensating effect of uranium content increment in inner core fuel.

Figure 5: Effect of setting outer core region to upper and lower part of inner core assembly

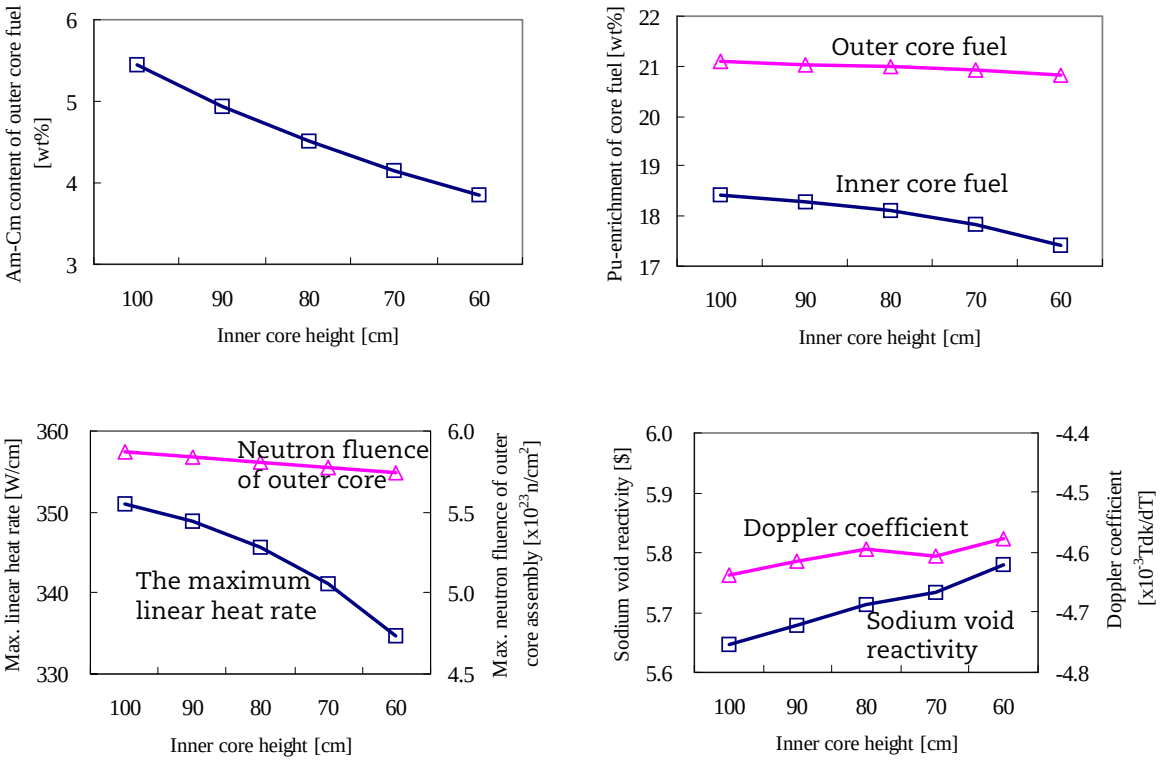

The representative core configurations

Setting axial outer core region in inner core assembly, we confirmed the fact that the maximum linear heat rate and the neutron fluence of outer core assembly are decreased. For seeking more attractive core concept, the fraction of inner and outer core fuel assemblies was changed. By setting outer core region to more outside position, it was found that the safety parameters improved. And, even though MA content of outer core fuel was increased, the maximum linear heat rate and the neutron fluence of outer core assembly were lower than the previous core configuration. Case 1 and Case 2 in Table 2 were selected as representative core configurations which took the minimum values in maximum linear heat rate within the parameter survey of the inner core height.

Eventually, compare to the reference case, the cores with two different TRU-composition regions in radial and axial directions have high-MA-content outer core fuel in order to improve safety parameters. In the case of using high-MA-content fuel, it may cause some difficulties in fuel design. But, as shown in Table 2, the cores presented here can lower the maximum linear heat rate and the enveloped reactor power. Furthermore, despite the outer core fuel includes much MA, maximum rare gases productions per a fuel pin are comparable level to the reference case. That means we can mitigate the impacts on safety parameters and fuel design when high-MA-content fuel is used.

Table 2: Core characteristics of reference core and two different TRU regions core

Items	Reference	Am-Cm division	Case1	Case2
Inner core height [cm]	100	←	65	75
Number of outer core assembly layers	4	←	3	2
Number of core fuel assemblies [-] (inner/outer core)	288/274	←	332/230	392/170
Pu-enrichment: Pu/HM [wt.%] (inner/outer core)	18.2/21.1	18.4/21.1	17.4/21.5	17.4/23.3
Am+Cm content: (Am+Cm)/HM [wt.%] (inner/outer core)	2.4/2.8	0.0/5.4	0.0/4.3	0.0/5.7
MA content: MA/HM [wt.%] (inner/outer core)	3.9/4.5	1.4/7.1	1.3/6.0	1.3/7.5
Burn-up reactivity [%Δk/kk′]	1.4	1.7	1.4	1.3
Breeding ratio [-]	1.11	1.11	1.11	1.11
Max. linear heat rate [W/cm] *1	351	351	329	321
Max. neutron fluence of outer core assembly [10^{23}n/cm^2] *2	5.9	5.9	5.4	4.6
Max. fast neutron fluence [10^{23}n/cm^2] *3	4.9	4.8	4.8	4.7
Sodium void reactivity [$]*4	5.8	5.6	5.8	5.7
Doppler coefficient [10^{-3}Tdk/dT] *4	-4.3	-4.6	-4.8	-4.8
Enveloped reactor power [MW]	3 904	3 857	3 832	3 832
Max. rare gases production per a fuel pin [mol] (inner/outer core) *5	.127/.124	.114/.146	.125/.128	.121/.126
MA transmutation rate [%] *6	42	37	38	36

*1 Result of two-dimensional calculation.

*2 Average of core fuel.

*3 Neutron energy > 0.1 MeV.

*4 At the end of equilibrium cycle.

*5 Contributions from (n,α) reaction, α decay and fission.

*6 $(M_i-M_f)/M_i$: M_i = MA loading amounts, M_f = MA discharged amounts.

Conclusion

In the transition stage from LWR to FBR, it can be assumed for FBR to use high-MA-content fuel recovered from LWR SF. The high-MA-content fuel may cause decrement of design margin for safety parameters. As an effective MA-loading method, Am-Cm concentration in outer core fuel was proposed in this study, which leads to the improvement of safety parameters. It also causes the reduction of required coolant flow rate that results from the suppression of power distribution mismatch. On the other hand, high-MA-content fuel may bring difficulties in fuel design, for example, the reduction of melting point of fuel and the increment of helium production. The author employed an enhanced core concept which has two TRU-composition regions not only in the radial direction but also in the axial direction. This concept leads to the decreasing of the maximum linear heat rate and the maximum rare gases production of high-MA-content fuel. As a result of these improvements, main core characteristics were improved in comparison with the reference core. It is concluded that the new core concept proposed in this paper has the potential to mitigate the impacts on safety parameters and fuel design when high-MA-content fuel is loaded.

Acknowledgements

The author would like to thank S. Ohki and T. Mizuno for useful comments and fruitful discussions.

References

[1] Ohki, S., *et al.*, "FBR Core Concepts in the "FaCT" Project in Japan", *Proc. PHYSOR 2008*, Interlaken, Switzerland, 14-19 September 2008, Interlaken, Switzerland (2008).

[2] Mizuno, T., *et al.*, "Advanced Oxide Fuel Core Design Study for SFR in the "Feasibility Study" in Japan", *Proc. GLOBAL 2005*, Tsukuba, Japan, 9-13 October 2005, Paper No. 434 (2005).

[3] Ishikawa, M., *et al.*, "Development of a Unified Cross-section Set ADJ2000 Based on Adjustment Technique for Fast Reactor Analysis", *J. Nucl. Sci. Tech.*, Supplement 2, p. 1073 (2002).

[4] Hazama, T., *et al.*, *Development of the Unified Cross-section Set ADJ2000R for Fast Reactor Analysis*, JNC TN9400 2002-064 (2002) [in Japanese].

Verification of the RELAP5 code against the MEGAPIE irradiation experiment

Paride Meloni, Pietro Agostini
ENEA, Italy

Mariarosa Giardina, Maddalena Casamirra, Francesco Castiglia, Calogera Lombardo
Università di Palermo, Italy

Abstract

The paper deals with the verification of the RELAP5 code version modified for LBE and Lead cooling systems against the thermal-hydraulic data made available within the framework of MEGAPIE initiative, an irradiation experiment performed at SINQ proton accelerator of PSI (CH) on a lead-bismuth eutectic liquid target. The code has been firstly assessed on the preparatory T-H experiments (single-pin tests and MEGAPIE Integral Tests). In a second phase the work has focused on the post-test analysis of selected data from the MEGAPIE irradiation operation including both steady-state and transient conditions. The calculation results have shown the good capability of the code to simulate the thermal-hydraulics of the cooling circuit both in steady-state conditions, where the temperatures calculated along the loop are in very good agreement with the experimental values, and in transient conditions, where the loop response following accelerator trip events is correctly simulated.

Introduction

MEGAPIE (Megawatt Pilot Target Experiment) is an international project conducted at SINQ proton accelerator of the Paul Sherrer Institute (PSI) to demonstrate the feasibility of a liquid lead-bismuth spallation target up to a maximum beam power level of 1 MW. The MEGAPIE international consortium, which has been also supported by the 6th Framework Programme of the European Community, includes scientific groups from Switzerland (PSI), Belgium (SCK•CEN), France (CEA, CNRS), Germany (FZK), Italy (ENEA), Japan (JAERI), Korea (KAERI) and USA (DOE).

The main goals achieved after about four months of irradiation of the target have been to collect a design database for liquid lead-bismuth targets, to gain experience in operating such an apparatus with the present accelerator performances and to manage the licensing process for such a target system. The demonstration of the feasibility of a liquid metal target has been an important step in the way to develop a spallation target for accelerator-driven system to be used in the nuclear waste transmutation, moreover the huge amount of data produced during the different phases of the experiment are available for assessing and validating the numerical tools for design and analysis of related components and systems.

In particular, during the preparatory testing phase, the single-pin tests performed in CHEOPE (BRASIMONE) [1] and MEGAPIE Integral Tests (MIT) [2] supplied some useful experimental data on the T-H behaviour of the cooling system. These data allowed the FPN (Nuclear Fusion and Fission, and related technologies) department of ENEA to undertake, in co-operation with the University of Palermo, a validation activity of the RELAP5 code version mod3.2.2β modified for LBE and lead-cooling systems, which is its reference system code for transient and safety analysis of heavy liquid metal (HLM) reactors. This activity has been completed with the post-test analysis of the thermal-hydraulic behaviour of the SINQ during the MEGAPIE irradiation experiment.

The target cooling was one of the most important aspects of the target system design, it was carried out with a triple-loop, three-fluid circuit: the primary LBE loop, an intermediate loop filled with oil (Diphyl THT) and a water loop to reject the heat in the SINQ main cooling loop. The RELAP5 code, which was used in the design phase to simulate the behaviour of the target cooling system at different operational and off-normal conditions, showed some difficulties in calculating the thermal performance of the LBE-oil heat exchanger connecting the first two loops. The code inadequacy in simulating the thermal exchange in the HX oil side, where the thermal exchange conditions are improved by means of a spiral welded on the wall, affected in a relevant way the prediction of the overall behaviour of the cooling system.

The paper describes the two phases of the validation activity. In the first phase the re-calculation of the single pin and MIT tests has allowed to assess a new correlation for the heat transfer coefficient that was implemented in RELAP5 to take into account the improvement of the thermal exchange conditions. In the second phase the new code version has been applied for the post-test analysis of a selected set of the MEGAPIE Irradiation data. This part has concerned the re-calculation of thermal-hydraulic steady state conditions obtained by averaging the measured loop parameters for a convenient time interval without unexpected proton beam trips. In addition the code assessment has been completed with the simulation of the transient behaviour of the MEGAPIE cooling loop following proton beam trips of the SINQ source.

RELAP5 assessment on single pin and MIT data

The single pin tests were conducted in the CHEOPE (CHEmical OPErational transient) facility at the ENEA Brasimone Centre [1] as a preliminary study of the heat exchange performances of LBE primary fluid with an organic oil (Diphyl THT) secondary one in one out of the twelve bayonet-type cooling pins foreseen in the Target Heat Exchanger (THX) of the MEGAPIE cooling circuit (Figure 1) The LBE primary fluid enters the top and, flowing down along the external cylindrical shell, transfers the power absorbed from the heater to the oil secondary fluid. The secondary coolant flows down through a central annulus diameter of 18 mm and rises through the outer annulus, 2 mm gap width, and leaves the pin at the top. Spiralling ridge is welded on the outer wall of the central annulus. This creates an oil spiralling annular flow path around the diameter of the cooling pin improving the heat exchange performances. The spire is about 2 mm width and runs upward, around the circumference of the tube in a pitch of 77 mm and 30° inclination angle.

Figure 1: CHEOPE single cooling pin

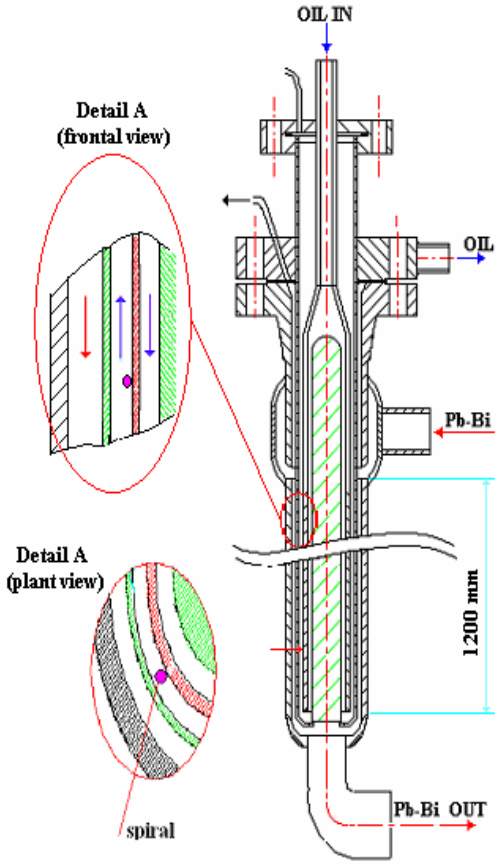

The preliminary analyses of the experimental data [3] showed that the one-dimensional RELAP5 code does not allow to take into account the 3-D effects induced in the oil bulk by the facilities peculiar geometry, it was decided to implement new correlations for the heat transfer coefficient and the pressure losses capable to simulate the thermal exchange conditions and to describe near helical hydraulic performances.

Implementation of the Gnielinski correlation

A literature survey showed that, on the basis of available experimental results, various authors suggested many correlations (unfortunately not always in agreement to one another) to be used to calculate heat transfer and friction factors in curved tubes. Among these correlations we thought to utilise the Gnielinski correlation (1) for the heat transfer, together with the Ito's one for friction factors (Table 1). The correlation developed by Gnielinski [4] was proposed at first for straight tubes, it has subsequently also been extensively tested for curved ducts and, once that suitable friction factors are employed together it, good performances in foreseen the Nusselt number has been found also in this case. The Gnielinski formula is:

$$Nu = \frac{(f_c/2)Re\,Pr}{1+12.7\sqrt{f_c/2}\left(Pr^{2/3}-1\right)}\left(\frac{Pr}{Pr_w}\right)^{0.14} \qquad (1)$$

where Nu, Re and Pr are, respectively, the Nusselt, Reynolds and the Prandtl numbers; Pr_w is the Pr evaluated at wall temperature and, finally, f_c is the friction factor. The friction factor losses from Ito's proposals [5] are shown in Table 1 at different Reynolds number intervals. In this table D is the helical diameter and d the internal duct one.

Table 1: Friction factor losses from Ito correlation

$f_c = \frac{16}{Re}$	$Re < 13.5(D/d)^{-0.5}$
$f_c = \frac{344(D/d)^{-0.5}}{\left\{1.56 + log_{10}\left[Re(D/d)^{-0.5}\right]\right\}^{5.73}}$	$13.5(D/d)^{0.5} < Re < 13.5(D/d)^{-0.5}$
$f_c = 0.076\ Re^{-0.25} + 0.0075\left(\frac{D}{d}\right)^{-0.5}$	$Re > 15000$

Indeed, in case of the single pin tests the flow of the oil was not merely helical because of a relevant gap between the spiral and the outer oil shell (0.6 mm), thus allowing a vertical out-flow of about 30% of the total oil mass flow rate, whose effects had to be accounted for. In fact, the presence of the gap limits the improvement in the heat transfer characteristics in consequence of the increase of the flow area that reduces the oil velocity. For this reason we obtained very good agreement [6] between experimental results and RELAP with Gnielinski describing in the model the oil path as a straight annulus rather than a helical coil.

Assessment of thermal exchange correlations on MITS test

As above said, in the MEGAPIE experiment, the LBE fluid is used as target material on which 580 MeV high energy proton current is injected to produce spallation neutrons necessary to core criticality. The proton beam deposits into the target about 540 kW power that must be removed to keep the operating target temperature. The target and the ancillary systems were preliminary set up and tested in a dedicated facility called MEGAPIE Integral Test Stand (MITS) [2], where the LBE heating was provided by replacing the MEGAPIE irradiation window with an electrical heater.

The MEGAPIE cooling system consists of separated three closed loops filled with different coolant fluids [Figure 2(b)]. The first loop is the Target Heat Exchanger (THX) in which the LBE primary fluid is used both as target material and as coolant. The secondary side of the THX, called Intermediate Cooling Loop (ICL), is filled with an organic oil (Diphyl THT) that removes heat from LBE fluid. In this system an Intermediate Heat eXchanger (IHX) transfers heat to other water loop (Water Coolant loop, WCL), placed between the ICL and the cooling plant of the experiment hall.

The difference between the MITS and SINQ configurations is that in the MITS, the proton beam was simulated by an electrical heater, called the Liquid Metal Container Heater (LMCH) mounted at the bottom of the target. The heater power in MITS configuration was ~157 kW, while the proton beam power in the steady-state SINQ configuration is ~540 kW. There were also certain slight differences in the configuration of the water loop piping between MITS and SINQ configurations. By using this ancillary system, a first experimental campaign was performed under different flow rates, temperatures, and heating power.

The THX is an assembly of 12 individual cooling pins inserted into 12 separated channels on the primary side, arranged in semicircles in the upper target [Figure 2(a)]. There are two relevant differences respect to the single pin tested in CHEOPE: the gap between the spiral welded on the inner surface and the outer surface was 0.6 mm by design in the single-pin tests while a maximum value of 0.175 mm for the tolerances is possible in the MEGAPIE design, an increased number of spires in about the same length of pipe. Both these differences have determined a better thermal exchange performance in MEGAPIE rather than in the single pin tests. They have been taken into account in the model by means of a different description of the oil cooling path. In fact, in the MEGAPIE cooling pin model it has been modelled as a helical pipe instead of the straight pipe previously used.

MITS steady states have been used for the assessment of the RELAP5 heat exchange correlations in the THX exchanger, the most critical component for a correct simulation of the MEGAPIE cooling loop. To this purpose a simple RELAP5 model of the component has been applied for the re-calculation of some selected steady states representative of the range of tested thermal-hydraulic conditions. The correlation of Seban-Shimazky (2) proposed for liquid metal flow in pipe [7] has been adopted in the THX LBE side. The new correlation of Gnielinski (1) has been used in the Oil side. Calculation results

Figure 2: Section of the THX in the upper target (a) and scheme of the MEGAPIE cooling system with location of the Instrumentation (b)

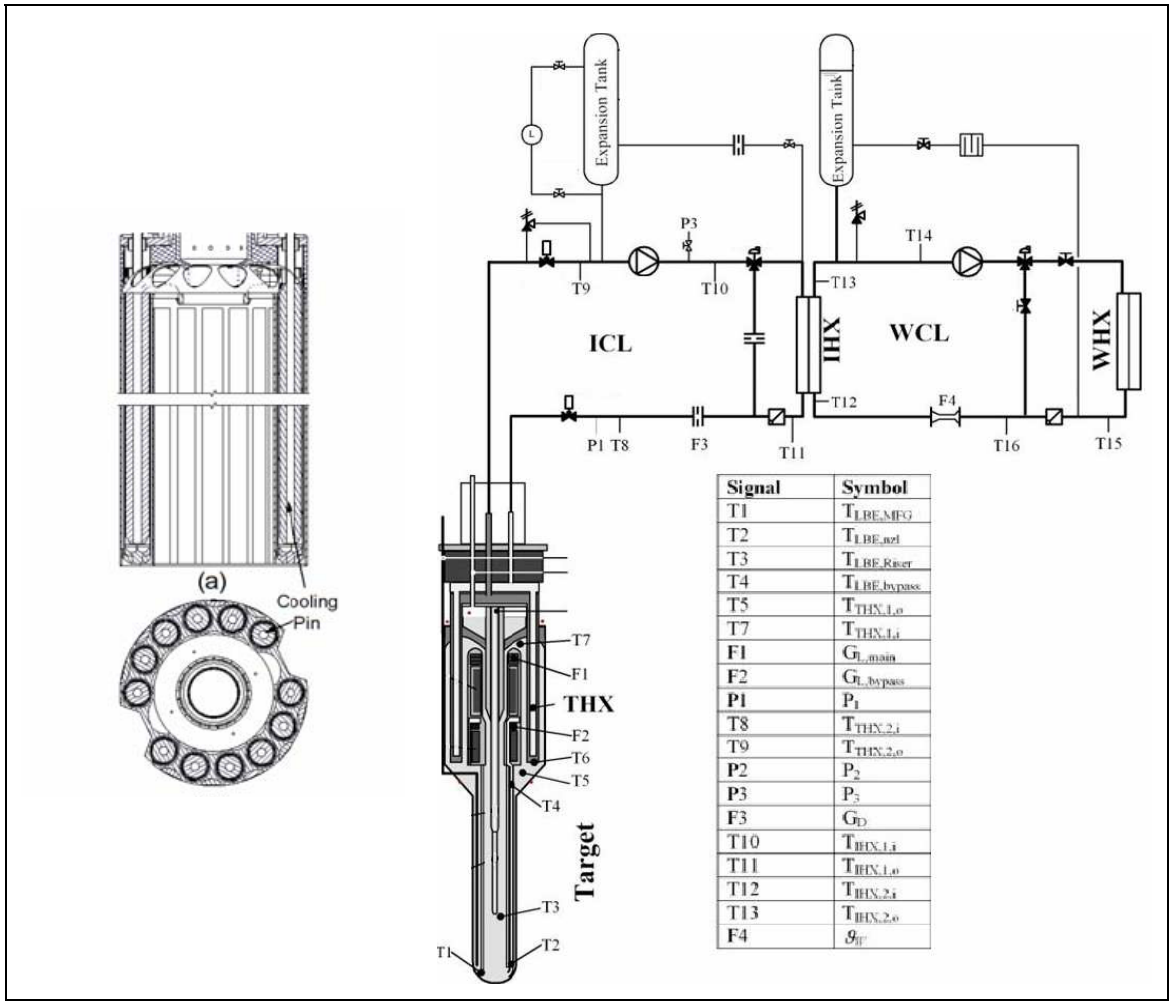

have been compared with the experimental data and with previous results obtained with the standard version of RELAP5, where the correlation of Dittus-Boelter (3) was used for heat exchange coefficient in the oil side.

$$Nu = 5.0 + 0.025 Pe^{0.8} \tag{2}$$

$$Nu = 0.023 Re^{0.8} Pr^{0.4} \tag{3}$$

The exchanged power and the increase of temperature in the oil side are reported in Figures 3 as the more significant parameters to evaluate the code capability in predicting the THX performance. This performance is better predicted with the new correlation implemented in RELAP5, in fact in the standard calculation the relative error on the exchanged power is within 10%, whereas the error for Glienlinsky is within 5% well below the level of uncertainty we have evaluated for the experimental data.

RELAP5 post-test analysis of the MEGAPIE irradiation experiment

The RELAP5 model of the cooling circuit used for the post-test analysis of the MEGAPIE irradiation experiment has been directly derived from the one used by PSI in the design phase and already assessed on the MITS tests [2]. The cooling system layout in the SINQ configuration for the MEGAPIE

Figure 3: MITS tests – comparison between experimental and calculated main parameters

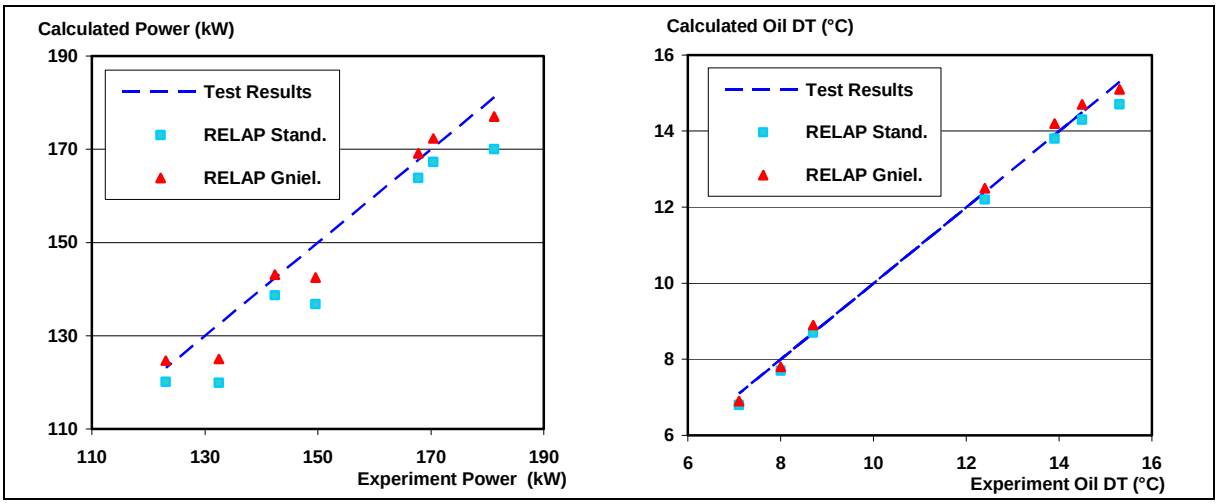

irradiation experiment was just slightly different from the previous layout in Figure 2. Basically, in the SINQ configuration, the control of the water loop was off, the three-way valve in this loop was blocked at a fixed opening therefore the water mass flow rate through the IHX was constant. Thus, the only relevant modifications of the model have concerned the THX component, which differs from the original one's both in the geometrical description of the helical oil path and in the associated correlation (Gnielinski), and a substantial simplification in the description of the water loop, which is limited to the simulation of the IHX water side by imposing the water inlet conditions by boundary conditions.

Re-calculation of the MEGAPIE experiment steady-state conditions

During the MEGAPIE irradiation experiment the thermal-hydraulic conditions of the SINQ cooling circuit had limited variations except for the start-up phase. After 13 days the beam current ranged from 1 200 to 1 400 μA for more than 110 days except for the periods of the beam interruption and a few short intervals. In this long period the power ranged from 500 to 572 kW, considering a conversion factor of 415 kW/mA, as estimated by PSI on the basis of Monte Carlo simulations [8]. Due to the limited variations of the temperature in the three different cooling loops only one reference steady state has been considered sufficient to represent the behaviour of the MEGAPIE cooling system for the most part of the experiment. In order to have almost average thermal-hydraulic conditions, the steady state selected for assessing RELAP5 corresponds to a target power of 540 kW [9]. The correspondent measured and calculated circuit temperatures are reported in Table 2.

The improvement of the RELAP5 predictions with the use of the Gnielinski correlation instead of the Dittus-Boelter standard correlation is more evident than in the component calculations showed in the previous paragraph. This is because a slight underestimation of the THX performance is amplified by the control logic of the three-way valve in the oil loop that tends to decrease the oil inlet temperature until the right performance is reproduced. All temperatures calculated with the new code version are within a range of 3°C from the measured ones, such an accuracy is undoubtedly acceptable considering the uncertainties related to the temperature measurements and the amount of thermal power in the target, as well as the difficulty to represent the real heat losses in the circuit owing to the lack of information.

Simulation of the MEGAPIE cooling system in transient conditions following proton beam trip

In order to verify the new RELAP5 model also in transient conditions, among nearly 4 500 beam trips of the SINQ source recorded during the 127 days of the MEGAPIE target irradiation, we have selected a beam interruption happened on 2 December at about midnight, according to SINQ acquisition system. The total beam interruption lasted only about 20 seconds but the falling-off period in two steps (115 s) and the rising period in four steps (250 s) were enough slow to influence the thermal-hydraulic behaviour of the cooling loop in a significant way.

Figure 4: Sketch of the RELAP5 nodalisation for the MEGAPIE cooling system

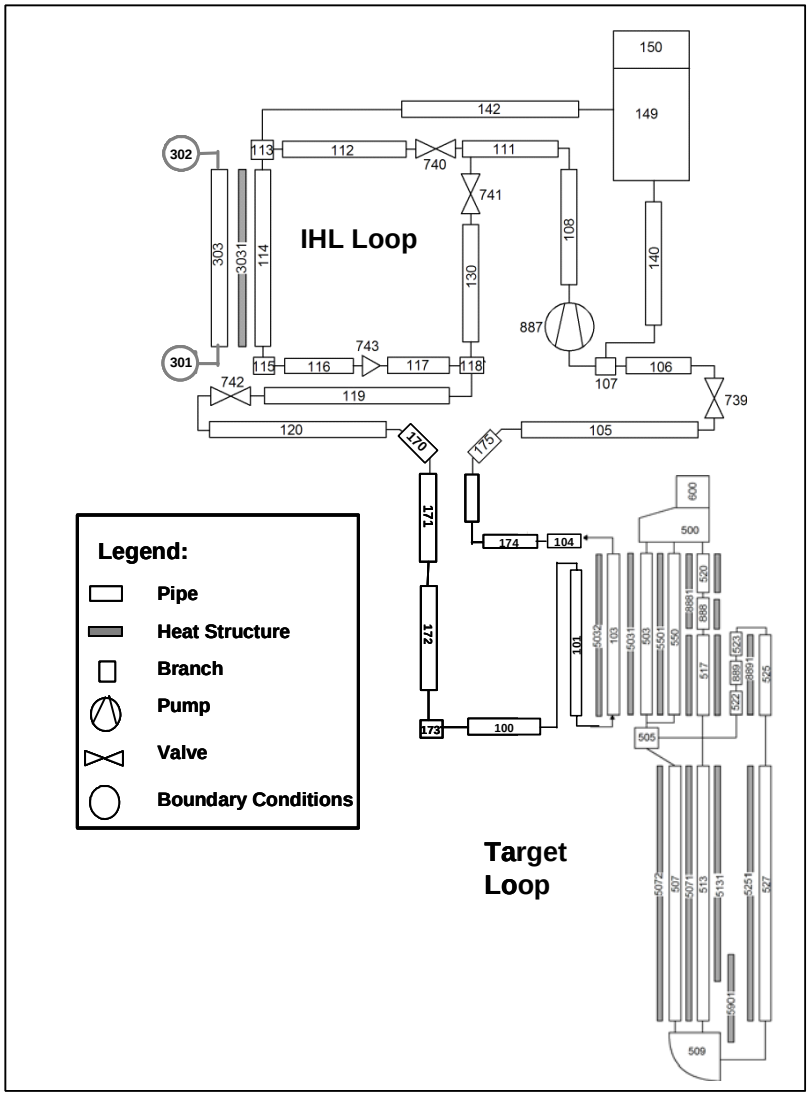

Table 2: MEGAPIE cooling system reference steady state

Target power 540.3 kW		Exp.	RELAP5 standard	RELAP Gnielinsky
THX LBE	Mflow (kg/s)*	41.23	Imposed	Imposed
	T1 (inlet) °C	319.6	316.2	316.2
	T2 (outlet) °C	229.5	Imposed	Imposed
THX oil	Mflow (kg/s)	9.25	Imposed	Imposed
	T3 (inlet) °C*	185.8	175.4	185.3
	T4 (outlet) °C	212.9	203.5	212.6
IHX oil	Mflow (kg/s)	NA	2.93	2.72
	T5 (inlet) °C	214.4	204.1	212.9
	T6 (outlet) °C	112.0	109.4	110.7
IHX water	Mflow (kg/s)	8.04	Imposed	Imposed
	T7 (inlet) °C	33.8	Imposed	Imposed
	T8 (outlet) °C	49.3	50.3	50.1

The post-test analysis of the beam trip transient has been performed with the RELAP5 model of the MEGAPIE cooling system set up for the steady state calculations and described in the previous paragraph. The interruption and switch on of the beam have been simulated in RELAP5 through a time description of the thermal power deposited in the target. As in the experiment LBE and oil pumps have operated at constant velocities during the whole transient, while the three-way valve in the oil loop has been maintained in operation to control the LBE temperature at the THX outlet. The mass flow rate and temperature of the water at the IHX inlet have been imposed in the calculation as time functions.

RELAP5 temperature trends are compared with the measured ones in Figures 4 and 5. They show a good capability of the model to predict the thermal-hydraulic response of the circuit at the beam interruption in term of the time scale. Although the three-way valve control, originally simulated in the code by means of a proportional-integral component and already tested on MITS transients [1], reacts to the LBE temperature decrease with a realistic delay (the three-way valve reaches the complete opening in a quite correct time), the decrease of LBE temperature calculated in the target loop is more accentuated than in the experiment (Figure 4). This behaviour affects also the oil temperature at the THX inlet and in IHX (Figure 5). A possible explanation for these slight discrepancies in the transient simulation could be an overestimation of the heat losses in the target that brings to a faster cooling of the LBE in the THX component.

Figure 4: Short beam trip: THX LBE and oil temperatures

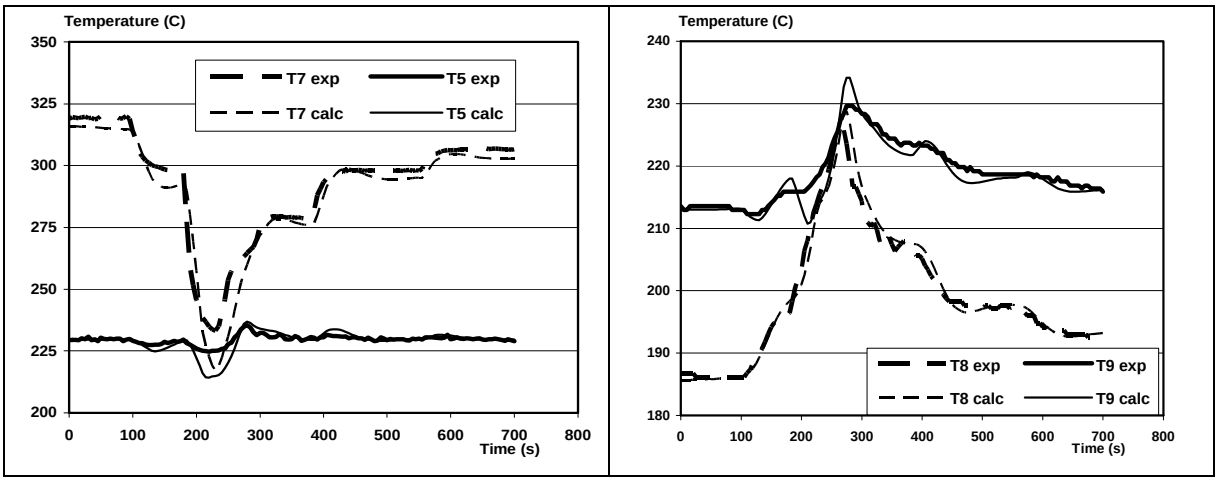

Figure 5: Short beam trip: IHX oil and water temperatures

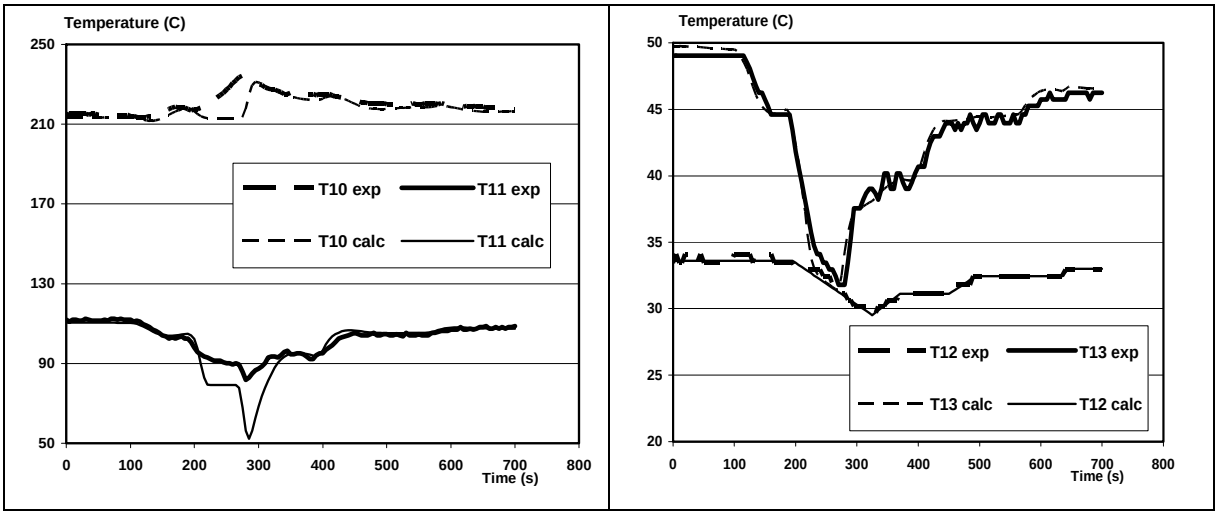

Conclusions

The ENEA participation in the post-test analysis of the MEGAPIE irradiation experiment has allowed to validate RELAP5 (mod3.2.2β version), its reference system code for transient and safety analysis of systems driven by accelerator (ADS), against thermal-hydraulics data related to a real liquid-metal target coupled with a proton accelerator.

The post-test calculations have been performed with a code version preliminary modified to improve the code capability in simulating the thermal exchange performance of the LBE-oil heat exchanger. The modification, which mainly concerned the computation of the heat transfer coefficient of the helical flow path in the oil side, has been preliminary assessed against the component data from single pin and MITS tests.

The post-test calculations have demonstrated the good capability of the code to simulate the thermal-hydraulics of the cooling circuit during the MEGAPIE normal operation. In steady-state conditions all temperatures have been predicted by the RELAP5 model of the loop in very good agreement with the experimental values, if one takes into account the uncertainties that affect the measurements and the heat losses of the cooling loop. Moreover, the applicability of the code to the transient conditions has been positively verified against an accelerator trip event.

References

[1] Agostini, P., *Observations Resulting from MEGAPIE Cooling Pin Tests in Brasimone*, EC Contract FIKW-CT-2001-00159 Megapie-Test report on Task 2.1

[2] Leung, W.H., *The MITS Test Results: Thermal Hydraulic Analyses*, PSI Technical Report MPR-MIT-LW34-003/0, Switzerland (2006).

[3] Casamirra, M., *et al.*, "RELAP5 Modification for CHEOPE Simulations", *International Conference Nuclear Energy for New Europe*, Bled, Slovenia, 5-8 September (2005).

[4] Gnielinski, V., "New Equations for Heat and Mass Transfer in Turbulent Pipe and Channel Flow", *International Chemical Engineering*, Vol. 16, pp. 359-368 (1976.)

[5] Ito, H., "Friction Factors for Turbulent Flow in Curved Pipes", *Journal of Basic Engineering, Trans. Amer. Soc. Mech. Engrs.*, Vol. D81, pp. 123-134 (1959).

[6] Casamirra, M., *et al.*, "Modifying RELAP5 Code to Deal with Helical Coiled Ducts", *XXIV Congresso Nazionale UIT sulla Trasmissione del Calore*, Naples, Italy, 21-23 June (2006).

[7] Meloni, P., *et al.*, "Implementation and Preliminary Verification of the RELAP5/PARCS Code for Pb-Bi Cooled Subcritical Systems", *Proc. of the International Conference on Accelerator Applications (AccApp01)*, American Nuclear Society, Reno, US (2001).

[8] Leung, W., P. Blair, *Date of the MEGAPIE Target Operation in SINQ*, PSI Technical Report (DRAFT).

[9] Meloni, P., *MEGAPIE Post-test Analysis for the RELAP5 Code Verification*, ENEA Technical Report, FPN – P9EH-009, January (2008).

Evaluation of JSFR oxide fuel core TRU burning capability

Masayuki Naganuma, Fumiaki Kono, Tomoyasu Mizuno
Japan Atomic Energy Agency, Japan

Shigenobu Kubo
The Japan Atomic Power Company, Japan

Abstract

In the Fast Reactor Cycle Technology Development Project (FaCT Project) launched in 2006, a sodium-cooled fast breeder reactor (FBR) with mixed-oxide fuel was selected as the primary candidate. A design study for the reactor, known as the Japan Atomic Energy Agency (JAEA) Sodium-cooled Fast Reactor (JSFR), has been conducted. In the study, the transition stage from light water reactors (LWR) to FBR was regarded as an important issue. This is because a wide variety of recycled LWR spent fuels might be supplied to the JSFR core, affecting the fuel designs from the viewpoint of minor actinide (MA) content. Thus, the effect of MA content on the fuel mechanical and thermal designs was quantitatively evaluated in the present paper. The results are as follows.

In fuel mechanical design, MA content affects the gas yield and the history of cladding temperature. Effects on specifications such as gas plenum length, etc., were evaluated under conditions that satisfy the typical mechanical limit. As a result, the contribution of the gas yield was found to be dominant. And, when a factor of 2.0 was tentatively assumed for the uncertainty of helium gas generation for conservativeness, the extension of the gas plenum length was approximately 15% per 1 wt.% of Am+Cm. The effect on the linear power limits in a steady operation was evaluated in the fuel thermal design. In this evaluation, the melting point and thermal conductivity obtained recently by the JAEA were applied. The results indicated that decreases in the linear power limit were 7 W/cm and 3.5 W/cm per 1 wt.% of Am+Cm for BOL and EOL, respectively. Hereafter, these results will contribute to the evaluation of irradiation conditions and fuel specifications of the JSFR core.

Introduction

In Japan, a joint Japan Atomic Energy Agency (JAEA)/Japan Atomic Power Company (JAPC) team has been involved in a project for the commercialisation of the fast reactor cycle since 2006 named the Fast Reactor Cycle Technology Development Project (FaCT Project) [1,2]. A sodium-cooled fast breeder reactor (FBR) with mixed-oxide fuel, the JAEA Sodium-cooled Fast Reactor (JSFR), has been selected as the primary candidate. The development targets of the FaCT Project are as follows: safety and reliability, sustainability (reduction of environmental burden, waste management and efficient utilisation of nuclear fuel resources), economic competitiveness and proliferation resistance. The design study for the JSFR has progressed based on the development targets.

In this design study, a transition stage from light water reactors (LWR) to FBR is regarded as an important issue [3,4]. This is because the transuranium (TRU) composition of fuel significantly affects the design. During this stage, as a number of LWR would coexist with FBR, TRU recycled from LWR spent fuel might be supplied as fuel for the FBR. The composition of the recycled TRU depends on burn-up, storage period and the recycle scenario of the LWR fuel. There is a possibility that the FBR core will contain a wide-range of minor actinide (MA). If the fuel has a high MA content, the following effects on the core and fuel designs are considered:

i) High MA content degrades the neutronic reactivity characteristics (sodium-void reactivity, Doppler coefficient, etc.), affecting the safety characteristics.

ii) High MA content raises the inner gas pressure due to increased helium gas generation, affecting the fuel's mechanical integrity. And, it decreases the melting point and thermal conductivity of mixed-oxide fuel, reducing the margin to fuel melting.

Therefore, it is necessary to understand the effects of MA content on design. The present paper places a particular focus on the fuel design of the JSFR oxide fuel core. For the fuel design, thermal and mechanical design are important factors. Parametric surveys of MA content were conducted in consideration of the design conditions, requirements, limits and fuel specifications of the JSFR. Then, the effects on the both fuel designs were quantitatively evaluated.

Design conditions, requirements and limits of the JSFR

The typical design conditions, requirements and limits of the JSFR [2,3] are shown in Table 1, and the parametric surveys were conducted based on these. The major items related to this evaluation are explained below.

Table 1: Typical design conditions, requirements and limits of the JSFR core

	Items	Values
Plant conditions	Power output (large-scale reactor) Coolant temp. (outlet/inlet) Shielding region diameter	1 500/3 530 [MW_e/MW_t] 550/395 [°C] < approx. 7.0 [m]
Core performance conditions	Breeding ratio (LBC/HBC) Average discharge burn-up core total (core+blanket) (HBC/LBC) Operation cycle length	1.1~1.0/1.2 150 [GWd/t] > 60/> 80 [GWd/t] > 24 [month]
Safety requirements	Sodium void reactivity Core height Average core specific heat Measures to prevent re-criticality	< approx. 6 [$] < 100 [cm] > approx. 40 [kW/kg-MOX] FAIDUS type subassembly
Fuel conditions	TRU composition Residual fission products	MA content is from 1 to 5 wt.%. Low-decontaminated fuel
Fuel integrity limits	Max. linear power Max. cladding temp. (mid-wall) CDF (steady state) Max. fast neutron fluence (E > 0.1 MeV)	< approx. 430 [W/cm] < 700 [°C] < 0.5 < approx. 5×10^{23} [n/cm^2]
Thermal-hydraulic condition	Bundle pressure drop	< approx. 0.2 [MPa]

Plant conditions

In the FaCT Project, design studies for large- and medium-scale reactors have been conducted. In this paper, a 3 530 MWt large-scale reactor was evaluated. The core outlet and inlet temperatures are 550°C and 395°C, respectively.

Core performance conditions

In the FaCT Project, flexible breeding capability is required not only for the efficient utilisation of nuclear fuel resources but also to meet other conditions such as economical advantage, etc. Thus, two breeding-type cores, the Low Breeding Core (LBC) and High Breeding Core (HBC), have been designed. The breeding ratio of the LBC ranges from 1.03 to 1.1, and that of the HBC is approximately 1.2. The total average discharge burn-up values (including core and blanket) of the LBC and HBC are 80 GWd/t and 60 GWd/t, respectively. The high burn-up in the LBC contributes to the reduction of fuel cycle cost, increasing its economical advantage.

Fuel conditions

The fuel of the JSFR core contains MA for uranium resource utilisation, the reduction of environmental burden, etc. A wide range of MA content is considered in the transition stage from LWR to FBR. MA content up to approximately 5 wt.% is regarded as a tentative target.

Fuel integrity limits

The tentative target of the linear power limit is 430 W/cm at BOL. As MA content affects properties of a mixed-oxide fuel, the limit may change according to MA content in the transition stage. The fuel cladding mid-wall maximum temperature is 700°C or less, and the fuel cladding cumulative damage fraction (CDF) under steady operation is 0.5 or less. The current target of fast neutron fluence ($E > 0.1$ MeV) is approximately 5×10^{23} n/cm^2.

Major fuel specifications and core characteristics of the reference core of the JSFR

In this paper, parametric surveys regarding MA content were conducted for the JSFR core. Thus, the major fuel specifications and core characteristics are introduced. As the reference core of the JSFR, a high internal conversion (HIC) type core has been adopted [5]. This type core aims to reduce fuel cycle cost by increasing total average discharge burn-up, including core and blanket. As a practical method, large diameter fuel pin was applied to increase internal conversion ratio to reduce the amount of blanket as much as possible. The core configuration is shown in Figure 1. Here, LBC with breeding ratio 1.1 was selected as the typical core, which has one layer of radial blanket subassemblies.

Figure 1: Core configurations of the JSFR (LBC, BR = 1.1)

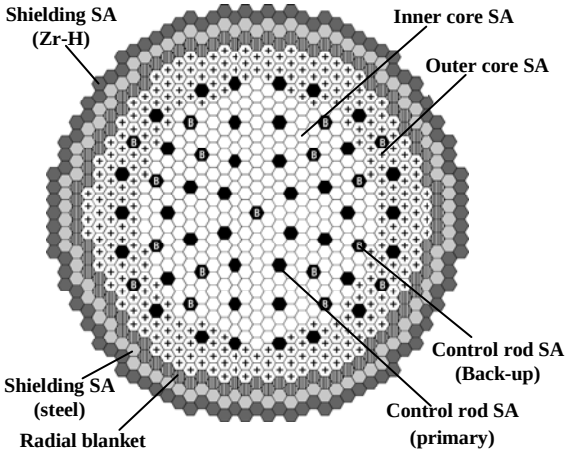

The major fuel specifications of LBC are shown in Table 2. The outer diameter of fuel pin is 10.4 mm. Oxide dispersion strengthened (ODS) steel [6], which withstands high neutron doses and has excellent high temperature strength, is adopted as cladding material to satisfy the design conditions of high burn-up and high core outlet temperature. The fuel pin has a lower gas plenum to reduce the bundle pressure loss by shorting the plenum length. The smear density is limited to 82% TD to attain high burn-up up. Thus, the annular pellet is selected. In addition, the fuel assembly with inner duct structure (FAIDUS) type subassembly [7] shown in Figure 2 is adopted for the prevention of re-criticality. This type subassembly has an inner duct installed at one corner as a measure for the early discharge of molten fuel to prevent re-criticality in a core disruptive accident (CDA). The major core characteristics are shown in Table 3. These are characteristic of LBC with FBR multi-recycle TRU composition [3]. Pu enrichments of the inner and outer core are 18 wt.% and 21 wt.%, respectively. The breeding ratio is 1.1. The peak linear power is approximately 400 W/cm.

Table 2: Major fuel specifications of the JSFR (LBC)

Items	Specifications
Fuel type	(U, Pu, MA)O_2 (Annul pellet)
Cladding material	ODS
Outer pin diameter [mm]	10.4
Cladding thickness [mm]	0.71
Column length [cm]	100
Axial blanket [cm] (upper./lower)	10 / 110
Bond material	He
Smear density [%TD]	82
Fuel density [%TD]	95

Figure 2: Conceptual view of the FAIDUS type subassembly

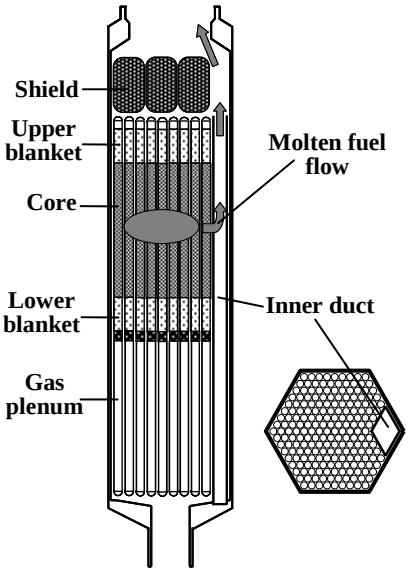

Table 3: Major core characteristics of the JSFR (LBC)

Items	Characteristics*
Operation cycle length [EFPM]	26.3
Fuel reloaded batch (core / rad. blank.) [-]	4 / 4
Pu enrich. (inn. core / out. core) [wt.%]	18.2 / 20.6
Average discharge burnup (core / total (core+blank.)) [GWd/t]	145 / 89
Burnup reactivity [%Δk/kk']	2.5
Breeding ratio (core / ax. blank. / rad. blank. / total) [-]	0.83 / 0.19 / 0.07 / 1.1
Max. linear power (inn. core / out. core)	403 / 402
Max. fast neutron fluence [$x10^{23}$ n/cm^2 (E>0.1 MeV)]	4.9

* These are characteristics of LBC with FBR multi-recycle TRU composition [3].

Outline of the effect of MA content on the fuel mechanical and thermal designs

Fuel mechanical design

In general, with increasing MA content, two effects are generally considered. One is the effect on the inner gas pressure of the fuel pin. This is induced by increased helium gas generation. The generation of helium gas is due to the following nuclear reactions:

- ternary fission of fissile nuclides;
- (n,α) reaction [mainly, $^{16}O(n,\alpha)^{13}C$];
- α decay of TRU nuclides.

The most dominant reaction is the third, especially, α decay of ^{242}Cm generated from ^{241}Am. This reaction depends on the increase of MA content, which raises the inner gas pressure. The other is the effect on the history of the cladding temperature. The fuel power decreases as the burn-up increases; however, the extent of power reduction is reduced or the linear power rather may increase with increasing MA content. This is because MA nuclides behave as superior fertile nuclides. This induces the cladding temperature in the end period of life to increase. The hoop stress of the cladding is large in the end period of life due to the accumulation of inner gas. Accordingly, the increased cladding temperature might affect the CDF of the cladding.

Fuel thermal design

As MA content increases, the thermal conductivity and melting point have a tendency to decrease. It is necessary to characterise these properties sufficiently because they may reduce the margin to fuel melting. Thus, the data of the mixed-oxide fuel with relatively low Am content were examined in the JAEA [8]. Figure 3 shows melting points evaluated based on the results. The ideal solution model was applied with the O/M ratio set at 2.00 for conservativeness here. As 1 wt.% of Am is contained, the melting point decreases by approximately 5°C. Figure 4 shows thermal conductivities evaluated based on the results. The effect of Am content is relatively small. It is especially slight in the high temperature region.

Figure 3: Melting point of Am-bearing mixed-oxide fuel

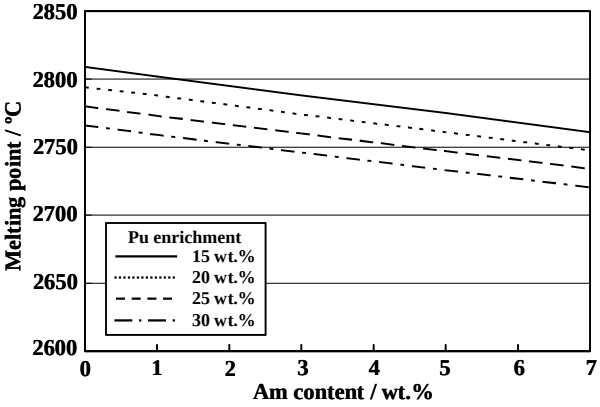

Figure 4: Thermal conductivity of Am-bearing mixed-oxide fuel

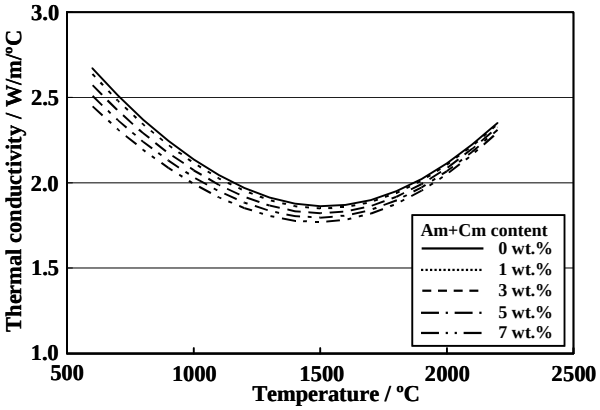

Evaluation of the effect on the fuel mechanical and thermal designs

Fuel mechanical design

In mechanical design, the gas yield and the history of cladding temperature are important, as described above. Their effect is mainly on the gas plenum length and the clad thickness due to CDF in the fuel pin design. In this section, first, the effect on the gas yield and the history of cladding temperature are evaluated for a wide range of MA content. After that, the effect on the gas plenum length and the clad thickness are evaluated based on the results, providing CDF satisfies the design limit.

Evaluation methods and conditions

i) MA content

- Am and Cm were assumed to be recovered separately from Pu and Np. And, Np was assumed to be co-recovered with Pu. As for the TRU composition, that of ALWR, with an average discharge burn-up of 60 GWd/t and storage period of 40 years, was applied based on Ref. [3].
- Am+Cm content was regarded as a parameter. Am+Cm contents of 0, 1, 3, 5 and 7 wt.% were selected as evaluation cases to caver the design condition of JSFR.

ii) History of cladding temperature

- The fuel power history was calculated using neutron diffusion theory for two-dimensional R-Z geometry. The history of the clad temperature was evaluated based on the result.

iii) Gas yield

- Gas yields for every Am+Cm content were evaluated in a point-depletion calculation code ORIGEN2.
- All Am and Cm was assumed to be ^{241}Am for conservativeness in the yield evaluation.
- As for the uncertainty of helium gas generation, a factor of 2.0 was tentatively assumed for conservativeness.

iv) CDF

- Only creep damage was considered in this CDF evaluation because the contribution of fatigue was negligible at the severest position of the FBR fuel pin.
- As for creep strength, inner and outer corrosion of ODS steel, design models that JAEA evaluated [9] were applied.
- It is necessary to consider various uncertainties such as fuel fabrication tolerances and temperature calculation error. In this CDF evaluation, the method to handle these uncertainties statistically was applied.

Results

Evaluated results of the gas yield are shown in Table 4. The yield increases as Am+Cm content increases, and the ratio is approximately 0.04 per 1 wt.% of Am+Cm content. The histories of peak cladding temperature for every Am+Cm content are shown in Figure 5. The cladding temperatures at EOL are recognised to become higher as Am+Cm content increases.

Table 4: Results of the gas yields

	Am+Cm content				
	0 wt.%	1 wt.%	3 wt.%	5 wt.%	7 wt.%
Gas yield (Xe, Kr, He, etc.)	0.29	0.32	0.40	0.48	0.56

Figure 5: History of the peak cladding temperature

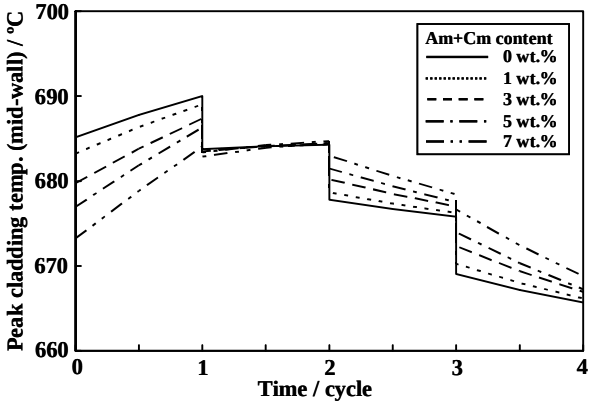

Based on these results, the fuel pin specifications were evaluated for every Am+Cm content with CDF at 0.5. The evaluated results are plotted in Figure 6 as a map to show the relationship between the gas plenum length and the cladding thickness. Here, the horizontal axis is the gas plenum length, and the longitudinal axis is the cladding thickness. As Am+Cm content increases, the gas plenum length must be extended, and the cladding thickness is increased. As a result, the extension of the gas plenum length is approximately 15% per 1 wt.% of Am+Cm content, while that of the cladding thickness is approximately 0.01 mm per 1 wt.% of Am+Cm content. In order to compare the contributions of the gas yield and the history of the cladding temperature, the effect of both factors on the gas plenum length were evaluated separately. The result reveals that the contribution of the gas yield is nearly

Figure 6: Map of gas plenum length and cladding thickness providing CDF = 0.5

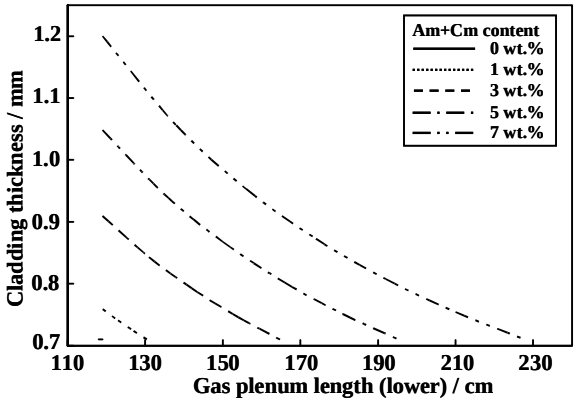

15% per 1 wt.% of Am+Cm content and is dominant. Here, it is necessary to note that these were results when the uncertainty of helium generation was assumed to be a factor of 2.0. If the uncertainty is studied minutely in the future, the influence might be revised.

Fuel thermal design

Material properties of mixed-oxide fuel such as the melting point and the thermal conductivity decrease with increased MA content, as described above. In this section, effect of MA content on the limit of linear power under steady operation is evaluated. First, the power to melt is calculated based on the JAEA-evaluated material property models. After that, the limit of linear power under steady operation is evaluated in consideration of an overpower factor, which means the ratio of fuel pin power at the normal trip level to that under steady operation. The evaluations are conducted at both BOL and EOL because the material properties are different at these times.

Evaluation method and conditions

i) *MA content*

- The contents of Pu+Np and Am+Cm were regarded as parameters. Pu+Np content ranged from 15 wt.% to 30 wt.%, and Am+Cm content ranged from 0 wt.% to 7 wt.%.

ii) *Limit temperature to melt*

- As for melting point, the JAEA evaluated model shown in Figure 3 was applied.
- Cm was regarded as Am, and Np was regarded as Pu, tentatively.
- In deciding limit temperature to melt, error of measurement of melting point and redistribution of Pu and Am were considered. The redistribution behaviour of Am was assumed to be equivalent to that of Pu [10].
- Decrease of melting point with burn-up was considered -7°C per 10 000 MWd/t.
- Nuclear transmutation of both Am and Cm were considered for the melting point at EOL.

iii) *Thermal conductivity*

- The JAEA-evaluated model shown in Figure 4 was applied.
- Cm was regarded as Am, and Np was regarded as Pu, tentatively.

iv) *Other*

- As for gap conductance, the model tentatively determined based on the above melting point and thermal conductivity and power to melt tests was applied.
- Hot spot factor (uncertainties in analysis, fuel specification and operation) was considered in the evaluation of fuel centre temperature.

Results

As examples of the results, the limits of linear power evaluated for 0, 1, 3, 5 and 7 wt.% of Am+Cm content are shown in Table 5. Pu+Np content for every case was 22 wt.%. The limits of linear power of 0 wt.% were 443 W/cm at BOL and 398 W/cm at EOL. The limit at EOL is found to be smaller than that at BOL by approximately 40 W/cm. This is due mainly to the reduction of melting points with burn-up. The limit temperature to melt falls by 150°C from BOL to EOL, as shown in Table 5. The decrease of the linear power limit at BOL is approximately 7 W/cm per 1 wt.% of Am+Cm content, and that at EOL is approximately 3.5 W/cm. The reason that the sensitivity at EOL is small is due to the consideration of the nuclear transmutation of Am and Cm for the melting point at EOL.

Table 5: Results of linear power limits under steady operation

	Am+Cm content: 0 wt.%		Am+Cm content: 1 wt.%		Am+Cm content: 3 wt.%		Am+Cm content: 5 wt.%		Am+Cm content: 7 wt.%	
	BOL	EOL	BOL	EOL	BOL	EOL	BOL	EOL	BOL	EOL
Pu+Np content [wt.%]	22.0	22.0	22.0	22.0	22.0	22.0	22.0	22.0	22.0	22.0
Limit temperature to melt [°C]	2 733	2 563	2 724	2 562	2 707	2 555	2 690	2 546	2 673	2 537
Power to melt [W/cm]	542	486	532	482	515	474	499	465	484	456
Limit of linear power under steady operation [W/cm]	443	398	435	394	421	387	408	380	396	373

The maps of linear power limits are shown in Figure 7 for BOL and EOL. The curves with the same linear power limit are plotted there. Decrease in the linear power limit is found to be nearly linearly related to Am+Cm content in the range of this evaluation. The map also shows that decreases in the linear power limit for BOL are approximately 7 W/cm per 1 wt.% of Am+Cm content. When Pu enrichment is 22 wt.%, the design target of linear power, 430 W/cm, is satisfied up to approximately 2 wt.% of Am+Cm content at BOL. At the same time, decreases in the linear power limit for EOL are 3.5 W/cm per 1 wt.%. It is necessary to pay attention to the limit at EOL as well as BOL in the thermal design of MA bearing fuel because the extent of power reduction is related to increasing MA content, as described in the previous section.

Figure 7: Maps of linear power limits under steady operation as factions of Am+Cm content and Pu+Np content (BOL and EOL)

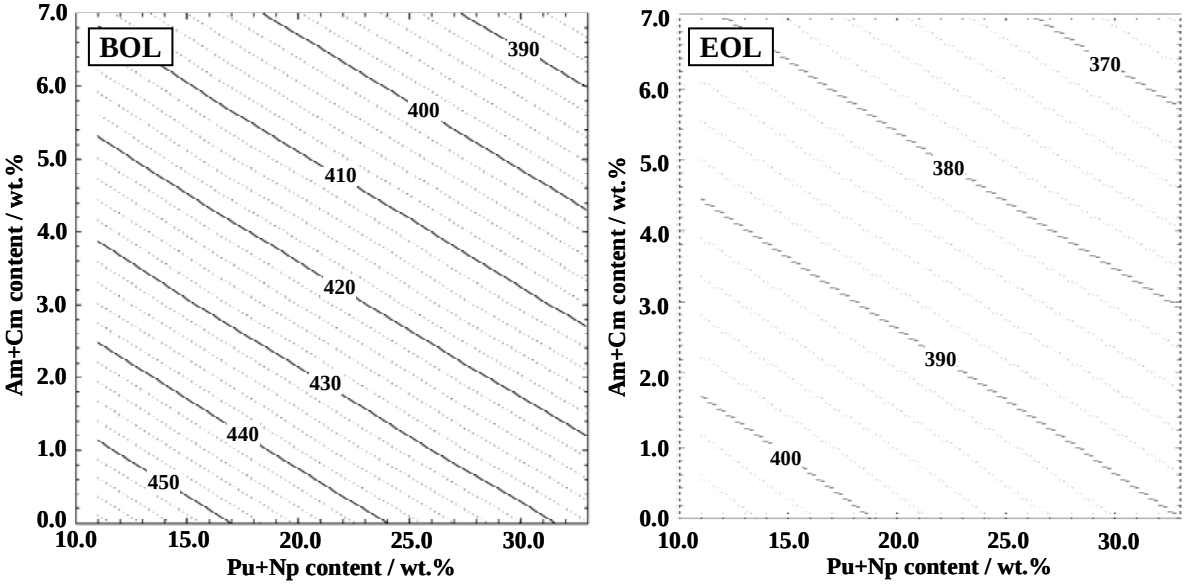

Conclusion

The effect of MA content on the fuel mechanical and thermal designs were quantitatively evaluated for the JSFR oxide fuel core. The results are as follows: in fuel mechanical design, MA content affects the gas yield and history of cladding temperature. Effects on specifications such as gas plenum length, etc., were evaluated under conditions that satisfy the typical mechanical limit, which was CDF under steady operation. As a result, the contribution of the gas yield was found to be dominant. And, when a factor of 2.0 was tentatively assumed as the uncertainty of helium gas generation for conservativeness, the extension of the gas plenum length was approximately 15% per 1 wt.% of Am+Cm. In fuel thermal design, the effect on the linear power limits under steady operation was evaluated. In this evaluation, the melting point and thermal conductivity examined by the JAEA were applied. The results indicated that decreases in the linear power limit were 7 W/cm and 3.5 W/cm per 1 wt.% of Am+Cm at BOL and EOL, respectively. Hereafter, these results will contribute to the evaluations of irradiation conditions and fuel specifications of the JSFR core. At the same time, they will be revised according to additional studies for material properties, the uncertainty of helium gas generation and so on.

Acknowledgements

This paper includes the outcome of a collaborative study carried out by the JAEA and the JAPC (representative of nine electric utilities, the Electric Power Development Company and the JAPC) in accordance with the "Agreement Concerning the Development of a Commercial Fast Breeder Reactor Cycle System".

References

[1] Niwa, H., K. Aoto, M. Morishita, "Current Status and Perspective of Advanced Loop Type Fast Reactor in Fast Reactor Cycle Technology Development Project", *GLOBAL 2007*, Idaho, US, pp. 62-70 (2007).

[2] Kotake, S., T. Mihara, S. Kubo, *et al.*, "Development of Advanced Loop-type Fast Reactor in Japan (1): Current Status of JSFR Development", *ICAPP '08*, Anaheim, CA, USA, Paper 8226 (2008).

[3] Ohki, S., T. Ogawa, N. Kobayashi, *et al.*, "FBR Core Concepts in the 'FaCT' Project in Japan", *Physor08*, Interlaken, Switzerland, Paper 649 (2008).

[4] Naganuma, M., T. Ogawa, S. Ohki, *et al.*, "Development of Advanced Loop-type Fast Reactor in Japan (6): Minor Actinide Containing Oxide Fuel Core Design Study for the JSFR", *ICAPP '08*, Anaheim, CA, USA, Paper 8082 (2008).

[5] Mizuno, T., T. Ogawa, M. Naganuma, T. Aida, "Advanced Oxide Fuel Core Design Study for SFR in the 'Feasibility Study' in Japan", *GLOBAL 2005*, Tsukuba, Japan, Paper 434 (2005).

[6] Kaito, T., S. Ohtsuka, M. Inoue, "Progress in the R&D Project on Oxide Dispersion Strengthened and Precipitation Hardened Ferritic Steels for Sodium Cooled Fast Breeder Reactor Fuels", *GLOBAL 2007*, pp.37-42, Idaho, US (2007).

[7] Mizuno, T., H. Niwa, "Advanced MOX Core Design Study of Sodium-cooled Reactor in Current Feasibility Study on Commercialized Fast Reactor Cycle System in Japan", *Nuclear Technology*, Vol. 46 (2004).

[8] Kato, M., K. Morimoto, *et al.*, *Evaluation of Thermal Physical Properties for Fast Reactor Fuels – Melting Point and Thermal Conductivities*, JAEA-Technology 2006-049 (2006) [in Japanese].

[9] Ogawa, T., I. Sato, T. Aida, *et al.*, *Study on Reactor Core and Fuel Design of Sodium Cooled Fast Reactor (Mixed Oxide Fuel Core) – Results in JFY2005*, JAEA-Research 2006-061 (2006) [in Japanese].

[10] Hisada, M., S. Koyama, K. Yamamoto, *Americium Redistribution in Americium Containing MOX Fuel (B8-HAM)*, JNC TN9430 2000-002, (2000) [in Japanese].